Reconstitution of the RNA polymerase I initiation complex from recombinant initiation factors and regulation of its activity

DISSERTATION ZUR ERLANGUNG DES DOKTORGRADES DER NATURWISSENSCHAFTEN (DR. RER. NAT.)
DER FAKULTÄT FÜR BIOLOGIE UND VORKLINISCHE MEDIZIN
DER UNIVERSTIÄT REGENSBURG

vorgelegt von
Michael Pilsl

aus
Passau

im Jahr
2021

Das Promotionsgesuch wurde eingereicht am:
09.07.2021

Die Arbeit wurde angeleitet von:
Prof. Dr. Herbert Tschochner

Unterschrift:

Pubilications:

Parts of the analysis of the Pol I/Rrn3 complex, Pol I monomers and dimers was published in:
Pilsl, Michael; Crucifix, Corinne; Papai, Gabor; Krupp, Ferdinand; Steinbauer, Robert; Griesenbeck, Joachim et al. (2016a): Structure of the initiation-competent RNA polymerase I and its implication for transcription. In: *Nature communications* 7, S. 12126. DOI: 10.1038/ncomms12126.

Contributions:
M.P. and R.S., performed biochemical experiments; G.P., C.C., F.K. and P.S. collected and analysed the cryo-EM data, and calculated and refined the EM densities. J.G. and P.M. participated in planning experiments, data interpretation and manuscript writing. P.S. and H.T. planned experiments and supervised the work. M.P., H.T. and P.S. prepared the figures and wrote the manuscript together.

Studies on an early intermediate Pol I PIC were published in:
Pilsl, Michael; Engel, Christoph (2020): Structural basis of RNA polymerase I pre-initiation complex formation and promoter melting. In: *Nat Comms* 11 (1), S. 1206. DOI: 10.1038/s41467-020-15052-y.

Contributions:
M.P. carried out experiments and data analysis. C.E. designed and supervised research. M.P. and C.E. carried out model building and prepared the manuscript.

Merkl, Philipp; Perez-Fernandez, Jorge; **Pilsl, Michael**; Reiter, Alarich; Williams, Lydia; Gerber, Jochen et al. (2014): Binding of the termination factor Nsi1 to its cognate DNA site is sufficient to terminate RNA polymerase I transcription in vitro and to induce termination in vivo. In: *Mol Cell Biol* 34 (20), S. 3817–3827. DOI: 10.1128/MCB.00395-14.

Pilsl, Michael; Crucifix, Corinne; Papai, Gabor; Krupp, Ferdinand; Steinbauer, Robert; Griesenbeck, Joachim et al. (2016a): Structure of the initiation-competent RNA polymerase I and its implication for transcription. In: *Nature communications* 7, S. 12126. DOI: 10.1038/ncomms12126.

Pilsl, Michael; Merkl, Philipp E.; Milkereit, Philipp; Griesenbeck, Joachim; Tschochner, Herbert (2016b): Analysis of S. cerevisiae RNA Polymerase I Transcription In Vitro. In: *Methods in molecular biology (Clifton, N.J.)* 1455, S. 99–108. DOI: 10.1007/978-1-4939-3792-9_8.

Darrière, Tommy; **Pilsl, Michael**; Sarthou, Marie-Kerguelen; Chauvier, Adrien; Genty, Titouan; Audibert, Sylvain et al. (2019): Genetic analyses led to the discovery of a super-active mutant of the RNA polymerase I. In: *PLoS genetics* 15 (5), e1008157. DOI: 10.1371/journal.pgen.1008157.

Hannig, Katharina; Babl, Virginia; Hergert, Kristin; Maier, Andreas; **Pilsl, Michael**; Schächner, Christopher et al. (2019): The C-terminal region of Net1 is an activator of RNA polymerase I transcription with conserved features from yeast to human. In: *PLoS Genet* 15 (2). DOI: 10.1371/journal.pgen.1008006.

Merkl, Philipp E.; **Pilsl, Michael***; Fremter, Tobias; Schwank, Katrin; Engel, Christoph; Längst, Gernot et al. (2020): RNA polymerase I (Pol I) passage through nucleosomes depends on Pol I subunits binding its lobe structure. In: *J. Biol. Chem.* DOI: 10.1074/jbc.RA119.011827.

Pilsl, Michael; Engel, Christoph (2020): Structural basis of RNA polymerase I pre-initiation complex formation and promoter melting. In: *Nat Comms* 11 (1), S. 1206. DOI: 10.1038/s41467-020-15052-y.

Ramsay, Ewan Phillip; Abascal-Palacios, Guillermo; Daiß, Julia L.; King, Helen; Gouge, Jerome; **Pilsl, Michael** et al. (2020): Structure of human RNA polymerase III. In: *Nat Comms* 11 (1), S. 6409. DOI: 10.1038/s41467-020-20262-5.
* contributed equally

Table of Content

1. Introduction

1.1. Making Ribosomes

The ability to translate genetic messages into functional proteins is essential for all lifeforms on our planet. Intermediary messenger RNAs (mRNAs) are translated into functional proteins. This process is achieved by a large enzymatic complex, the ribosome. Ribosomes of the yeast *S. cerevisiae* (hereafter called yeast) consist of ~80 proteins and 4 ribosomal RNAs (rRNA). rRNA accounts for more than two thirds of the ribosomal mass, has structural and catalytic functions. The ribosome consists of two subunits, the small subunit (SSU/40S) decodes mRNA, while formation of peptide-bonds is catalyzed in the large subunit (LSU/60S) of a translating ribosome (80S). Prominent ribosomal species can be separated in density gradients and assigned with their respective sedimentation co-efficient (in Svedberg units, S).

Synthesis of ribosomes starts with the transcription of the 35S rRNA gene by RNA Polymerase I (Pol I). This polycistronic precursor is processed into the 18S, 5,8S and 25S rRNA of the major small and large ribosomal subunits. The small 40S subunit consists of the 18S rRNA and 33 ribosomal proteins. In the large 60S subunit, 25S, 5,8S and 5S rRNAs associate with 46 ribosomal proteins. More than 200 additional factors, including proteins, protein complexes and small nucleolar ribonucleoproteins (snoRNPs), are required for the assembly of ribosomes. These assembly factors transiently associate in a hierarchically manner with maturating ribosomes (reviewed in (Woolford and Baserga 2013; Klinge and Woolford 2019)) .Ribosome biogenesis represents a major metabolic effort of a cell. 2000 ribosomes are produces per minute in fast growing yeast cells. For this process, 50% of Pol II transcribed genes encode for ribosomal proteins. Further, 60% of total transcription is devoted to rRNA (Warner 1999; Rudra and Warner 2004).

1.2. The rDNA locus

1.2.1. Nuclear sub-compartmentation - the nucleolus

The biosynthesis of ribosomes takes place at a dedicated sub-compartment within the nucleus, the nucleolus. The nucleolus is a prominent example of functional sub-compartmentation and was observed in early microscopic studies. In yeast cells it appears as a crescent shaped structure within the nucleus and occupies about one third of its volume. In thin sections of cryo-fixated and freeze-substituted yeast cells, three distinct compartments can be distinguished. Electron-transparent zones resembling fibrillar centers (FC) are surrounded by a dense fibrillar component (DFC) and forms a network within the nucleolus. The rest of the nucleolar structure is composed of the granular component (GC) (Léger-Silvestre et al. 1999). Immuno-staining revealed that Pol I is enriched at the boundary of the DNA containing FC and the DFC. This indicates the site of rRNA transcription and hypothesized that nascent rRNA is protruding into the DFC, where early steps of ribosome assembly and rRNA processing occur (Léger-Silvestre et al. 1999). Besides being the starting place for ribosome

synthesis, the highly dynamic structure can harbor biogenesis of other RNP complexes and functions in stress response and can control cellular activity. (Raska et al. 2006; Moss et al. 2007).

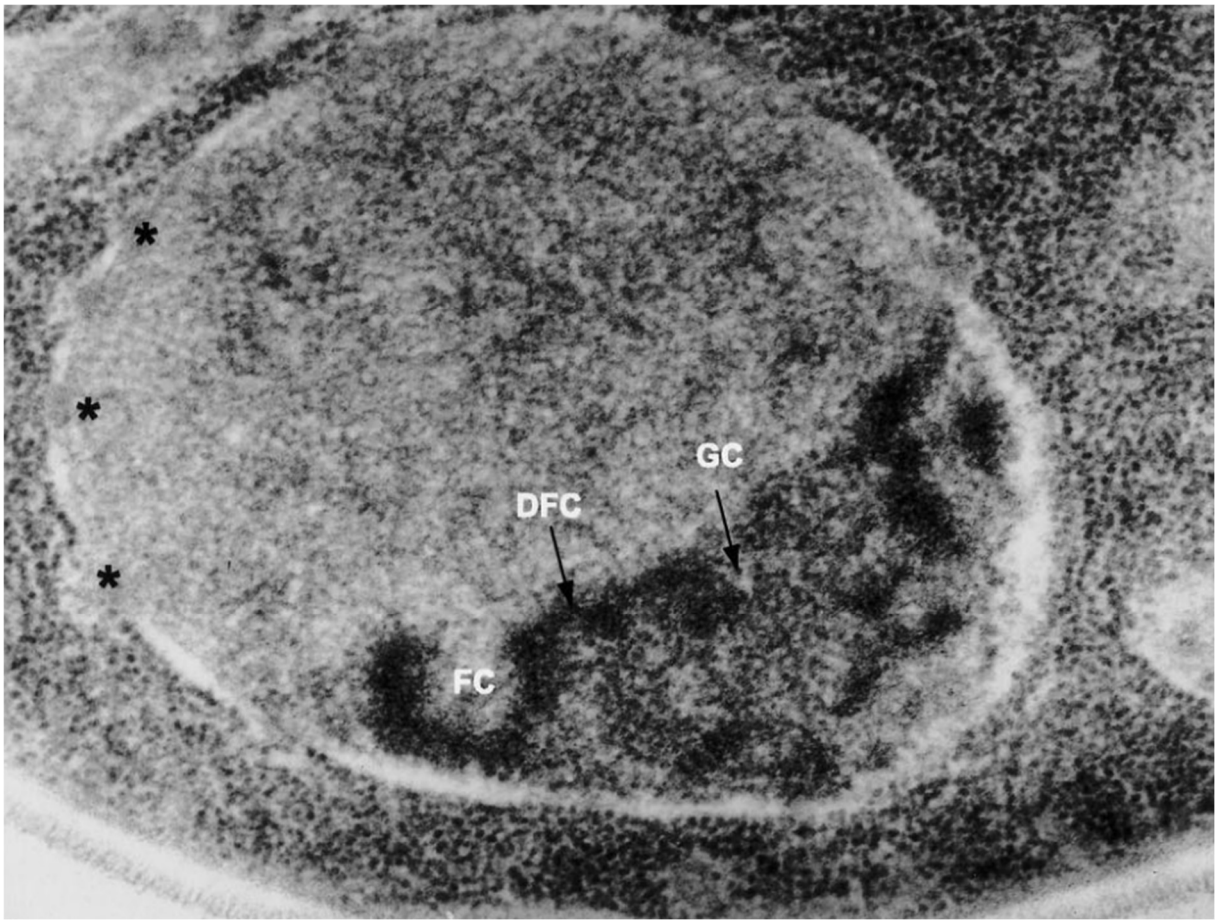

Figure 1: Morphology of Saccharomyces cerevisiae cells after cryo-fixation and freeze-substitution. The nucleus is seen to be outlined by a double envelope with pores (asterisks). In the nucleolus, three distinct morphological compartments are identified: electron-lucid zones resembling fibrillar centers (FC) are detected near the nuclear envelope. These electron-lucid zones are surrounded by a dense fibrillar component (DFC) that extends as a network throughout the nucleolar volume. A granular component (GC) is dispersed throughout the rest of the nucleolus, from (Léger-Silvestre et al. 1999).

In mammals the rRNA genes are found on the short arms of acrocentric chromosomes and can form multiple nucleoli. Nucleolar organization regions (NORs) were already observed in early microscopic studies (McClintock 1934). Size and morphology can vary in response to cellular stress. Further, the 5S rRNA gene is separated from the nucleolar rRNA genes (Moss et al. 2007; McStay 2016). In haploid yeast nuclei, only one nucleolus is found. It harbors 100-300 copies of rRNA genes. These rDNA transcription units make up about 10% of the yeast genome and are clustered on chromosome XII in a head to tail orientation. A schematic representation of the yeast rDNA locus is shown in *Figure 2* A.

An rDNA unit is composed of the 35S rRNA gene, which is transcribed by Pol I, and an intergenic spacer (IGS, or NTS for non-transcribed spacer). The IGS contains the 5S rRNA gene, which is transcribed by Pol III and is oriented in the opposite direction. (Warner 1999; Petes 1979; Srivastava and Schlessinger 1991). A bi-directional Pol II promoter (expansion-promoter, E-pro) is also located in the ITS. E-pro is

responsible for recombination-based amplification of rDNA (Kobayashi et al. 2001; Kobayashi 2011). Transcription from this promoter is normally repressed by Sir2. When the rDNA copy number is reduced, Sir2 repression is removed and the amplification is induced (Kobayashi and Ganley 2005; Iida and Kobayashi 2019b).

Due to the enormous amount of Pol I transcription, actively transcribed rRNA genes can be visualized using a spreading method (Miller and Beatty 1969). Transcribed 35S rDNA genes form 'Christmas-tree' like structures (*Figure 2* ,B). The gene body is packed with transcribing polymerase molecules and forms the stem, nascent RNA with increasing length form the branches. In terminal knobs, early assembly intermediates of nascent ribosomes can be detected. In fast growing cells only half of the rDNA copies are transcribed and over one hundred Pol I molecules can associate with a single rDNA gene. (French et al. 2003; Schneider et al. 2007; Neyer et al. 2016; Dammann et al. 1993).

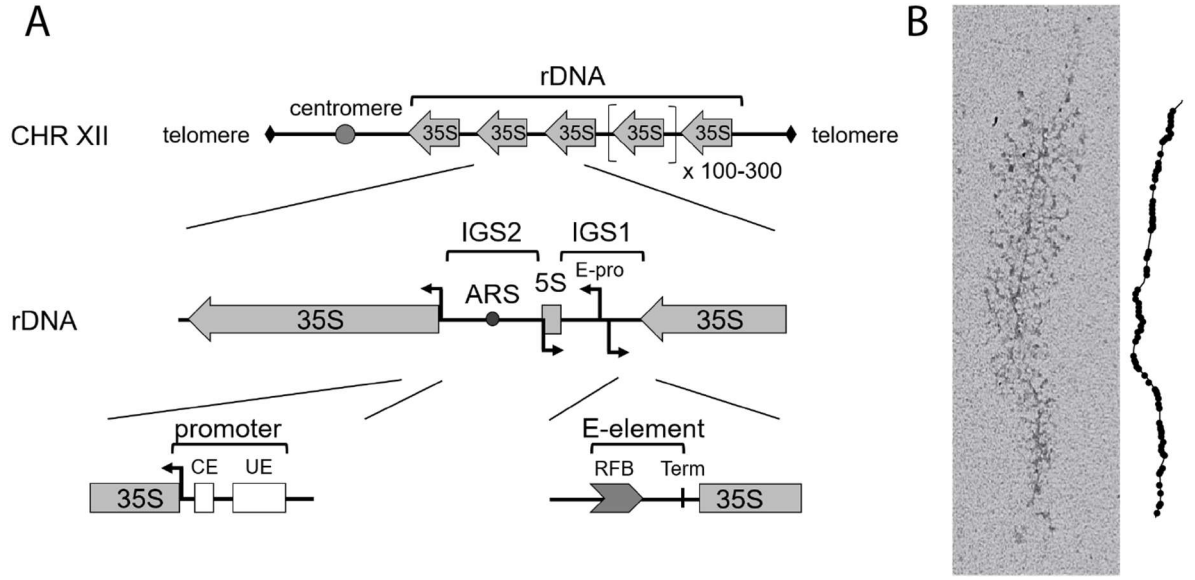

Figure 2: Overview of the rDNA locus

A) Schematic representation of the yeast rDNA locus. Chromosome XII harbors ~100-300 repeats of rDNA units. Enlargement of one rDNA unit, consisting of Pol I transcribed 35S rRNA, bi-directional Pol II promoter (E-pro) Pol III transcribed 5S rRNA gene, an autonomous replication sequence (ARS) and intergenic sequences 1 and 2 (IGS1,2). 35S rRNA gene promoter and the IGS1 region are shown in detail: The promoter consists of the upstream element (UE) and the core element (CE). Enhancer element (E-element) containing replication fork barrier RFB and terminator element, (adapted from (Hannig et al. 2019)) B) left: Electron micrograph 'miller spread' of a yeast rRNA gene transcribed by Pol I, right: over 90 Pol I molecules can be located on the gene body, schematic representation of Pol I distribution (from (Darrière et al. 2019)).

1.2.2. Chromatin composition and states at the rDNA locus

In the nucleus, chromatin is the template for all DNA-dependent processes as replication, recombination or transcription (Kornberg 1974; Kornberg and Stryer 1988). The DNA-genome is wrapped around histone octamers, forming nucleosomes (Arents et al. 1991; Arents and Moudrianakis 1993). This unit competes for DNA access with transcription machineries or other chromatin components (Kornberg and Lorch 2020). Chromatin is dynamically associated with and modified by

diverse nuclear complexes including RNA-processing machineries, architectural components, chromatin remodeling enzymes and transcription factors. Interaction of many factors with the rDNA loci have been described and were identified in proteomic studies (Hamperl et al. 2014). Genomic loci adopt specific functional states to regulate gene expression. The yeast rDNA genes are found in at least two different states, an 'open' actively transcribed conformation and a nucleosomal 'closed' state. The HMG-box protein Hmo1 associates with actively transcribed rRNA genes and was suggested to maintain the open chromatin state (Conconi et al. 1989; Merz et al. 2008; Wittner et al. 2011; Goetze et al. 2010; Gadal et al. 2002). In mammals, maintenance of an open chromatin state might be functionally conserved in the HMG-box containing factor UBF, in addition to the role of UBF on pre-initiation complex (PIC) formation. Actively transcribed rRNA genes are largely devoid of nucleosomes (Albert et al. 2013; Herdman et al. 2017; Merz et al. 2008).

Net1 and the RENT complex

Net1 interacts with Cdc14 and Sir2 to form the RENT 'regulator of nucleolar silencing and telophase' complex. Net1 and the RENT complex link important cellular processes and functions, from genome stability to Pol I transcription and to regulation of the cell cycle. The role of Net1 and Cdc14 in cell cycle regulation has been studied in detail. Net1 inhibits and sequesters Cdc14 phosphatase to the nucleolus throughout the cell cycle, distinct phosphorylation of Net1 in late anaphase release Cdc14 from the nucleolus, the delocalized phosphatase can act on its nuclear and/or cytoplasmic substrates and enable completion of anaphase and progression to G1 phase (Visintin et al. 1999; Shou et al. 1999; Azzam et al. 2004). Net1 and Sir2 associate with two regions on the rDNA, the rDNA promoter and the replication fork barrier (RFB) at the 3'end of the rRNA gene (Huang and Moazed 2003). At the RFB, Fob1 mediates recruitment of Sir2 by Net1, whereas at the rDNA promoter UAF is required to recruit Net1 (Huang and Moazed 2003; Bairwa et al. 2010; Goetze et al. 2010). Sir2 is important for genome stability and for maintenance of rDNA copy-number. Sir2 represses recombination-based amplification of rDNA in response to rDNA copy number (Kobayashi and Ganley 2005; Kobayashi 2011; Iida and Kobayashi 2019b). Furthermore, components of the RENT complex can directly affect Pol I transcription. Cdc14 phosphatase might inhibit Pol I transcription during the cell-cycle. (Clemente-Blanco et al. 2009). and Net1 was found to be important for Pol I transcription initiation. Genetic and physical interactions of Net1 and Pol I have been shown *in vivo* and *in vitro* (Straight et al. 1999; Shou et al. 2001; Goetze et al. 2010; Hannig et al. 2019).

1.3. RNA polymerases

The genetic information stored in DNA needs to be transcribed into RNA. For this process, a distinct class of enzymes evolved, DNA-dependent RNA polymerases (Pols). DNA-dependent RNA polymerases catalyze the synthesis of RNA from a DNA template. Over 50 years ago, three distinct forms of RNA-polymerases were identified in eukaryotic cells (Roeder and Rutter 1969, 1970). The order of elution

from an anion exchange column implicated the nomenclature, RNA Polymerase I, II and III (or A, B and C). In plants, two more forms of RNA-polymerases exist, Pol IV and Pol V, these enzymes are closer related to Pol II and function in gene silencing (Pikaard 2006; Douet et al. 2009; Haag and Pikaard 2011; Herr et al. 2005). These Pols were later found to transcribe different classes of genes. Pol I synthesizes the polycistronic precursor of three of the four ribosomal RNAs (Reeder and Roeder 1972; Nogi et al. 1991b). Pol II produces mRNA and several small non-coding RNAs and Pol III transcribes genes of small structured RNAs, like the transfer RNA (tRNA) or 5S rRNA.

Pol I, Pol II and Pol III vary in their sensitivity to α-amanitin, a toxic cyclic peptide found in the death cab mushroom *Amanita phalloides*. Pol I is almost insensitive to the drug, Pol III can resist higher concentrations while Pol II in inhibited under low concentrations. (Lindell et al. 1970; Wieland 1968). The toxin binds to a pocket at the active site of Pol II and inhibits RNA chain elongation by trapping the trigger loop, a mobile element important for catalysis and translocation. (Bushnell et al. 2002; Liu et al. 2018; Brueckner and Cramer 2008). In Pol I this binding pocket is not conserved, additionally the location can be occupied by the C-term of Pol I subunit A12.2 (Engel et al. 2013).

RNA Polymerase architecture

Multi-subunit Pols share a common architecture. In eukaryotes, the two largest subunits form the core of the enzyme. The large subunits are homologous A190 and A135, Rpb1 and Rpb2, and C160 and C128 in Pol I, Pol II and Pol III, respectively and harbor the active site (Cramer 2002). Five subunits Rpb5, Rpb6, Rpb8, Rpb10 and Rpb12 are shared between the Pols. Together with AC40/AC19 shared between Pol I and Pol III, or Rpb3/Rpb11 counterpart in Pol II, these subunits form the core-polymerase. Other peripheral subunits associate with this core enzyme. The stalk subunits A43/A14 in Pol I and its homologs Rpb4/Rpb7 in Pol II and C17/C25 in Pol III protrude from the polymerase core. In addition to the 12 shared or homologous subunits, Pol I and Pol III have additional subunits, A49/A34.5 or C37/C53, respectively. Additionally, Pol III contains a specific heterotrimer C82/C34/C31. (Cramer et al. 2008; Vannini and Cramer 2012; Cramer 2019; Lalo et al. 1993; Klinger et al. 1996; Kuhn et al. 2007; Geiger et al. 2010; Geiger et al. 2008; Fernández-Tornero et al. 2007; Hoffmann et al. 2015; Ramsay et al. 2020).

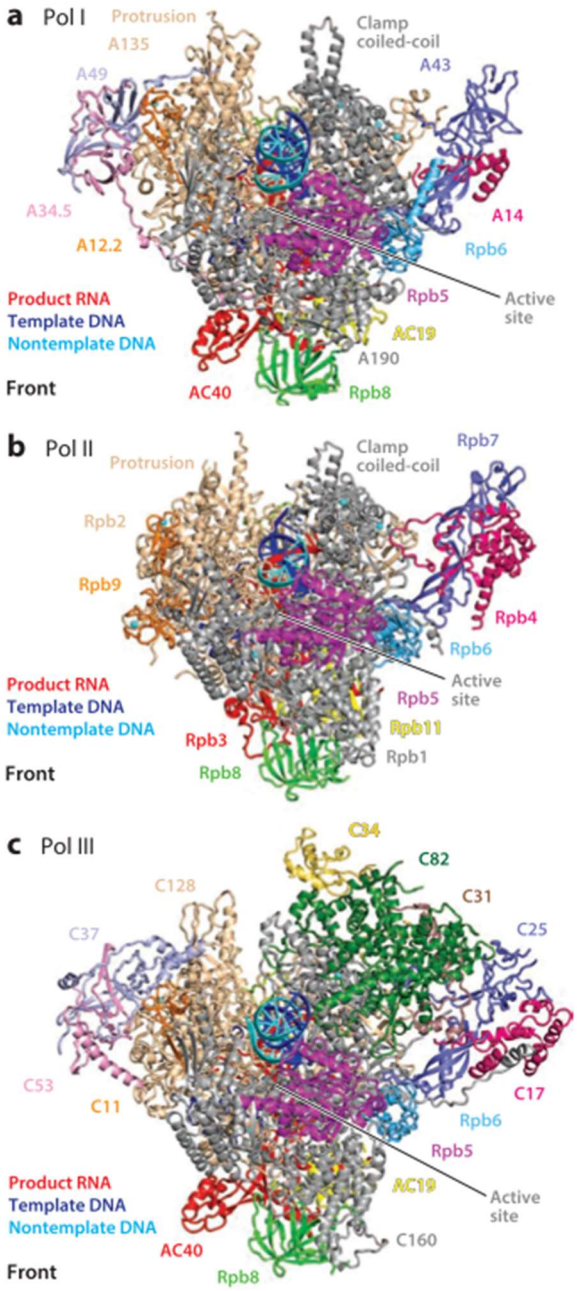

Figure 3: Conservation of RNA polymerase subunits
Historically, nomenclature of Pol II subunits is given as Rpb1-12; Pol I and Pol III, are termed by letters A for Pol I and C for Pol III, followed by their apparent molecular mass (e.g. A190 for largest Pol I subunit). Elongation complexes of a) Pol I, b) Pol II and c) Pol III are shown. Subunit counterparts are shown in same colors. Figure from (Engel et al. 2018), details see text.

Pol I specific subunits resemble built-in transcription factors

Built-in transcription factors of Pol I may contribute to the adaptation of the enzyme to its task of transcribing only one specific gene at very high rates. Subunits A49/34.5 are related to Pol II transcription factor TFIIF (Geiger et al. 2010; Kuhn et al. 2007). The A49/34.5 heterodimer consists of three functional parts. The N-terminal part of A49 (amino-acids 1-110) associates with the A34.5 subunit and forms the dimerization module, related to TFIIF, a linker domain (111-185) and a C-

terminal tandem winged helix (186-415) (Geiger et al. 2010). A34.5 depends on the N-terminal part of A49 to bind to Pol I, while its deletion causes no severe growth defects (Gadal et al. 1997). In vitro analyses suggested a role for the C-terminal tandem winged helix (tWH) domain of A49 in DNA binding and Pol I processivity/elongation whereas the dimerization module A49/34.5 stimulated RNA cleavage (Geiger et al. 2010), whereas the linker and tWH domain (A49-C) are important for Pol I transcription initiation *in vivo* (Beckouet et al. 2008). A49-C is highly flexible but can be located over the Pol I cleft (Bischler et al. 2002; Jennebach et al. 2012). Recent cryo-EM structures revealed distinct position of A49-tWH in Pol I in context of initially transcribing complexes (ITC), open complexes (OC) and elongating complexes (EC). Further, parts of the A49-linker can stabilizes the transcription bubble (Tafur et al. 2016; Han et al. 2017; Sadian et al. 2019). The position of A49-tWH in the EC, in contrast to the ITC, is not compatible with Rrn3 binding. Repositioning of this domain could trigger Rrn3 release (Sadian et al. 2019), A49 mediated release of Rrn3 during the transition from initiation to processive elongation would agree with increased Rrn3 levels in gene-bodies in ChIP experiments when A49 was depleted (Beckouet et al. 2008). Subunits A49/34.5 are not essential, but growth is strongly impaired in these mutants. Interestingly, yeast cells can overcome these growth defects by the generation of suppressor mutants in Pol I subunits that affect the intrinsic flexibility of the enzyme (Darrière et al. 2019).

A stalled Pol I enzyme could result in the pile-up of following Pols and, thus, halt the transcription of an entire rDNA repeat, which can be loaded with up to hundred Pol I molecules (Hontz et al. 2008; Albert et al. 2011). Pol I has high intrinsic RNA cleavage activity, which can help to overcome Pol I stalling due to backtracking or nucleotide misincorporation. Subunit A12.2 contains a TFIIS-related domain at its C-terminus, while the N-terminal part is related to Rpb9, which anchors the subunit at the Pol I lobe. This direct attachment helps to efficiently recover backtracked Pol I or stalled complexes induced by UV damage (van Mullem et al. 2002; Lisica et al. 2016; Sanz-Murillo et al. 2018). A12.2 might destabilize Pol I elongation complexes and support transcription termination (Prescott et al. 2004; Appling et al. 2018). Interestingly, the C-terminal part of A12.2 can adopt different positions within Pol I. In inactive dimers it can be located near the active site, whereas it is excluded in elongation complexes and flexible. (Engel et al. 2013; Pilsl et al. 2016a; Neyer et al. 2016; Tafur et al. 2016). Besides, the C-terminal part of A12.2 could occupy a position at the Pol I lobe, displacing the A49/34.5 heterodimer (Tafur et al. 2019). Further, A49/34.5 and A12.2 can facilitate Pol I passage through nucleosomal templates (Merkl et al. 2020).

1.4. The transcription cycle

Transcription of DNA templates by RNA polymerases can be subdivided in three phases. In order to start transcription, RNA polymerases have to recognize a DNA sequence at the beginning of the gene to be transcribed. At this promoter region, the enzyme displaces the two strands of the DNA duplex

and starts synthesis of RNA (initiation). The enzyme then extends the nascent RNA chain, matching the DNA template strands (elongation). Finally, Pol stops elongation and dissociates from the template DNA and the synthesized RNA (termination), becoming available for the next round of transcription (reviewed in (Cramer 2019)).

Following initiation, RNA polymerases adapts an actively elongating conformation and starts with processive RNA synthesis. Therefore, the DNA cleft contracts to tightly bind downstream DNA and the DNA-RNA hybrid (Tafur et al. 2016; Neyer et al. 2016). The catalytic mechanism of RNA chain elongation is similar to Pol II (Scull et al. 2019). Elongating Pol I can be influenced by additional elongation factors as Spt4/5, the Paf1-complex or Spt6. These factors can act independently or co-operate and might help to ensure high processivity of Pol I. (Anderson et al. 2011; Engel et al.; Schneider 2012; Viktorovskaya et al. 2011; Viktorovskaya and Schneider 2015; Zhang et al. 2009; Zhang et al. 2010; Ucuncuoglu et al. 2016).

Several sequence elements and factors were described to be involved in transcription termination. Different molecular mechanisms for this process were suggested. Secondary structure elements in the nascent RNA chain can cause pausing and destabilization of ternary complexes without additional factors (Nielsen et al. 2013; Peters et al. 2011). A 'torpedo'-model is based on rapid 5'-3' exo-nucleolytic cleavage, after an endo-nucleolytic cut. Higher processivity of exonuclease will lead to collision with elongating polymerases and resulting clashes facilitate dissociation of the enzyme from DNA (Tollervey 2004). Pol I transcripts are processed at its 3'-ends but also cis elements and factors required for efficient termination were identified. The yeast Pol I terminator region contains a T-rich sequence followed by a 'Reb1' binding site. It was reported, that Reb1 or mammalian TTF1 can terminate Pol I transcription *in vitro* (Lang and Reeder 1993; Mason et al. 1997), however in growing yeast cells Nsi1 occupies the terminator-Reb1 binding site and helps to terminate Pol I transcription. (Reiter et al. 2012; Merkl et al. 2014; Németh et al. 2013).

1.5. The RNA Polymerase I transcription initiation machinery

1.5.1. The rDNA promoter and its transcription factors

Mainly two experimental approaches identified and defined the yeast Pol I promoter and the Pol I transcription factors. First, the Pol I cis-acting elements were identified with a linker scanning mutagenesis approach (LSM). A centromeric plasmid bearing a shortened rDNA gene and a reporter sequence to monitor rRNA synthesis was used, to compare mutated versions of the Pol I promoter (Musters et al. 1989). A follow up study complemented this *in vivo* study with data of a Pol I dependent *in vitro* transcription system, using fractionated crude cell extracts (Kulkens et al. 1991) and tried to clearer define the DNA regions important for Pol I transcription initiation (Choe et al. 1992). These studies revealed a core promoter element/core element (CE) from position -38 to +8 relative to the transcription start site (TSS), which is sufficient for low level transcription. Further, a stimulatory

upstream element (UE) that stretches up to nucleotide -155. A mutational hot-spot was identified at -89 to -42 as well as the observation that the spacing between the UE and CE elements is important (Kulkens et al. 1991; Choe et al. 1992; Musters et al. 1989). Interestingly, the Pol I promoter shows a remarkable low degree of conservation throughout eukaryotes. It was suggested that intrinsic sequence features like bendability and meltability of the promoters are more important, than the defined nucleotide sequence (Engel et al. 2017; Engel et al. 2018). Most of the Pol I transcription factors were identified in an elegant genetic screen. The 35S rDNA gene could be transcribed from a galactose inducible promoter by Pol II. After mutagenesis, defects of Pol I factors are compensated in galactose-containing medium, but not in glucose-containing medium where Pol II transcription from galactose promoters is inhibited. This approach revealed that synthesis of the 35S rRNA precursor is the only essential function of Pol I in yeast (Nogi et al. 1991a; Nogi et al. 1991b). Further, genes with essential functions in the Pol I transcription process were identified. Beside essential Pol I subunits, several transcription factors were found – the RRN (rRNA deficient) genes (Nogi et al. 1991a). In the following four essential general transcription factors for Pol I were identified, the TATA binding protein (TBP), Rrn3 (Yamamoto et al. 1996) and two multi-protein complexes termed core factor (CF) (Keys et al. 1994; Lalo et al. 1996; Lin et al. 1996) and upstream activating factor (UAF) (Keys et al. 1996; Steffan et al. 1996; Keener et al. 1997). Together with Pol I, these factors form a preinitiation complex (PIC) and will be described in detail in the following sections.

1.5.2. Rrn3

Besides TBP which is utilized by all three nuclear RNA polymerases, Rrn3 is the Pol I transcription factor with the highest degree of conservation from yeast to human (Moorefield et al. 2000). Yeast Rrn3 interacts with Pol I independently of DNA (Yamamoto et al. 1996). In yeast cells, only a subpopulation of Pol I is able to initiate at the Pol I promoter, this initiation competent Pol I population is associated with Rrn3 (Milkereit and Tschochner 1998). Rrn3 interacts with Pol I subunit A43 and forms an initiation active complex (Peyroche et al. 2000; Blattner 2011). Biochemical studies suggested that Rrn3 interacts also with the CF subunit Rrn6 which could stabilize the preinitiation complex (Peyroche et al. 2000), but this could not be confirmed in high resolution structures of the pre-initiation complex (Pilsl et al. 2016a; Engel et al. 2016; Fernández-Tornero 2018). However, interaction of the acidic loop of Rrn3 with the Zn-ribbon domain of Rrn7 was observed, that could support recruitment of Pol I to the promoter (Sadian et al. 2019). Under certain conditions, Rrn3 might bind promoter DNA on its own, thereby supporting recruitment of Pol I (Stepanchick et al. 2013). Early after transcription initiation, Rrn3 dissociates from the polymerase (Bier et al. 2004; Herdman et al. 2017), and Pol I subunit A49 becomes important for disassembly (Beckouet et al. 2008; Sadian et al. 2019). However, complete dissociation of Rrn3 from the elongating Pol I seems not to be crucial for the transcribing enzyme, since yeast cells expressing a A43-Rrn3 fusion protein are viable (Laferté et al. 2006). Complex formation of

Pol I with Rrn3 was identified as a regulated key step in yeast and mammalian Pol I transcription initiation. Formation of the complex is regulated by the TOR (target of rapamycin) pathway and post-translational modifications play a role in complex formation (Powers and Walter 1999; Mayer et al. 2004; Mayer et al. 2005; Cavanaugh et al. 2002; Hirschler-Laszkiewicz et al. 2003). Inhibition of TOR-signaling with rapamycin leads to a decrease of Pol I/Rrn3 complex and consequently lower Pol I occupancy at the promoter which resembles the situation of cells in stationary phase (Claypool et al. 2004; Philippi et al. 2010). The overall phosphorylation pattern of bulk Pol I differs from its Rrn3 bound form and phosphorylation of Pol I is a prerequisite for transcription initiation (Fath et al. 2001; Fath et al. 2004). Furthermore, a conserved patch of Rrn3 in the interaction interface to Pol I subunit A43 was found, and phosphor-mimicking in this area reduced binding to Pol I (Blattner et al. 2011). Cryo-EM studies show how Pol I monomers can be bound by the initiation factor Rrn3 (Pilsl et al. 2016a; Engel et al. 2016; Torreira et al. 2017). This prevents the formation of transcriptionally inactive yeast Pol I dimers, which could be visualized with negative staining (Milkereit et al. 1997) and observed in protein crystals (Engel et al. 2013; Fernández-Tornero et al. 2013) or cryo-EM studies (Pilsl et al. 2016a). The physiological relevance of auto-inhibited Pol I dimers was under debate, until recently an elegant live cell imaging approach could prove the existence of Pol I dimers under certain physiological conditions in vivo. The authors suggested that the dimers represent a hibernating Pol I storage form under starvation conditions. (Torreira et al. 2017; Fernández-Tornero 2018). Interestingly, Pol I dimerization was also observed in Schizosaccharomyces pombe. There, Pol I uses different domains and interfaces for dimerization which suggest conservation of this regulatory mechanism (Heiss et al. 2021). We want to understand the requirements of Pol I/Rrn3 complex formation, how this complex formation is regulated and how the complex contributes to formation of the Pol I PIC.

1.5.3. TBP

For targeting their promoters and to facilitate transcription initiation, eukaryotic and archaeal RNA polymerases require specific sets of transcription factor complexes. The TATA-binding protein – TBP - is the only factor shared between these transcriptions systems (recently reviewed in (Kramm et al. 2019)). TBP is required by all three Pols in yeast cells (Cormack and Struhl 1992). TBP preferentially associates with AT rich sequences and was found at almost all transcribed genes in yeast cells (Rhee and Pugh 2012). Two pairs of conserved phenylalanine residues interact with the minor groove of a TATA element and introduce a ~90° kink at canonical TATA-sequences (Kim et al. 1993a; Kim et al. 1993b). TBP alone or in complex is essential for Pol II and Pol III initiation. Interestingly, this is not the case for the yeast Pol I initiation system, here Pol I in complex with Rrn3 and CF are sufficient for low levels initiation. TBP requires binding of UAF to the promoter to stimulate this basal activity. (Steffan et al. 1996; Keener et al. 1998; Siddiqi et al. 2001a). A contradictory report by Aprikian and co-workers, observed stimulation of TBP on this minimal system (Aprikian et al. 2000) and to less extent *in vitro*

(Bedwell et al. 2012). TBP is required for UAF dependent recruitment of CF to the rDNA promoter (Steffan et al. 1996). TBP interacts with UAF subunit Rrn9 and CF subunit Rrn6 *in vitro,* which might be important for CF recruitment (Steffan et al. 1998). For Pol I the molecular mechanism how TBP enhances transcription initiation is not very well understood and might diverge from Pol II and Pol III transcriptions systems (Kramm et al. 2019). Insertions in the cyclin domains of Rrn7 would prevent TBP-DNA contacts observed in TFIIB and Brf1 complexes (Engel et al. 2017). Fittingly, Pol I specific interactions of TBP are presumably mediated with the N-terminal TBP lobe rather than the C-terminal repeat, that has conserved interfaces with Pol II and Pol III factors (Ravarani et al. 2020). Photo-crosslinking experiments, in *Acanthamoeba castellanii*, suggest that TBP might not contact promoter DNA with its saddle domain. This could imply a divergent mechanism for TBP in Pol I initiation, than in the Pol II and Pol III complexes (Radebaugh et al. 1994; Gong et al. 1995; Bric et al. 2004). Further, in yeast TBP mutations were described that specifically affect Pol I, Pol II or Pol III promoters (Schultz et al. 1992; Kim and Roeder 1994). The role of TBP in Pol I transcription is not fully understood. It is not completely clear if its activity depends on UAF, how TBP is recruited to the promoter and how it stabilizes CF and helps to recruit Pol I.

1.5.4. CF

CF consist of three subunits Rrn6, Rrn7 and Rrn11 (Keys et al. 1994; Lalo et al. 1996; Lin et al. 1996). CF recognizes a part of the CE at the promoter, together with TBP and UAF CF forms a promoter-bound platform to which a complex of Pol I with Rrn3 is recruited. (Steffan et al. 1996; Milkereit and Tschochner 1998). CF subunit Rrn7 is related to TFIIB and Brf1 and is conserved in higher eukaryotes (Knutson and Hahn 2011; Naidu et al. 2011). Similarities between Rrn7 and TFIIB/Brf1 lead to models of the Pol I PIC (Blattner et al. 2011; Knutson et al. 2014), which have been challenged by recent structures of Pol PICs (Engel et al. 2017; Han et al. 2017; Sadian et al. 2017). Albeit some sequence motifs were found to be related between Rrn7 and TFIIB and Brf1, interactions with TBP may diverge (Knutson and Hahn 2013; Engel et al. 2017; Ravarani et al. 2020). CF binds a ~12 bp GC rich sequence within the CE and might be sensitive to DNA intercalators (Jackobel et al. 2019). All CF subunits can independently interact with TBP, but Rrn6 showed the strongest interaction (Steffan et al. 1996; Steffan et al. 1998). CF together with Pol I and Rrn3 is sufficient to initiate transcription, even in absence of TBP at a basal level (Keener et al. 1998; Bedwell et al. 2012). A crystal structure of CF elucidated the architecture of the heterotrimeric factor and cryo-EM reconstructions described interfaces with Pol I - Rrn3 and suggested mechanisms for Pol I initiation. Overall architecture of these complexes is similar, although the complexes differ in details. (Engel et al. 2017; Han et al. 2017; Sadian et al. 2019; Sadian et al. 2017). Two models how CF enables Pol I initiation were suggested. First, association of CF-DNA and polymerase might depend on promoter pliability, and only DNA fragments with a certain degree of ‘bendability’ and ‘meltability’ enable contacts between CF, DNA and Pol I

(Engel et al. 2017). Second, a ratcheting motion of CF-DNA upstream of Pol I would feed DNA toward Pol I and support promoter melting, however these complexes exist in conformations that fail to bind Rrn3 (Han et al. 2017). These studies relied on an artificially mismatched DNA scaffold with annealed RNA primer, reflecting post-initiation states referred as 'initially transcribing complexes' ITCs. Early steps of Pol I PIC formation including promoter recognition by CF and DNA melting remain to be studied in detail.

1.5.5. UAF

The upstream activating factor (UAF) consists of six subunits, Rrn5, Rrn9, Rrn10, Uaf30 and the two histone proteins H3 and H4. It targets the UE promoter and commits the Pol I complex to its template. (Keys et al. 1996; Keener et al. 1997). UAF is dispensable for a basal level of transcription *in vitro*, but required for high levels of transcription *in vivo* and *in* vitro (Keener et al. 1998). Together with TBP, UAF recruits CF and stimulates Pol I transcription. Interactions of UAF subunit Rrn9 with TBP were found to be important for transcription stimulation (Steffan et al. 1996; Steffan et al. 1998). In addition to its function on Pol I initiation, UAF helps to establish a specialized chromatin state at the rDNA promoter. Deletion of Rrn5, Rrn9, Rrn10 or Uaf30 causes a so called polymerase switch phenotype, where Pol II starts to transcribe the rRNA gene from its chromosomal locus. (Vu et al. 1999; Oakes et al. 1999; Siddiqi et al. 2001b). Therefore, UAF maintains a chromatin state, that represses Pol II and Pol III transcription (Goetze et al. 2010). UAF is not only found at the rDNA promoter in the nucleolus, but also at the Sir2 gene-locus. There, UAF represses Pol II dependent synthesis of Sir2-mRNA in response to rDNA copy loss number (Iida and Kobayashi 2019b, 2019a). Together with the repression of Pol II transcription at the rDNA locus, this highlights the important role of UAF in balancing Pol I transcription and maintenance of rDNA copy number. I want to better understand the role of UAF in formation of the Pol I PIC. As the nucleating factor its interplay with TBP is poorly understood. We want to study the molecular mechanisms how UAF recruits and stabilizes TBP, CF and supports Pol I initiation.

1.6. Objectives

In this work I try to address some problems on the fascinating question how 80% of the total cellular RNA can be produced from the rRNA genes and its dedicated Pol I transcription machinery. Contradictory to the massive output of the Pol I transcription machinery, the protein levels of the initiation complexes are relatively low. Only a few hundred copies of UAF, CF and the initiation competent Pol I/Rrn3 are found within a cell (Bier et al. 2004). These amounts, however, are sufficient for efficiently targeting the promoter, melting the DNA and starting processive transcription. This highly efficient initiation system is not completely understood yet, and information about the precise molecular role of the single components of the initiation complex is lacking. To get better insights in this process, Pol I transcription initiation should be reconstituted *in vitro*. First attempts to reconstitute

Pol I transcription in vitro relied on the separation of crude extracts as shown in (Riggs and Nomura 1990; Tschochner 1996; Milkereit and Tschochner 1998). Combinations of such fractions could restore promoter dependent Pol I transcription activity. Fractions which influence transcriptional activity should be further purified, or replaced with pure recombinant factors. An *in vitro* transcription system reconstituted from highly purified proteins should be used to better define functional parts of the Pol I transcription machinery and to elaborate molecular mechanisms that allow its high transcriptional output. Further, Pol I PIC and sub-complexes should be analyzed by electron (cryo) microscopy. For a detailed functional and structural analysis of Pol I PIC components, individual components have to be purified in large quantities and high quality.

In particular, we try to understand how only a subpopulation of Pol I, associates with Rrn3 and is competent for transcription initiation. Furthermore, we want to elucidate the requirements of UAF and TBP binding to the upstream promoter to enhance Pol I transcription initiation. High resolution structures of the complete pre-initiation complex in combination with biochemical assays should help to understand the detailed mechanism how Pol I recognizes its promoter and how it achieves its high transcriptional output remain. It was suggested that UAF, TBP and CF bind the promoter and form a platform to which Rrn3 bound Pol I is recruited. We want to understand the concerted assembly of UAF and TBP and their interaction with CF, Rrn3 and Pol I to form the full Pol I preinitiation complex as well as their role to stimulate Pol I activity.

2. Results

2.1. Purification of Pol I transcription factors TBP, Rrn3 and CF

Previous results suggested, that Pol I promoter dependent transcription depends on Pol I, Rrn3 and CF (Keener et al. 1998) and TBP might stimulate basal initiation (Bedwell et al. 2012). To understand the molecular mechanism allowing Pol I initiation, I first aim to reconstitute Pol I transcription initiation from highly purified recombinant transcription factors. TBP was expressed in *E. coli* and purified to homogeneity (methods 5.7.1). Multi-step purification strategies for Rrn3 and CF were described earlier (Blattner et al. 2011; Bedwell et al. 2012; Knutson et al. 2014; Engel et al. 2017). Protocols were adapted and slightly modified, see methods 5.7.2 for Rrn3 and 5.7.3 for CF. These factors could be purified in milligram amounts. A Coomassie stained SDS-PAGE gel of individual purified factors used for *in vitro* reconstitution confirms homogeneity of protein preparations (see Figure 13).

2.2. Analysis of initiation competent Pol I/Rrn3 complex in comparison to bulk Pol I

2.2.1. Purification of the initiation competent Pol I/Rrn3 complex

In fast growing yeast only about 2% of Pol I molecules are associated with Rrn3 cells and only this subpopulations is able to start transcription at the rDNA promoter (Milkereit and Tschochner 1998). The portion of the initiation competent Pol I/Rrn3 complex can be increased by overexpression of Rrn3, however cell growth is affected under these conditions (Steinbauer 2010). Despite the essential role of Rrn3, the molecular mechanism of Pol I activation and the complex formation is still missing. For a detailed biochemical, structural and functional analysis of this complex, we established a purification protocol for the active Pol I/Rrn3 complex and compared it to bulk Pol I, which is not associated with Rrn3. We overexpressed Rrn3 using a plasmid in which Rrn3 is expressed under the control of a galactose inducible promoter for three hours. At this timepoint increased levels of Pol I/Rrn3 were detected, although no significant growth defects were observable. Pol I and its initiation machinery can be enriched by biochemical fractionation of cell lysates. In these protocols, after pre-fractionation, Pol I is precipitated from cell lysates in low conductivity buffers. After ultra-centrifugation Pol I and factors that allow promoter dependent transcription can be resuspended in high-salt buffers and further analyzed, fractionation scheme see Figure 4 A (Tschochner 1996; Milkereit and Tschochner 1998). In fraction PA600, I quantified an enrichment >350 fold of Pol I in relation to total protein amount in whole cell lysates in my master thesis (Pilsl 2013). Pol I is almost quantitatively precipitated from the dialysate II fraction and can be resuspended in high-salt buffer after ultra-centrifugation see Figure 4 B, details in methods 5.6.1). The protocol not only enriched Pol I, but final fractions were partially depleted by the overexpressed factor Rrn3. Minor amounts of Rrn3 were detected in the flow-through of the DEAE column (fraction not shown), while the major part of Rrn3 was found in the soluble supernatant of the dialyzed sample (T0-SN, Figure 4 B). Immuno- or affinity-purification of Rrn3 from the PA600-fraction yielded almost stoichiometric amounts of co-purified Pol I (Figure 4 C, D). Likely,

only the subpopulation of Rrn3, that was associated with Pol I precipitated in the low conductivity buffer and could be separated from excess of unbound factor. While Rrn3 binds quantitatively to the affinity-matrix only 40% of Pol I was bound (Figure 4B), which agrees with initial observations of Robert Steinbauer (Steinbauer 2010). The portion of Pol I associated with Rrn3 could be increased from 2% to over 30% by overexpression of the factor (Steinbauer 2010). Stringent salt conditions in wash buffer strongly reduced unspecific binding, thereby the complex remained stably associated. This is in line with early biochemical characterization of the salt resistant initiation competent Pol I form (Milkereit and Tschochner 1998). The partially purified complex from talon affinity purification was further purified on a MonoQ anion exchange column and resulted in a homogenous and stoichiometric complex (Figure 4 C).

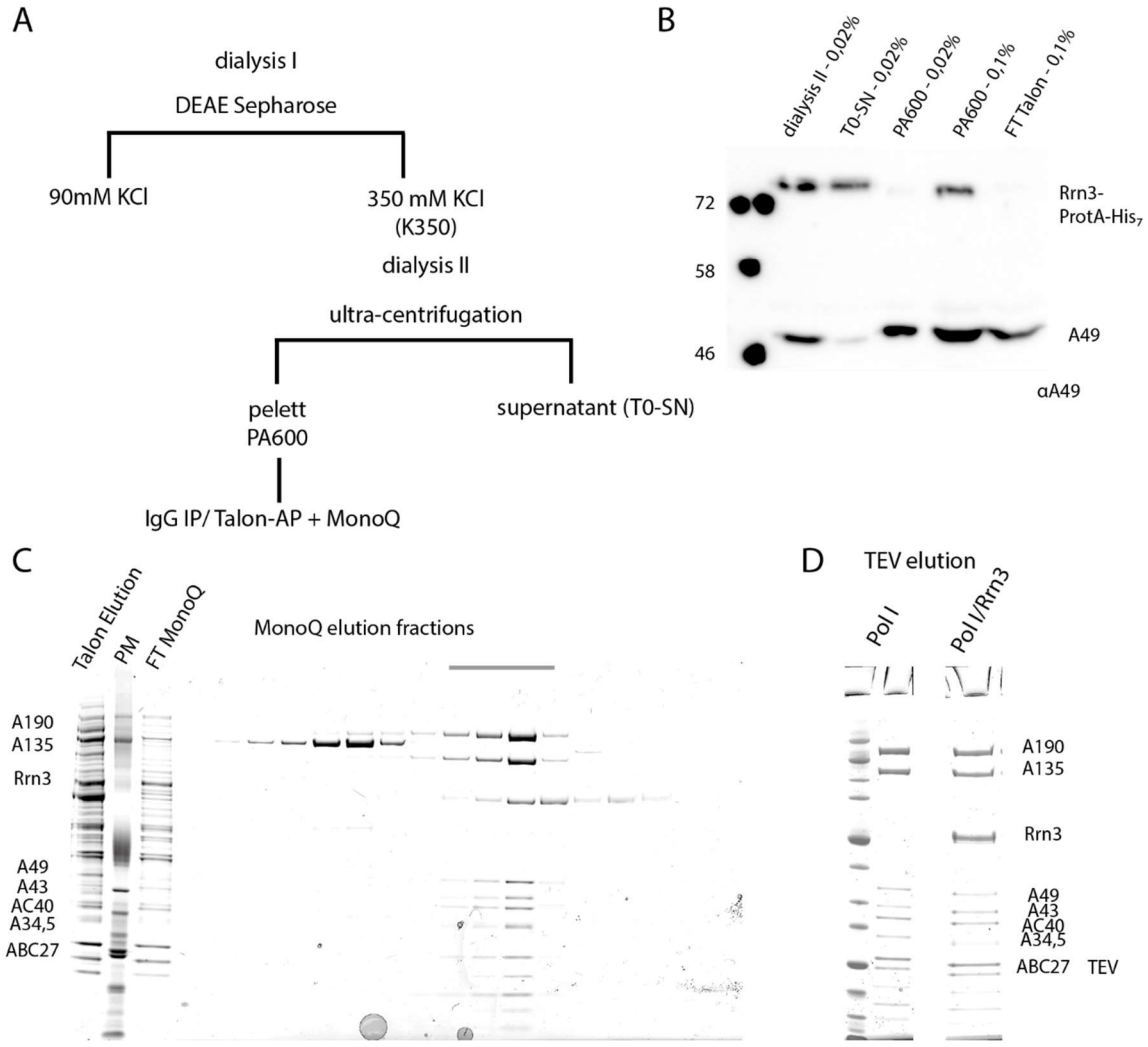

Figure 4: Purification of Pol I/Rrn3.

A) Fractionation scheme of yeast cell lysates B) Western Blot of selected fractions shows enrichment of Pol I and Rrn3. polyclonal anti-body against Pol I subunit A49 (#...) was used to detect Pol I; Rrn3 is immuno-stained by cross-reactivity of rabbit IgG with Protein-A tag, percentage of total fraction volume loaded on Western Blot is given, same amount (0,02%) of the second dialysate, the supernatant after ultracentrifugation (T0-SN) and the resuspended pellet (PA600) were loaded, fivefold amount of PA600 fraction and the FT (0,1%) of the Talon-purification shows quantitative binding of re-solubilized Rrn3 from the PA600 fraction. C) Coomassie stained SDS PAGE gels from Talon

affinity-purification and subsequent MonoQ anion-exchange chromatography shows homogenous and stoichiometric complexes, Pol I and Rrn3 containing peak fractions (grey bar) were pooled for further biochemical analysis. D) Coomassie stained SDS PAGE of Pol I and Pol I/Rrn3 purified via IgG coupled magnetic Beads and TEV elution.

A similarly prepared yeast extract from a different strain served as source to purify a Pol I complex, which was largely devoid of Rrn3, and will be termed 'bulk Pol I'. Yeast cells carrying a TEV cleavable Protein A tag on Pol I subunit A135 were cultivated under same conditions as the Rrn3 overexpression strain and purified from the PA600 fraction (methods 5.6.1). The same strategy was applied for Pol I/Rrn3, which yielded pure and stoichiometric complexes for Pol I and Pol I/Rrn3 (Figure 4 D). We did not observe differences in activity of Pol I purified from the PA600 fraction after carbon source switch, nor found any modifications of the enzyme by mass spectrometry, in comparison to our routine purification protocol directly from cell lysates (methods 5.6.4). Next, we wanted to compare the biochemical activity of our purified Pol I complexes.

2.2.2. Reconstitution of basal transcription initiation *in vitro*

Purified Rrn3, from yeast, or recombinant source in E.coli can be used to reconstitute functional complexes (Yamamoto et al. 1996; Keener et al. 1998; Blattner et al. 2011). Complex formation of Pol I and Rrn3 is not very efficient *in vitro*. Large amounts of Rrn3 protein and long incubations times were required (Keener et al. 1998; Blattner et al. 2011). Bulk Pol I requires large excess of recombinant Rrn3 for efficient initiation *in vitro*. Up to 100 x fold molecular excess stimulated initiation activity in my experimental conditions. Further, pre-incubation times of 2-16 hours are far from physiological conditions, but long incubation times can hint towards a conformational change. A minimal system allowing promoter dependent Pol I transcription contains CF and the initiation competent form of Pol I, which is associated with Rrn3 and a promoter DNA containing at least 38 bp upstream the TSS (Keener et al. 1998). Previous attempts to reconstitute promoter dependent transcription from purified components were not successful in out lab. The newly established protocol to purify the endogenous Pol I/Rrn3 complex allows to reconstitute a minimal Pol I dependent initiation system *in vitro*. Yeast Pol I/Rrn3 together with recombinant CF produced RNA from a promoter-containing DNA template (Figure 5 A, lane 2), Pol I/Rrn3 alone showed no activity. Further, improvements in recombinant expression and purification of Rrn3 enabled us finally to reconstitute Pol I transcription initiation with yeast Pol I and recombinant CF and Rrn3 (Figure 5 B). The recombinant factors alone or in combination did not show activity, but together with Pol I they synthesized RNA from a promoter scaffold.

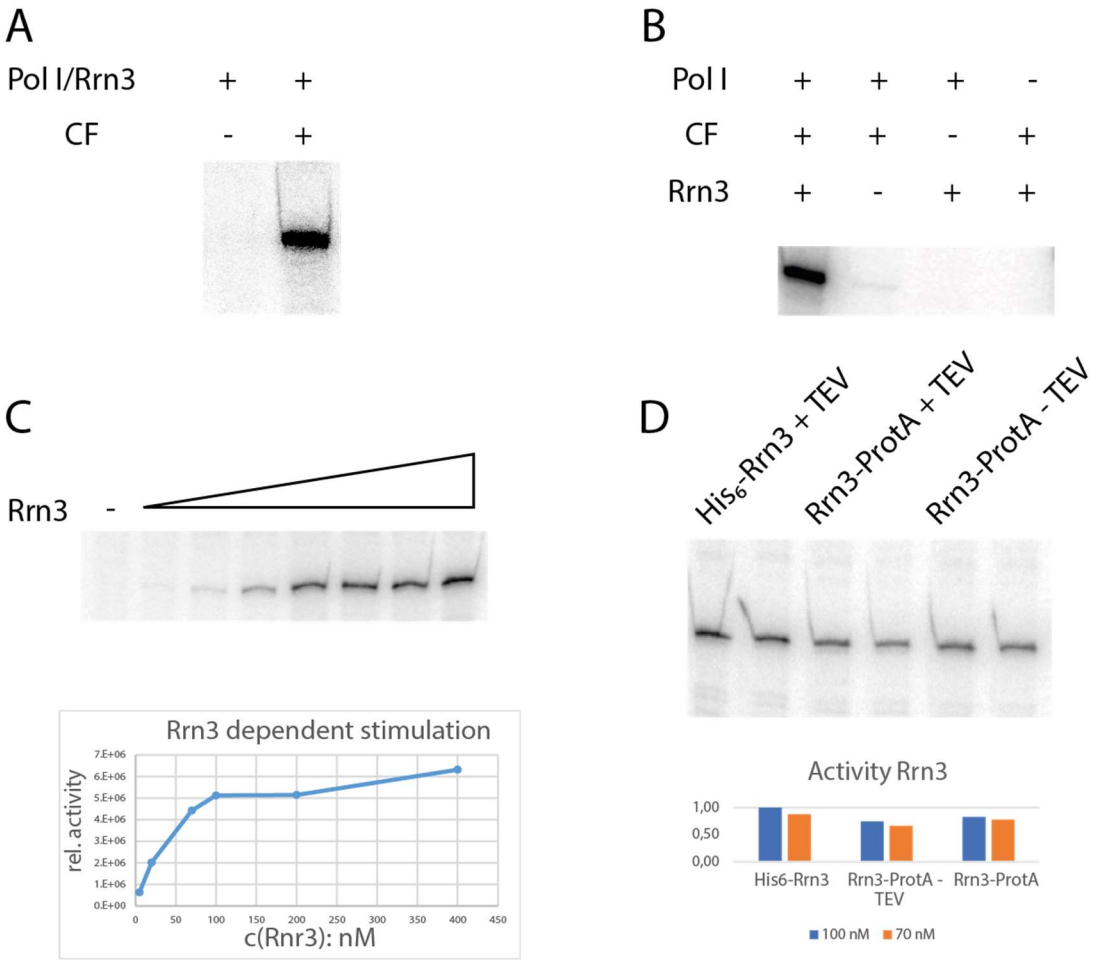

Figure 5: Reconstitution of basal transcription initiation in vitro
Promoter-dependent *in vitro* transcription assay A) Reconstitution of Pol I transcription initiation with purified Pol I/Rrn3 complex. B) Reconstitution of Pol I transcription initiation with purified Pol I and recombinant Rrn3. C) Optimal amount of Rrn3 at a given concentration of Pol I (4 nM) and CF (20 nM) was determined in titration experiment. Upper panel autoradiogram, lower panel transcription activity was plotted against Rrn3 concentration. Initiation activity reaches a plateau around 70-100 nM Rrn3 D) Rrn3 epitope fusions don't strongly affect initiation activity. Two concentrations of Rrn3 (70, 100 nM) with N-terminal His6 Tag, C-terminal Protein A tag, and Protein A tag, which was removed by proteolytic cleavage (TEV) were used in reconstituted *in vitro* transcription assay.

2.2.2.1. Optimization of transcription using recombinant Rrn3

Long preincubation (>18 h) of Pol I and excess (2,5 to 9x fold) of Rrn3 drive complex formation (Keener et al. 1998; Blattner et al. 2011). To find optimal reaction conditions, recombinant Rrn3 was titrated to constant amounts of yeast Pol I (100 fmol/4 nM per reaction) and incubated for three hours on ice. Promoter dependent transcription activity strongly increases up to 70 nM -100 nM end-concentration Rrn3 and reaches a plateau (Figure 5 C). The reactions could be further stimulated with up to 100x fold excess of Rrn3. In all following presented *in vitro* transcription initiation assays 14x fold excess of Rrn3 over Pol I was used. Overnight incubations of Pol I alone or together with Rrn3 did not affect Pol I activity in tailed-template transcriptions (not shown).

Truncations and/or epitopes on the N- and C-termini of Rrn3 can influence its stability in yeast cells (Philippi et al. 2010). Therefore, it was important to exclude that the position of epitope tags impairs the activity of the factor. We expressed Rrn3, with the same epitope Rrn3-TEV-ProtA-His_7 used for the *ex vivo* purification of Pol I/Rrn3 in *E. coli* cells and could purify the recombinant factor as described (see 5.7.2). We compared Rrn3-TEV-ProtA-His_7, Rrn3-TEV-ProtA-His_7 that was TEV-cleaved and His_6-Rrn3 in promoter dependent *in vitro* transcription reactions and observed a similar activity for these constructs (Figure 5, D). Thus, in my *in vitro* experiments, the epitope fusion did not affect Rrn3 function. In further experiments His_6-Rrn3 was used, if not stated otherwise. In initial experiments we observed a higher promoter dependent activity for the yeast Pol I/Rrn3 complex compared to the reconstituted system from Pol I and recombinant Rrn3. Therefore, we carefully characterized the specific activities of the enzyme forms.

2.2.2.2. Ex vivo purified Pol I/Rrn3 is primed for transcription initiation

RNA Polymerases can start transcription from single stranded 3' overhangs. (Kadesch and Chamberlin 1982). This non-specific assay can be used to compare activities of different Pols (Merkl et al. 2014; Merkl et al. 2020). Comparison of the transcriptional activity of the two Pol I-containing fractions showed clear differences. Bulk Pol I is ~ 2,5 times more active than ex vivo purified Pol I/Rrn3, in the non-specific assay (Figure 6 A, B). In contrast, Pol I/Rrn3 is ~3,5 times more active than bulk Pol I in the initiation dependent assay. Normalized to unspecific tail-template transcription activity, *ex vivo* purified Pol I/Rrn3 is up to ten folds more active in promoter-dependent transcription than bulk Pol I (Figure 6 B).

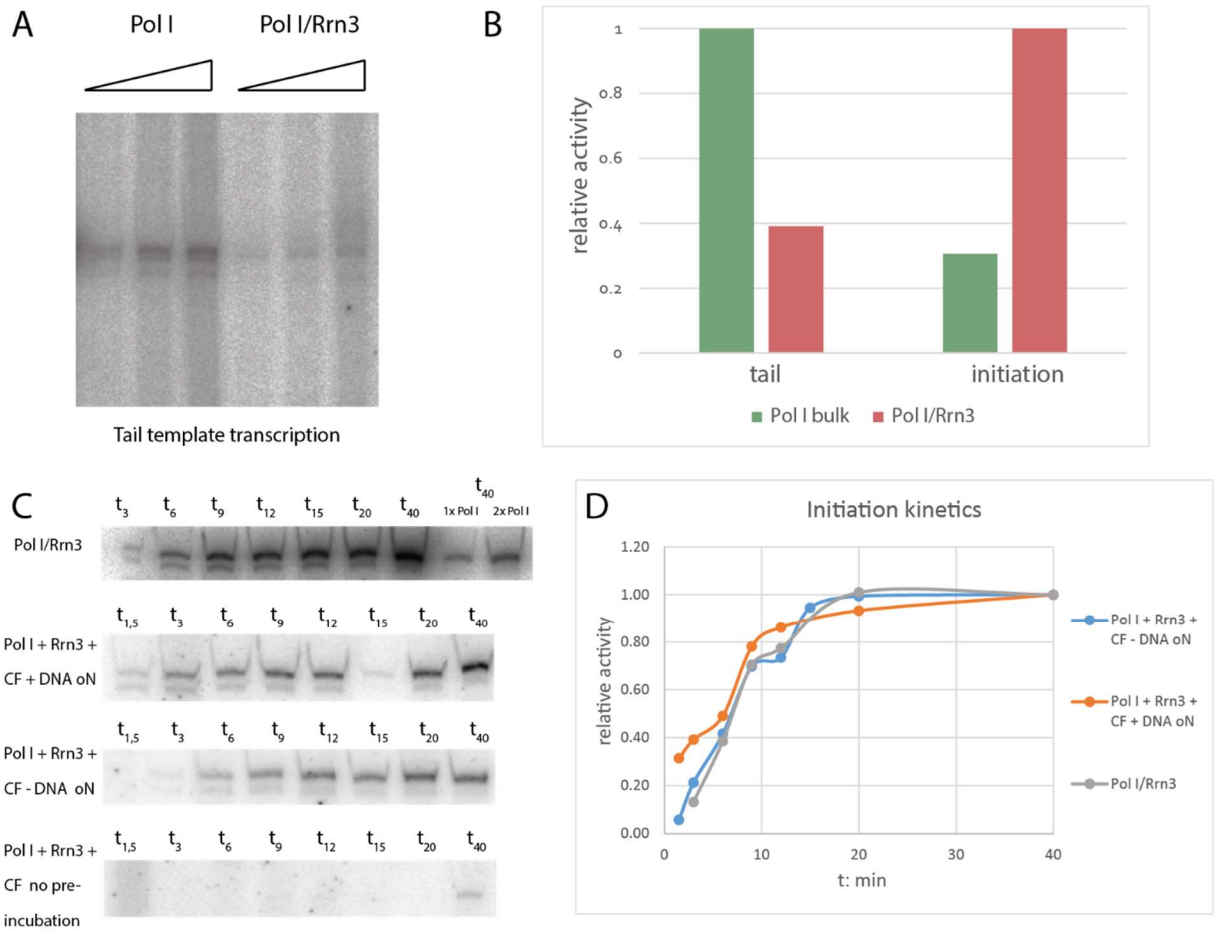

Figure 6: Pol I/Rrn3 shows high specific initiation activity

A) Tail template transcription with increasing amounts (0,125; 0,25; 0,5 pmol) of bulk Pol I or Pol I/Rrn3 B) Representation of specific activities of bulk Pol I and Pol I/Rrn3; Pol I (green) shows higher activity in tail template assay (left) while Pol I/Rrn3 (red) is more active in promoter-dependent assay (right) C) Initiation rates of different pre-incubated complexes are compared. Reaction were started by addition of transcription buffer including NTPs. Pol I/Rrn3 was directly mixed with CF and template DNA (Pol I/Rrn3, grey); Pol I, recombinant Rrn3 and CF were pre-incubated over-night in presence or absence of DNA (PCR +/- DNA, orange/blue). Autoradiograms of reactions are shown; timepoints are indicated over respective lane; endpoint reactions of Pol I preincubated with Rrn3 (lane 8,9 row 1, same and double amounts of Pol I) indicate high specific activity of endogenous Pol I/Rrn3. D) Normalized transcription activity shown in C (normalized to endpoint activity) was blotted against reaction time. Preincubation of components are indicated.

Efficient reconstitution of Pol I and Rrn3 requires long incubation time. The observed discrepancy in activity of endogenous Pol I/Rrn3 and the reconstituted complex could be caused by a delayed reaction kinetic. I used complexes with different pre-incubation conditions and compared initiation reactions in time course experiments. Over-night assembly reactions of Pol I with optimized amounts of Rrn3 (70 nM) and CF (40 nM) in presence or absence of promoter DNA were compared to yeast Pol I/Rrn3. Without pre-incubation, activity of the reconstituted system with recombinant Rrn3 is rather inefficient and strongly delayed (see Figure 6, C row 4). A faint band appeared at the 40 minutes timepoint, which is about 5-10% of endpoint-activity of the pre-incubated complex. Pre-incubation of

Pol I, Rrn3 and CF showed essentially the same reaction kinetic as freshly added Pol I/Rrn3. Pre-incubation together with promoter DNA show increased transcription rates at early timepoints. For all conditions, with the exception of the freshly added factors, maximal RNA synthesis was achieved within ~15 minutes (Figure 6, D).

Thus, Pol I/Rrn3 complex formation can limit Pol I initiation rates *in vitro*, but this can be overcome by preincubation of Pol I with recombinant factors. This facilitates initiation to similar reaction kinetics as the *in vivo* formed Pol I/Rrn3 complex. Recruitment of a minimal PIC to the promoter occurs rather fast and efficient, as preincubation with promoter DNA increases transcription only at early time points (1,5/3 min) but lead to same transcription levels at later timepoints. Remarkably, transcriptional output in these promoter dependent assay of Pol I/Rrn3 were ~3,5x higher compared to Pol I preincubated with Rrn3 at end point reactions Figure 6, B. Summarized, our newly established purification protocol for the initiation competent Pol I/Rrn3 resulted in a homogenous sample with a high specific activity in promoter dependent transcription. This encouraged us to study the complex by electron cryo-microscopy.

2.2.3. Electron cryo microscopy of the Pol I/Rrn3 complex

The association of Rrn3 with Pol I is mediated via interactions of the transcription factor with Pol I subunit A43 (Peyroche et al. 2000). The crystal structure of Rrn3 has been solved. Distance restraints derived from crosslinking-mass-spectrometry data of the bis(sulfosuccinimidyl)suberate (BS3) crosslinked complex (Rrn3 Lysine K558 with A190 K582 and AC40 K329 (Figure 7, D) and mutational analysis suggested the binding location of Rrn3 on the Pol I surface. The proposed model for the position of Rrn3 on Pol I was composed of a Pol I homology model and the Rrn3 crystal structure. (Blattner et al. 2011). Up to then, the validation of this model by a high-resolution structure, which could reveal insights in the molecular mechanism of Pol I activation was missing. We established a protocol to purify the endogenous Pol I/Rrn3 complex, which yielded an almost homogenous complex, that is primed for transcription initiation. We used cryo-EM to study the complex in more detail. Grid-preparation and optimization, data collection and processing on Pol I/Rrn3 and Pol I monomers and dimers was carried out in the group of Patrick Schultz under guidance of Corinne Crucifix at the IGBMC Strasbourg (Pilsl et al. 2016a), details see methods 5.8.5.

We obtained a refined 3D EM-density from these particles with and an overall resolution of 7.5 Å (0,143 FSC criterion) which allowed us to visualize secondary structure elements like alpha helices of Pol I and its transcription factor Rrn3. This enabled us to fit the independently solved x-ray structures of Pol I (Fernández-Tornero et al. 2013; Engel et al. 2013) and Rrn3 (Blattner et al. 2011) into our cryo-EM map.

2.2.3.1. Pol I specific interactions with Rrn3

In our Pol I/Rrn3 structure the elongate Rrn3 molecule interacts through its N-terminus with the A43/A14 ‘stalk’, contacts the ‘dock’ region of subunit A190 and reaches the AC40 and AC19 subunits

with its C-terminal end (Figure 7, A) as suggested by cross-linking and topological information from early EM work (Blattner et al. 2011; Peyroche et al. 2000). While the position of the A14 subunit is not affected when its residues 83–85 interacts with residue 224 of Rrn3, the A43 subunit is reorganized upon interaction. The 'connector' residues 274–316 of A43 are not detected and are probably re-positioned upon Rrn3 binding. A43 connector can interact with the cleft of a neighboring Pol I molecule, leading to dimerization of two Pol I molecules (Engel et al. 2013). Finally, the Rrn3 serine-patch identified as important for Pol I binding (Blattner et al. 2011) is involved in the interface. Modification of serine residues in this patch alter normal cell growth and impair PIC assembly in vivo, as shown in ChIP experiments (Blattner et al. 2011). In mammals, phosphorylation of serine side-chains in this location inhibits Pol I transcription, likely by interfering with mammalian Rrn3/TIF-IA binding (Mayer et al. 2004; Mayer et al. 2005).

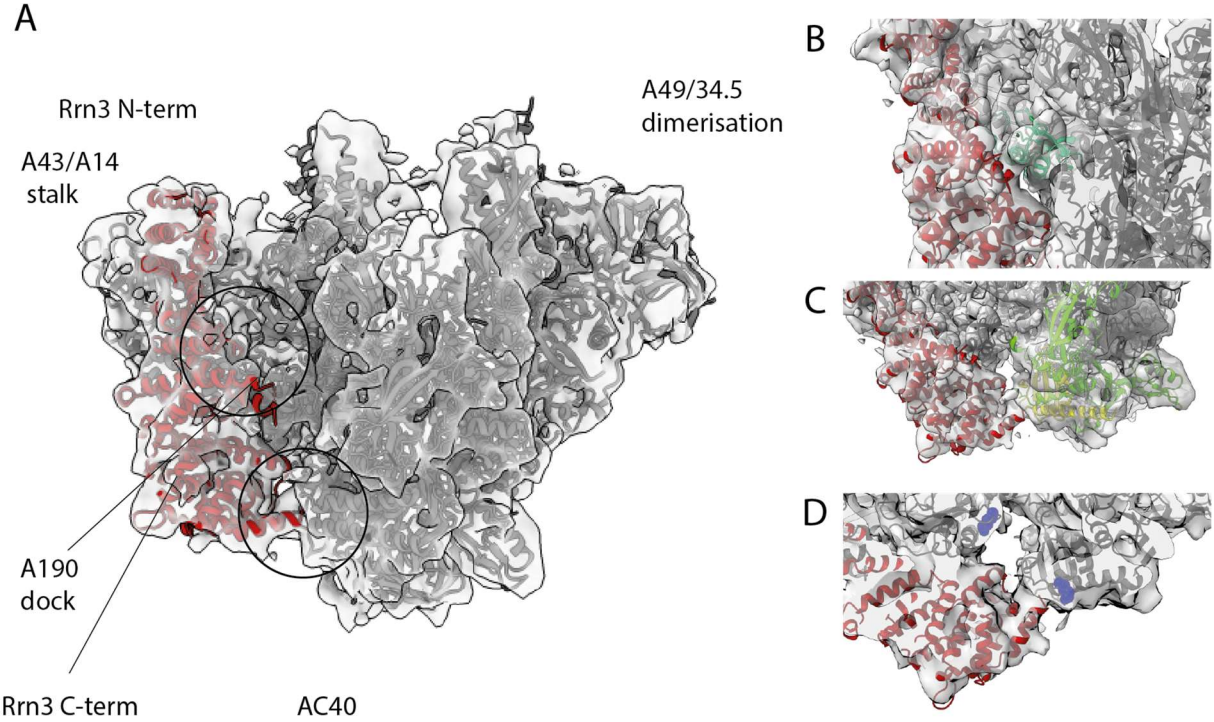

Figure 7: Cryo-EM structure of Pol I/Rrn3
A) Atomic structure of Pol I (black, PDB accession numbers 4C2M) and of Rrn3 (red, 3TJ1) docked into the cryo-EM density of the Pol I/Rrn3 complex (transparent grey envelope). Rrn3 binds along the backside of Pol I and interacts with the A43/14 stalk, Pol I dock domain and contacts AC40/19 with its C-terminus. Regions enlarged in B-C are highlighted. B) Close-up view of the Pol I/Rrn3 complex on the central domain of Rrn3 interacting with the dock domain of the largest Pol I subunit A190 containing the Pol I-specific region α12a (dark green) C) Enlarged view of the Pol I/Rrn3 complex showing interaction of the C-terminus of Rrn3 (red) with AC40 (green) and AC19 (yellow). D) Enlarged view of the Pol I/Rrn3 complex; AC40 lysine 329 and A190-lysine 582, BS3 crosslinked to lysine 558 of Rrn3 are highlighted as blue sphere, Rrn3 K558 is located in a flexible loop, but neighboring residues would fulfill distance restraints.

The helix-forming residues 243–251 of Rrn3 contact the 'dock' domain of the largest A190 subunit and particularly helix 549–564 and residues 564–573 which are part of the Pol I-specific region a12a (Figure

7, B). Finally, the end of helix-forming residues 554–542 of Rrn3 are in close contact with C-terminal and N-terminal loops of AC40 (residues 334) and AC19 (residues 44–49), respectively (Figure 7, C). This is consistent with cross-linking data using BS3 (bis-sulfosuccinimidyl-suberate), which identified with high confidence a contact between lysine 558 of Rrn3 and AC40 lysine 329 and A190 lysine 582 (Figure 7, D)., respectively (Blattner et al. 2011).

2.2.3.2. Fitting Pol I into the Pol I-Rrn3 cryo-EM model

Interestingly, significant changes were observed in the structure of Pol I. The active center cleft is more contracted in the Pol I/Rrn3 cryo-EM map than in the crystal structure. Comparing the crystal form with a molecular Pol I model fitted into the Pol I/Rrn3 density, shows that the 'clamp' domain and the A43-A14 stalk moved inwards (Figure 8 A). The two long helices that form the clamp core domain of A190 are displaced by 8 Å. On the other side of the DNA-binding cleft an inward movement of 3.5 Å is also measured at the tip of the 'protrusion' domain of A135, indicating that the cleft closes by 11.5 Å when compared with the crystal structures. The A190 'lid loop' (residues 368–380) is perfectly resolved in the EM map, but its position within the RNA exit-channel is slightly shifted (Figure 8,B), suggesting that the RNA exit channel is less occluded than in the Pol I crystal structure. Another important difference to the crystal structure is found within the active site. While all helices are resolved, no density is observed for the Pol I-specific 'expander domain' and the 'expander helix/ DNA mimicking loop', an element present in the active site in several crystal structures (Figure 8 C) (Engel et al. 2013; Fernández-Tornero et al. 2013). The fact that the expander helix/extended loop is missing in some crystal forms (Kostrewa et al. 2015) and could not be traced in the electron density map suggests that it is partially flexible.

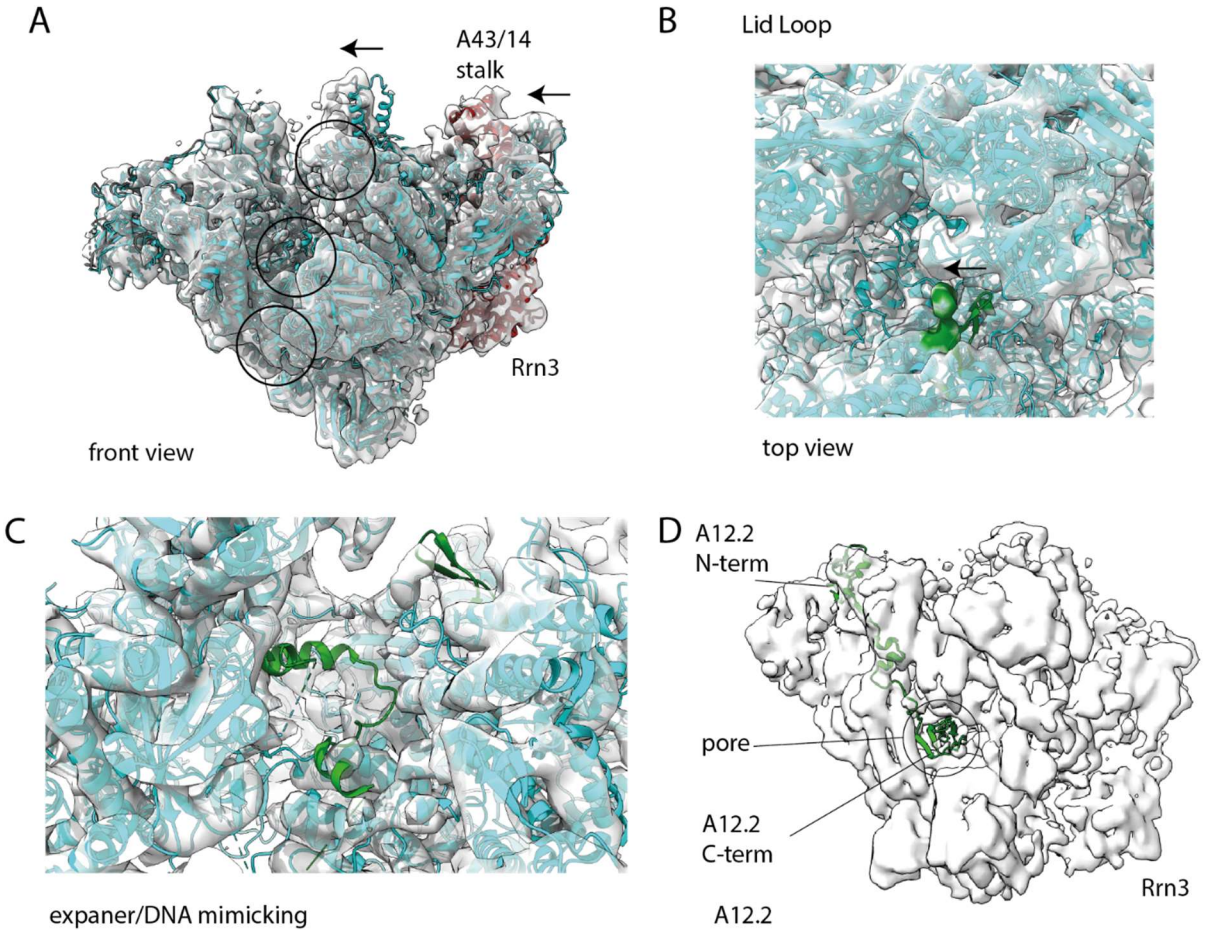

Figure 8: Structural changes of Pol I in the Rrn3-bound conformation as compared with the crystal form

A) Pol I/Rrn3 model (grey) fitted into cryo-EM density of Pol I/Rrn3 (grey envelope) compared to Pol I x-ray structure (cyan, pdb 4c2m). Subunit A135 of both molecular models were aligned and show closing of the cleft and the upward movement of the A43-A14 stalk in Pol I/Rrn3 (indicated with black arrows). Regions enlarged in B-D are highlighted by circles. B) Position of the lid loop of subunit A190 (residues 368–380) in the crystal structure (green ribbons) as compared with the cryo-EM structure (green envelope). Molecular model of Pol I X-ray structure in cyan, (pdb 4c2m) and EM density of Pol I/Rrn3 grey envelope. C) Expander helix in X-ray structure (green ribbon) of the A190 subunit (residues 1360–1400) which is not resolved in the cryo-EM structure. D) Crystal structure of the A12.2 subunit (green ribbon). A12.2 N-terminal Rpb9 related domain is associated with the Pol I lobe, its C-terminal TFIIS-like domain is not located in the pore of the Pol I-Rrn3 cryo-EM structure (grey envelope).

In addition, the C-terminal part of A12.2, which holds the TFIIS homology region, is absent in the cryo-EM map while it is positioned in the pore in the crystal structure (Figure 8 D). The inserted C-terminus of TFIIS stimulates RNA cleavage to resume Pol II-dependent RNA chain elongation (Kettenberger et al. 2003). In a Pol I ITC reconstruction the RNA primer was lost and the C-terminal domain of subunit A12.2 inserted into the funnel domain of Pol I, as would be expected for RNA cleavage events (Sadian et al. 2017). Absence of A12.2 C-terminal domain was not caused by subunit dissociation, since the N-terminal part, homologous to Rbp9, including two helices is perfectly resolved and is located similar to its position in the crystal structure on the Pol I lobe (Figure 8 D). This observation indicated that the C-

terminal domain of A12.2 dissociates from the active site and is probably flexible since no similar density was detected in our map.

2.2.3.3. Rrn3-free Pol I monomers differ from Pol I dimers.

In Pol I crystal structures, the C-terminus of the Pol I subunit A43 (connector) interacts with the cleft of a neighboring Pol I molecule, leading to dimerization of two Pol I molecules (Engel et al. 2013; Fernández-Tornero et al. 2013). Transition of an inactive enzyme with an expanded cleft into a more contracted Pol II-like monomeric, but transcriptional active Pol I was suggested to be involved in transcription regulation (Engel et al. 2013). So far, no high-resolution data of an active Pol II-like Pol I conformation existed. We wanted to compare this Rrn3 free monomeric Pol I to its Rrn3 bound state, to attribute the effects of Rrn3 on the conformational changes of the molecule. In solution, Pol I monomers, dimers and a very small portion of Pol I/Rrn3 co-exist (Milkereit and Tschochner 1998). From 2934 cryo-EM images we extracted and separated Pol I monomers (108.214 particles 28%) and dimers (141.024 particles 72%) *in silico*.

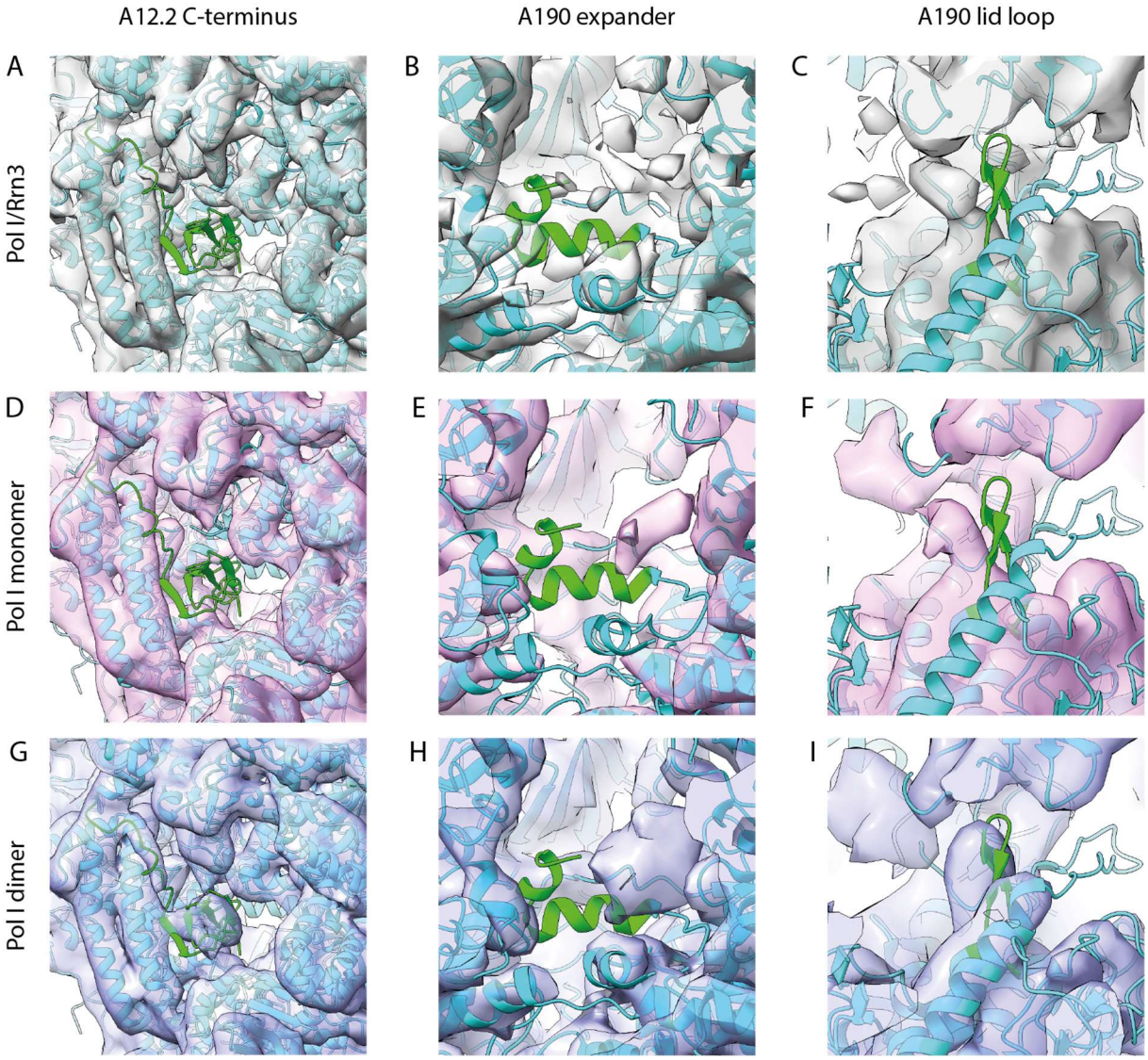

Figure 9: Comparison of key structural features in different Pol I conformational states
The position of the A12.2 C-terminus (**A, D , G**) the A190 expander helix (**B, E, H**) and the A190 lid loop (**C, F, I**) are shown in the cryo-EM maps of the Pol I- Rrn3 complex (**A-C**) the Pol I monomer (**D-F**) and the Pol I dimer (**G-H**) relative to the dimeric crystal structure (pdb: 4c2m) blue cartoon representation, key structural elements are highlighted in green.

At a resolution of 7.5 Å, the isolated Pol I monomer structure was very similar to the Rrn3-bound enzyme (Figure 31). In particular, the C-terminal domain of A12.2 is not detected, whereas it is present in the center of the dimer (Figure 9 A, D , G; Supplementary Fig. 7) and the position of the clamp is almost identical in both structures indicating that the cleft has the same width. The lid loop was positioned slightly differently than in the crystal structure but still in a way that it partly occludes the RNA exit channel (Figure 9 C, F, I). The expander helix was clearly not in the same position as in the early crystal structures but a new density is placed in the active site which could correspond to a different position of the expander domain (Figure 9 B, E, H). The monomeric Pol I form seems to be slightly depleted in A49/34.5 since the corresponding density is weaker than in the Pol I-Rrn3 complex, but the bridge over the cleft is detected as a faint electron density (data not shown). Altogether, this comparison indicated that the major conformational changes in Pol I are not specific for the Rrn3 bound complex, but rather properties of monomeric Pol I.

2.2.3.4. Cryo-EM structure of Pol I dimers resemble the crystal structure

The analysis of the dimeric Pol I form by cryo-EM was important to understand the differences with the crystal structures. A final resolution of 7,8 Å was obtained for the entire dimer, which shows a slight movement between the two monomers. This movement is in agreement with alterative conformations found in Pol I crystals (Kostrewa et al. 2015). We could partially correct this flexibility by analyzing a single monomer thus reaching a resolution of 6.8 Å. The A43/A14 stalk is essential for dimerization and the stalk of one monomer interacts with the DNA-binding cleft of the second monomer. The connector helix in A43 plays a crucial role for dimerization and contacts the 'protrusion' domain of A135 close to the Pol I-specific insertion α11a. Whereas, the A43 connector helix is poorly resolved in the monomeric form of Pol I, and is displaced on binding of Rrn3, it is perfectly resolved in the dimer at the position determined by X-ray crystallography (Figure 31). Moreover, the cryo-EM dimer map is comparable to the crystal structure with regard to cleft opening, and for the density corresponding to the C-terminal domain of A12.2, which is clearly detected at the same position (Figure 9 G).

However, the expander helix observed in some of the crystal structures, is not in the same position, while a new density appears in the active site as seen for the isolated monomer (Figure 9 H). Interestingly, in all three structures the catalytically important 'bridge' helix appeared to be partially unwound in its central part, indicating that even when the expander helix is absent the bridge helix does not fold properly (Supplementary Fig. 9). The A190 lid loop is well resolved in the cryo-EM dimer map and it adopts the same position than in the crystal form (Figure 9 I). Furthermore, the density

bridging the DNA-binding cleft is weakly detected in all maps suggesting that the corresponding protein domain is not stably positioned.

In summary, we purified a highly active Pol I/Rrn3 complex and compared its EM structure to bulk Pol I which exists in monomeric and dimeric conformations. While our *in-solution* structure of Pol I dimers resembles an inactive state observed in protein crystals, monomeric Pol I and Pol I/Rrn3 appear in a similar conformation. Rrn3 may stabilize this active monomeric state and therefore allow promoter recruitment and transcription initiations. Whereas Pol I oligomerization state and complex formation with Rrn3 is independent of DNA; additional factors are required for targeting the activated enzyme to its promoter.

2.3. Reconstitution of the complete Pol I pre-initiation complex

So far, I established protocols to reconstitute basal Pol I transcription using recombinant CF and either Pol I/Rrn3 purified from yeast, or reconstituted with recombinant Rrn3. However, efficient transcription initiation depends on additional factors. UAF requires TBP to enable high levels of transcription (Steffan et al. 1996; Keener et al. 1998). Further, Net1 associates with the promoter and stimulates Pol I transcription (Shou et al. 2001; Hannig et al. 2019). The molecular mechanisms how these factors allow high levels of Pol I initiation are not completely understood. Therefore, we wanted to reconstitute the complete Pol I PIC to better understand how individual components support Pol I transcription initiation.

2.3.1. Purification of UAF complex

Efficient Pol I transcription initiation depends on the initiation competent Pol I/Rrn3, CF, TBP and UAF. The upstream activating factor consists of six subunits, Rrn5, Rrn9, Rrn10, Uaf30 and the two histone proteins H3 and H4 (Keys et al. 1996; Keener et al. 1997). UAF is dispensable for a basal level of transcription *in vitro*, but is required for high levels of transcription *in vivo* and *in vitro* (Keener et al. 1998). Together with TBP, UAF recruits CF and stimulates Pol I transcription (Steffan et al. 1996). The low cellular abundance of UAF was limiting a detailed structural and functional analysis of the complex. Only a few hundred molecules are present in yeast cells (Bier et al. 2004). Purification of the endogenous complex enabled identification of all complex subunits and a functional characterization of UAF (Keys et al. 1996; Keener et al. 1997). However, the protocol does not yield sufficient amounts of pure protein for a detailed structural and functional study. Therefore, we wanted to establish a purification strategy for UAF from recombinant source.

2.3.1.1. Purification of recombinant UAF

Purification of pure protein(-complexes) in sufficient amounts is a prerequisite for functional and structural studies. The MultiBac baculovirus expression system (methods 5.5) was demonstrated to be suitable for multi-protein complex expression and purification (Berger et al. 2004; Fitzgerald et al. 2006). The system offers genetic tools, that enable construction of plasmids for parallel expression of multiple proteins. Expression cassettes are integrated in a viral genome precursor, which can be

transfected into insect-cell-lines. The amplificated virus can infect large volumes of suspension culture cells and therefore can be scaled up to large quantities (Fitzgerald et al. 2007).

We used this baculovirus expression system to express and purify the UAF complex. Therefore, we co-expressed the six UAF subunits (Rrn5, Rrn9, Rrn10, Uaf30, H3, H4) in baculovirus infected insect cells. HA, Flag and 7xHis of epitope-tags on subunits Rrn5, Rrn9 and Uaf30 respectively allowed different purification strategies, the most efficient in terms of purity and yield is presented (Figure 10, details see methods 5.7.4).

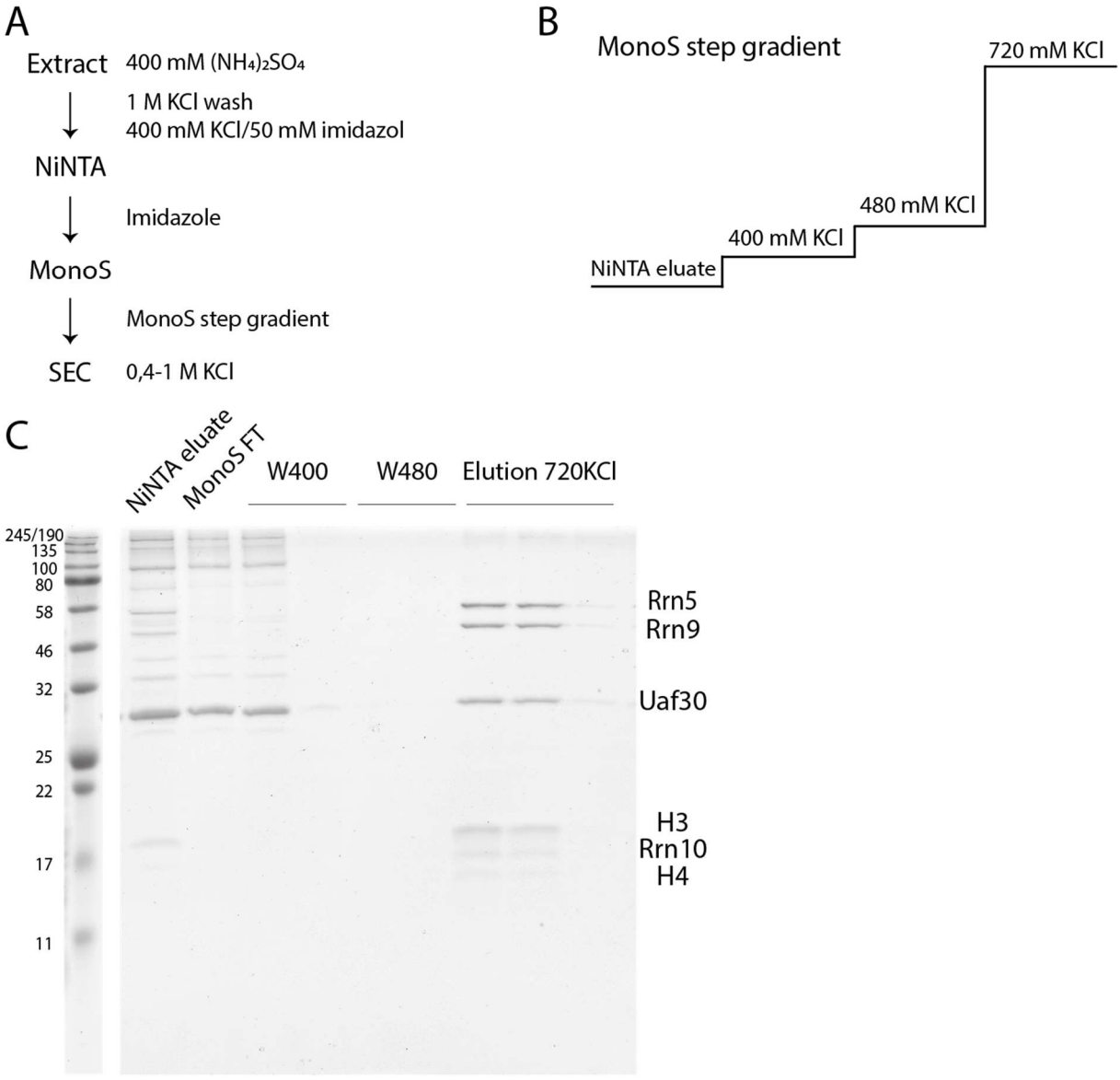

Figure 10: Purification of recombinant UAF from BIIC

A) Multistep purification scheme of UAF from baculo-virus infected insect cells includes a NiNTA capture, a cation exchange step and an optional size exclusion polishing step. Important buffer conditions are indicated. B) Optimized MonoS step gradient used for UAF purification. C) Coomassie stained 12% SDS PAGE gel with selected fractions of UAF purification. UAF is enriched in NiNTA with excess of bait protein Uaf30, contaminants including excess Uaf30 were found in MonoS flow-through (FT), highly purified UAF complex elutes at 720 mM KCl in a step gradient. Individual UAF subunits are indicated on the right, size of marker in kDa on the left.

A buffer containing 400 mM ammonium sulphate was used to inhibit DNA interactions and to solubilize the recombinant UAF-complex. Then, we used the 7xHis-tag on Uaf30 subunit to efficiently capture the UAF complex on NiNTA agarose beads. Recombinant UAF is stable under high salt conditions and does not dissociate during wash steps up to 1 M KCl, which is well in line with the characterization of the endogenous complex (Keys et al. 1996; Milkereit and Tschochner 1998). We further purified the NiNTA eluate by ion-exchange chromatography (Figure 10 B, C), using the strong affinity of the complex for the MonoS cation-exchange resin, to >95% purity. Most contaminants that co-purified on NiNTA affinity resin did not bind to the MonoS matrix under the chosen conditions, or were removed during the wash-steps (Figure 10 C, compare NiNTA eluate and MonoS FT). UAF components are depleted in the MonoS flow-through, while other contaminants and excess of NiNTA bait-protein Uaf30 is efficiently removed and found in the flow-through or wash fractions. Likely, the high pI values and resulting positive charges of the histone proteins contribute to the strong binding. Finally, UAF could be eluted from the cation-exchange column at 720 mM KCl in a step gradient (details see method section 5.7.4). This protocol yielded 100-200 µg pure UAF complex from 1 L baculo virus infected insect cells. These amounts of the factor allowed a detailed biochemical, structural and functional analysis of the complex.

2.3.1.2. UAF migrates as a stable 360 kDa complex on gelfiltration columns

In previous studies, a 240 kDa TBP containing complex was described that stimulated Pol I transcription initiation levels (Milkereit and Tschochner 1998). Further, in a recent study with recombinant UAF purified from *E. coli* two complex populations were observed on gelfiltration columns (Smith et al. 2018). UAF migrates with apparent molecular weights of 415 kDa and 194 kDa, suggesting the appearance of dimers and monomers respectively. Native mass spectrometry allowed this group to determine a molecular mass of 174,3 kDa. This suggested a complex composition with two H3 subunits and one copy each of Rrn5, Rrn9, Rrn10, Uaf30 and H4 for the monomeric complex (Smith et al. 2018).

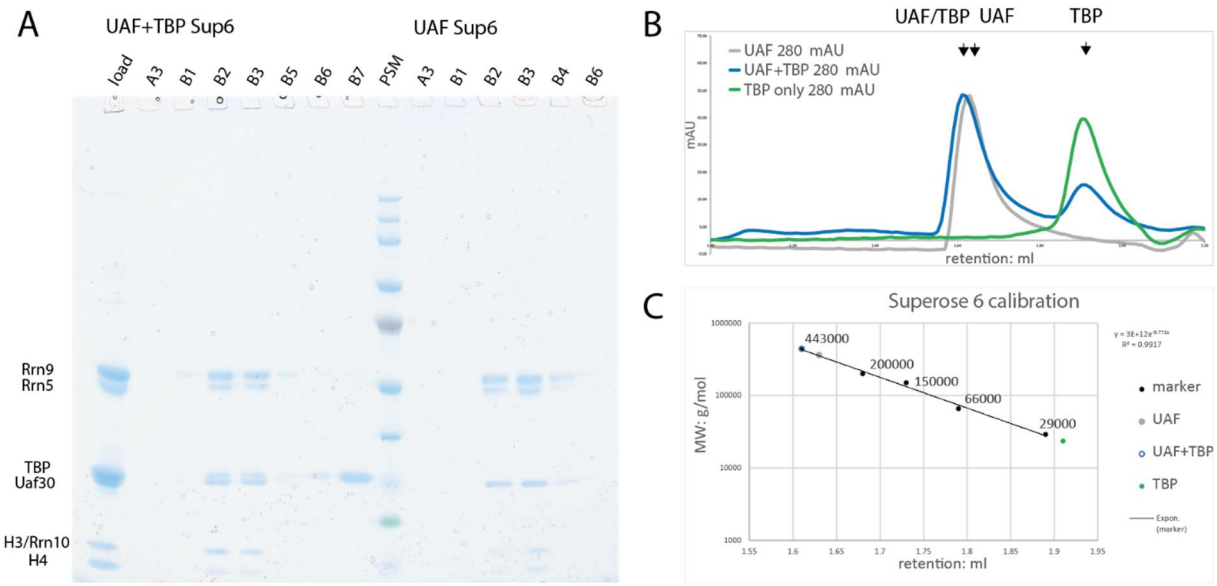

Figure 11: UAF migrates as a 360 kDa complex and stably associates with TBP
A) Coomassie stained 4-12% NuPAGE gel of indicated Superose 6 elution fractions. UAF preincubated with recombinant TBP on the left, UAF only fractions on the right, individual subunits are indicated on the right. An extra protein band corresponding to TBP co-migrates with UAF and is separated from excess TBP (fraction B6/7) B) SEC profiles (280 nm UV absorption) of the individual runs, UAF only in grey, UAF preincubated with TBP in blue, TBP only in green. C) Calibration of Superose 6 column. Globular marker proteins (443 kDa apo-ferritin, 200 kDa b-amylase, 150 kDa alcohol-dehydrogenase, 66 kDa albumin, 29 kDa carbo-anhydrase - all purchased from sigma) were used to calibrate the sizing column, molecular weights of marker proteins in g/mol are indicated in diagram. Slope of the regression line was used to estimate molecular weights of UAF complexes. Elution peaks of UAF, UAF/TBP and TBP only are indicated as grey, blue and green dots respectively.

We performed analytical size exclusion chromatography (SEC) to estimate molecular weight of the recombinant UAF complex and to study interactions of UAF and TBP. In initial experiments with salt concentrations close to physiological conditions (20 mM HEPES pH7,8; 200 mM KCl) and in absence of promoter DNA, we did not observe stable migration of UAF complex on gelfiltration columns. Interestingly, increasing the conductivity in the gelfiltration buffer up to 1 M KCl, stabilized the UAF complex to migrate as a distinct population (Figure 11). Likely, the high conductivity in the buffer prevented ionic-interactions of the heavily charged UAF surface that would lead to aggregation of the complex. In high conductivity buffers, all UAF subunits elute in approximately stoichiometric amounts (Figure 11 A) from the Superose 6 Increase 3,2/300 column. UV-light absorption at A280 nm and A260 nm confirmed absence of DNA in elution profiles (not shown). Preincubated with TBP, UAF eluted slightly earlier from the SEC column, suggesting a higher molecular mass, and an additional band, corresponding to the molecular weight of TBP appeared in the SDS-gel (Figure 11 A, B).

The molecular weight of globular marker proteins was blotted against their retention volume (Figure 11 C). An approximate linear relationship between the logarithmic weight and retention allowed the estimation of molecular weights of globular proteins. We calculated an apparent molecular weight of 362 kDa for the UAF complex. Preincubated with TBP the determined molecular mass was about 440

kDa and, thus, slightly higher. The estimated size for TBP alone was 23,5 kDa and close to the expected 27 kDa. The molecular weight values for UAF were close to the expected mass of dimeric complexes, assuming the stoichiometry suggested by Smith et al. (approx. 348,6 kDa for dimers). Our UAF constructs carry 3xHA, Flag and 7xHis tag, which contribute for around 12 kDa additional molecular weight. No monomeric complexes were observed under my experimental conditions. It should be noted that in the study of Smith et al. the complex was artificially stabilized by the addition of large amounts of arginine in the SEC buffer (Smith et al. 2018). the mechanism how it stabilizes protein oligomers is not well understood. Arginine is weakly interacting with proteins, and might partially support unfolding of proteins (Arakawa et al. 2007; Kim et al. 2016).

2.3.2. Expression and purification of Net1

Beside the well-studied functions of Net1 in its role as a RENT component, its involvement in Pol I transcription initiation has been described. Overexpression of Rrn3 can rescue growth phenotypes caused by temperature sensitive Net1 mutations and purified Net1 protein stimulates Pol I transcription *in vitro* (Shou et al. 2001). The molecular mechanism how this factor enhances Pol I initiation however remains poorly understood. Systematic truncations of Net1 protein which were performed in the group of Wolfgang Seufert identified the C-terminal part of Net1 (Net1-C) to be responsible for Pol I dependent functions of Net1. In a combined effort we showed that Net1-C supports loading of Pol I to the rDNA and normal cell-growth (Hannig et al. 2019) which encouraged us to understand the basic mechanisms of Pol I stimulation by this protein. To understand its interplay with Pol I PIC components, we included Net1 and its truncations in our reconstituted *in vitro* assays.

In first attempts I tried to purify Flag-tagged Net1-C from yeast cells. Albeit the protein was overexpressed, yields were limiting for an in-depth structural and functional analysis. Net1 variants purified from *E. coli* in the group of Wolfgang Seufert showed no stimulation of Pol I transcription in my *in vitro* experiments which could be due to impaired phosphorylation of bacterial expressed recombinant proteins. The baculo virus expression system uses an eukaryotic posttranslational modification machinery, not present in *E.coli* cells (Fitzgerald et al. 2006), and should be appropriate to express heavily phosphorylated Net1 protein (69 annotated phosphosites in phosphoGRID database in June 2021). We expressed TAP-tagged versions of full length Net1, Net1-ΔC (amino acids 1-1051) and Net1-C (1052-1189) in baculo virus infected insect cells (BIICs) (Figure 12 A). Proteins were purified on IgG-coupled Sepharose and eluted by proteolytic TEV cleavage (see 5.7.5). Net1-FL and Net1-ΔC are prone to degradation during protein purification. Albeit lysate and buffers were supplemented with protease inhibitors and kept on ice to minimize these effects, degradation-products of full length Net1 and Net1-ΔC were present (Figure 12 B). Nevertheless, the un-degraded form accounts for the main population. In SDS-PAGE gels, Net1-C migrates as a diffuse band at an apparent molecular weight of about 30 kDa (Figure 12 B), albeit its theoretical mass is 18 kDa. The protein is phosphorylated *in vivo*,

several phosphosites have been annotated, and phosphorylation seems to play a functional role as the phosphorylation pattern changes in different growth states and only phosphorylated Net1-C seems to interact with Pol I (Hannig et al. 2019).

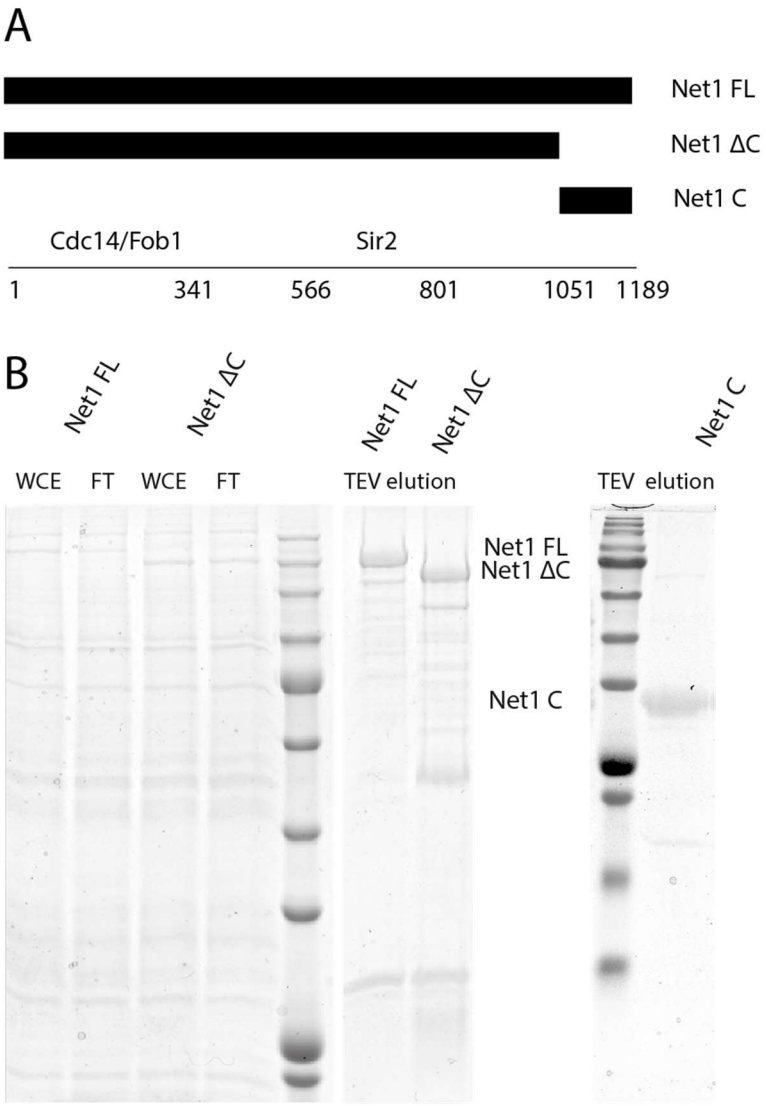

Figure 12: Expression and purification of Net1 truncation constructs
A) Schematic representation of expression constructs for full length Net1 (Net1 FL), Net1 ΔC missing C-terminal amino-acids from position 1051 and Net1-C, containing only the C-terminal part of Net1 starting from amino-acid 1052. Net1 domains interacting with Cdc14, Fob1 or Sir2 are indicated, details see text, figure adapted from Hannig 2019, modified. B) Coomassie stained SDS gels of recombinant Net1 variants; left, 10% SDS gel with cell lysates (WCE) and IgG Sepharose flow through (FT) fractions from insect cells expressing TAP-fusion proteins of either full length Net1 or Net1 ΔC are shown. TEV elution fractions of the constructs contain degradation products; right 15% SDS gel with TEV elution of Net1-C

Thus, we can purify Net1 FL and its truncations in large quantities from recombinant source. During expression in BIICs, proteins can become post-translationally modified, which might be essential for their function. In the next step we tested the purified Net1 constructs in our *in vitro* transcription assays.

2.3.3. Reconstitution of Pol I transcription initiation *in vitro* from recombinant purified factors

Next, I reconstituted Pol I transcription initiation from recombinant purified Pol I transcription factors. Therefore, I incubated the recombinant purified transcription factors with yeast Pol I (Coomassie stained gel of individual components in Supplemental Figure 12 D) and DNA-templates. The first template contains the WT rDNA sequence from position -212 to +147 (relative to the TSS) including the complete promoter. In a second, shorter (+119 bp downstream) reference template the UE (-155 -39) was mutated. The construct lacking the UE allows a basal CF-Pol I-Rrn3 dependent initiation, but not enhanced levels of transcription (Keener et al. 1998) and serves as an internal control. Specific initiation from the WT template results in the synthesis of an RNA product with 147 nt or accordingly 119 nt from the ΔUE-DNA.

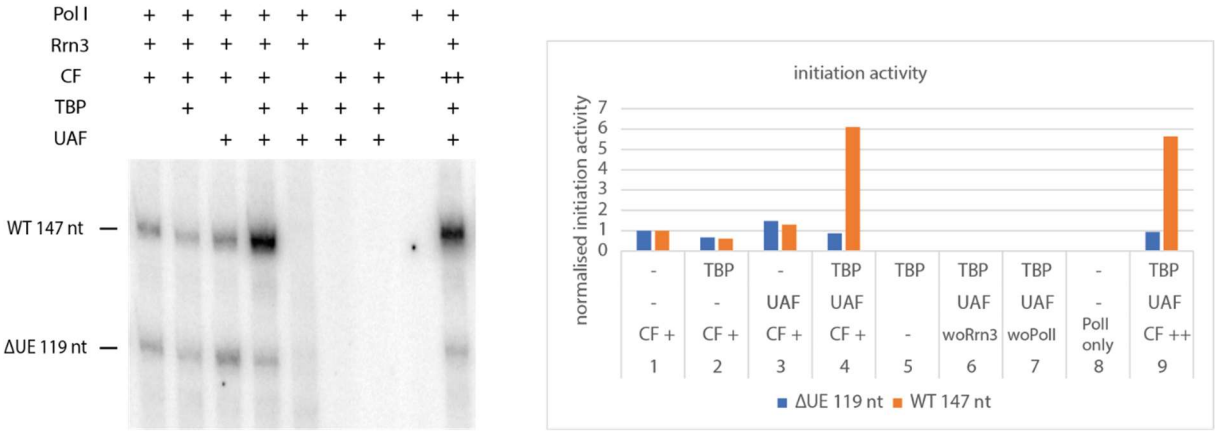

Figure 13: Reconstitution of Pol I transcription initiation in vitro with recombinant UAF
In vitro transcription assay demonstrated functional recombinant UAF complex. Left, autoradiogram of *in vitro* initiation assays. Transcription from a WT rDNA fragment and a template with mutated UE resulted in 147 nt or 119 nt run-off product, respectively. Each reaction contained both DNA templates and the indicated factors. Right, quantification of the autoradiogram. Reactions were normalized to basal transcription level of the minimal system analyzed in lane 1.

In paragraph 2.2.2, a minimal transcription initiation system containing recombinant CF, Rrn3 and yeast Pol I or Pol I/Rrn3 was introduced (Figure 5). A minimal system comprising recombinant CF and Rrn3 together with Pol I enables transcription initiation from both templates with similar efficiency (Figure 13, lane 1). Addition of either purified recombinant TBP or UAF mildly affects the basal initiation rates alone (lane 2; 3). Combination of all five factors leads to increased transcription initiation from the WT promoter, but not from the reference template with mutated UE sequence (lane 4). Omission of CF, Rrn3 or Pol I abolished specific transcription, and also Pol I alone did not show any specific activity. Finally, a reaction with double amount of CF did not further stimulate the system, confirming that the factor is not limiting under these conditions (lane 9). UAF together with TBP stimulated the

basal transcription system in these reactions by a factor of 6 (compare transcription level from WT rDNA in lane 1 to lane 4). The stimulation is even higher, when compared to the internal ΔUE reference. Thus, we purified a transcriptionally active recombinant UAF complex and could reproduce TBP dependent stimulation by UAF on basal Pol I transcription initiation (Steffan et al. 1996; Keener et al. 1998). This reconstituted transcription system from purified transcription factors was used to better characterize the role of UAF and TBP in Pol I transcription.

2.3.3.1. Net1-FL and Net1-C stimulate promoter dependent transcription to high levels

We aimed to better characterize the stimulatory effects of Net1 on Pol I initiation and therefore included recombinant Net1 in our complete reconstituted *in vitro* system.

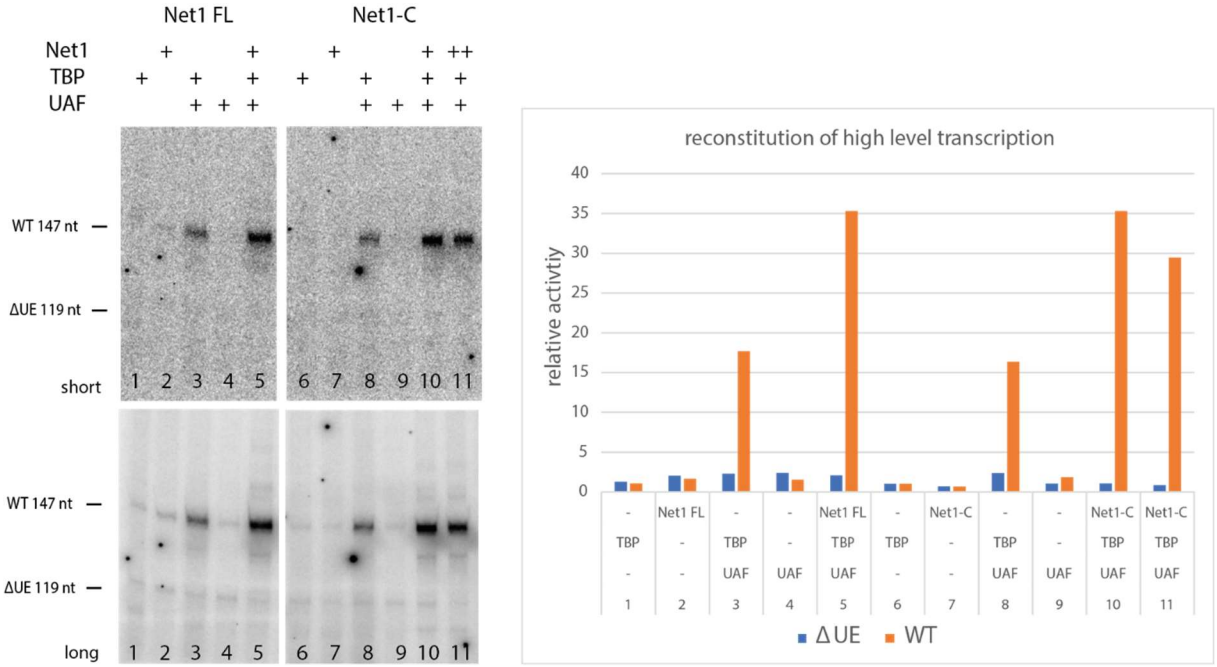

Figure 14: High level stimulation of Pol I initiation by Net1 FL and Net1-C

Reconstitution of efficient Pol I transcription initiation *in vitro*. Reactions contain a WT rDNA fragment from -212 to +147 relative to transcription start site and a second reference template containing a mutated UE sequence resulting in a 147 nt run off transcript from the WT promoter and 119 nt from the ΔUE promoter. Reactions contained Net1 FL or, Net1-C, UAF and TBP as indicated and constant amounts of Pol I, Rrn3, CF. Short (top) and longer (bottom) exposure to phosphoscreen are shown. (Lanes 5, 10 and 11 were oversaturated at longer exposures;) on the left. Right: quantification of the depicted transcription reactions.

We observed a more than 35-fold stimulation of the fully reconstituted system compared to the minimal system (compare lane 1 to 5). Stimulation in comparison to the internal reference lacking the UE site is even higher, but could be biased by competition effects between the WT promoter sequence and the reference DNA for protein factors. In UAF containing reactions transcription is reduced by 20-40% from the reference compared to the minimal system. The effects of Net1 and UAF/TBP appear to be independent. UAF/TBP dependent stimulation was found to be up to 15-fold and Net1 stimulated

the reactions by a factor of 2-4. In a minimal transcription initiation system baculo-virus expressed Net1-FL stimulated Pol I transcription approximately by a factor of three (Supplemental Figure 1 A) which is in line with previous reports (Shou et al. 2001). The C-terminal truncated protein Net1-ΔC showed almost no effect on transcription efficiency, but importantly we could assign the stimulatory activity of Net1 to its C-terminal part. Transcription activation by Net1-C was almost as efficient as by the full-length protein (Supplemental Figure 1 A, C). Accordingly, Net1-C was sufficient for this robust stimulation and allowed stimulation of transcription to the same extend as the full-length Net1 protein.

2.3.3.2. Net1 does not stimulate tailed template transcription but is specific for initiation from the Pol I promoter

In previous reports a promoter-dependent *in vitro* transcription assay showed the stimulatory effect of Net1 on Pol I transcription. (Shou et al. 2001; Hannig et al. 2019). Direct physical interaction of Net1 with Pol I has been shown (Shou et al. 2001; Hannig 2016) and would enable Net1 to influence transcribing/elongating Pol I. Indeed, Net1 can be found downstream of the Pol I promoter and might travel with Pol I after successful initiation (Huang and Moazed 2003; Goetze et al. 2010). A control experiment using tailed-templates should show, whether the activity of Net1 domains is specific for the initiation phase of Pol I, or the factor might be of importance during Pol I transcription elongation. In tailed template experiments, RNA polymerases start transcription from single-stranded 3' DNA overhangs and do not require any other factors (Dedrick and Chamberlin 1985). We observed no stimulation of transcription in our tailed-template assay, for neither of the constructs (Supplemental Figure 1 B, D). In contrast, transcription rates are slightly decreased in presence of the recombinant proteins. Thus, Net1 and its C-terminal part affect the initiation phase of Pol I. Next, we wanted to further analyses how the enhanced initiation rates observed in the presence of Net1 could be reached and aimed to study this effect in more detail.

Summarized, we were able to reconstitute Pol I transcription initiation from purified factors *in vitro*. UAF together with TBP stimulated a minimal transcription system, consisting of Pol I, CF and Rrn3 up to 10-15-fold. Addition of Net1-FL or Net1-C allowed high levels of transcription, up to 35-fold over the basal level, expanding the set of Pol I initiations factors by Net1. We established protocols, that yield sufficient amounts of all components that allow efficient Pol I initiation *in vitro*. In the following, we used these factors to reconstitute the Pol I PIC and to study the molecular details that allow this high transcriptional output. We aim to understand, how the individual factors contribute to this highly efficient process of transcription initiation.

2.4. Protein-Protein interactions in the Pol I PIC

First, protein-protein crosslinking coupled to mass-spectrometry was used to obtain architectural information of the complex and to gain information about protein-protein interactions within this mega-Dalton complex. Chemistry of the cross-linking reagent restrains spatial distance of residue-pairs. We used BS3 (bis(sulfosuccinimidyl)suberate) for crosslinking the complete PIC. BS3 crosslinks

primary amine groups with a C-alpha distance closer than 30-40 Å (Schmidt and Urlaub 2017). For transcription factors only (UAF-TBP-CF-Net1-C assembled on promoter DNA, without Pol I and Rrn3) we collected three datasets each with a different crosslinker; i) BS3, ii) DSS (disuccinimidyl suberate) a more hydrophobic chemical analogue of BS3 and iii) EDC (1-Ethyl-3-[3-dimethylaminopropyl]carbodiimide hydrochloride) a 'zero-length' crosslinker that activates carboxyl groups for spontaneous reaction with primary amines (details see methods 5.9). Complexes were assembled, crosslinked and purified on SEC columns. Purified, crosslinked complexes were processed and analyzed by Alexandra Stützer and Momchil Ninov in the lab of Henning Urlaub. Interaction maps of individual experiments are presented in Supplemental Figure 2 -4. Raw data of all crosslinked peptides is available upon request from Herbert Tschochner, Christoph Engel or Michael Pilsl.

2.4.1. TBP and Net1-C mediate interactions between the core PIC and UAF

Overall, crosslinking-mass spectrometry analysis of the complete PIC suggested a rather modular complex architecture with limited inter-complex contacts. Almost all crosslinks between Pol I subunits, CF and Rrn3 subunits could be mapped on known molecular structures and full-fill distance criteria (131 out of 136 (96%) residues pair within 30 Å Cα-Cα distance), assuring quality of the dataset (Supplemental Figure 2). Protein-protein interactions were dominated by intra-complex crosslinks and reflected promoter architecture with UAF and CF binding sites. We did observe little interactions between UAF and CF or Pol I. TBP bridged between CF and UAF and Net1-C interacted with UAF and Pol I.

UAF extensively crosslinked to TBP, this includes previously described interactions with Rrn9 (Steffan et al. 1998) but TBP also interacted with other UAF components as H3. Further, we observed strong crosslinking of UAF to Net1-C, whereas UAF appeared to be isolated from CF or Pol I. Thus, TBP and Net1-C may form an interaction hub and mediate between UAF on the upstream-promoter side and CF-Pol I around the transcription start side.

2.4.2. X-link MS reveals interaction network of Net1-C in Pol I PIC complex

Whereas association of UAF and CF with their dedicated promoter elements determine PIC architecture to a certain extent, Net1-C interactions are less clear. Physical interactions of Net1 with Pol I have been previously described (Shou et al. 2001; Hannig et al. 2019). Further, Net1 association with the Pol I promoter seems to depend on UAF (Goetze et al. 2010). We had a closer look on Net1-C interactions within the complete PIC, therefore we selected high confidential cross-links of Net1-C (>1 residue pair and score >2). Net1-C interacted with Pol I at its stalk domain and its associated factor Rrn3 (8 residue pairs in 27 peptides were identified, TBP (11; 38) and UAF components Rrn10 and H3 (Figure 15 A).

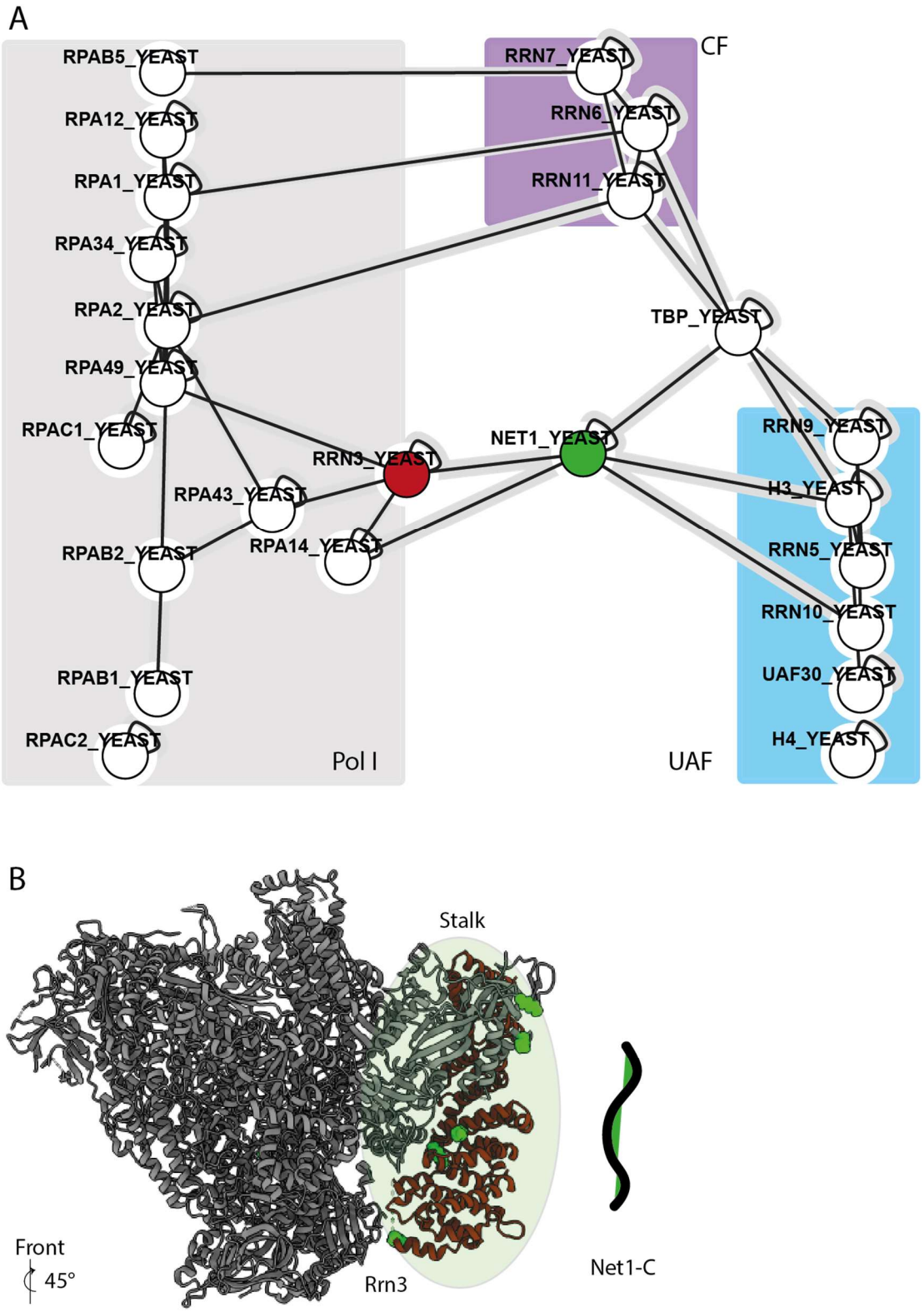

Figure 15: Net1-C interactions within the Pol I PIC
A) Protein interaction network at the Pol I PIC visualized with xiview webserver (xiVIEW) (Graham et al. 2019). BS3 crosslinked. B) Net1-C interacting residues in Pol I/Rrn3 are displayed as green spheres; interaction cluster in a surface at the Pol I stalk and Rrn3 is highlighted in green; Additional crosslinks to flexible residues in this region were found, that could not be mapped directly to the structure. Residue 558 is in a flexible loop, R551 in proximity is shown. Further crosslinks in stalk subunit A14 K117, K131 were not resolved, but are located within this interaction hot-spot at the Pol I stalk.

2.5 The acidic region of human UBF1 shares conserved features with Net1-C and stimulated Pol I transcription initiation

Net1 co-purifies with different Pol I subunits (Shou et al. 2001; Huang and Moazed 2003; Hannig et al. 2019), however how this interaction is mediated was not clear. Our protein-protein crosslinking data allowed to closer define Net1 interactions with Pol I and Rrn3. Mapping Net1-C interacting residues in the Pol I/Rrn3 atomic model revealed an interaction hotspot at the Pol I stalk. Net1-C appears close to stalk subunits A43 and A14 and Rrn3 (Figure 15 B). The method gives information about proximity of two peptides, but does not necessarily allow to distinguish multiple interaction of individual proteins. Therefore, it is not clear if interactions with Pol I stalk, Rrn3 and UAF/TBP co-occur and if Net1-C is truly bridging between these factors or rather interacting with each of these components individually in different intermediate states or timepoints.

2.5. The acidic region of human UBF1 shares conserved features with Net1-C and stimulated Pol I transcription initiation

The C-terminal part of multifunctional protein Net1 contains an acidic and serine rich region which shares similarities with the C-terminal part of UBF (Hannig et al. 2019) and is predicted to be largely unstructured (Figure 16 A). Also many of the Pol II trans-activation domains are predicted to be largely unstructured, are enriched in acidic residues and contain hydrophobic residues near acidic side chains (Erijman et al. 2020; Hirai et al. 2010). Similarly the Pol III subunit C31 is largely unstructured and contains an acidic C-terminus, that is required for efficient initiation (Thuillier et al. 1995; Abascal-Palacios et al. 2018). The acidic tail of UBF1 has been shown to be involved in Pol I transcription activation in higher eukaryotes (McStay et al. 1991; Tuan et al. 1999). Interestingly, some transactivation functions seem to be inter-changeable between species (McStay et al. 1991; Voit et al. 1992; Tuan et al. 1999; McStay et al. 1997). Yeast cells expressing a chimeric Net1 protein in which the C-terminal part is replaced by the human UBF1 activation region was shown to partially suppress the Net1-ΔC phenotype. Thus, stimulation of Pol I initiation could be functionally conserved (Hannig et al. 2019). For a better understanding of this effect, I analyzed this putative Pol I activation domain in our *in vitro* assays. Analogously to the Net1 constructs, we expressed the C-terminal region of the human UBF1 protein (hUBF1-CTR), containing a hydrophobic patch and the acidic tail region, as TAP fusion protein in baculovirus infected insect cells. Compared to Net1-C, the expression-level and yield of hUBF1-CTR was lower (Figure 16 B, C), but sufficient for *in vitro* characterization. In *in vitro* transcription reactions we observed small effects of hUBF1 on Pol I transcription (Figure 16 D). Net1-FL and Net1-C enhanced transcription levels (lane 5, 15) while Net1-ΔC (7-10) did not stimulate transcription. hUBF1 barely influenced basal transcription levels (11, 12) but stimulated UAF dependent transcription (13, 14). Although stimulation was not as pronounced as by Net1-FL and Net1-C the moderate stimulation of transcription would correlate with moderate effects on cellular growth in Net1-hUBF-C fusion strains (Hannig et al. 2019). Multifunctional mammalian UBF complex defines the chromatin structure at the mammalian Pol I promoter, with its HMG-box-domains it associates

throughout the functional rRNA gene unit (Herdman et al. 2017). Interactions with other factors as SL1, or TTF1 may help to position UBF at the promoter region (Herdman et al. 2017; Moss et al. 2007). UBF can interact with SL1 via its C-terminal domain and is required for PIC formation (Tuan et al. 1999; Herdman et al. 2017).

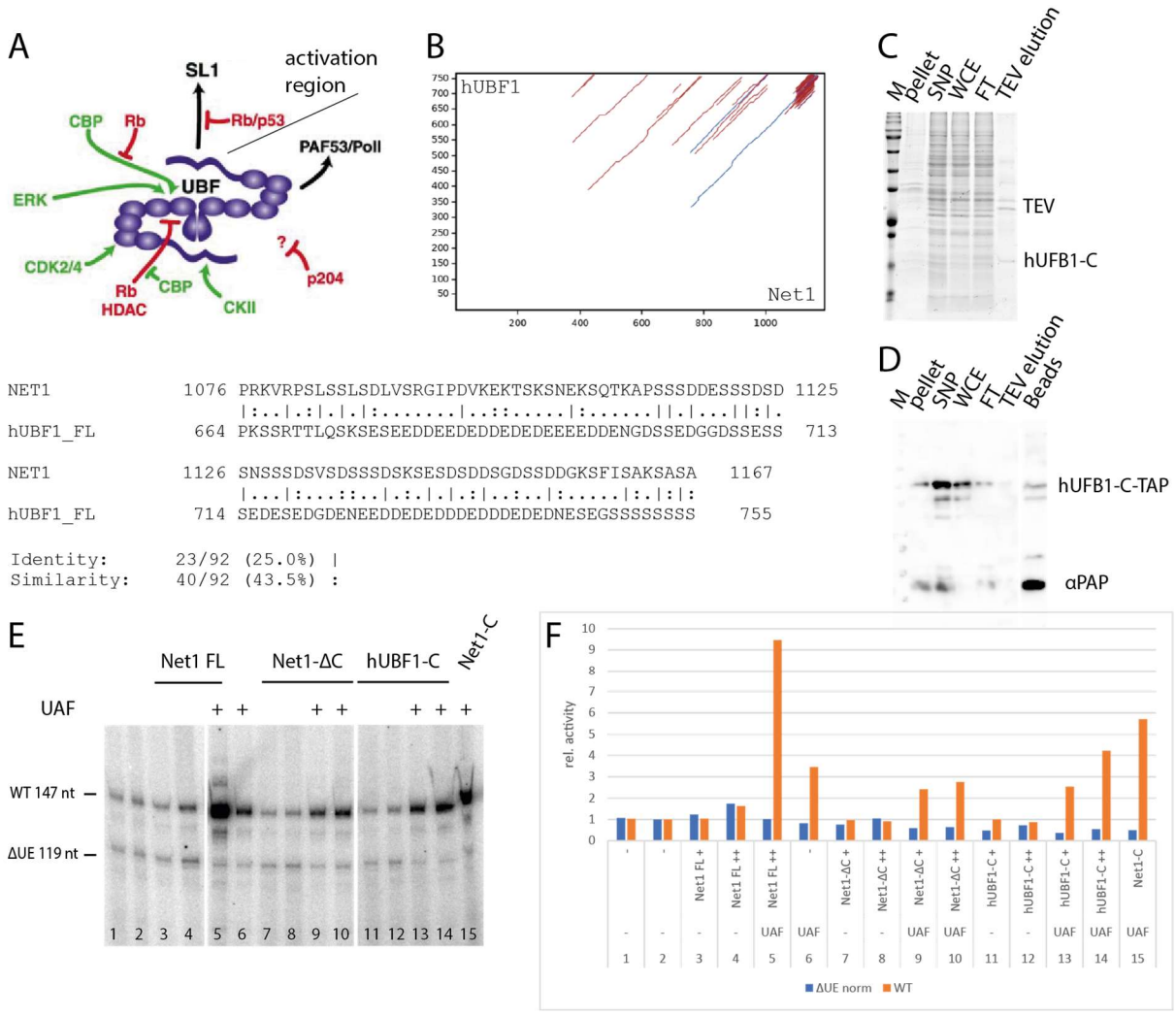

Figure 16: Acidic tail of hUBF1 enhances Pol I transcription initiation
A) Domain architecture of hUBF1, hUBF1 consists of 7 HMG boxes (violet blobs) and an acidic carboxyterminal activation region (waved line) (from (Moss and Stefanovsky 2002). B) Pairwise local sequence alignment (https://www.ebi.ac.uk/Tools/psa/) of Net1 and hUBF1 (amino-acids 627-765) C) Coomassie stained 15% SDS PAGE of recombinant hUBF1-C purification; Pellet after centrifugation, lysate before centrifugation (SNP), soluble supernatant (WCE), IgG Sepharose flow-through (FT) and TEV-protease elution fraction; D) same fractions were analyzed on Western-Blot with immune-staining using antibody #105 (anti-Protein A Peroxidase/PAP). E) Autoradiogram of *in vitro* transcription reaction. All reactions contained Pol I, Rrn3, CF and TBP and were supplemented with UAF (+) and Net1 FL, Net1-ΔC, hUBF1-C or Net1-C as indicated. F) quantification of *in vitro* transcription reactions, Net1-C quantification might be biased by shape of the lane (15).

2.6. DNA interactions at the Pol I promoter

We reconstituted a highly active Pol I PIC. Our cross-linking data gave a first view on the molecular architecture of the initiation factors which participate in PIC formation. To elucidate the requirements and hierarchy of promoter binding and to attribute the function of specific DNA sequences for factor binding and PIC assembly, I established protocols to directly analyze DNA-protein associations at the Pol I promoter and used it to re-investigate its DNA cis-elements.

2.6.1. Sequence specific DNA binding by UAF

Transcription factors have to specifically identify and bind their target sequences. The upstream promoter element is required for UAF dependent activation and template commitment (Keys et al. 1996). Previous studies aimed to characterized UAF-promoter interactions. Keys and colleagues complemented fractionated cellular extracts with purified endogenous UAF and evaluated the transcriptional output (Keys et al. 1996; Steffan et al. 1996). Definition of the minimal DNA sequence required for UAF dependent functions was not totally consistent in the published reports (Kulkens et al. 1991; Steffan et al. 1996; Keener et al. 1998; Aprikian et al. 2000). Electrophoretic mobility shift assays (EMSA) analyze the DNA binding of factors more directly. In these assays, the mobility of nucleic acids in native (acrylamide) gels in an electric field are analyzed. When components interact with DNA or RNA, migration in gels becomes slower. To date a detailed analysis of UAF - promoter engagement is lacking. We established EMSA experiments with recombinant UAF to better characterize its DNA interactions. Therefore, we compared UAF binding to two fluorescently labelled DNA templates. A WT rDNA fragment (-212 to +119 bp relative to TSS), labelled with Cy5, should help to detect *bona fide* UAF and/or CF binding, whereas an equivalent Cy3 labelled template where UE sequence (-155 to -39) is mutated should serve as non-specific control for UAF binding (schematic representation see Figure 17 B).

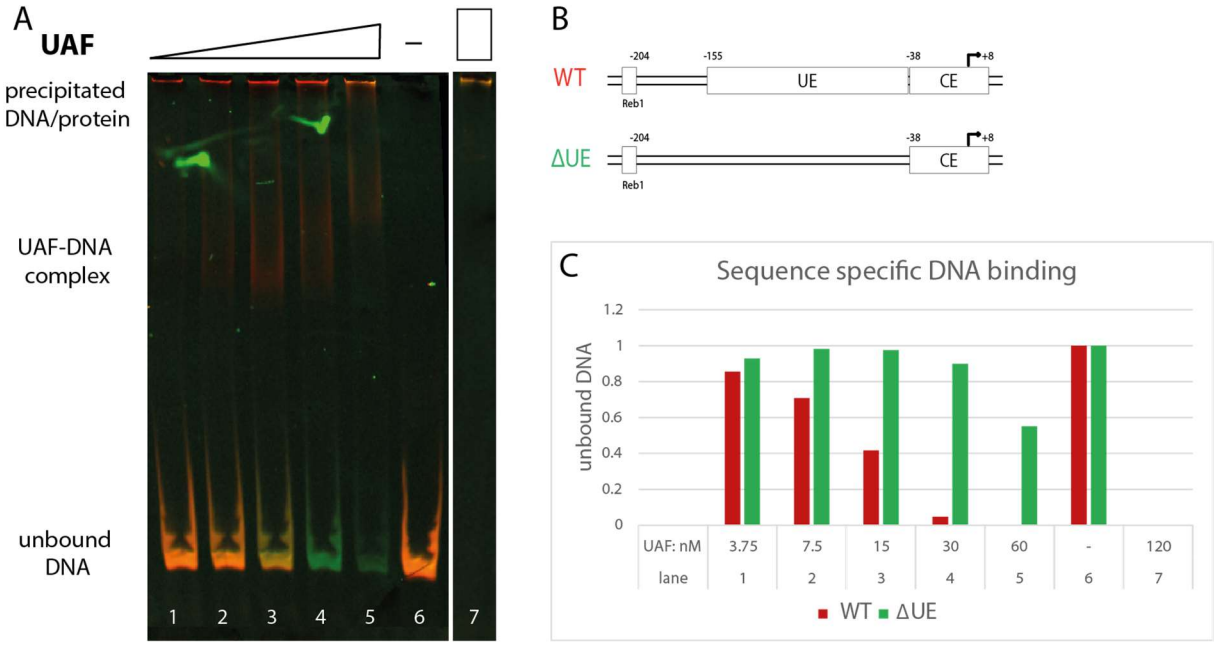

Figure 17: UAF specifically recognizes Pol I promoter DNA

UAF shows highly specific binding in EMSA experiment. A) native PAGE gel, merged Cy5 (red) and Cy3 (green) channels are displayed in orange at equal amounts, increasing amounts of UAF (3,8; 7,5; 15; 30; 60 and 120 nM) are titrated to mixture of Cy5-labelled WT DNA (red) and Cy3 labelled ΔUE (green). Three DNA populations can be distinguished on native acrylamide gels: Unbound DNA, a UAF-DNA complex which decreased DNA mobility, and precipitated DNA-protein complex does not migrate into gel and remains in pockets. B) Schematic representation of DNA templates; Cy5 labelled WT DNA (red) and Cy3 labelled ΔUE (green). C) Quantification of unbound DNA in each lane from individual fluorescence channels, colored as above, reveals highly specific binding of WT DNA. Signals were normalized on input DNA signals in lane 1.

In EMSA experiments we observed three distinct populations of DNA, free/unbound DNA, a UAF-DNA complex with decreased mobility, and precipitated DNA-protein complex which did not migrate into gel and remained in the gel-pockets. With increasing amounts of UAF the WT fragment was preferentially shifted to a higher molecular weight. In lane 4, essentially all of the WT fragment (95%) is bound, while ΔUE is almost not affected (10% decrease of unbound DNA). Only when the WT fragment is quantitatively bound, ΔUE becomes affected (lanes 5+7). Higher UAF concentrations caused precipitation of both DNA fragments and prevented migration into the gel (lane 7). In lane 1-4 the precipitated complex specifically contained the WT fragment, arguing for sequence-specific UAF-DNA interaction (compare DNase I footprinting in Figure 20 & Supplemental Figure 5, 6). The population of UAF-bound DNA migrating into the gel appeared as a diffuse band. Contrast differences at the boundaries of the pockets caused artefacts and prevented direct quantification of the 'precipitated' fractions. UAF showed highly specific binding of the WT promoter DNA and strongly discriminated between the promoter sequence and a mutated sequence which suggests that it plays an important role in Pol I promoter recognition.

2.6.2. Net1 C-term supports UAF DNA Binding Net1-C supports UAF association with promoter DNA *in vitro*

Net1 can associate with two regions on the rDNA gene, the Pol I promoter and NTS1 region. While recruitment to NTS1 region interplays with the replication fork barrier and Fob1 (Huang and Moazed 2003), the recruitment of Net1 depends on association of UAF at the Pol I promoter (Goetze et al. 2010). Net1-C is also required for Net1 and Cdc14 association with the 35S rDNA promoter (Hannig et al. 2019). Moreover, we observed protein-protein interactions of Net1 with DNA binding factor UAF. Therefore, we included Net1 FL and Net1-C proteins in our DNA binding analysis.

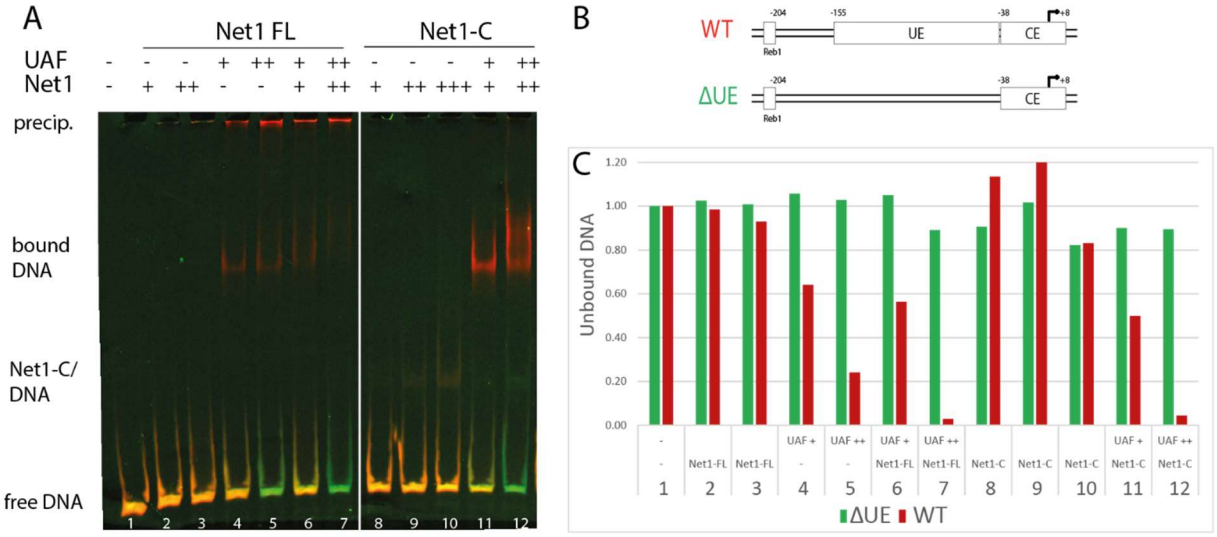

Figure 18: Net1-C supports UAF association with promoter DNA *in vitro*
Electrophoretic mobility shift assay (EMSA). A) Competition between Cy5 labelled WT promoter (red) and Cy3 labelled promoter with mutated UE (green), merged Cy5 and Cy3 channel are shown. Same intensities for both fragments are color-coded in yellow, see input/free DNA in lane 1. Full length Net1, or Net1-C were titrated with or without UAF to DNA fragments. Three distinct populations of DNA were observed: free/unbound DNA, bound promoter DNA in complex with UAF migrating into the acrylamide gel and a species that remains in the pockets and did not enter the gel (precipitated). B) Schematic representation of DNA fragments, WT Cy5, red and ΔUE, Cy3, green C) Quantification of unbound DNA in individual fluorescence channels.

Full length Net1 weakly bound to both templates with slight preference for the WT promoter. Net1-DNA complexes did not migrate into acrylamide gels (lane 2, 3). As shown above (Figure 17) UAF selectively bound WT promoter DNA and a main population did not enter the gel (lane 4, 5). Addition of Net1 FL increased both WT promoter binding and precipitation, although effects from both factors might be independent. Net1-C alone weakly bound to both templates (lane 8-10). Strikingly, when incubated together with UAF, the DNA bound complex separated quantitatively from the unbound fraction in the acrylamide gel (11, 12). The amount of bound WT promoter is slightly increased when Net1-C is incubated with UAF (compare 4, 5 to 11, 12). The pronounced effect of Net1-C on UAF association with promoter DNA was surprising. In Net1-ΔC strains, Pol I recruitment to the 35S rRNA

gene is strongly impaired (Hannig et al. 2019), however promoter occupancy of UAF in ChEC and ChIP experiments was only mildly affected (Achim Griesenbeck, unpublished).

2.6.3. Net1-C stimulates Pol I initiation after assembly of a DNA bound UAF-TBP-CF complex

We tried to dissect Net1-C functions on UAF assembly and Pol I recruitment in a transcription assay using immobilized templates. In this assay, we coupled biotinylated DNA to streptavidin-covered magnetic beads. We assembled Pol I and its transcription factors on immobilized DNA, purified stable interacting complexes and tested the activity of the bound factors (Figure 19). We used WT promoter DNA and compared this to a fragment with mutated UE, but containing the CF binding site CE. On both templates, we assembled PIC complexes and washed away unbound factors. After removing unstable bound factors, transcription reaction could be started by addition of NTPs or the templates could be supplemented with additional factors. In our experimental conditions no stable PIC associated with the templates since almost no activity was observed after the washing steps (lane 1,7). This means that at least one crucial factor for PIC formation and/or Pol I was removed by the washing steps. Addition of Pol I/Rrn3 was sufficient to rescue transcription from the WT promoter, suggesting a stable UAF-TBP-CF complex on the immobilized WT promoter. In contrast to the WT promoter, the template containing CE but with mutated UAF binding site showed no/very weak activity when supplemented with Pol I/Rrn3. Apparently, only some residual CF remained at the DNA and additional CF and Pol I/Rrn3 would be required to commence transcription (Figure 19 B). Thus, UAF/TBP are essential for stable binding of CF to the promoter DNA. This is well in line with results from commitment assays, that showed that DNA-bound UAF complexes did not exchange to competitor templates (Keys et al. 1996; Steffan et al. 1996). Next, we used this stable DNA UAF-TBP-CF complex to test if Net1-C also functions after formation of this DNA-bound platform. Addition of Net1-C together with Pol I/Rrn3 enhanced transcription, arguing for a (partially) UAF independent mechanism of Net1-C stimulation. This agreed with experiments using the minimal initiation system, where Net1 stimulated transcription in absence of UAF (see above (Figure 14) and (Hannig et al. 2019)).

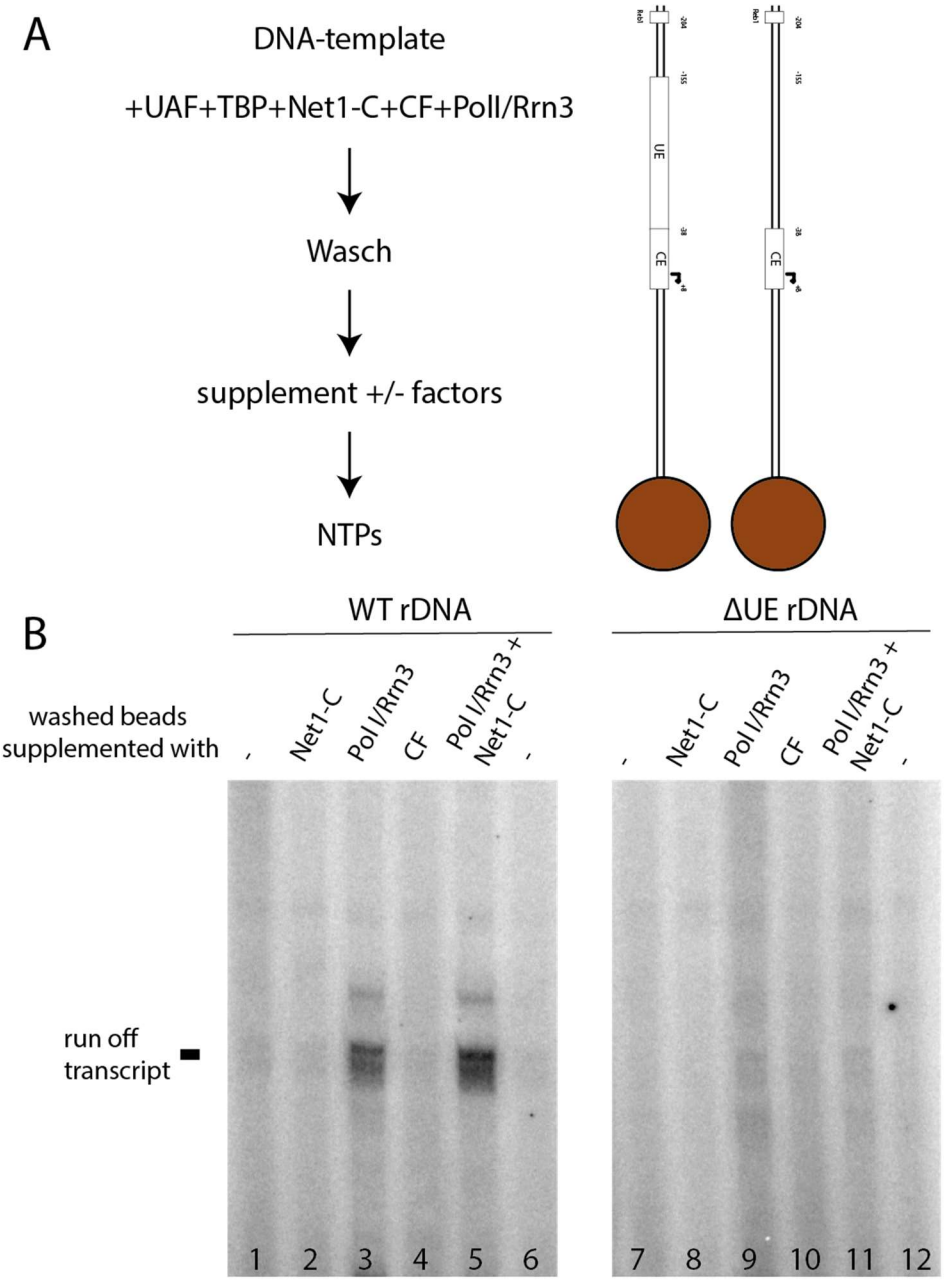
A
DNA-template
+UAF+TBP+Net1-C+CF+PolI/Rrn3
Wasch
supplement +/- factors
NTPs
B
WT rDNA
ΔUE rDNA
washed beads supplemented with
-
Net1-C
Pol I/Rrn3
CF
Pol I/Rrn3 + Net1-C
-
run off transcript
1 2 3 4 5 6
7 8 9 10 11 12
C
PIC complexes on WT promoter
initiation activity
0
1
2
3
4
- - - 1
- - Net1-C 2
- Pol I + Rrn3 - 3
CF - - 4
- Pol I + Rrn3 Net1-C 5
- - - 6

Figure 19: Net1-C stimulates Pol I initiation post UAF association
Immobilized template transcription assays suggest a role of Net1-C after formation of a stable DNA bound UAF-TBP-CF complex; A) schematic representation of the immobilized template assay; PIC complexes were assembled on biotinylated DNA promoter fragments which were immobilized on streptavidin-coupled magnetic beads. Factors not stably bound were removed in wash steps, reactions were supplemented with or without additional proteins before transcription reaction was started by addition of NTPs. B) Autoradiogram of the immobilized transcription assay; DNA bound complexes were purified as described above on a WT (left) or ΔUE promoter fragment (right); purified complexes were supplemented with factors as indicated. C) Quantification of transcription from WT fragment in B); addition of Pol I preincubated with Rrn3 restores initiation activity and can be further stimulated by Net1-C.

2.6.4. DNase I footprinting suggests intimate UAF DNA interactions

Footprinting experiments can be used to identify direct and sequence-specific DNA contacts of transcription factors. Tight interactions with proteins protect DNA from enzymatic digestion, or chemical modification. Digested DNA fragments can be visualized on denaturing urea-page sequencing gels. Proteins associated with DNA protect segments of nucleic acids and leave a characteristic pattern of undigested DNA (footprints). This method was used in earlier studies to determine interactions of the Pol I initiation machinery *in vivo* and *in vitro* (Vogelauer et al. 1998; Bordi et al. 2001; Hontz et al. 2008). Micrococcal nuclease (MNase) and DNase I digestion were used to characterize interactions of DNA-binding factors at the rDNA promoter region *in vivo*. These studies identified DNA contacts at the Pol I promoter and support the assignment of -160 -50/-40 of the UE. The promoter element was initially defined based on *in vitro* transcription reactions (Kulkens et al. 1991; Choe et al. 1992; Keys et al. 1996). Later, binding of UAF lacking Uaf30 subunit was analyzed by DNase I footprint. Complete UAF showed protection from -48 to -107 while UAF devoid of subunit Uaf30 still associates with promoter but lost 10-15 bp protection in the upstream direction (Hontz et al. 2008).

We used DNase I footprinting to closer analyze DNA-protein interactions in our reconstituted Pol I PIC complexes. Sequencing reactions allow the precise mapping of DNase I sensitive sites. Both DNA strands were analyzed in independent reactions. Complexes were assembled as described (5.10) and treated with DNase I (methods 5.10.1). We monitored the quality of complex assembly on native PAGE gels. Therefore, we loaded a part of the binding reaction to a native page gel, prior to DNase I digest (Figure 20 B). Cy3 signal of reference ΔUE DNA was only weakly visible, digestion-pattern resembled in all reaction control digestion without factors. Only Cy5 channel is shown on sequencing gel (Figure 20 A).

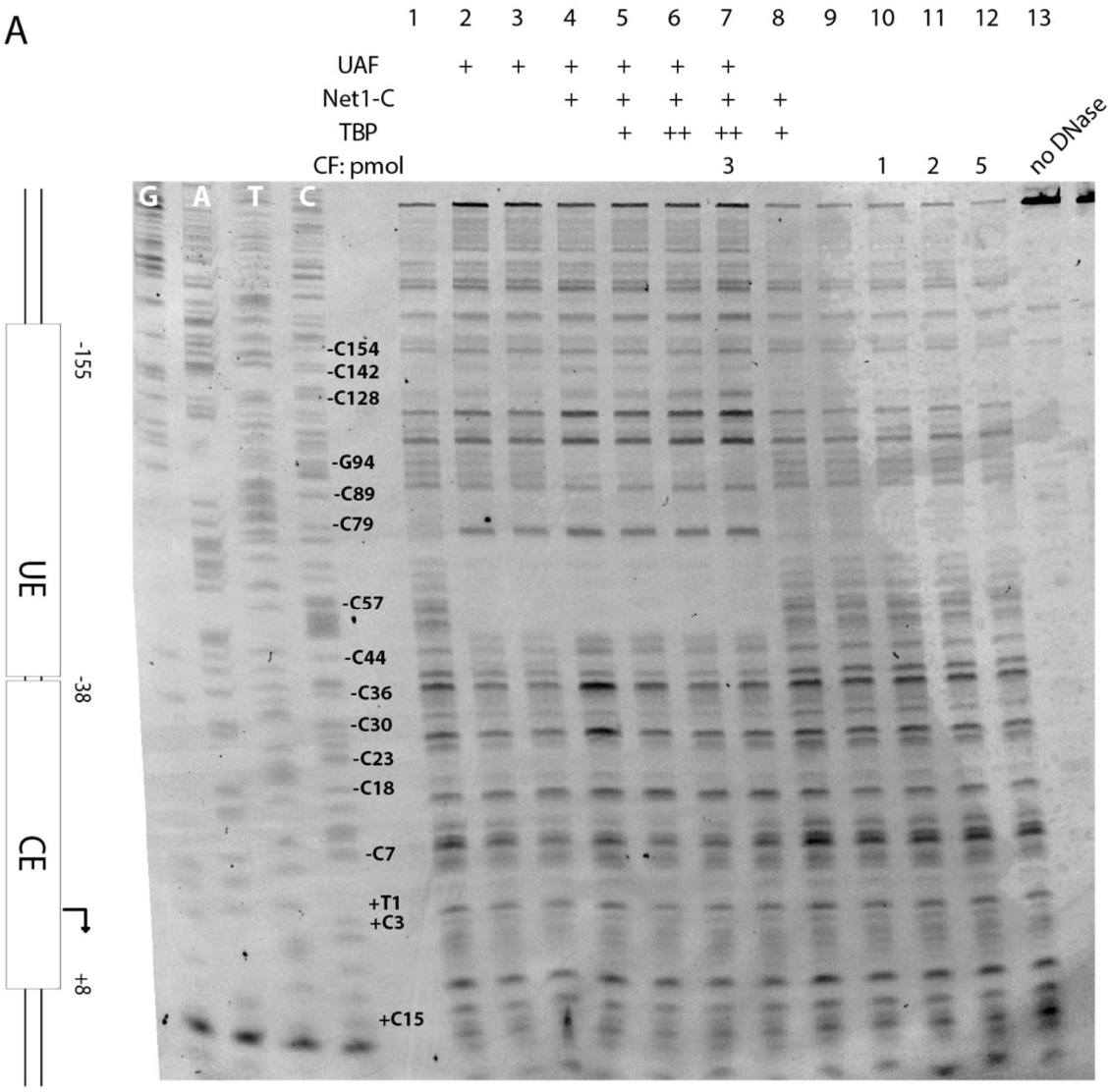

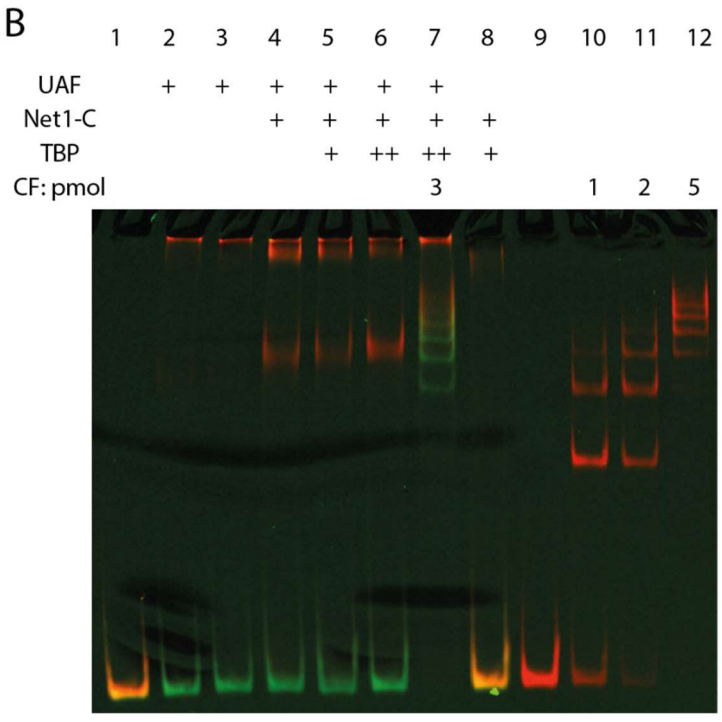

C
TTTCCAAACTCTTTTCG
AACTTGTCTTCAACTGC
TTTCGCATGAAGTACCT
CCCAACTACTTTTCCTCA
C A C T T G T A C T C
CATGACTAAACCCCCCC
TCCCATTACAAACTAAA
ATCTTACTTTTATTTTCT
TTTGCCCTCTCTGTCGCT
C T G C C T T A A C
TACGTATTTCTCGCCGAG
AAAAACTTCAATTTAAG
CTATTCTCCAAAAATCTT
AGCGTATATTTTTTTTCC
A A A G T G A C A

Figure 20: DNase I footprinting suggest intimate UAF DNA interactions
A) 7% UREA-PAGE sequencing gel of DNase I footprinting reaction; on the left a schematic representation of the Pol I promoter region is depicted; sequencing reactions with di-deoxy-nucleotides (ddNTPs) allow precise mapping of DNA fragments, the di-deoxy-nucleotides used in the respective sequencing reaction are indicated on top of each lane. Selected bases are indicated relative to the TSS; DNase I footprinting reaction in lane 1-13, reactions contain factors as indicated and were digested with constant amounts of DNase I. Reactions in lane 1-8 contained Cy5-labelled WT DNA and equal amounts of Cy3-labelled ΔUE DNA, only Cy5 signal is shown. B) EMSA experiments confirmed DNA occupancy. An aliquot of the assembly reaction was loaded onto a native PAGE gel prior to DNA digestion; reactions in lane 1-8 contained Cy5-labelled WT DNA and equal amounts of Cy3-labelled ΔUE DNA, lane 9-13 contained only CF and Cy5 labelled WT promoter DNA. Merged Cy3 and Cy5 channels are depicted C) DNA Sequence of the template strand, the Cy5 labelled oligonucleotide used for amplification and sequencing reactions is highlighted in magenta, the TSS in bold.

UAF alone protected WT DNA strongly between -48 and -92/93 with a hypersensitive site observed at position -76/77. The proximal boundary around downstream -48 was not sharp and may extend to -40 in downstream direction (Figure 20 and Supplemental Figure 5). Addition of Net1-C extended the protected area to -107 in the upstream direction, whereas position -92/93 remained unaffected, and generated a sharper boundary at -48. Further, sites at -37 and -26 were more accessible. In the distal UE we observed additional hypersensitive sites at -107, -122, 132 and -145. Strong protection from -48 to -92 argue for intimate protein-DNA interactions. Sequences more upstream were rather weakly protected but showed fainter signals than in control reactions.

Mapping of DNA interaction sites at the Pol I promoter revealed prominent UAF-interactions. This encouraged us to characterize in detail the binding behavior of UAF and CF to the corresponding promoter cis-elements.

2.7. Cis element analysis

The Pol I promoter was mapped to a relative large stretch of DNA reaching from -155 to +7 relative to the transcription initiation site (Musters et al. 1989; Kulkens et al. 1991; Choe et al. 1992). The CE was assigned to position -38 to +7 relative to TSS. Mutation in 10 bp windows from -1 to -30 abolished transcription in a minimal transcription system (Engel et al. 2017). Higher eukaryotes share a bipartite organization of the Pol I promoter, a core element that is essential and a regulatory upstream control element (Moss 2004; Herdman et al. 2017). Beside this topology, the Pol I promoter shows a remarkable low degree of conservation throughout eukaryotes (Moss et al. 2007). However, it was suggested that intrinsic sequence features like bendability and meltability of the promoters are more important, than the defined nucleotide sequence (Engel et al. 2017).

The UE reaching from -155 to -38 is a relatively long recognition sequence for a transcription factor. Definition of the UE was not totally consistent. Agreement was achieved for the 5' boundary of the Pol I promoter, allocated around -155 (Musters et al. 1989; Kulkens et al. 1991; Choe et al. 1992).

Discrepancies were found in sequences required for UAF binding. 3' deletions extending to -70 caused full reduction in ability to bind UAF in one study (Keys et al. 1996), but larger deletions were required to observe this effect before (Kulkens et al. 1991). 5' mutations to -119 or -91 strongly decreased template activity (Keys et al. 1996). Commitment assays helped to distinguish effects from factor association and template activity. These studies however relied on cell extracts. In these crude fractions other components are present, that could influence the formation of initiation complexes and their activity. Later, in a transcription system reconstituted from purified factors, sequences upstream of -60 were required for high level transcription, but upstream of -76 were dispensable for this activation (Keener et al. 1998).

The determination of the minimal DNA region essential for stable CF, UAF or TBP binding remained unclear. Therefore, we wanted to closer define the minimal DNA sequence required for Pol I dependent transcription initiation. We generated a library containing several Pol I promoter variants including previously described mutants. We mutated promoter sequences to random DNA stretches with the same length, to preserve spacing of sequence elements relative to each other (Figure 21). The abbreviation Δ in the figure legend does not refer to truncations but the exchange of nucleotides, the distance relative to TSS is given in squared brackets. A schematic overview of the promoter-variants is given in Figure 21. We sorted the mutants into three main categories; UE variants, CE variants and mutants which could affect relative positioning of UE and CE.

Additionally, to the initiation activity with our reconstituted *in vitro* transcription system, we were able to systematically assay the DNA-binding capacity of our recombinant transcription factors to the cis-element promoter constructs. Complementary *in vivo* assays were performed by Joachim Griesenbeck and Christopher Schächner to confirm the importance of the DNA sequences in yeast cells. Furthermore, the Chromatin Endogenous Cleavage (ChEC) technique allowed to map factor-binding sites and to study co-dependence of factors and cis-elements. In context with my EMSA analysis the different approaches allow a comprehensive picture about the functional PIC architecture *in vitro* and in vivo. For the EMSA and *in vitro* transcription analyses fluorescently labelled oligonucleotides were designed to amplify a 331 bp dsDNA fragment of the 35 S rDNA gene (position -212 to +119 relative to TSS). The concentration range of UAF to efficiently bind its DNA template and to efficiently stimulate transcription was found to be rather small. Excess of the factor could lead to precipitation of the complex together with DNA and omitted transcription initiation. In order to exclude these effects, reactions with assembled UAF-DNA complexes were split, one part was loaded on native acrylamide gels to ensure the integrity of the complex, the other part was used as template in *in vitro* transcription assays.

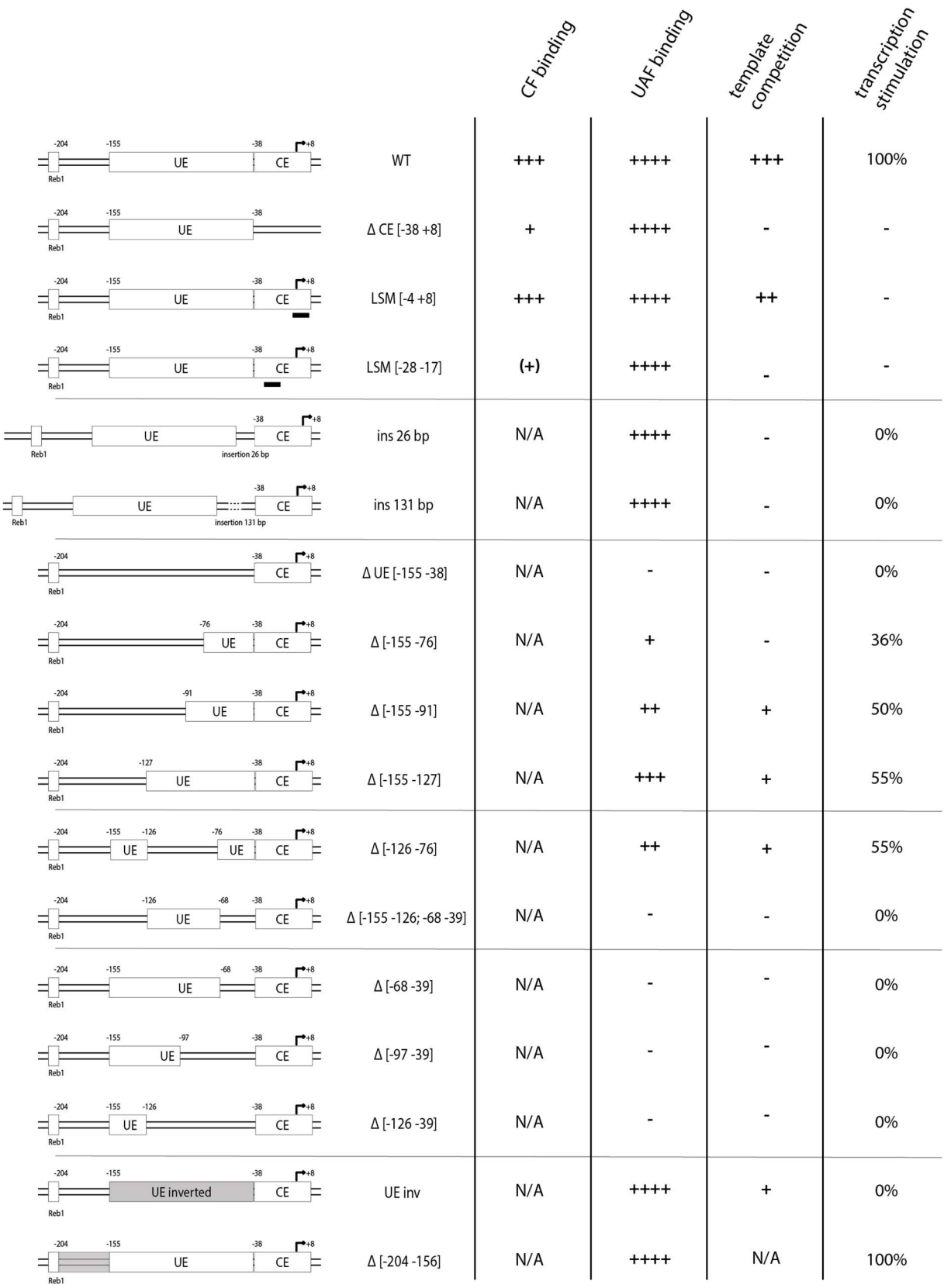

Figure 21: Pol I promoter cis element analysis

Pol I promoter cis elements mutants were analyzed in factor binding and transcription efficiency. From left to the right: schematic representation of the variants; CF binding analyzed in EMSA experiments; UAF binding analyzed in EMSA experiments; template competition ability calculated from reference

templates in initiation assays (+++ < 40%; ++ < 60% + < 80% reduction of reference template in presence of UAF/TBP); transcription stimulation: UAF-TBP dependent stimulation of transcription relative to WT template, individual assays and quantification see Supplemental Figure 7 - 9.

2.7.1. Mutagenesis of the core promoter

Mutation [-8 +4] around the TSS and [-28 -17] completely abolished Pol I transcription in an *in vitro* transcription system (Kulkens et al. 1991). The mechanism causing these initiation defects were not totally clear and we could closer analyze these mutants with our defined *in vitro* experiments. We-analyzed these mutations together with a mutant with a completely randomized CE [-38 +8].

First, in EMSA experiments binding of recombinant CF to WT promoter fragments in competition to mutated CE fragments was compared (Supplemental Figure 7). In control reactions, two WT fragments with either Cy5, or fluorescent labels were bound with similar affinities. At higher CF concentration additional bands appear, probably caused by multimeric factor binding. This multimeric binding events are unspecific and also happened on different substrates like 5S rDNA fragments (not shown). Accordingly, this resulted rather from low-sequence specific binding events, than from a functional oligomerization of CF. The 331 bp DNA fragment would be long enough to accommodate multiple CF molecules. Binding-properties of the TSS mutant [-8 +4] resembled the WT fragment, while the completely randomized CE [-38 +8] showed reduced CF binding compared to the WT fragment. Mutation of 12 bp within the CE [-28 -17] had the strongest effect, about 80% of the Cy5 labelled fragment remained unbound, in contrast to only 20% of the WT competitor (Supplemental Figure 7) UAF efficiently bound to all of these constructs (Supplemental Figure 7, summarized in Figure 21). None of the constructs supported Pol I initiation *in vitro*. Interestingly, the TSS mutant [-8 +4], but not [-38 +8] or [-28 -17] repressed transcription of the reference template in presence of UAF and TBP (Supplemental Figure 9 A). Thus, different steps in promoter engagement might be affected.

2.7.2. UE mutants

Keener and colleges showed that promoter DNA upstream position -76 is dispensable for high level activation in a reconstituted system, while a truncation to position -60 or -38 reduced transcription level to a basal level (Keener et al. 1998). Therefore, we wanted to re-investigate in detail how UE mutations affect promoter binding and how this correlate to transcription initiation in our combined assays.

5’ UE mutations were specifically recognized by UAF

The Pol I promoter was truncated from its 5’ end. In mutation [-204 -156] sequences upstream the UE were mutated, preserving a Reb1 binding site, which could play a topological role *in vivo* and served as a control for correct mapping of the 5’ boundary. Previously, it has been shown that mutations of few base-pairs (8-10) in the UE only mildly affected Pol I activity (Kulkens et al. 1991; Choe et al. 1992). Thus, larger windows of mutations were chosen, truncating the UE from its previously defined upstream end (-155) to -127, -91 and -76. The ability to bind to promoter DNA was compared to a

fragment which has the complete UE mutated ΔUE [-155 -39]. UAF binds constructs – [-204 -156], [-155 -127], and [-155 -91] as selective as WT promoter DNA. [-155 -76] shows higher preference than the ΔUE [-155 -39], but compared to the WT and mutations upstream -91, binding is reduced (Supplemental Figure 8).

Competition experiments of the WT gave further information, which sequences were required for stable and efficient factor binding. Consequently, the 5'mutations which showed efficient binding were also compared to a WT promoter fragment. In a control reaction two WT fragments, (one labelled with Cy5, the other with Cy3) are bound with same efficiency (ratio unbound Cy5/Cy3 ~1). Interestingly, in these reactions UAF associated preferentially with the WT DNA.

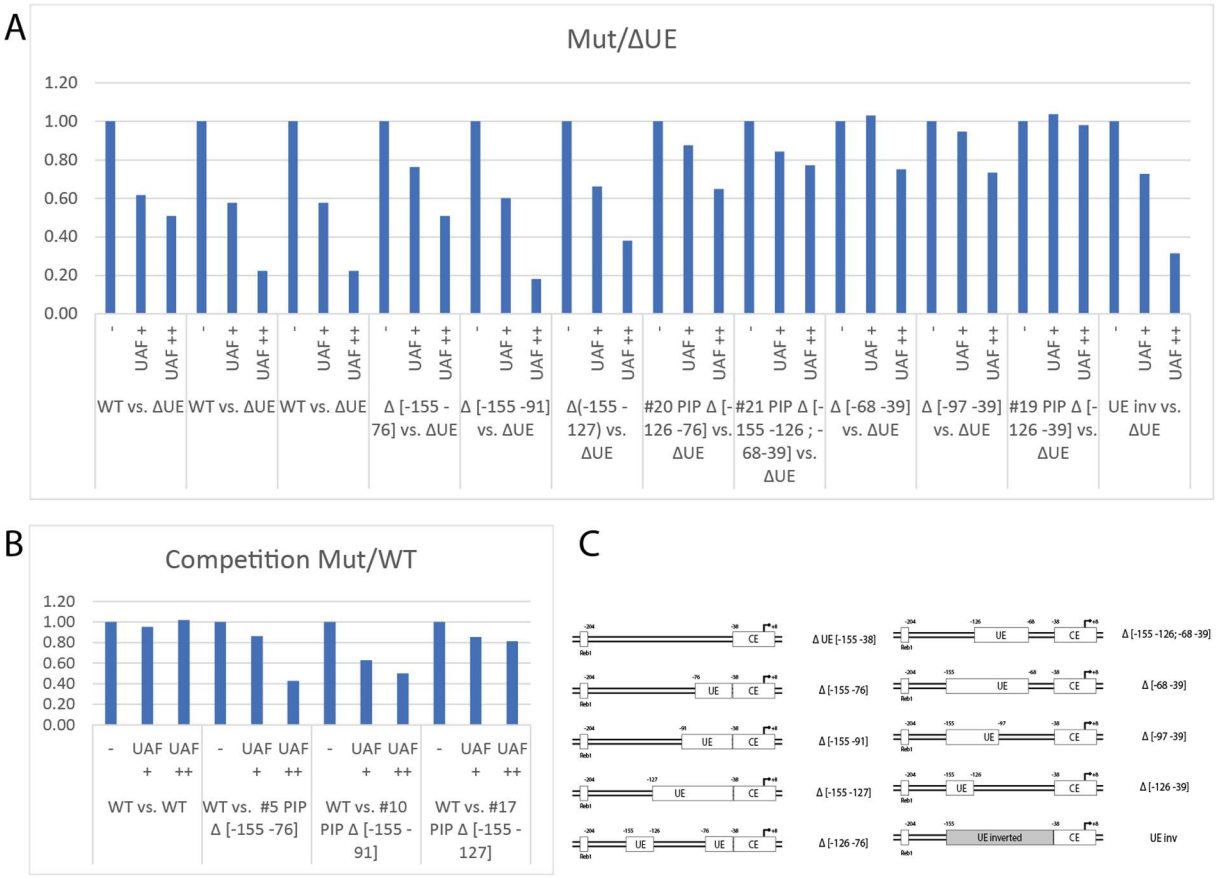

Figure 22: UAF recognizes a proximal UE

Competition EMSA experiments A) Summary of multiple EMSA reactions, for individual reactions see Supplemental Figure 7, 8. Increasing amounts of UAF + (15 nM), ++ (30 nM) were incubated with UE mutants in competition to ΔUE DNA, mutated sequences are given in square brackets; unbound DNA was quantified and ratio of UE mutant over ΔUE is depicted. B) Binding of UE mutants, compared to WT promoter, unbound DNA was quantified and ration of WT over competitor is depicted. C) Schematic representation of UE mutants.

Interestingly, mutants [-155 -127] and [-155 -91] that were efficiently bound by UAF in analogous competition experiments with ΔUE were found to be discriminated against the WT fragment. Binding to [-155 -76] was reduced, but still preferential to the ΔUE competitor in (Supplemental Figure 8).

Compared to the WT promoter, binding of [-155 -91] and [-155 -76] mutated DNA fragments was strongly decreased. Mutations at the UE 5' boundary [-155 -127] have a milder but notable effect.

3' UE mutations strongly reduce UAF recognition

Mutations affecting the 3' end of the UE proximal to the CE, [-126 -39], [-97 -39], [-68 -39] strongly affected UAF binding. Mutant [-126 -39] completely lost preferential UAF binding compared to ΔUE. UAF binding to [-97 -39] and [-68 -39] mutants were impaired to a similar degree. A mutant combining 5' and 3' UE mutations [-155 -127; -68 -39] showed similar defects as the 3' mutants [-68 -39] and [-97 -39] (Supplemental Figure 8, Figure 21). Mutant [-126 -76] associated better with UAF, then the 3' mutants but not as efficient as WT DNA.

Overall, sequences upstream of the CE starting upstream position -38 towards -68/-76 play an important role for sequence specific recruitment of UAF. Sequences from -38 to -91 allow efficient sequence dependent recruitment of UAF. Sequences upstream of -91 stabilized factor association and caused preferential binding.

***In vitro* transcription activity was reduced in all mutants**

Next, we tested the promoter variants in our reconstituted *in vitro* transcription system. A second template, slightly longer, lacking the UE element served as internal reference. Net1-C stabilized UAF-DNA interactions, therefore, all reactions contained Net1-C, and, hence produced in general elevated transcription levels relative to the minimal system. This system allowed to observe mainly two different effects. Firstly, UAF/TBP dependent stimulation of basal transcription levels could be measured. Moreover, activity of the reference template could give information about the formation of a stable committed complex on the other DNA fragment. If a stable complex is established, factors might be sequestered from the reference and its activity decreases. Preassembled UAF-DNA complex was evaluated on native PAGE gels. About 75% of the WT promoter were decorated with the factor, assuring the use of a UAF bound DNA template.

None of the UE constructs was able to activate transcription to WT levels. Only the [-204 -156] mutant efficiently activated transcription, agreeing with the previously defined 5' boundary of the UE around -155 bp (Kulkens et al. 1991; Choe et al. 1992). Activity decreased with the length of 5' mutation. [-155 -127] showed robust but reduced stimulation, [-155 -91] is stronger impaired and [-155 -76] almost completely lost capability of transcription activation (Supplemental Figure 9). This observation is contradictory to previous work, in which sequences upstream -76 were found to be dispensable for stimulation to WT levels (Keener et al. 1998). [-155 -76] showed reduced UAF association in EMSA experiments see (Supplemental Figure 8). However, [-155 -127] and [-155 -91] templates were well decorated with UAF, but with reduced affinity compared to the WT promoter. Interestingly, fragment [-126 -76] containing WT sequences on the 5' and 3' UE boundaries was able to activate transcription, while the individual parts did not, or only at a low level. Consistently [-155 -127; -68-39] preserving WT

sequences in the middle part of the UE did not result in UAF/TBP dependent stimulation. Mutants affecting the 3' UE end of the UE [-68 -39], [-126 -39] [-155 -127; -68 -39] were defective in transcription activation and template competition. Constructs with mutation in the UE were not directly tested for CF binding in EMSA experiments, yet all constructs showed basal transcription activity, which proves CF association.

Relative positioning of UE and CE elements towards each other is important for their functionality

Another set of mutants was generated to examine the position of the UE and CE relative to each other. The UE [-155 -39] was reversed (UE rev), the CE now flanking the originally upstream end of UE. Further, we created insertions of 26 and 131 bp (ins 26 bp; ins 131 bp) between the UE and CE. UAF stably associates with these constructs in EMSA experiments (Supplemental Figure 7, 8). However, no stimulation of transcription initiation was observed from these constructs. As the reference template also remained unaffected, likely no stable committed complex could be formed efficiently. Complementary ChEC analysis by Christopher Schächner and Joachim Griesenbeck revealed that minor amounts of CF were recruited independently of the CE position *in vivo*.

Experiments of the cis element analysis are summarized in Figure 21. Altogether, the experiments were in agreement with early characterization of the Pol I promoter *in vivo* and *in vitro* (Musters et al. 1989; Kulkens et al. 1991). CE mutations abolished Pol I transcription, affecting different stages of initiation. Whereas CF recruitment is affected in [-28 -17] and [-38 +8], TSS mutant [-8 +4] was capable for factor binding and competition, but not initiation.

The activity of the Pol I promoter decreases with length of 5' truncations until position -76. Further, the experiments indicated, that UAF association with the promoter relies on an extended network of protein-DNA interactions. Stable UAF binding was only observed to the WT promoter. Sequence specific binding could be assigned to a proximal upstream element between -91/-76 to -38. In EMSA experiments, distal parts of the UE stabilized interactions, but were less important for promoter recognition. Consistently, none of the mutants enabled RNA production to WT levels in *in vitro* transcription reactions. For enhanced levels of transcription, the proximal UE was required. Transcriptional output from mutated UE constructs correlated well with factor association in EMSA experiments and consequently with the transcription reactions which were challenged with the competitor promoter.

2.8. Functional analysis of UAF and TBP in Pol I PIC

Re-investigation of the promoter elements gave insights how UAF and CF interact with promoter DNA. We aim to better understand how this factor interactions contribute to this high transcriptional output. We could not directly observe interactions of TBP with the Pol I promoter. The TATA-binding protein is essential for UAF dependent transcription stimulation (Steffan et al. 1996; Siddiqi et al. 2001a). A direct interaction of TBP with UAF subunit Rrn9 *in vitro* and in a yeast two-hybrid system was shown

(Steffan et al. 1998). Photo-crosslinking experiments indicated that TBP might use a different DNA interface in Pol I initiation complexes (Bric et al. 2004). Further, a TBP containing complex stimulated basal Pol I transcription initiation in fractionated extracts (Milkereit and Tschochner 1998). On the other hand, conflicting reports on the need of UAF for TBP dependent stimulation were reported (Aprikian et al. 2000; Siddiqi et al. 2001a; Bedwell et al. 2012). Interactions of TBP with PIC components are poorly understood so far. A crosslinking-mass-spectrometry approach tried to map CF-TBP interactions (Knutson et al. 2014), albeit no biochemically stable complex between CF and TBP could be formed so far by us and others (Engel et al. 2017). The requirement of TBP for Pol I transcription initiation has been well described, although the molecular mechanism of this process is not well understood. I wanted to use the newly established *in vitro* assays, to better understand TBP function in Pol I transcription.

2.8.1. Stimulation of Pol I transcription depends on UAF and TBP

Conflicting reports on the need of UAF for TBP dependent stimulation were reported. Whereas UAF was strictly required for TBP dependent stimulation in experiments from the Nomura group (Steffan et al. 1996; Keener et al. 1998; Siddiqi et al. 2001a), UAF was dispensable for TBP-dependent stimulation in disputed reports (Aprikian et al. 2000; Bedwell et al. 2012). We re-investigated this question in our *in vitro* transcription system.

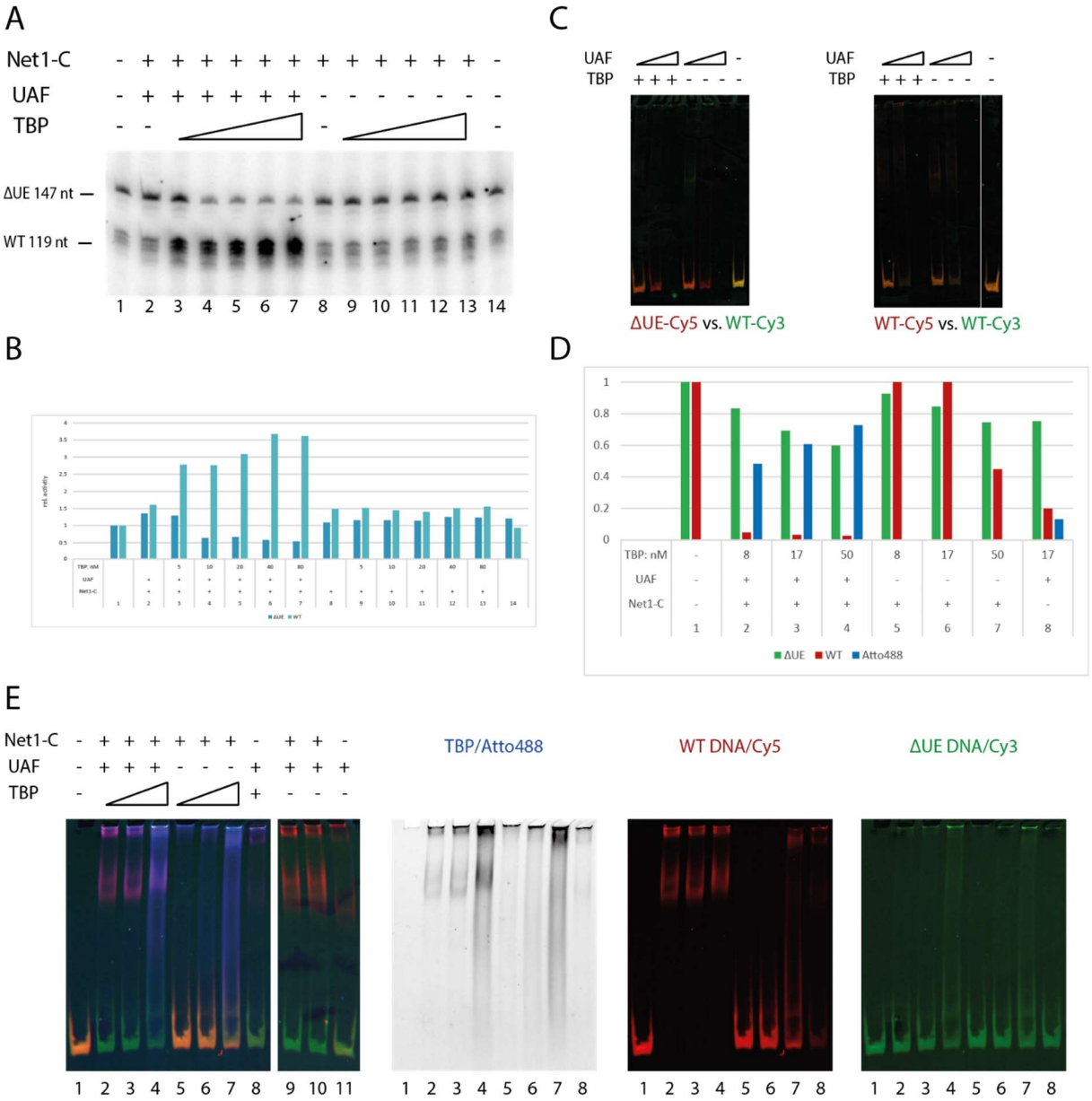

Figure 23: UAF recruits TBP to the Pol I promoter and is required for TBP dependent stimulation
A) Autoradiogram of *in vitro* transcription initiation assay. Increasing amounts of recombinant TBP (5, 10, 20, 40, 80 nM end-concentration) were added to transcription reactions. Reactions contained same amounts of Pol I, Rrn3 and CF plus additional factors as indicated (+); Transcription from WT promoter fragment results in 119 nt run off RNA product, or 147 nt from reference with mutated UE sequence. TBP strictly depends on UAF for transcription B) Quantification of TBP dependent transcription reaction in A, WT and ΔUE are depicted in dark blue and light blue respectively. C) EMSA, TBP does not alter UAF binding properties, increasing amounts of UAF were incubated in presence or absence of TBP with fluorescently labelled promoter fragments. Left WT-Cy3 (green) ΔUE-Cy5 (red); right two WT fragments, WT-Cy3 (green) WT-Cy5 (red), merged channels are depicted. D) EMSA experiment shows association of TBP together with UAF and WT DNA. Quantification of fluorescence signals in E atto488-TBP (blue); WT DNA Cy5 (red) ΔUE DNA Cy3 (green) E) native PAGE gel of EMSA experiments. Increasing amounts of atto488 labelled TBP (8, 17, 50 nM) were incubated with fluorescent DNA templates in presence or absence of UAF. Factor UAF and Net1-C were added as indicated; panels from left to right: Left panel: merged fluorescence signals atto488 (blue); WT DNA Cy5 (red) ΔUE DNA Cy3 (green); for better visualization atto488 TBP is depicted in grey, WT-Cy5 labelled DNA in red and ΔUE-Cy3 in green, control reactions without TBP lane 9-11 are not shown

We titrated increasing amounts of recombinant TBP to reactions with or without UAF (Figure 23, A). The basal level (lane 1, 14) of transcription was stimulated by ~50% by Net1 (8). Addition of UAF to the reaction did not further stimulate the activity (lane 2), only after addition of recombinant TBP transcription initiation from the WT promoter was stimulated (lanes 3-7). Correlating with UAF/TBP dependent activation of WT transcription, we observed decreased transcription from the ΔUE reference template. 5 nM TBP were sufficient for robust stimulation from WT promoter, but not for repression of initiation from the ΔUE reference (3). This repression was observed at higher TBP concentrations (4-7), which stimulated transcription from the WT template to slightly higher levels. In contrast, reactions lacking UAF were largely unaffected by addition of TBP (8-13). We neither observed stimulation of the WT or reference template, nor observed inhibition of ΔUE reference transcription. Thus, this experiment supports the observations by Nomura and co-workers, who reported that TBP functions in Pol I transcription completely depend on UAF.

2.8.2. UAF-TBP interaction is independent of DNA

Next, we wanted to better understand how UAF and TBP cooperate to enhance transcription. In fractionated cell extracts a salt stable TBP containing complex of about 240 kDa stimulated basal Pol I transcription initiation (Milkereit and Tschochner 1998). However, TBP was reported to be absent in *ex vivo* purified UAF complexes, but required for its activity (Steffan et al. 1996; Steffan et al. 1998). Further, direct interaction of TBP with UAF subunit Rrn9 *in vitro* and in a yeast two-hybrid system was shown (Steffan et al. 1998). Therefore, we wanted to find out under which conditions the UAF-TBP complex can be formed.

We purified recombinant UAF complex in large amounts and used this to analyze UAF-TBP interactions. Co-expression of TBP with UAF in insect cells resulted in sub-stoichiometric amounts of TBP, therefore we reconstituted UAF-TBP interactions with recombinant TBP, expressed in *E. coli*. We preincubated purified UAF complexes with recombinant TBP and performed analytical size exclusion chromatography in high conductivity buffer and compared them with the UAF complex without TBP (apo-UAF complex). An extra protein band, corresponding to TBP appeared (Figure 11 A) and we observed a slight shift towards a higher molecular mass (Figure 11 B). We estimated a molecular weight of 360 kDa for UAF alone and 440 kDa for UAF in complex with TBP (Figure 11 C). The remaining 75 kDa could correspond to three TBP molecules, but for this rather small sub-unit, stoichiometry estimation might not be reliable. Remarkably, UAF-TBP interaction is solid in absence of any (promoter) DNA and stable on SEC column in high conductivity buffers. Further, we observe intense protein-protein crosslinking of TBP in promoter assembled complexes. Thereby, TBP seems to associate with various UAF components (Supplemental Figure 3, 4).

2.8.3. UAF recruits TBP to the rDNA promoter

The Pol I promoter doesn't contain a canonical TATA-recognition sequence. Stimulation of transcription initiation inter-depends on UAF and TBP. We performed EMSA experiments to examine, whether TBP might influence binding of UAF to the rDNA promoter or vice versa. We incubated UAF with fluorescently labelled promoter fragments in presence or absence of TBP. TBP appeared not to affect binding properties of UAF under chosen conditions. We detected neither more specific binding, nor a higher affinity in the presence of TBP (Figure 23 C). Albeit we found activation of transcription from these fractions (see Figure 23, A), we could not directly proof presence of TBP in the shifted DNA-protein complex in this assay. Resolution of the native acrylamide gel didn't allow us to unambiguously distinguish UAF from UAF+TBP on the DNA template. To analyze how TBP is targeted to the Pol I promoter, we performed EMSA experiments using fluorescently labelled TBP (atto488, generous gift from Prof. Grohmann). TBP could bind the Pol I promoter independently of UAF (Figure 23 E, lane 5-7) in a nonspecific way. In fact, minor amounts of both the WT promoter sequence and the reference with mutated UE are bound at low TBP concentrations (8 nM; 17 nM, sufficient for robust stimulation). Increasing the TBP (50 nM) concentration we quantified a slight preference for the WT sequence. UAF at the chosen concentration decorated 95% of the WT promoter fragments, but less than 10% of the ΔUE reference, suggesting specific UAF binding and high UAF occupancy. When titrating TBP together with UAF to the reactions, we observed prominent co-migration of the atto488-TBP signal (blue, violet in merged channels) together with the UAF-WT-DNA band (Figure 23 E). This co-localization prominently occurred at lower TBP concentrations, that are sufficient for efficient transcription stimulation (see Figure 23, A). Although this assay didn't allow to quantify the portion of recruited TBP it gave a good impression for the selective recruitment of TBP in the presence of UAF.

2.8.4. UAF-TBP recruit CF to the Pol I promoter

UAF stably associates with the rDNA promoter, while other initiation factors dissociate after transcription initiation. We observed high sequence specific binding of UAF, while CF showed more promiscuous binding, further I could reconstitute high levels of transcription *in vitro* in the presence of UAF. For basal Pol I initiation, TBP and UAF are not essential (Keener et al. 1998). In a simple model UAF might act as a stably associated binding platform, that helps to increase local concentration of CF to enable Pol I transcription initiation. To test this, we titrated CF amounts in our reconstituted initiation assay. UAF, TBP and Net1-C were preassembled on promoter DNA for 30 minutes. Increasing amounts of CF were added, preincubated Pol I and Rrn3 was supplemented and reactions incubated for another 30 minutes, before transcription reaction was started with buffer containing NTPs.

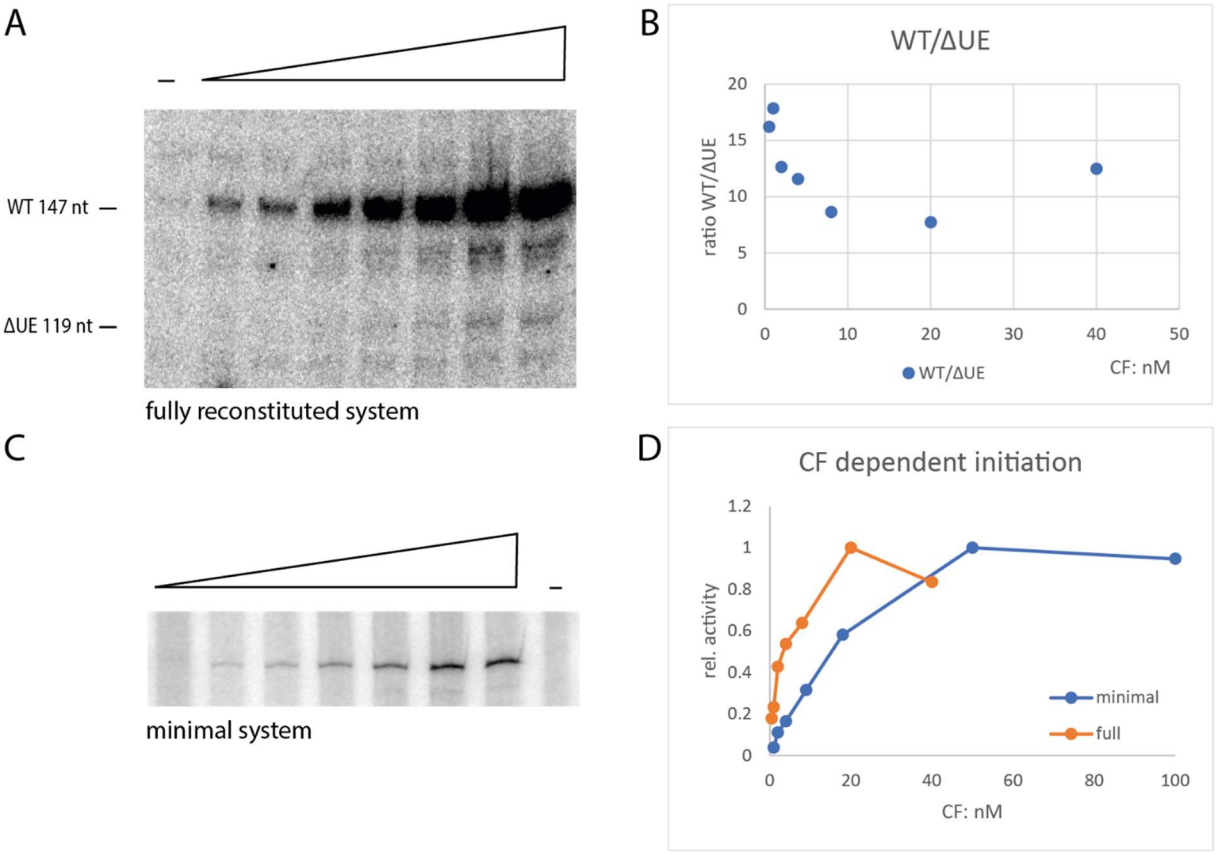

Figure 24: UAF/TBP enhance CF recruitment to the promoter
A) Fully reconstituted *in vitro* transcription assay, including Net1-C with increasing CF amounts (0,5; 1; 2; 4; 8; 20; 40 nM). Expected length of run-off transcript from WT (147 nt) and ΔUE (119 nt) template are indicated. WT template is efficiently transcribed under low CF concentrations. B) ratio of transcription from WT over ΔUE transcription in A) was blotted against CF concentrations. At low CF concentrations ≤ 4 nM the ratio is increased. C) minimal *in vitro* transcription assay, with increasing CF amounts (1; 2; 4; 9; 18; 50; 100 nM) reveals optimal CF concentration around 50 nM D) maximal CF dependent activity of fully reconstituted system from WT template and minimal system highlight efficient UAF/TBP dependent transcription at limiting CF concentrations and a reduced optimal CF concentration.

UAF allowed robust transcription at low levels (0,5 -1 nM) of CF from the WT promoter (Figure 24 A). UAF dependent commitment to the WT promoter was not absolute under the chosen conditions, at limiting CF concentrations, a free CF population exists, that allowed initiation from the ΔUE template. We blotted the ration of initiation rates from WT over ΔUE templates against the CF concentration. The ratio should be constant, if CF is recruited with similar affinity to both templates. Interestingly, we found increased values especially at low CF concentrations. The WT template is preferentially used, which would argue for a UAF dependent preference. Under higher CF concentrations (> 4 nM), the ratio stayed relatively constant. Transcription from the ΔUE template was relatively weak why quantification can be error prone. Further, factors might be sequestered from the reference template. Therefore, we compared initiation rates independently in a minimal transcription system (Figure 24 C). The optimal amount of CF is reduced in the fully reconstituted initiation system and higher activity is found at low CF concentrations in UAF/TBP dependent reactions (Figure 24 D). The minimal system

showed maximal transcription rates around 50 nM CF, in the fully reconstituted system maximal activity was already achieved using 20 nM CF.

Summarized, high levels of Pol I transcription depended on UAF and TBP. UAF and TBP can interact independently of DNA. Whereas presence of TBP did not strongly affect DNA binding properties of UAF, TBP preferentially associates with UAF decorated promoter templates. Together, UAF and TBP efficiently recruit and stabilize CF at the Pol I promoter. Moreover, these factors may have functions beyond recruitment of CF, as transcription levels are enhanced at saturated CF levels.

2.9. Structural basis of RNA polymerase I pre-initiation complex formation and promoter melting

Pol II and Pol III use related mechanisms to initiate transcription, the process substantially diverges in Pol I, reviewed in (Khatter et al. 2017; Jochem et al. 2017; Engel et al. 2018). A minimal system sufficient for Pol I initiation consists of promoter DNA, containing the CE with the CF binding site, CF and the initiation competent Pol I form associated with Rrn3. High resolution structures of this core complex could be determined, giving insights in the complex architecture, DNA contacts and factor Pol I interactions and suggested an unique mechanism for Pol I initiation, relying on intrinsic promoter properties as bendability and meltability (Engel et al. 2017; Han et al. 2017; Sadian et al. 2017). These studies are based on an artificially stabilized ternary complex with a preformed mismatched transcription bubble and an annealed RNA oligomer, resembling a post-initiated state, referred as ‘initially transcribing complex’ (ITC). This experimental approach originates from the analysis of Pol II elongation complexes (ECs), preventing heterogenic sample conformations and making use of the tight DNA/RNA hybrid association with the polymerase (Gnatt et al. 2001; Kettenberger et al. 2004). These strategy revealed late initiation intermediates, leaving room for speculation with regard to the functional roles and temporal classification of the analyzed conformations and can be prone to artefacts as in one approach the essential factor Rrn3 is absent (Han et al. 2017). During the process of transcription initiation, Pols are recruited to their promoters by a set of general transcription factors, forming a ‘closed complex’ (CC). Melting of double-stranded DNA establishes an ‘open complex’ (OC) which can start RNA synthesis and transitions to a ITC and is finally transferred in a processive elongation complex (EC) reviewed in (Engel et al. 2018).

In a complete Pol I initiation system, UAF cooperates with TBP to stabilize CF association at the rDNA promoter. Together with Net1-C Pol I initiation rates could be increased up to 35-fold (

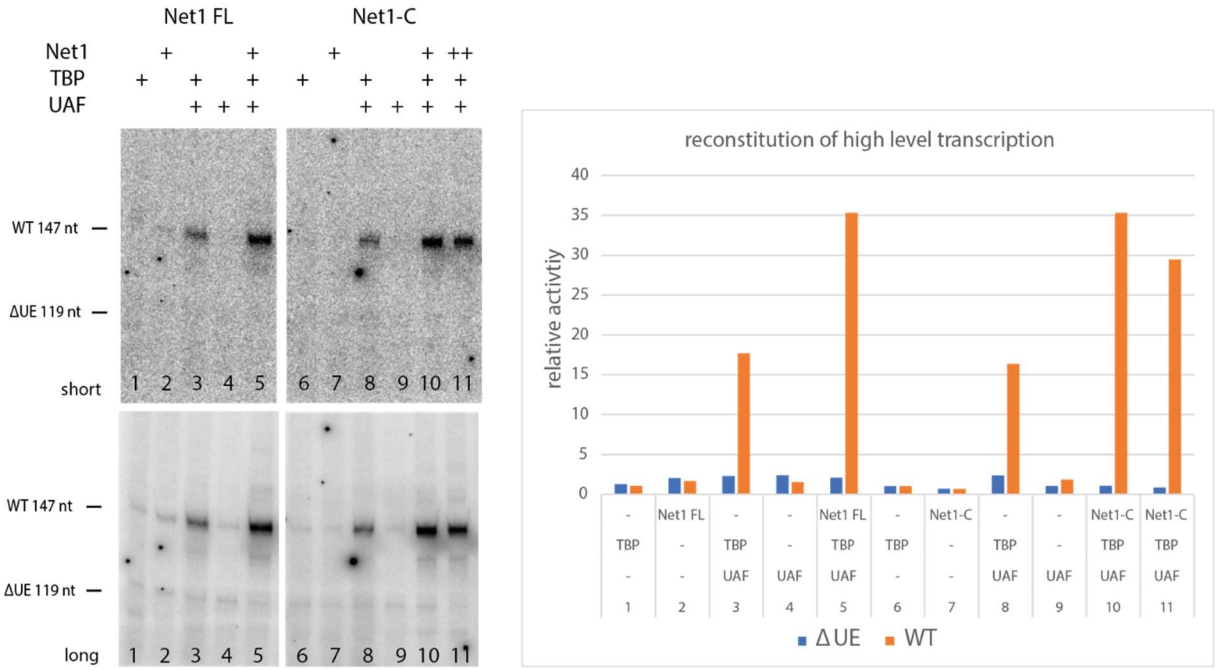

Figure 14) (Keener et al. 1998; Hannig et al. 2019). However, structural data of such a complete initiation system are lacking. We used the complete initiation system to analyze early steps in Pol I initiation and determined the structure of an early intermediate Pol I PIC, which gave insights into Pol I PIC formation and the mechanism underling promoter melting. These results were recently published (Pilsl and Engel 2020).

2.9.1. A truncated DNA scaffold is defective in Pol I initiation

We truncated the dsDNA template on its downstream edge at position +8, maintaining all important promoter cis elements, including the TSS, but preventing DNA contacts with Pol I clamp core and jaw domains. Avoiding downstream Pol I contacts might eventually favor a Pol I closed-complex-conformation, which would be a missing part of the Pol I initiation puzzle. We tested the truncated template in our *in vitro* transcription assay, and compared it to a longer +28 template (see schematic representation). We did not observe RNA synthesis from the truncated template, neither the minimal nor the complete initiation system is active. In contrast, RNA is produced from the longer template in the minimal system and at elevated levels in presence of Net1-C and in the complete reaction. Omitting the downstream DNA contacts abolished Pol I transcription and encouraged us to structurally characterize this effect.

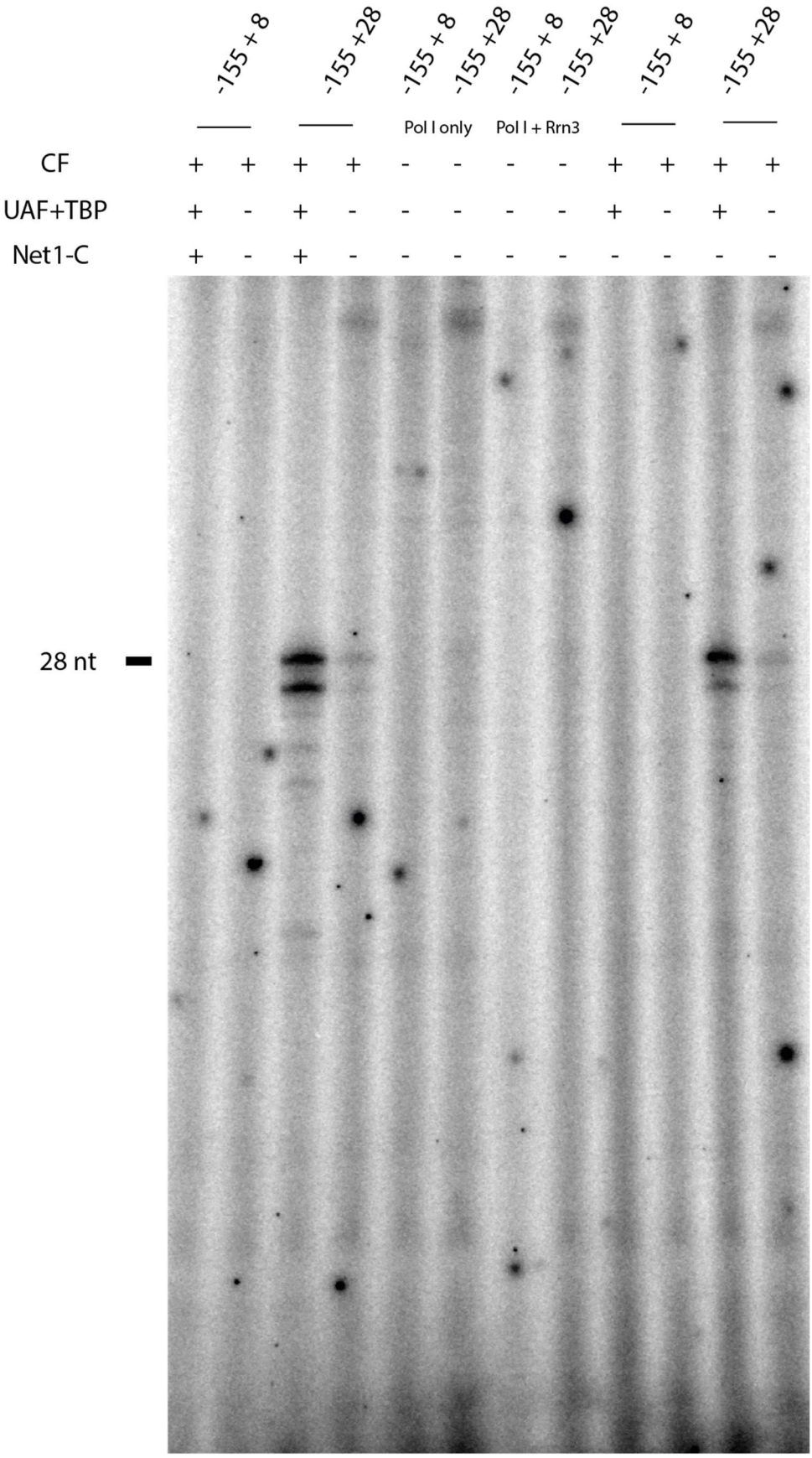

Figure 25: Truncated scaffold is defective in Pol I initiation
20% UREA PAGE gel of *in vitro* transcription reactions of different DNA templates. Positions relative to TSS are indicated above reaction lanes. Reactions contained Pol I + Rrn3 and were supplemented with

factors as indicated. No activity was observed from template –155 + 8, the longer –155 + 28 template allowed basal and enhanced levels of transcription.

2.9.2. Pol I initiation components assemble on downstream truncated promoter DNA to a stable complex

We assembled UAF, TBP, CF, and Net1-C, on a short double-stranded promoter DNA (-155 +8). Together with Pol I preincubated with Rrn3, we tried to reconstitute the complete Pol I PIC complex *in vitro.* Analysis on size-exclusion chromatography revealed an almost stoichiometric complex containing UAF, TBP, CF, Pol I and Rrn3 (Supplemental Figure 10 A). The polymerase apparently associated stably with the UAF/TBP/CF DNA-platform, even without its downstream DNA contacts.

To stabilize the complex for cryo-grid preparation, the complex was crosslinked with 1 mM BS3 prior to size-exclusion chromatography, peak fractions were applied on carbon-coated Quantifoil grids and plunged into liquid ethane to obtain frozen hydrated complexes (methods 5.8.6). 4.088 molecular movies were recorded on a Cs-corrected Titan Krios microscope (FEI), operated at 300 kV equipped with a 4k × 4k Gatan K2 summit direct electron detector (Gatan) in super-resolution mode at a nominal magnification of 105.000x. Following pre-processing, we started with 311.557 initial molecular images, performed two-dimensional (2D)- and three-dimensional (3D)-classification in RELION (Zivanov et al. 2018), and selected a total of 122,099 particles. These particles were refined to a final cryo-EM reconstruction with an overall resolution of 3,5 Å (Methods; Supplemental Figure 10). The reconstructions showed and early intermediate Pol I PIC state (eiPIC, Figure 26). The cryo-EM density clearly revealed secondary structure features for the entire particle and side chain orientations in most regions (Figure 26 C and Supplemental Figure 11 A-F)).

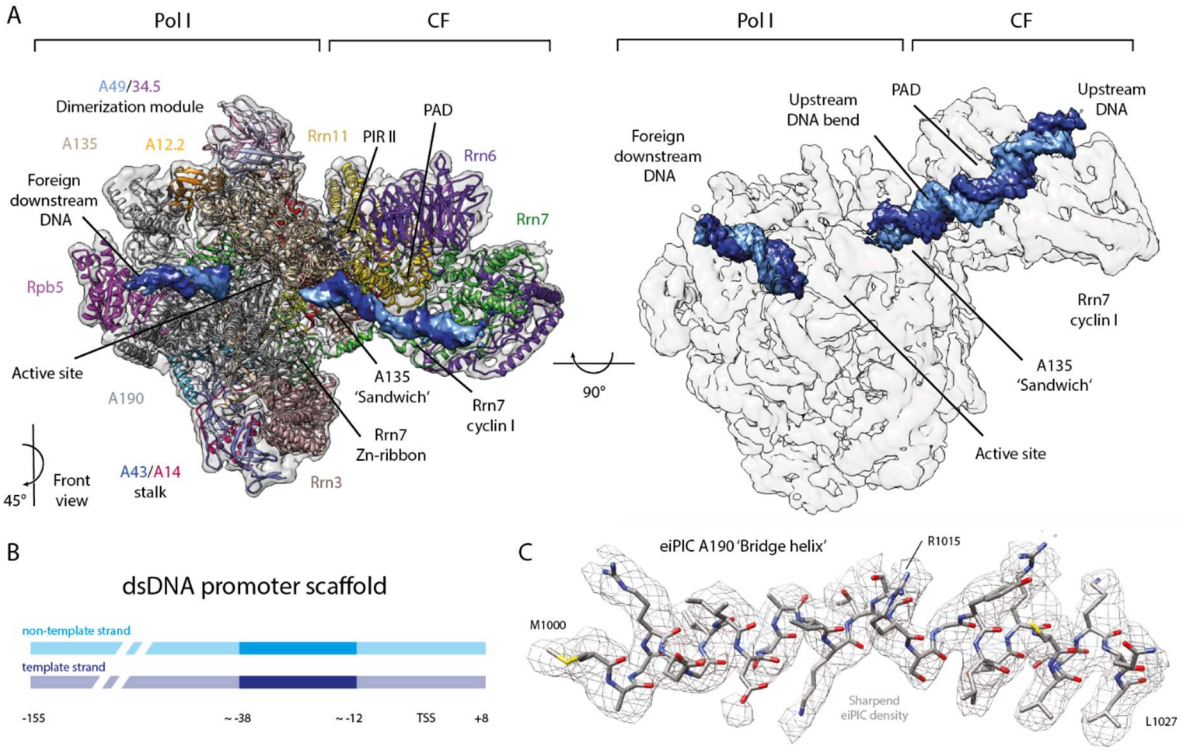

Figure 26: Cryo-EM reconstruction of a Pol I early intermediate PIC.
A) Overview of the Pol I eiPIC cryo-EM reconstruction at 3.5 Å resolution (unsharpened; transparent gray envelope) overlaid with the PDB model (colored ribbon) and DNA (space filing). The right panel shows transparent density (gray) for protein components and solid density for the DNA path (template strand in blue and non-template in light blue). PAD promoter-associated domain (of Rrn11); PIR polymerase interacting region (of CF). B Schematic representation of promoter dsDNA used for PIC assembly, densities observed in the eiPIC reconstruction are highlighted in blue and light blue for template strand and non-template strand, respectively. C Atomic model of the bridge helix in subunit A190 overlaid with sharpened eiPIC density (gray mesh) indicates residue orientations.

2.9.3. Architecture of the early intermediate PIC (eiPIC)

We could allocate template and non-template DNA strands, Pol I, CF subunits, and Rrn3. Despite protein–protein crosslinking, TBP, UAF, and Net1-C remained flexible, and we could not detect distinct EM-densities for them. However, in the very same elution fractions we detected protein-protein crosslinks of all PIC components including UAF, TBP and Net1-C, by mass-spectrometry (see paragraph 2.4). These components seemed to stabilize CF in the Pol I PIC, a similar effect was observed by the co-activator 'mediator' in context of a Pol II PIC (Plaschka et al. 2016). After manual model building and real space refinement we obtained a model of high quality (Supplemental Figure 11). Upstream DNA was well-ordered between CF-interacting regions and entry into the Pol I active center cleft. Following the canonical DNA-path further downstream, however, no density was visible around the active center itself, but ≥12 well-defined base-pairs could be placed on the downstream edge between bridge helix and the clamp-head/jaw domains, even though our scaffold should not extend this far. Contacts of downstream DNA with the enzymes clamp core and jaw domains are conserved (Bernecky et al. 2016) and likely, the highly charged region is bound by foreign DNA or the far upstream end of our scaffold. A similar effect was observed for patches of the nucleosome, after transcription by Pol II 'peeled' off supercoiled DNA (Kujirai et al. 2018).

Rrn3 was tightly bound to Pol I 'stalk' and 'dock' subdomains as previously observed (Pilsl et al. 2016a; Engel et al. 2016). CF binds the Pol I core via its polymerase interacting regions (PIR) similar to ITC conformations (Engel et al. 2017; Han et al. 2017; Sadian et al. 2017). The quality of the cryo-EM density allowed us, to rebuild the CF subunits Rrn6, Rrn7 and Rrn11, consolidating divergent assignments in the crystal structure PDB 5O7X) and an ITC EM-based model (PDB 5W66, (Han et al. 2017). In contrast to inactive Pol I (Engel et al. 2013; Fernández-Tornero et al. 2013; Pilsl et al. 2016a), the 'expander' and 'connector' subdomains were flexible and the central bridge helix was refolded in the eiPIC (Figure 26 C). The C-terminal domain of subunit A12.2 showed only residual density in the funnel domain of subunit A190 (Supplemental Figure 11 B). Our eiPIC reconstruction showed strong density for the A49/A34.5 dimerization and A34.5 C-terminal tail domains (Supplemental Figure 11 E), indicating that the heterodimer is constitutively attached. The tWH and linker domains of subunit A49 are detached in the eiPIC.

2.9.3.1. CF DNA contacts

The eiPIC density allowed the construction of a CF model, which we found to resemble the overall ITC conformation. To define the structural changes that take place upon promoter recruitment, we compared the architecture of CF in free (PDB 5O7X) (Engel et al. 2017) and promoter-engaged eiPIC conformation (Supplemental Figure 12). CF module I and II retracted from each other by up to 12 Å upon binding of the CE promoter sequence. This retraction lead to the exposure of positively charged residues that are now free to engage the phosphate backbone (Supplemental Figure 12 A, B). These DNA-binding regions lie within the Rrn11 promoter-associated domain ('PAD') and the cyclin domains of Rrn7. The same regions engage the DNA in ITCs (Engel et al. 2017; Sadian et al. 2017) and have been described in detail in late ITCs devoid of Rrn3 (Han et al. 2017). Remarkably, the Rrn7 residues involved in DNA-binding were not conserved within TFIIB or Brf1, which share a similarity in their overall fold (Knutson and Hahn 2011; Naidu et al. 2011; Knutson et al. 2014) and would clash with TBP in canonical TFIIB-TBP or Brf1-TBP complex (Engel et al. 2017; Vorländer et al. 2018; Abascal-Palacios et al. 2018).

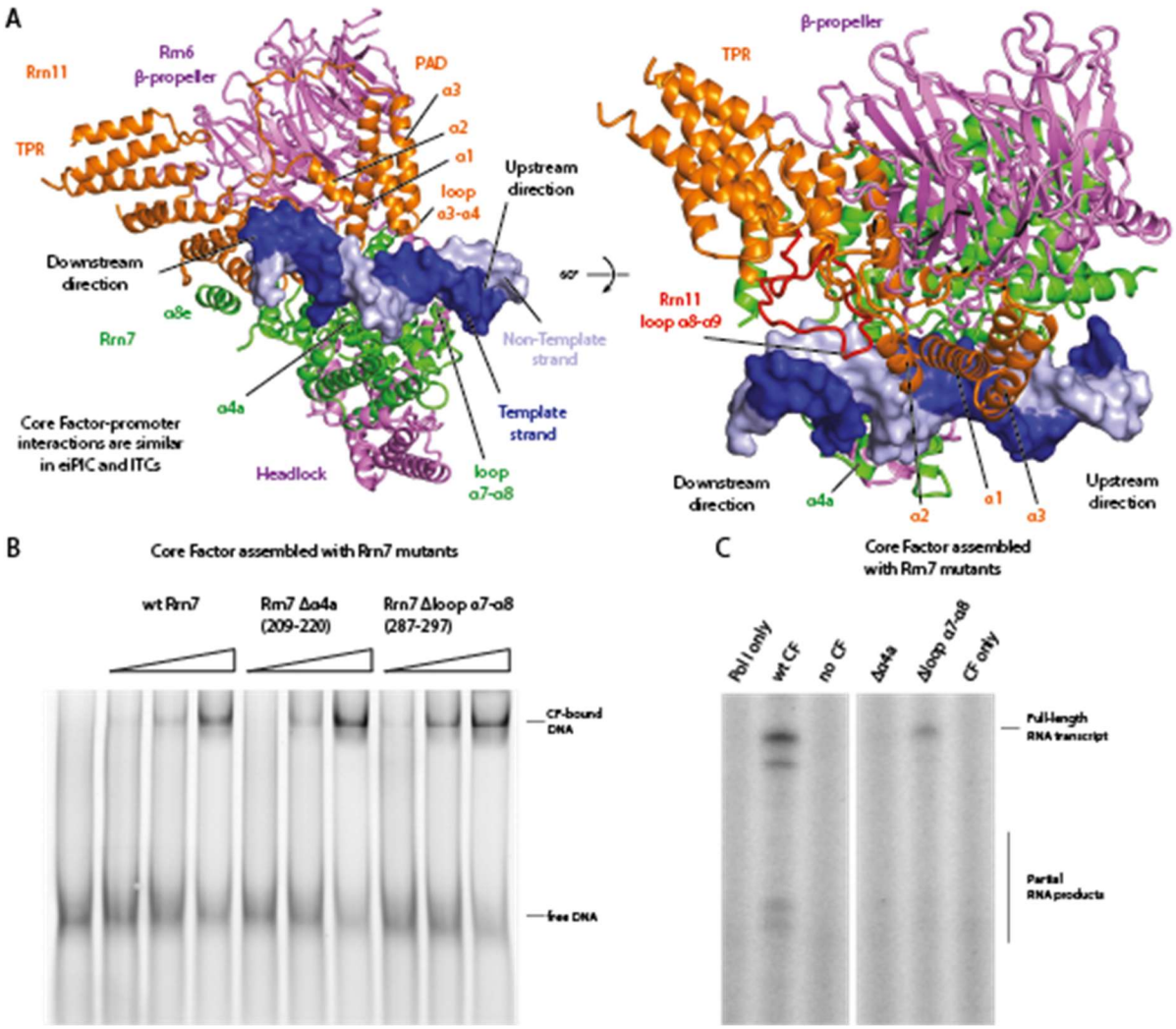

Figure 27: CF – promoter interactions in eiPIC

A Model of promoter-bound CF in the eiPIC. The same regions of Rrn7 and Rrn11 contribute to promoter phosphate backbone interactions compared to ITC reconstructions. B Electrophoretic

mobility shift assay (EMSA) shows that wild-type CF interacts with double-stranded promoter DNA (0.25 pmol, 0.5 pmol, and 1 pmol CF added). Mutation of Rrn7 (Δα4a and Δloop α7-α8) does not impair promoter-DNA association. C In contrast to DNA binding, initiation efficiency of CF assembled with Rrn7 mutants Δα4a and Δloop α7-α8 is impaired (promoter-dependent *in vitro* transcription assay from a minimal scaffold)

Comparison of free and promoter-engaged CF also showed that the Rrn7-specific helix α4a in the N-terminal cyclin domain shifts and was inserted into the minor groove of the CE promoter DNA, while loop α7-α8 in cyclin II became well-structured and contacted the major groove further upstream upon eiPIC formation (Figure 27 A). Thereby, the distal upstream DNA-path was modified towards the C-terminal domain of Rrn7 and the β-propeller-domain of Rrn6. Thus, promoter binding by Rrn7 specific regions on one face and by the TFIIB-unrelated CF subunit Rrn11 on the opposite face tightly squeeze the DNA. This may explain why the basal Pol I initiation system does not require TBP association opposite of the Rrn7 cyclins. To address the importance of these residues, we constructed CF mutants with deletions in helix α4a and in loop α7-α8. Both could still associate with promoter DNA (Figure 27 B), but showed defects in basal initiation *in vitro* (Figure 27 C). Engagement of these regions may therefore be important to induce a specific DNA conformation required for Pol I recruitment or promoter melting.

2.9.3.2. The Pol I 'sandwich' region is important for PIC formation.

Previously, a Pol-I-specific proximal upstream promoter-binding region was described. This region consists of loop α11a-α12 (residues 452–456) and the loop β28-β28 (residues 815–818) in the protrusion and wall domains of Pol I subunit A135, respectively (Engel et al. 2017). In the eiPIC, a positively charged loop (892–895, wall domain of subunit A135) re-orients towards the promoter DNA, contributing additional phosphate-backbone interactions (Figure 28), similar to other ITC/PIC structures, termed 'sandwich' region (Han et al. 2017; Sadian et al. 2017; Sadian et al. 2019). These promoter interactions are all specific to Pol I, because the residues are not conserved in Pol II (Cramer et al. 2001) and III (Hoffmann et al. 2015). Furthermore, DNA is occluded from the corresponding region in Pol II and III PICs by the N-terminal cyclin domains of TFIIB (Plaschka et al. 2015; Dienemann et al. 2019) and Brf1/Brf2, respectively (Vorländer et al. 2018; Abascal-Palacios et al. 2018; Gouge et al. 2015). This suggested a Pol I specific mechanism for promoter interaction.

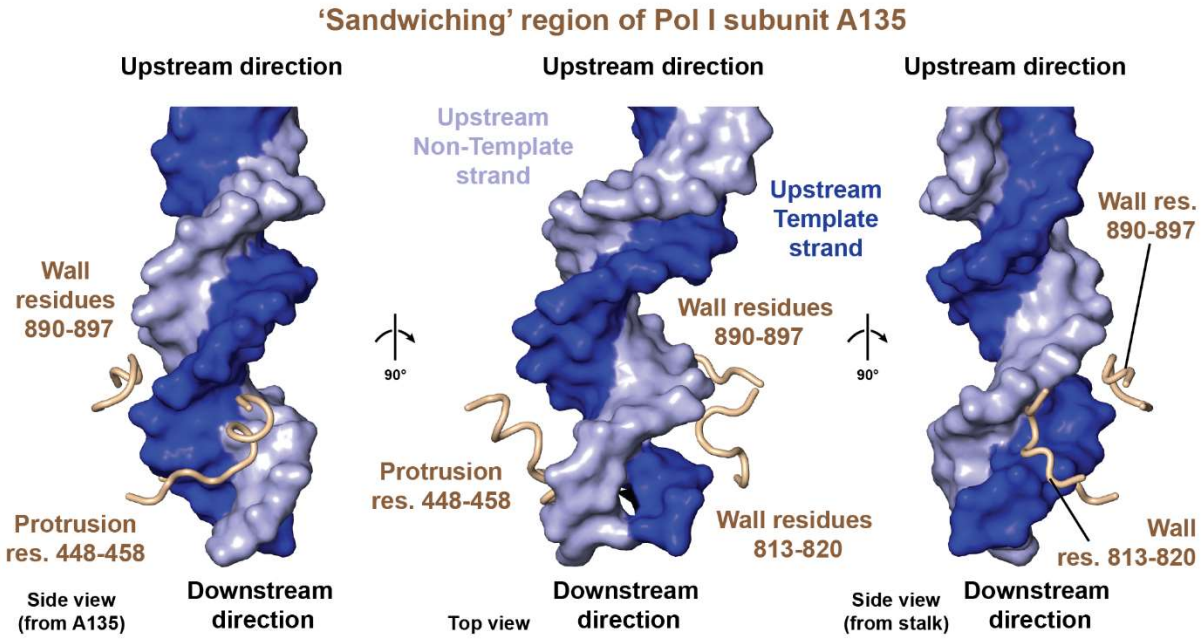

Figure 28: Pol I specific loops of subunit A135 form sandwich region
PDB model of proximal upstream promoter DNA in the eiPIC (space-filling, blue) shows how A135 residues (ribbon, wheat) approach the backbone of both DNA strands.

In the eiPIC, the sandwich region tightly holds the promoter in place between the wall and protrusion domains at the bottom of the cleft. Sandwich elements contact both DNA strands, therefore rendering it specific for an un-melted duplex. Density for the DNA directly downstream of the sandwich is not observed, indicating a higher degree of flexibility. Consequently, the recruitment of the Pol-I-Rrn3 complex seems to mainly rely on (1) contacts between the promoter and the sandwich and (2) protein–protein contacts between CF and the Pol-I-Rrn3 complex. In contrast, further promoter contacts with the Pol I cleft or downstream elements and/or A49 appear not to be required for recruitment.

2.9.3.3. TFIIB-related elements in Rrn7 adopt divergent positions.

The TFIIB-related 'reader' and 'linker' elements within Rrn7 (Knutson and Hahn 2013; Naidu et al. 2011) are mostly ordered in the active center cleft of the eiPIC (Figure 29), with the exception of the residues 46–56 (B-reader homologous). The protein backbone extends from the N-terminal zinc ribbon into the Pol I cleft, apparently trapping the well-ordered 'lid' subdomain of Pol I subunit A190 before forming two anti-parallel strands and exiting the Pol I upstream face on the side of the shelf module (Figure 29 A). The path of Rrn7 differs from a Pol I ITC (Han et al. 2017) and from TFIIB in complex with Pol II (Supplemental Figure 13). During Pol II initiation, the TFIIB-reader-loop contacts the 'rudder' and the 'fork loop I' domains, while the TFIIB-linker binds the top of the rudder and forms a helix that interacts with the clamp core domain (Sainsbury et al. 2013). In the eiPIC, rudder and fork loop I apparently interact neither with each other nor with the TFIIB-reader-homologous regions of Rrn7. Instead, rudder and fork loop I are oriented towards the bridge helix and a Rrn7 helix that is similar to the TFIIB linker connects to CF module II. In addition to a divergent path of Rrn7 compared to TFIIB, the residues contacting the template strand in a Pol I ITC (Han et al. 2017) and Pol II ITC are mostly flexible in the

eiPIC, but not in Pol II CCs (Dienemann et al. 2019) or in a Pol II-TFIIB (Sainsbury et al. 2013) complex. Furthermore, TFIIB reader-loop arginine residue 78, which is important for TSS selection by Pol II (Chen and Hampsey 2004), does not exist in Rrn7. This adds to overall sequence and architecture differences between Rrn7 and TFIIB.

To clarify the importance of Rrn7 loop residues which are disordered in the eiPIC, we mutated the entire loop or smaller stretches and analyzed CF initiation activity in a basal assay (Figure 29 B). The loop deletion Rrn7 mutant showed strongly reduced initiation— efficiency, which can mainly be attributed to the residues 51–56, but not to residues 43–50. The Rrn7 version with loop-deletion still assembled well with Rrn6 and Rrn11 and was able to form a basal PIC *in vitro* (Supplemental Figure 12 D, E). Thus, the Rrn7-reader-loop is likely important for promoter melting.

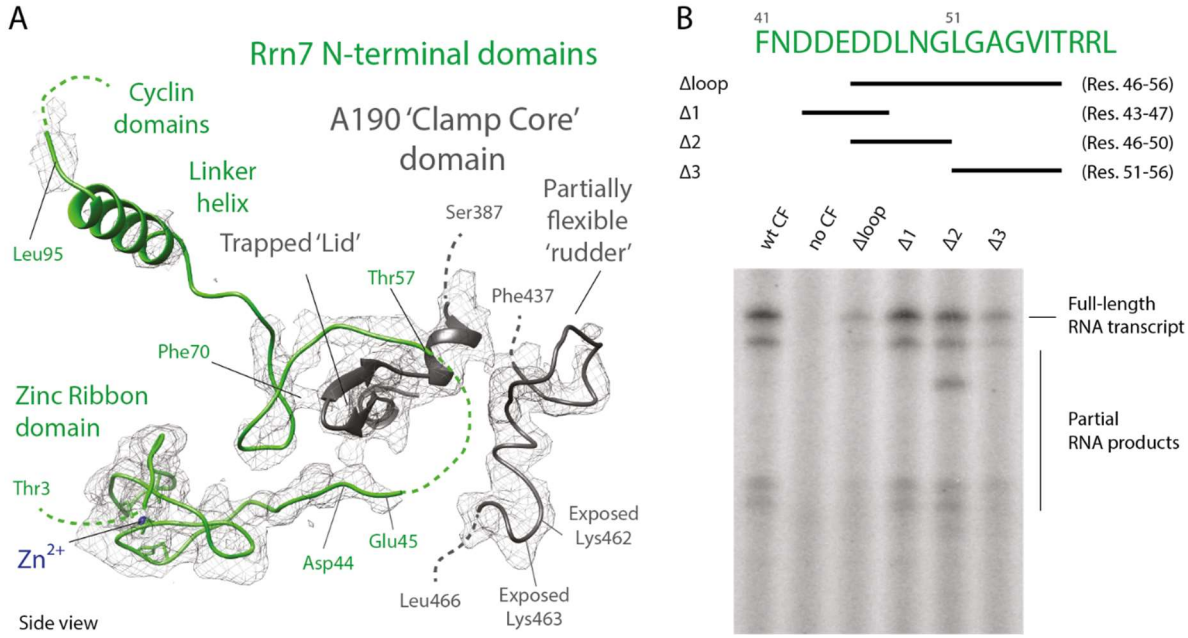

Figure 29: The N-terminal region of Rrn7 is partially ordered within the eiPIC.
A Ribbon model of TFIIB-homologous regions in the N-terminus of Rrn7 (green) overlaid with sharpened eiPIC density (gray mesh). The lid domain of Pol I subunit A190 (dark gray ribbon) is trapped between well-ordered regions of Rrn7. Residues 46 to 56 of Rrn7 are partially flexible, hinting at a function during promoter melting. B Amino acid sequence of flexible Rrn7 region is shown in green with schematic representation of deletion mutants indicated by black bars. Basal *in vitro* initiation assay shows the effect of Rrn7 mutations within this loop: Deletion of the entire loop and its C-terminal part (51 to 56) show reduced initiation activity.

2.9.3.4. Pol I is primed for initiation at the eiPIC stage

Modeling of the active center based on our eiPIC density indicated, that aspartate 629 in subunit A190 (Asp483 in Pol II subunit Rpb1) has apparently changed its orientation with respect to the dimeric crystal structures (Fernández-Tornero et al. 2013; Engel et al. 2013) (Figure 30). Adapting its active orientation in the eiPIC, Asp629 now allows coordination of the catalytic magnesium ion ('metal A'), together with Asp627 and Asp631 for which we observed a clear cryo-EM density peak (Figure 30 B). In addition, the hybrid-binding domain of subunit A135 re-arranges to form a one-turn helix in the eiPIC. This helix also resembles the active Pol I, II, and III EC conformations and its formation exposes

histidine 1038 to the bottom of the cleft, which is now free to contact the hybrid upon initial transcription as observed in ITCs. Furthermore, the previously buried lysins 462 and 463 in subunit A190 become exposed in the eiPIC (Supplemental Figure 11 F), now resembling the active Pol-II-fold (Armache et al. 2005) and contacting the first visible downstream DNA base pair. This may contribute to a high affinity for foreign DNA and to the Pol I preference for initiation from ends of dsDNA. With the described structural changes upon eiPIC formation, Pol I enters a conformation that is primed for initial transcription via a conserved mechanism (Cheung and Cramer 2012) in the presence of NTPs.

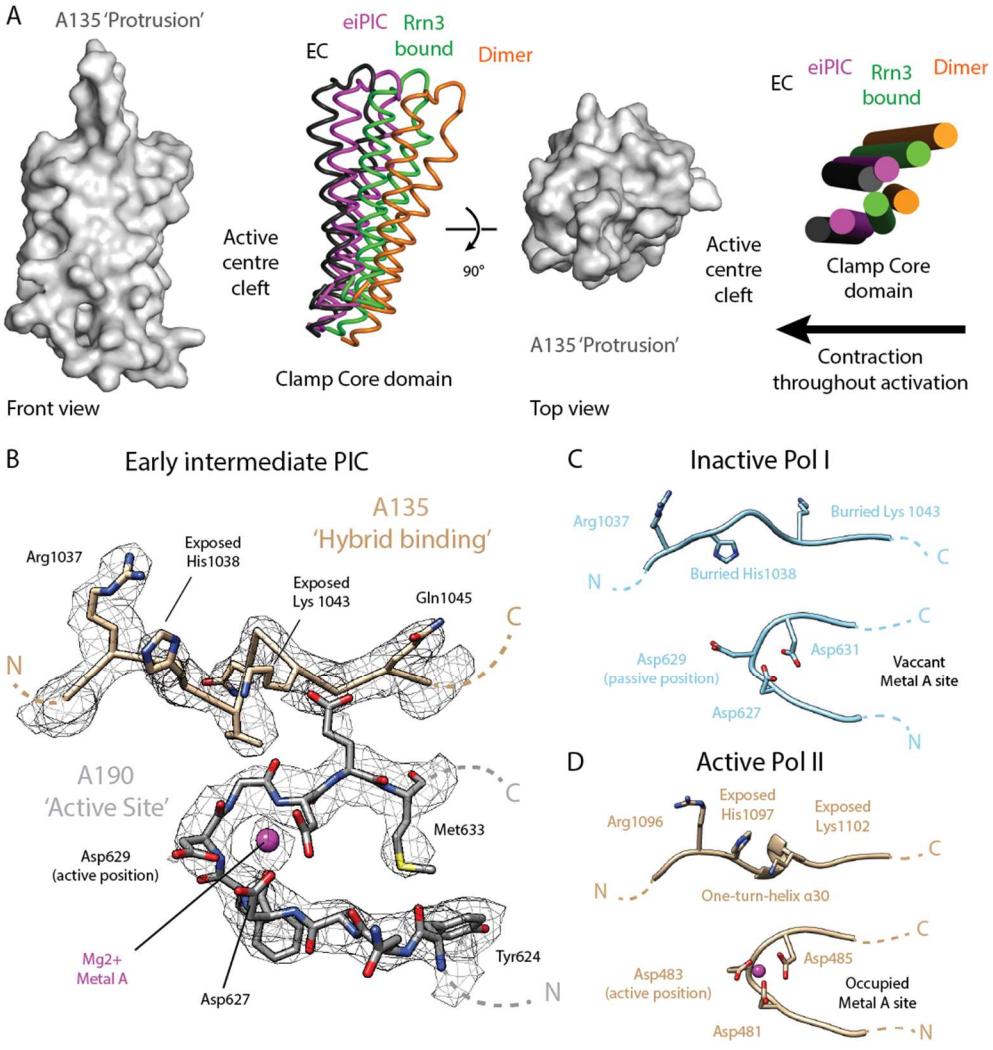

Figure 30: Pol I is primed for initiation in the eiPIC
Cleft contraction throughout activation stages. A) Pol I structural models were overlaid via their A135 subunits (protrusion subdomain in gray, space filling). Cleft contraction is indicated by colored clamp core helices (subunit A190). Monomeric Pol I and ITC stages are similar to Rrn3-bound- and EC-conformations, respectively (not shown for clarity). PDB models displayed: 4C2M (orange), 5G5L (green), eiPIC (magenta) and 5M3F (black). B) Atomic model of the active center and hybrid-binding domains within Pol I subunits A190 and A135, respectively. Overlaid with sharpened eiPIC density (gray mesh). The metal A site is occupied and a one-turn-helix α30 is formed in A135, exposing positively charged residues. C) Inactive Pol I (PDB 4C2M) region for comparison to B. D) Active Pol II region for comparison to B and C.

We also observed, that the Pol I cleft continues to contract downstream of the sandwich region, adapting an intermediate conformation between the Rrn3-bound and ITC/actively elongating states (Figure 30 A). This adds an additional intermediate to the set of Pol I structures (Engel et al. 2018), but is in line with the suggestion, that cleft modulation is a major regulatory mechanism of Pol I transcription (Torreira et al. 2017; Engel et al. 2013). At the stage of DNA-melting during the transition from CC to OC states, dsDNA cannot be accommodated between clamp core and protrusion domains any longer (Engel et al. 2017). Hence, simultaneous promoter loading and cleft contraction allosterically destabilize the upstream duplex at the position of the clamp core and may foster spontaneous melting at this position. Notably, the initially melted region shows the highest conservation among rDNA promoters identified thus far (Ganley et al. 2005). Thus, the eiPIC apparently represents a trapped CC-OC transition intermediate conformation, which is important for spontaneous DNA-melting and takes place during promoter association of the polymerase.

3. Discussion

Structural and functional investigation of transcriptional multi-protein complexes is essential to our understanding of gene regulation. For Pol I transcription, various strategies were used to identify, characterize and purify components of the pre-initiation-complex (Nogi et al. 1991a; Keys et al. 1996; Keys et al. 1994; Milkereit et al. 1997; Milkereit and Tschochner 1998; Keener et al. 1998; Bischler et al. 2002). Most of these protocols did not yield enough material and/or provided not sufficiently pure components for a detailed structural and functional analysis. Long-lasting efforts revealed the Pol I crystal structure in 2013 (Engel et al. 2013; Fernández-Tornero et al. 2013). In the recent years, the 'resolution revolution' in electron cryo microscopy (Kühlbrandt 2014) made cryo EM to the method of choice in structural biology to study macromolecular assemblies as the transcription machinery. In this work, purification protocols for components of the yeast Pol I PIC from endogenous and recombinant source were established. The highly purified factors showed high activities in reconstituted *in vitro* assays and were suitable for further cryo EM analysis. The ability to reconstitute the Pol I PIC and subcomplexes in large amounts allowed us to re-investigate the role of TBP in this context. Further, we were able to assign stimulatory activity of the Net1 protein, to its C-terminal part and found this part to be functionally conserved in mammalian UBF. In summary, we were able to suggest a model how the factors interact in a timely and spatial manner to form a stable and functional PIC. Finally, we observed an early intermediate of the Pol I PIC and describe functional parts in CF, that facilitate Pol I initiation.

3.1. Pol I/Rrn3 is competent for transcription initiation

3.1.1. Ex vivo purified Pol I/Rrn3 is primed for transcription initiation

Rrn3 directly interacts with Pol I independently of DNA (Yamamoto et al. 1996). In fast growing cells, only 2% of Pol I molecules are associated with Rrn3 and only this subpopulation is able to initiate transcription (Milkereit and Tschochner 1998). Poor factor occupancy limited biochemical and structural characterization of the complex. Key findings for efficient purification of the yeast Pol I/Rrn3 were increased factor occupancy upon Rrn3 overexpression and biochemical enrichment of the complex before immune/affinity purification. Major enrichment step in this protocol was precipitation of the complex in a low conductivity buffer (Figure 4). This fraction can be separated by ultra-centrifugation and resuspended. Immuno- or affinity purification of Rrn3 yields almost stoichiometric amounts Pol I.

Initiation of Pol I transcription in yeast cell extracts depends on the formation of a complex between Pol I and the initiation factor Rrn3 (Milkereit and Tschochner 1998). Purified Pol I/Rrn3 complex together with recombinant CF, was active in a minimal promoter-dependent transcription system (Figure 5, A). Incubation of Rrn3-free Pol I with over-stoichiometric amounts of purified recombinant Rrn3 and CF (Figure 5, B) resulted in promoter-dependent transcription, whereas no transcript was

detected in reactions lacking either CF or Pol I. Minor activity (about 1% of activity of full reaction) was detected without addition of recombinant Rrn3 (Figure 5 B, lane 2). This residual activity was observed at long exposure times and could result from co-purified endogenous Rrn3 from Pol I preparations as it was only observed in presence of CF.

Whereas bulk Pol I produces higher amounts of RNA in promoter-independent transcription from tailed templates, in relation Pol I/Rrn3 complex was up to 10x-fold more active in the initiation assay. Thereby initiation rates are similar for both complexes (Figure 6). A large excess of Rrn3 was required to efficiently enable transcription initiation (Figure 5 C). In experiments to reconstitute the Pol I PIC, over-night preincubations with five-fold Rrn3 were sufficient to obtain stoichiometric amounts of Rrn3 co-migrating with the initiation complex on sizing-columns (see Supplemental Figure 10) but might be stabilized by other transcription factors as CF. However, preincubation with CF and/or DNA template could not restore transcription levels of the *ex vivo* Pol I/Rrn3 (Figure 6). Complex formation of bulk Pol I and recombinant Rrn3 *in vitro* might be poor under these conditions. This is in agreement with earlier studies (Yamamoto et al. 1996; Keener et al. 1998; Blattner et al. 2011). Long incubation times and excess of factor were required for complex formation, this could hint towards a conformational change.

3.1.2. Rrn3 stabilizes Pol I monomeric conformation and drives pre-initiation complex formation

Purified Pol I adopts two oligomeric states in solution, monomers and dimers (Milkereit et al. 1997). Pol I/Rrn3 is strictly monomeric and position of Rrn3 was initially observed at the Pol I stalk using immuno-detection of anti-bodies directed against Rrn3 (Milkereit and Tschochner 1998; Peyroche et al. 2000). The crystal structure of Rrn3 was solved and combined with crosslinking-mass-spectrometry a model for the Pol I/Rrn3 complex was made. Rrn3 arrangement on Pol I in our cryo-EM map is similar to a model predicted from cross-linking data combined with the Rrn3 x-ray structure and a Pol I homology model (Blattner et al. 2011). Rrn3 is oriented towards subunit A43 making contacts via the Rrn3 serine patch, and stretches along subunits A190 and A135 down to subunit AC40/19, explaining protein crosslinks between Rrn3 and AC40 (Figure 7). The orientation of Rrn3 towards the OB fold of subunit A43 is in accordance with previous genetic, biochemical as well as with previous EM data (Peyroche et al. 2000).

Reorganization of the Pol I connector helix in Pol I/Rrn3 could prevent dimerization

A consequence of Rrn3 binding is the re-organization of the A43 C-terminus and the interference with Pol I dimerization by displacing the Pol I–Pol I interaction through the connector helix. The connector helix is an essential determinant of Pol I dimerization (Engel et al. 2013; Fernández-Tornero et al. 2013; Kostrewa et al. 2015; Torreira et al. 2017), suggesting that the binding of Rrn3 interferes with dimer formation. Indeed, Pol I dimer formation could not be triggered in vivo under starvation conditions if

A43 connector was missing (Torreira et al. 2017). Dimer dissociation is important for the structural rearrangements yielding initiation competent Pol I. Interestingly, Rrn3 resembles the 'mediator' head domain of the Pol II transcription system in its structure as well as in its interaction with the respective polymerase stalk (Soutourina et al. 2011; Plaschka et al. 2015). Thus, the comparative structural analysis of Pol I and Pol II may reveal common principles in pre-initiation structure and formation. The crystal structures of Pol I and Pol II revealed some clear differences, which can be due to the specialization of the enzymes for transcription or an artefact of the particular requirements for crystallization. The most significant differences were that Pol I has an ~10 Å more open cleft, an extended loop (expander) in the cleft, which might mimic DNA and an active center, which resembles a reactivated backtracked polymerase (Cheung and Cramer 2011; Wang et al. 2009). Furthermore, Pol I crystallized as a dimer in which the C-terminal part of subunit A43 reaches into the cleft of a neighboring Pol I molecule. Many of these features suggested that Pol I had to undergo conformational changes to initiate transcription. Determination of the cryo-EM structures for Pol I-Rrn3 (and Rrn3-free Pol I) represents an important step to understand the formation of the Pol I pre-initiation complex. The cryo-EM structure of the dimeric form of Pol I strongly resembled the Pol I crystal structure. The structures of Pol I/Rrn3 and the Rrn3-free monomeric form of Pol I, in contrast, are more compatible with a transcriptional active enzyme. The cleft is closed by about 11 Å and neither the expander loop, nor the A12.2 C-terminus are found in the active center. The position of the expander loop seen in some of the crystal structures may hamper interaction with the template. In contrast to Pol II, purified Pol I needs over-stoichiometric amounts of tailed template for efficient RNA synthesis *in vitro* (Engel et al. 2013). This might point to the possibility that excess template is required to displace the expander loop (and the C-terminal domain of A12.2 (see below)) from the active center, thereby converting inactive Pol I into a more transcription competent Pol II-like conformation. Our data suggest that Pol I may adopt a conformation, which is likely compatible with transcription even in the absence of DNA. The interaction between Pol I and Rrn3 could either stabilize or induce such structural changes (see also discussion below).

Rearrangement of A12.2 C-terminal domain

In the Pol I crystal structure the TFIIS-like C-terminal domain of A12.2 occupied the active center in the crystal structure. Its position is very similar to that of TFIIS in Pol II after backtracking when TFIIS stimulates intrinsic Pol II cleavage of the RNA extension (Cheung and Cramer 2011; Wang et al. 2009). Our cryo-EM analyses revealed that, in analogy to the homologous Pol III subunit C11 (Hoffmann et al. 2015) and the Pol II factor TFIIS, the C-terminal domain of A12.2 is not an integral part of the active center, and that it can be removed from its position in the nucleotide entry pore. However, in contrast to Pol II, and similar to C11, the RNA cleavage supporting polypeptide chain is tightly associated with Pol I as another example for 'built-in transcription factors' in the enzyme (Kuhn et al. 2007; Geiger et

al. 2010). Similar to TFIIS this might help to remove stalled transcription complexes more efficiently (Reines et al. 1992), thus increasing processivity (Ishibashi et al. 2014; Sigurdsson et al. 2010). Consistently, Pol I recovered mostly by RNA cleavage for backtracks larger than 3 nt, whereas Pol II without TFIIS uses also 1-D diffusion to regain transcription elongation. The 'built-in' cleavage activity may prevent frequently occurring transcriptional arrests which would be especially disadvantageous for the highly transcribed rRNA genes of fast dividing cells (Lisica et al. 2016).

Cleft contraction and bridge-helix-folding during Pol I activation

One remaining significant difference within the active center of Pol II when compared with the active centers of the three different cryo-EM structures of Pol I (Pol I dimer, Pol I monomer and Pol I/Rrn3) is the conformation of the bridge helix. For Pol II a mechanism was proposed in which a switch between a partially unfolded and a completely folded bridge helix and the resulting bending is important for DNA, and the DNA/RNA hybrid translocation (Gnatt et al. 2001; Silva et al. 2014). For Pol I it was proposed that the partially unfolded bridge helix is a consequence of the significantly wider cleft. Thus, it was predicted, that cleft closing might induce complete folding of the bridge helix and opening of the RNA exit channel with concomitant inside movement of A135 domains (Fernández-Tornero et al. 2013). This structural rearrangement would be necessary for anchoring of the transcription bubble. Whereas the latter two transitions can be seen in the initiation competent Pol I-Rrn3 complex and the Rrn3-free Pol I monomers, the bridge helix remained partially unfolded in all cryo-EM structures. It is possible that DNA binding is required for the complete folding, or that the unfolded bridge helix is a Pol I-specific feature at this stage. Fittingly, in later cryo-EM structures of elongating Pol I, the cleft is further contracted and the bridge-helix completely folded, further A12.2 C-terminus and the expander/DNA-mimicking loop are displaced from the active site (Tafur et al. 2016; Neyer et al. 2016). In fact, exchange of two amino acids, which change the amino acid sequence of Pol I bridge helix into the amino acid sequence of the Pol II helix, led to alterations of transcription speed and processivity in the respective Pol I mutant (Michael Pilsl and Herbert Tschochner unpublished observations). This indicated that the Pol I-specific bridge helix is important for proper Pol I activity.

Enzyme hibernation by functional dimerization

For a long time, it was unknown, whether different subpopulations of Pol I monomers and dimers exist *in vivo*. It is, however, tempting to speculate that these two different forms of Pol I are involved in Pol I transcription regulation as it was previously suggested (Milkereit et al. 1997; Peyroche et al. 2000; Engel et al. 2013). Pol I dimers may be a stable storage pool for the enzyme, which is kept in an inactive state. In response to changes in physiological situations, the pool of Pol I dimers could be quickly activated into monomers to adjust cellular ribosome biosynthesis. In an elegant live cell imaging approach, the appearance of Pol I dimers could be demonstrated in yeast cells. In this study, dimer formation could be introduced under starvation conditions, supporting the model of a storage form,

or hibernating enzyme (Torreira et al. 2017; Fernández-Tornero 2018). Whereas dimer formation in S. cerevisiae depends on A43 connector domain, Pol I in Schizosaccharomyces pombe uses a completely different interface for dimerization. (Heiss et al. 2021). This functional conservation underlines the relevance of Pol I dimerization throughout different organisms. Regulatory processes like phosphorylation, DNA-association or binding of a transcription factor might be involved in this transition. According to our data, the presence of Rrn3 alone may not be sufficient to trigger formation of Pol I monomers (Pilsl et al. 2016a). However, it is possible that Rrn3 in addition to a yet unknown activity is required for dimer dissociation. Binding of Rrn3 might stabilize Pol I monomers resulting in a salt resistant initiation competent Pol I/Rrn3 complex (Milkereit and Tschochner 1998). At which stage of complex formation Rrn3 stabilizes the monomeric form remains to be determined. The connector seems to be essential for Pol I dimerization (Torreira et al. 2017), thus a simple mechanism could be hindrance of connector re-association in monomeric Pol I by Rrn3.

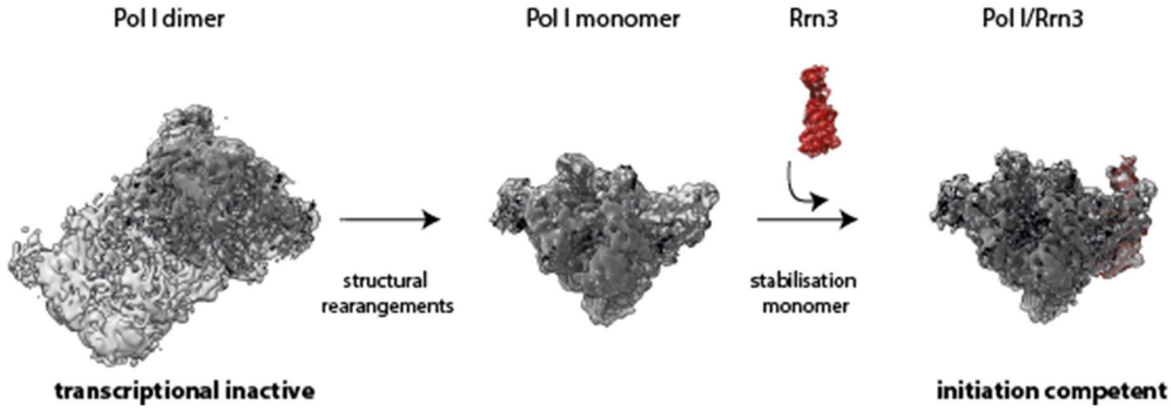

Figure 31: Rrn3 stabilizes Pol I monomeric conformation and drives pre-initiation complex formation
Model for transformation of inactive Pol I dimers to initiation competent Pol I/Rrn3. Cryo-EM densities of Pol I dimers, monomers, and in complex with Rrn3 are shown as grey envelope. Structural rearrangement of monomeric Pol I include cleft contraction, dis-location of A43-connector and position of the A12.2 C-terminus

3.1.3. Formation of the initiation competent Pol I/Rrn3 complex might be regulated by post-translational modifications

Regulation of enzymes by post-translational modification allows cells to rapidly adapt enzymatic activities to changing physiological conditions. Phosphorylation on the hydroxy-group of serine or threonine residues is one of the most common post-translational modification, and Pol I was described as a phosphoprotein complex (Gerber et al. 2008).

Interestingly, the overall phosphorylation pattern of bulk Pol I differs from its Rrn3 bound form and phosphorylation of Pol I is a prerequisite for transcription initiation and complex formation with Rrn3 (Fath et al. 2001). Furthermore, posttranslational modifications of mammalian Rrn3 have been described, that affect preinitiation complex formation (Cavanaugh et al. 2002; Mayer et al. 2004; Mayer et al. 2005). Phospho-mimicking mutations of conserved serine-residues impaired Rrn3 binding (Blattner et al. 2011). However, for yeast Rrn3 or Pol I no posttranslational modifications that affect

complex formation has been identified so far. While several phosphosites on Pol I were found, the physiological role of these modifications is still unclear (Gerber et al. 2008). Earlier studies analyzed bulk Pol I therefore, specific modifications of a subpopulation corresponding to the initiation active Pol I couldn't be investigated. The enrichment of the Pol I/Rrn3 complex allowed the reassessment of phosphosites in context of the initiation active Pol I and its associated factor Rrn3.

The interaction interface of Pol I subunit A43 and Rrn3 is conserved from yeast to human. A 22 amino acid peptide from this conserved patch in A43 could inhibit Pol I transcription by binding Rrn3 and sequestering the factor (Rothblum et al. 2014). In yeast the serine residues S141 and/or S143 are exposed to Rrn3 and would be an attractive target for potential regulation. These putative phosphosites were mutated to aspartic acid, to mimic constitutive phosphorylation, or to alanine which resembles the unmodified residue. A growth defect for the phospho-mimicking double mutant S141/143D was observed (Reiter 2011). However, the modified residues could not be detected by mass- spectrometry yet. Also, our trials to prove the appearance of phosphorylation of these residues was not successful. We could identify previously described phosphosites on Pol I, but did not observe any differential phosphorylation sites on Pol I and the Pol I/Rrn3 complex up to now. In our purification protocol, we selectively enriched Rrn3 that is associated with Pol I. We could identify phosphorylated residues located in a flexible acidic loop in Rrn3. Parts of this loop have recently been shown to interact with Pol I and to stabilize the Rrn7 Zn-ribbon domain (Sadian et al. 2019). The modified residues observed in the Pol I bound Rrn3 population however lie within the disordered part of this loop and as a deletion of the entire loop did not result in any growth-phenotype (Blattner 2011), thus an important regulatory function of these residues is unlikely.

Overexpression of factors limits information on the physiological role of potential modifications. The overexpression situation could not have been appropriate for the identification of physiological relevant modifications, as modifying enzymes might become limiting and could not act anymore on relevant targets. Furthermore, overexpression of Rrn3 was induced by the addition of galactose to cells previously cultured with raffinose as carbon source, this shift needs a reprogramming of the cells' metabolism, which also might have implications on the posttranslational modification pattern within a cell. Further, technical and analytical problems will limit the identification of all modifications, as modified residues can be underrepresented due to characteristics of the poly-peptide chains, like their 'fly ability' in the mass-spectrometer, or their proteolytic digestion pattern. Finally, essential but very transient modifications would not be detectable by the applied methods.

3.2. Reconstitution of the complete Pol I PIC

3.2.1. UAF can be purified from recombinant source and is stabilized in high conductivity buffers

A large-scale preparation protocol for UAF from yeast cells has been described. Only few micrograms of pure complex could be purified from 100 L yeast culture (Keener et al. 1998; Keys et al. 1996). The

low yield of this factor strongly limited its biochemical and structural characterization. Recently, a protocol for the recombinant purification of the UAF complex, expressed in E.coli was described, although the activity of the factor in a reconstituted transcription assay with purified factors was not demonstrated (Smith et al. 2018; Knutson et al. 2020). We established a purification protocol for UAF from recombinant source. A buffer containing 400 mM ammonium sulphate inhibits DNA interactions and was used to solubilize the recombinant complex. Then, we used the 7xHis-tag on Uaf30 subunit to efficiently capture the UAF complex with NiNTA agarose beads. Recombinant UAF was stable under high salt conditions and did not dissociate during wash steps up to 1 M KCl, which is well in line with the characterization of the endogenous complex (Keys et al. 1996; Milkereit and Tschochner 1998). On a subsequent MonoS cation exchange column excess of Uaf30 bait and most other contaminants were efficiently removed. Likely the strongly positively charged histone proteins contribute to this high-affinity binding.

UAF shares biochemical properties with nucleosomes

UAF stability depends on high conductivity buffers. UAF migrated with an apparent molecular mass of 360 kDa on a Superose 6 column in a high salt buffer (Figure 11). This would correspond to dimeric complexes, assuming the stoichiometry of recombinant UAF from *E.coli* (Smith et al. 2018). In contrast to this publication, we did not observe monomeric UAF complexes. Interaction of positively charged residues of the histone proteins with the DNA phosphate backbone are well described in context of the nucleosome. Similar interactions of histone proteins H3 and H4 are likely to play a role in UAF (Keener et al. 1997). Whereas UAF can form a stable complex with promoter DNA under moderate salt conditions, high conductivity buffers avoid DNA binding and stabilizes unbound UAF complex in solution (compare Figure 18, Figure 11). These biochemical properties are shared with nucleosomes, summarized by Caroline Luger: '*Unlike nucleosomes (i.e., octamers wrapped with DNA), histone octamers (and subcomplexes) are very unstable without DNA because of the electrostatic repulsion among the positively charged histones. Therefore, octamers do not exist as stand-alone structures under physiological conditions Nucleosome assembly depends in part on avoiding non-nucleosomal interactions between its components; this is accomplished by the use of salt gradients (in vitro) and histone chaperones (in vivo*)' (Andrews and Luger 2011). In this regard, the assembly of the UAF complex might be of further interest. It is not clear, how UAF or its components like the histone proteins H3/4 are delivered to the nucleolus, when and where complex assembly occurs. It was suggested that UAF might associate with the promoter directly after replication and this UAF-DNA complex persist as an activatable rDNA repeat (Keener et al. 1997). Several chaperones have been identified for H3/4 subcomplexes. Spt2; Asf1, CAF1 (Liu et al. 2012; Chen et al. 2015; Mattiroli et al. 2017). The yeast chromatin assembly factor1 (CAF1) binds and deposits H3/4 monomers to (newly synthesized) DNA. Upon interaction with a second complex, H3/4 dimerizes to the H3/4 tetramer and

the chaperone is released (Mattiroli et al. 2017; Sauer et al. 2017). It is not known if these chaperons play a role in UAF assembly, but it is unlikely that free H3/4 populations directly target the Pol I promoter. It is also unclear if and where UAF holo-complex is assembled. UAF might be assembled in the cytoplasm and imported into the nucleolus, or directly assembled at the Pol I promoter. An option might be that UAF replaces a nucleosome at the promoter, where Rrn5, 9, 10 and Uaf30 might associate with H3/4 and replace H2A/B tetramers. Again (histone)-chaperone activity is likely to be required. Various histone or nucleosome subcomplexes (e.g. tetrasomes, hexasomes, hemisomes …) have been observed, their physiological appearance and function is largely unknown (Zlatanova et al. 2009). UAF could be a specialized chimeric form of H3/H4 tetrasome as suggested by Knutson et. al. (Smith et al. 2018; Knutson et al. 2020). A large >80 bp footprint could be explained by histones H3/4-tetramer interactions, UAF specific subunits would recognize Pol I promoter DNA specifically.

3.2.2. Reconstitution of efficient Pol I initiation *in vitro* depends on UAF-TBP and Net1

Overall the stimulatory capacity observed for UAF/TBP in various experiments was between 3-15-fold compared to the minimal system. It should be noted that the final transcription assays contained six purified protein (complexes) plus the DNA template. It is unlikely that the optimal concentration of all factors could be found and the optimal ratio of all components could not be determined in these assays. The assays in this study contained constant amounts of Pol I (100 or 125 fmol), which results in enzyme concentration of 4 - 5 nM in the final reaction volume. Transcription factor Rrn3 was added in 14x fold molecular excess to efficiently stimulate transcription. DNA binding factors were added in similar amounts as the DNA template as higher concentrations were observed to inhibit transcription (UAF, TBP). Albeit quality of individual protein preparation was high, individual factors might suffer upon storage, freeze-thawing and concentration of active molecules can vary. The stimulatory effect of recombinant UAF (3-15-fold) observed under my experimental conditions is less than the reported up 10 to 50 fold stimulation of the endogenous complex (Keener et al. 1998). In the study of Keener et al., molar quantities of the transcription factors were not reported, and amounts of endogenous complexes were limiting a more detailed investigation. Later, recombinant CF showed higher specific activity than the endogenous complex (Bedwell et al. 2012). Functional modification of endogenous complexes, spurious contamination with other (enzymatic) factors, or simply damage during (multi-step) purification might cause different activities of recombinant factors. Further, UAF together with TBP likely act as recruiting factors for CF, therefore relative stimulation would be sensitive to limiting amounts of CF. In my experimental conditions, recombinant CF was added in excess and should not be limiting (Figure 13, lane 9). Addition of either Net1-FL or Net1-C to these reactions stimulated initiation-rates up to 35-fold over basal transcription levels. Thereby, effects of Net1 and UAF/TBP appeared to be largely independent.

3.2.3. Net1-C interacts with UAF/TBP and Pol I/Rrn3 and functions as a Pol I activation domain

We could reproduce Pol I stimulation by full length Net1 protein (Shou et al. 2001) and could assign Net1 stimulatory functions to its C-terminal part (

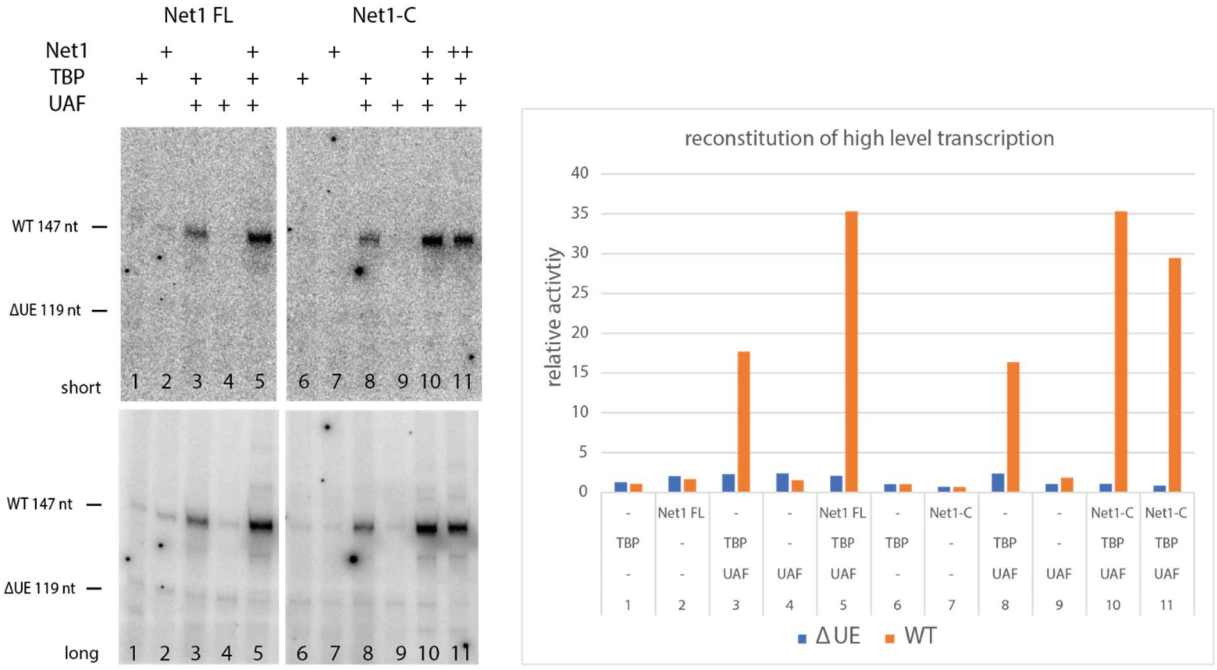

Figure 14). Net1-C enhanced Pol I loading on rRNA genes *in vivo* and promoter-dependent transcription in a minimal transcription system *in vitro (Hannig et al. 2019).* Fold stimulation of the minimal and fully reconstituted system were similar and seemed to be independent of stimulation by UAF/TBP. In immobilized template assays we could show, that Net1-C stimulated initiation reactions after UAF-TBP-CF complex was assembled on DNA (Figure 19). Protein-crosslinking revealed two main interaction sites for Net1-C, with UAF and the Pol I stalk region, including Rrn3.

Net1-C supports UAF-promoter assembly *in vitro*

Surprisingly, Net1-C strongly stabilized association of UAF with promoter DNA (Figure 18). In Net1-ΔC strains, Pol I recruitment to the 35S rRNA gene is strongly impaired (Hannig et al. 2019), however promoter occupancy of UAF in ChEC and ChIP experiments was only mildly affected (Achim Griesenbeck, unpublished). Cells may have redundant mechanisms for deposition of UAF to the promoter. Net1-C was predicted to be intrinsically disordered and no DNA-binding motif was predicted, still we observed faint interactions with both DNA templates (Figure 18, lane 8-10). Net1-C can interact with various genomic loci *in vivo*, while the full-length protein has more defined targets (Hannig et al. 2019; Huang and Moazed 2003). Positive residues of Net1-C may interact un-specifically with the DNA phosphate backbone. 19 out of 138 Net1-C amino-acids are lysine residues, which are enriched in the basic tail of the protein.

Sharing histone subunits H3 and H4, nucleosomes and the UAF complex have some common characteristic features. They are highly positively charged, ‘naked’ complexes require high conductivity

buffers and they target relatively long stretches of DNA. Nucleosome assembly depends in part on avoiding non-nucleosomal interactions between its components; this is accomplished by the use of salt gradients (*in vitro*) and histone chaperones (*in vivo*). To compensate effects from highly positively charged histone proteins, negatively charged components as RNA, or poly glutamic acid were successfully used to assemble nucleosomes. (Andrews and Luger 2011). Serine residues make up one third of Net1-C protein. Net1-C is heavily phosphorylated which is essential for its function (Hannig et al. 2019). This posttranslational modification will render the protein negatively charged. Charge compensation of positively charged residues may support UAF assembly onto promoter DNA, which might explain the *in vitro* effect to a certain degree. Poly glutamic acid showed no similar effect and the Net1-C effect seems to be more specific (not shown). The assembly of UAF-DNA *in vitro* is strongly supported by Net1-C (Figure 18). The precipitated fraction of UAF-DNA contains specifically bound complexes (Figure 17) and DNase I accessibility pattern of precipitated complexes is similar to those stabilized by Net1-C. Sharper boundaries of UAF footprints in presence of Net1-C may be another hint towards assembly functions of Net1-C. Charge dependent aggregation is not caused by a diffuse interaction pattern, but rather oligomeric interactions (Weijers et al. 2008). *In vivo*, UAF association with the Pol I promoter is only mildly affected in Net1-ΔC strains and Net1 is not known to play a role in nucleosome assembly.

Net1-C interactions with UAF/TBP and Pol I/Rrn3 might stabilize distinct PIC conformations

Net1-C strongly crosslinked to UAF, we observed crosslinks to subunits Rrn5, Rrn9, Rrn10 and strongly to H3, but not to H4. Further, we observed interactions with TBP, which itself might be tightly associated with the UAF complex. In contrast, only few interactions with Rrn6 were found. Crosslinking mass-spectrometry data was collected on complexes assembled on promoter DNA and therefore do not necessarily reflect pre-assembly or chaperoning states of the complex. However, interaction maps may support a model, where UAF helps to recruit or stabilizes Net1-C at the promoter. Net1-C can be passed on to Pol I or mediate interactions between the enzyme and UAF as a second interaction hot-spot at the Pol I stalk and Rrn3 implied (Figure 15). Net1-C stimulation *in vitro* does not depend on UAF, but likely interactions with Pol I play a role for this process. Interestingly, Pol III subunit C31 which is largely unstructured contains an acidic C-terminus and stabilizes the stalk and clamp domains in Pol III PICs (Abascal-Palacios et al. 2018). Net1 interactions with Pol I subunits A190, A135 and A43 have been shown and fusion of Net1-C to A190 suppresses growth defects in Net1-ΔC strains (Shou et al. 2001; Huang and Moazed 2003; Hannig et al. 2019). Interaction of Net1 with the Pol I promoter region was reduced, when PIC formation is impaired in a uaf30Δ strain, indicating that Net1 may interact with PIC components. (Goetze et al. 2010). Further, overexpression of Rrn3 rescued phenotypes in Net1 deletion strains (Shou et al. 2001). In ChIP and ChEC experiments Net1 is not totally restricted to the

promoter but also found in the 35S rDNA gene body (Huang and Moazed 2003; Goetze et al. 2010). This resembles the situation of Rrn3, which is trailing into the rDNA gene (Herdman et al. 2017).

Net1-C stimulated Pol I initiation and might be functionally conserved in mammalian UBF

We previously showed that the activation region of human UBF1 can partially rescue growth defects when fused to Net1 (Hannig et al. 2019). Recombinant hUBF1-C stimulates transcription initiation in our completely reconstituted yeast transcription system, but weaker than Net1. Thus, C-terminal region of human UBF1 could be a functionally conserved Pol I activation domain. *In vitro,* hUBF1-CTR does not stabilize UAF but its mode of activation might be related to Net1-C functions post UAF recruitment and mediated by direct Pol I interactions. Activation domains are often partially unstructured, acidic and rather short stretches of amino-acids with little primary sequence similarity. They rather share some biophysical properties, and are often enriched in acidic residues. These activation domains form promiscuous/fuzzy interactions with co-activator complexes and thereby stabilize intermediate conformations and association of the (Pol II) initiation machinery with promoters (Pacheco et al. 2018; Erijman et al. 2020; Keaveney and Struhl 1998). Activation of Pol I transcription by Net1-C may be an additional layer in regulation of Pol I transcription and help fine tuning of transcription levels. Phosphorylation seems to be important for Net1 function and its phosphorylation pattern changes during growth stages (Hannig et al. 2019). In Pol II transcription activation domains often act as last step in gene regulation cascades. My experiments suggest, that Net1-C might primarily function after formation of a stable DNA bound complex (Figure 19). Pol II transcription factors are often found with a bi-partite organization. A DNA-binding domain targets the factor to its genomic loci and an activation region, that stimulates gene expression. It was shown that purified Pol I and Net1 proteins physically interact (Shou et al. 2001). However, UAF-TBP-CF and Net1 could associate with the Pol I promoter in absence of Pol I or Rrn3 (Goetze et al. 2010). Association of Net1 with promoter bound UAF-TBP-CF may help loading of the protein to Pol I *in vivo*. First, interactions with UAF might tether Net1 to the promoter, after or during PIC formation Net1 forms contacts with the stalk region of Pol I/Rrn3. Net1 associates with Pol I/Rrn3 and upon successful initiation can travel with the polymerase into the 35S rRNA gene. *In vitro*, UAF-Net1-C interactions were not required for Net1-C dependent stimulation of transcription. Net1-C rather enhanced steps after formation of a stable DNA bound complex. Further investigation of native chromatin templates will help to elaborate mechanistic insights. It is possible that the ‘loading’ step onto Pol I could be overcome under *in vitro* conditions with high concentration and no spatial-temporal separation of factors.

3.2.4. UAF associates tightly with TBP independent of promoter DNA and is required for enhanced initiation rates

The multi-step purification scheme for UAF from yeast cells, that lead to the identification of its subunits (Keys et al. 1996; Keener et al. 1997) include two purification steps over MonoS or heparin columns. TBP alone can be purified over these columns and shows affinity to the resins (see TBP purification). In my experiments, TBP co-expressed with UAF in BIICs was (partially) depleted from UAF fractions after MonoS/Heparin steps, but more stable on NiNTA and subsequent SEC runs, which would be in agreement with observations in fractionated cell extracts (Milkereit and Tschochner 1998). Further, UAF-TBP interactions were characterized in more detail and found to be more robust, than interactions of CF with TBP (Steffan et al. 1996; Steffan et al. 1998). I could show that UAF can form a stable complex with TBP in the absence of DNA *in vitro* (Figure 11). Under similar buffer conditions (400 mM KCl), interaction of in vitro translated Rrn9 protein with TBP was strongly reduced (Steffan et al. 1996), suggesting that additional interactions of UAF components might stabilize TBP association with the complex. Fittingly, cross-linking mass-spectrometry identified proximity of all UAF subunits but H4 to TBP, most crosslinks were found to Rrn9 and H3. Interacting domains may be important for interaction (Supplemental Figure 3, 4). TBP preferentially associates with UAF decorated promoter DNA (Figure 23). Finally, I could show that enhanced initiation depends on UAF and TBP (Figure 23 A), supporting studies from the Nomura lab (Steffan et al. 1998; Siddiqi et al. 2001a).

3.2.5. UAF recruits TBP to the Pol I promoter

The Pol I promoter does not contain a canonical recognition sequence for TBP and it is not clear how TBP is targeted to the promoter. We observed a high affinity of TBP to UAF decorated DNA, together with size-exclusion chromatography analysis of DNA free, as well as promoter-DNA containing complexes we hypothesize that UAF might recruit TBP in a DNA independent manner to the Pol I promoter. TBP tightly bound to UAF under my experimental conditions, eventually different purification schemes might have defined TBP as a UAF-component. Observations by Joachim Griesenbeck/Christopher Schächner, that found ectopic recruitment of TBP on inverted UE in ChEC experiments (unpublished) underline the capacity of UAF to modulate TBP positioning at the promoter. Once recruited to the promoter, TBP might engage with DNA, recruit and/or stabilize CF at the promoter and help to introduce a specific conformation, that is prone for Pol I initiation.

About 85% of all Pol II promoters do not contain a canonical TATA-sequence (Rhee and Pugh 2012). Interestingly, in TFIID and SAGA, which are two Pol II multiprotein transcription factors that associate with TBP and deliver it to promoters, DNA binding by TBP appears to be one of the last steps towards promoter engagement. Thereby these factors can undergo large structural rearrangements. In SAGA and TFIID DNA binding by TBP is inhibited, while in TFIID the DNA binding surface is occupied, in SAGA steric hindrance by subunit Spt3 impairs DNA-association. Further, interaction sites that are required for subsequent recruitment of TFIIB and TFIIA are occupied (Patel et al. 2018; Papai et al. 2020) and

reviewed in (Esbin and Tjian 2020). Submodules of SAGA and TFIID that engage with TBP consist of octamers of histone-fold containing subunits. Histone folds are involved in both, protein-protein and protein-DNA interactions (Arents and Moudrianakis 1995). It is tempting to speculate about a relation of UAF to these TBP recruiting factors. To date, no homology of other subunits to SAGA or TFIID subdomains were found. In UAF, beside the histone-proteins H3/4 subunit Rrn5 is predicted to contain a histone fold. It was suggested, that the histone fold in Rrn5 might form a hybrid H3-H4-tetramer like structure (Knutson et al. 2020). A functional dimerization of two complexes can't be excluded. While the histone-fold-octamer containing subcomplex of SAGA does not bind DNA, UAF targets the Pol I promoter. This could reflect the nature of single to multi-gene regulation, the Pol I and Pol II transcription system.

In the Pol I system it is not clear if, or at which step TBP binds promoter DNA. Photo-crosslinking experiments suggested divergent DNA interaction of TBP in Pol I complexes (Bric et al. 2004). Mutations of conserved phenylalanine residues might address the question if the characteristic bend is introduced during Pol I initiation and thus TBP action at the Pol I promoter is conserved. However, TBP is likely to be located more upstream than in Pol II complexes, as CF interactions would be incompatible with TBP location (Engel et al. 2017). TBP interactions with the CF or the minimal PIC are weak. Interactions with all individual CF subunits Rrn6, Rrn7 and Rrn11 were observed, Rrn6 showing strongest interactions (Lalo et al. 1996; Steffan et al. 1996; Steffan et al. 1998). However, no stable CF/PIC complexes containing TBP could have been stabilized so far. Cryo-EM approaches contained TBP, but the protein was either lost during complex preparation, or highly flexible and was not observed in electron densities of the complexes (Engel et al. 2017; Sadian et al. 2017). We also did not yet observe TBP in cryo-EM densities in our UAF-containing early PIC intermediates on a truncated template, although cross-linking-mass-spectrometry proves interactions of TBP with PIC components.

3.2.6. Promoter cis elements

Re-investigation of Pol I promoter elements revealed a more detailed description how cis-acting elements and Pol I transcription factors could interact.

CE is composed of a CF binding site and the transcription start site, that functions independent of factor recruitment

We found that CF shows promiscuous DNA binding but has a preference to the CE sequence (Supplemental Figure 7, summarized in Figure 21). We could closer define the CF binding site to [-28 -17] a mutation which impaired binding of the factor, while mutations around the TSS did not affect CF binding. Thus, we identified different mechanisms for mutations described in earlier studies on the Pol I promoter (Musters et al. 1989; Kulkens et al. 1991). A similar study examined DNA binding by recombinant CF and competition with short oligonucleotides attributed the CF interacting DNA region exactly to -28 to -17 (Jackobel et al. 2019). Moreover, new cryo-EM structures identified CF-DNA interactions from -27 to -13 in a PIC context. These interactions are mediated by subunits Rrn7 and

Rrn11, which contact backbone DNA, as well as the minor and major grove. Mutations of few nucleotides in the corresponding DNA sequence or exchange of amino-acids which contact the DNA abolished initiation *in vitro* (Sadian et al. 2019).

All CE mutants were inactive in promoter dependent transcription assays (Supplemental Figure 9), underlining the essential role for proper CF recruitment and positioning. CF and UAF can associate with a TSS mutant [-4 +8] (see Supplemental Figure 7). This mutant, but not [-38 +8] or [-28 -17] reduces transcription levels from the reference template (Supplemental Figure 9, Figure 21). Formation of a stable UAF-TBP-CF complex, might sequester at least CF and/or Pol I/Rrn3 to the competitor template. Efficient formation of this committed complex *in vitro* depends not only on physical interaction between UAF, TBP and CF, but also requires the correct CF binding sequence. Complementary ChEC analysis by Christopher Schächner and Joachim Griesenbeck found a minor amount of CF recruited independently of the CE *in vivo*. *In vitro* transcription assays contained relatively high amounts of CF, close to saturation, therefore, subtle decrease of CF concentration will hardy be detectable under these conditions.

Thus, in the TSS mutant [-4 +8] steps after transcription factor assembly and recruitment could be affected. The experiment couldn't reveal if either Pol I/Rrn3 recruitment or later steps in transcription initiation are impaired. In the mutant sequence, the GC content around the TSS is increased (67 %) compared to WT (42 %), this could hinder both, stable Pol I recruitment, and DNA melting. We showed that different CE mutations affected different steps of Pol I initiation. CF interaction site is relatively clearly mapped to ~-28 to ~-13 relative to the TSS and proper DNA binding is essential for factor association and initiation. Mutation in this CF interacting region impair template competition ability, in contrast to the mutations around the TSS.

CF poorly protects promoter DNA in DNase I footprinting assays

We did not observe footprints of Pol I or CF (Supplemental Figure 5). Albeit PIC components co-eluted on sizing columns, buffer conditions might have been inappropriate for stable interaction of Pol I with the promoter (compare Figure 19) and in EMSA reactions different complex populations were not distinguishable (Figure 20 B and Supplemental Figure 5). CF interactions could not be unambiguously identified with this method. Naked DNA in control reaction is poorly digested in the predicted CF interaction sequence from -15 to -28. Adaption of DNA digest conditions may produce different DNA fragments. Longer pre-incubation-times can favor a stable UAF-TBP CF conformation and experiment might be repeated with adapted conditions. An exo-nuclease approach was suitable for analyzing CF-DNA interactions and high-resolution cryo-EM structures allowed to visualize CF-DNA interaction in detail (Sadian et al. 2019). Nevertheless, pattern of UAF-DNA contacts helps to reinvestigate functional parts of the rDNA promoter and UAF.

Interaction patter of UAF with promoter DNA is pronounced and in agreement with earlier studies on the endogenous complex (Hontz et al. 2008). We are able to efficiently bind UAF to the DNA template and assay promoter templates with higher factor occupancy, >90% of DNA is UAF bound. This allows more stringent digestion and more sensitive detection of DNA interaction at areas at the upstream end.

UAF recognized proximal UE with high specificity and could be stabilized by distal DNA contacts

UAF is the nucleating factor for PIC formation, its stable association with the Pol I promoter is crucial for efficient transcription initiation. UAF is the only PIC component, which remains at the Pol I promoter during different growth states of yeast cells. While Pol I/Rrn3 complex formation is disrupted in stationary cells and promoters are devoid of CF, UAF stably associates with the promoter (Claypool et al. 2004; Philippi et al. 2010; Goetze et al. 2010). *In vitro*, all other components of the Pol I PIC, but UAF, can dissociate from the DNA template after initiation (Aprikian et al. 2001).

A more proximal UAF binding region could be composed of UAF subunits Rrn5, Rrn9 and Rrn10 which would allow sequence specific binding of the factor (some more upstream of -91 to -40). UAF without the Uaf30-subunit still can be directed to the promoter and only affects a small DNA-interaction region around -100 (Hontz et al. 2008). This interaction might be stabilized by additional DNA-contacts of the histone proteins H3/H4. In the nucleosomal context, H3 and H4 mainly interact with DNA phosphate backbone and minor-grove (Luger et al. 1997). It is unlikely, that these subunits, that are spread over the whole genome in the nucleosome complex, account for highly specific DNA binding. On the other hand, this DNA-binding capacity is likely to support the stable interaction of UAF with its promoter.

The proximal UE was previously found to be sensitive for shorter (10-12 bp) mutations, leading to reduced, not completely abolished transcription, and initially termed ‘CE II’ position (-76 to -51) (Kulkens et al. 1991). Later, when the minimal requirements for promoter-dependent transcriptions were defined, this nomenclature was discarded and the promoter was described as bi-partite UE-CE architecture (Choe et al. 1992; Keys et al. 1996; Keener et al. 1998).

Fittingly the proximal UE-promoter region was strongly protected from DNase I cleavage in footprinting assays (Figure 20 and Supplemental Figure 5, 6) arguing for intense protein-DNA interactions in this region. UAF specifically associated with this proximal UE and was stabilized by the distal UE. This distal part was required for efficient transcription stimulation and stabilized UAF-DNA-interaction but did not show high specificity on its own. In DNA binding assays, the proximal UE up to -91 efficiently recruited UAF when compared to the ΔUE mutant. However, this is not reflected in *in vitro* transcription reactions, under my experimental conditions. Here, template activity was reduced to about 50% of the WT template. Together with the observation, that mutations in the distal UE (-155 -127) (-155 -91) (-155 -76) failed to efficiently compete with an WT fragment, the distal UE might have previously undescribed functions. First, it stabilizes UAF DNA interactions, locking the recruited

transcription factor to its genomic target and keeping it stably associated. Proper positioning might induce a stable conformation allowing recruitment and positioning of CF. Further, proper UAF association is needed for the recruitment and stable formation of the UAF/TBP/CF complex. Template competition ability is impaired in the distal UE mutants, suggesting a destabilization of the committed complex. Stable CF and/or Pol I association may depend on stable UAF binding in a distinct conformation. This would agree with a model for CF-promoter recognition. Engel et al suggested, that CF recognizes bend, or bendable DNA (Engel et al. 2017)

The importance of the relative position of the binding sites was shown. TBP is known as key factor for CF recruitment (Steffan et al. 1996). As shown above (Figure 11, 22) TBP-UAF interaction might be DNA independent, but for efficient CF recruitment correct positioning of the CF recognition sequence is mandatory. This rather static architecture might be of relevance for suggested initiation-mechanisms by Pol I. It was suggested, that intrinsic mobility of CF ratchets DNA towards the polymerase and thereby facilitates promoter melting (Han et al. 2017; Sadian et al. 2019). Likely, this movement and the requirement of flexible DNA elements are restraint by stable DNA and protein interactions.

Mutants affecting the relative position of UAF and CF binding sites (ins 26, ins 131, UE-rev) were not capable to stimulate Pol I transcription, while factors UAF and CF – independently - associated with the constructs *in vitro*. TBP is required for recruitment of CF and template commitment (Steffan et al. 1996). CF recruitment by TBP relies on a distinct spacing and positioning of the DNA recognition sequences. Albeit some CF can be ectopically recruited *in vivo (Christopher Schächner/Achim Griesenbeck, unpublished)*, incorrect positioning of the CE leads to inefficient complex formation *in vitro*, impairing competition to the refence template.

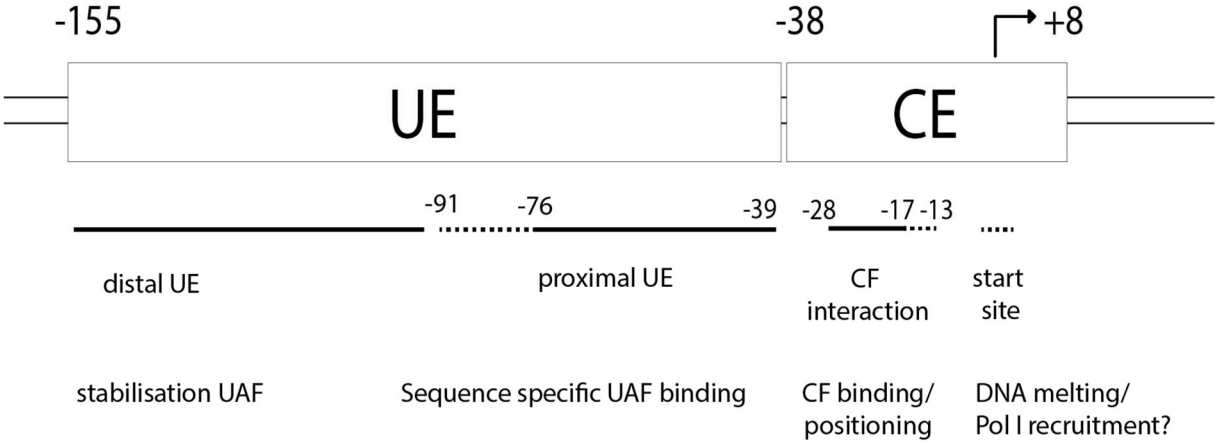

Figure 32: Model for Pol I promoter architecture
Re-investigation of sequence elements revealed a more detailed description of the Pol I promoter; CF interaction site could be mapped more precisely and was confirmed by other studies; proximal UE was found to be important for specific promoter recognition; distal UE could stabilize UAF promoter interactions,

We better defined DNA elements at the Pol I promoter. CF interactions were identified and agree with other studies (Engel et al. 2017; Sadian et al. 2019; Jackobel et al. 2019). We found supporting

information, that the relative positioning of DNA elements is important for activated transcription (Musters et al. 1989). Finally, the proximal UE is required for specific UAF binding, but additional sequences more upstream were required for stable association and high levels of transcription *in vitro*.

DNA structure at the rDNA gene

Different studies speculated about a specific DNA conformations or structures at the rDNA locus. Early studies suggested an 'ribomotor'-model, where enhancer elements and Reb1 form large gene loops (Kulkens et al. 1992). At the promoter, identification of histone proteins H3/4 as components of UAF suggested the idea that DNA might wrap around the transcription factor complex similar to nucleosomes (Keener et al. 1997). Nuclease cleavage patterns of CF in ChEC experiments (Goetze et al. 2010) support this idea. Further, two main interaction sites of TBP were identified in ChIP-exo experiments at the Pol I promoter, the first around the TSS, the second co-localizing with UAF (Uaf30) profiles around -60 (Rossi et al. 2021). It is not clear, if these observations are caused by different states of the multi-copy locus, or result from a conformation that would allow both contacts. Interestingly, a mechanism proposed that CF might recognize bendable DNA (Engel et al. 2017).

3.2.7. TBP and Net1-C form an interaction-hub between UAF and the core PIC

UAF as nucleating factor, that is stably associated with the Pol I promoter and resides there during multiple rounds of transcription, likely acts as a recruiting factor for the other PIC components. Crosslinking mass-spectrometry data and initial negative stain reconstructions suggest a bipartite promoter architecture. TBP together with Net1-C forms an interaction hub between UAF and core-PIC. Stepwise assembly of an active PIC, beginning with recruitment of TBP by promoter bound UAF, would provide several checkpoints (Steffan et al. 1996).

As nucleating factor UAF mediated recruitment of TBP and subsequent formation of the UAF/TBP/CF complex could be a target for Pol I regulation. UAF occupies its gene targets also in growth states and conditions, where Pol I transcription is shut-down (Claypool et al. 2004; Philippi et al. 2010; Goetze et al. 2010). Formation of the PIC likely relies on promoter contacts and protein-protein interactions of UAF, TBP and CF which could be targeted by post-translational modifications. Predestined to such modifications could be the histone-tails of H3 and H4 in UAF. Interestingly, we observe strong crosslinking of H3-tail to TBP and Rrn6. So far, no posttranslational modifications (PTMs) of Pol I factors that regulate its activity could be identified. The expression source used for UAF production and purification, baculo-virus infected insect cells, involved a eukaryotic PTM machinery and can strongly modify expressed proteins and their activity (as an example Net1 in this work). UAF can be reconstituted in *E.coli* cells, however its activity could be only shown in cellular extracts but not in a more defined system with purified components (Smith et al. 2018). Complexes purified from *E. coli* might be modified in crude yeast extracts, while complexes from eukaryotic cells (endogenous or recombinant) would carry functional modifications.

3.2.8. UAF stabilizes a promoter bound complex, that efficiently recruits Pol I

UAF recognizes the UE with high specificity. Transcription from a second reference template lacking the UE is repressed. This effect becomes more pronounced at elongated pre-incubation times. UAF-TBP might sequester factors from the reference, and Pol I should be the limiting factor in this reaction. (5 nM Pol I, 5 nM DNA templates >80 % decorated with UAF, 20 nM CF). Thus, a specific conformation of the DNA-bound UAF-TBP-CF-Net1-C complex might efficiently recruit Pol I/Rrn3. Studies on binding dynamics in live cells suggest that transcription factors mostly interact with chromatin DNA rather transiently. Interactions with TFIID or TFIIB and TFIIA, or TFIIIB stabilize TBP on Pol II and Pol III promoters, respectively. Longer residence time might increase probability of Pol recruitment and subsequent initiation (Zhang et al. 2016; Gouge et al. 2017b; Gietl et al. 2014).

A divergent mechanism for TBP in Pol I initiation compared to its role in Pol II and Pol III was suggested (Engel et al. 2017). Accordingly, FRET-experiments (by Kevin Kramm in the group of Dina Grohmann, unpublished) did not reveal strong signals of a 90° bend as observed for Pol II and Pol III (Gietl et al. 2014; Gouge et al. 2017a). TBP likely positions more upstream (~ -40) at the promoter than at its canonical position in Pol II. To introduce the characteristic bend, TBP utilizes two pairs or highly conserved phenylalanine residues, that are inserted into the DNA minor grove. Recruitment of TBP to UAF might happen independently of DNA contacts. It is neither clear if TBP association with the promoter is required or protein-protein interaction can be sufficient, nor if a TBP bend might play a functional role in Pol I transcription. In this context mutational analysis of TBP could help to get insights into divergent molecular mechanism of this conserved factor. Mutations on the less conserved N-terminal lobe linked to Pol I function (Ravarani et al. 2020). This is in good agreement with our crosslinking-mass-spectrometry data, where we observe mainly crosslinks in the N-terminal TBP lobe to both CF and UAF subunits

3.3. Structural basis of RNA polymerase I pre-initiation complex formation and promoter melting

Within this work, we describe an early intermediate initiation complex. The structure enables the independent discussion of promoter recruitment and DNA-melting in a sequential manner. Apparently, the polymerase is recruited to its dsDNA promoter but cannot complete the melting process due to a lack of fixated downstream DNA. We described the eiPIC reconstruction in the context of PIC formation and continue to update our model of Pol I recruitment and DNA-melting in light of these findings. Our interpretation is well in line with the idea that targeting of the initiation machinery to the rDNA promoter depends mostly on UAF, and TBP serves to position CF downstream of the UE, while interacting with the promoter using a divergent interface. Recruitment of the Pol-I-Rrn3 complex then relies on a specific DNA architecture, namely a bendability that allows interactions of the Rrn11 TPR domain with the Pol I protrusion and binding of a promoter element to the Pol I sandwich region

(Figure 28). (Kownin et al. 1987; Engel et al. 2017). Since our assembly originally comprised UAF and TBP, and only a single reconstruction was obtained from 39% of all recorded particles, it is likely that we capture a physiologically relevant conformation, while factors were artificially positioned by DNA/RNA hybrid scaffolds simulating initial transcription in previous analyses (Engel et al. 2017; Han et al. 2017; Sadian et al. 2017; Sadian et al. 2019), even though RNA was lost in one case (Sadian et al. 2017).

Pol I promoter opening could be highly efficient, combining steric and electrostatic mechanism

Within the eiPIC structure, re-arrangements between CF module I and II enable Rrn7 and Rrn11 to bind promoter DNA, mainly by phosphate backbone interactions of basic loops. This explains the (low) sequence specificity of DNA-binding by CF and thus the overall similar eiPIC architecture compared to ITCs and late PIC reconstructions. Likely, Rrn7-specific DNA-interacting loops contribute to DNA-conformational modulation (compare Figure 27). We further confirm cleft contraction between the protrusion and clamp core domains and exposure of basic residues at the bottom of the cleft during DNA-melting by Pol I in the eiPIC. While our findings do not oppose the idea of an upstream ratchetting mechanism to open Pol I promoter DNA, we also see no evidence to support such a mechanism deduced from shifts in CF-positions observed in ITC reconstructions (Han et al. 2017; Sadian et al. 2019). Instead, we propose a simplified melting-mechanism based on steric DNA-distortion and electrostatic single-strand trapping which, in this combination, is only possible in Pol I, but not in Pol II and III. Firstly, Pol I recruitment relies on DNA-duplex binding to the sandwiching region and DNA positioning within the expanded cleft of the Pol I/Rrn3 complex (Figure 30 A). Sequence specificity is determined by proximal upstream bendability (Engel et al. 2017; Jackobel et al. 2019) and distal upstream recognition by UAF, which is linked to the PIC via CF and TBP. Divergent TFIIB reader-loop elements within Rrn7 are placed in the Pol I cleft, may play a role in duplex-destabilization and bind the melted template strand similar to observations in ITCs (Han et al. 2017).

In addition, allosteric duplex-destabilization resulting from a cleft contraction between the clamp and protrusion domains observed in the eiPIC likely contributes to melting (Figure 30 A). This contraction primes Pol I for initial transcription by re-ordering previously inactivated regions (Figure 26, 30). Exposed basic residues can then contribute to stabilization of the initially melted template strand and ultimately the DNA/ RNA hybrid at the bottom of the cleft. Furthermore, the non-template strand may be bound by the A49 linker (as observed in (Han et al. 2017; Sadian et al. 2019), thereby preventing collapse of the early bubble similar to the σ-factor in bacterial Pol (Boyaci et al. 2019; Feklistov et al. 2017). Only after initial transcription, the growing RNA chain can interact with Rrn7 and would finally clash with reader/linker elements, freeing the exit channel and expelling Rrn7 from the polymerase. This is probably concerted with the association of the flexible A49 tWH domain at the back of the clamp

core domain, leading to dissociation of CF and Rrn3 and preventing re-association, thereby fostering promoter escape.

In Pol II and Pol III initiation complexes (He et al. 2016; Vorländer et al. 2018; Abascal-Palacios et al. 2018), TFIIB/Brf1 cyclin domains occlude the sandwiching region and reader/linker domains diverge from Rrn7, preventing a similar mechanism. Arguing for a model of combined adaptations, a number of CF mutations impaired *in vitro* initiation rates, but only large deletions completely abolished functionality (Knutson et al. 2014; Engel et al. 2017). Furthermore, a 12 subunit Pol I lacking A49/A34.5 is still able to initiate from its native promoter (although the lack of A49 linker-positioning strongly impaired the process) (Beckouet et al. 2008; Pilsl et al. 2016a; Darrière et al. 2019), TBP is not necessary for basal transcription (Keener et al. 1998) and single A49 mutations have only minor effects on Pol I function (Geiger et al. 2010). Thus, the overall functionality of the system is robust and highly adaptive to conditional variations. However, full initiation rates required for physiological growth depend on the combined action of all Pol-I-specific elements that have accumulated throughout evolutionary adaptation and are basically conserved throughout eukaryotic organisms (Moss et al. 2007; Russell and Zomerdijk, Joost C B M 2006; Moorefield et al. 2000). These adaptations increase initial transcription to such efficiency, that formation of a stable closed complex under physiological conditions appears unlikely. While such a state may be transiently established, the instant cleft contraction and Rrn7-dependent duplex-destabilization by the combined action of Pol I and CF elements directly lead to melting and prime the polymerase for initial transcription and hybrid stabilization.

3.4. Model for Pol I initiation

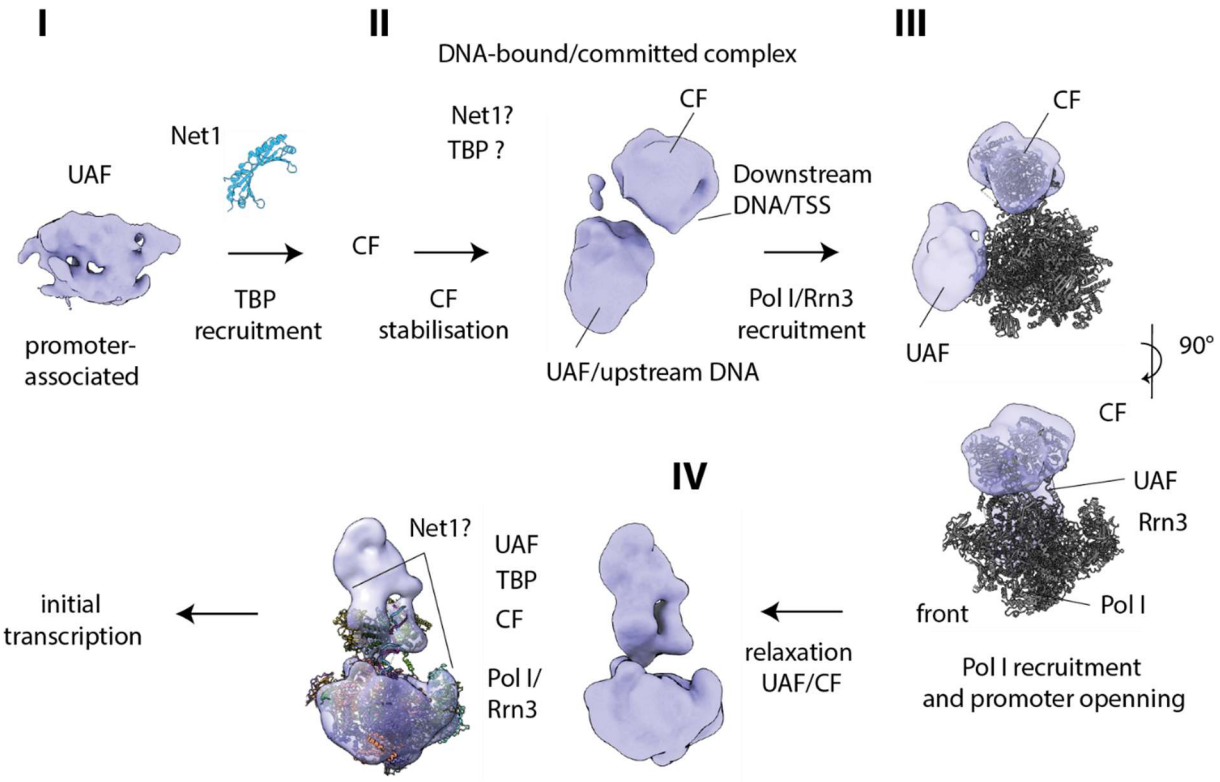

Figure 33: Model of Pol I initiation
I) UAF is associated with promoter DNA (low resolution cryo-EM map of UAF is depicted) and recruits DNA. UAF-TBP may introduce a DNA conformation that stabilises CF at the promoter. II) Stable UAF-TBP-CF complex is formed at the promoter (low resolution negative stain EM map of DNA bound UAF-TBP-CF complex is shown). III) Model for Pol I/Rrn3 recruitment. CF was fitted in EM density, superposition with CF in ITCs would allow Pol I recruitment without major sterically hindrance. IV) After Pol I/Rrn3 recruitment and promoter opening, DNA conformation and interactions of UAF, TBP and CF could relax into a different conformation and allow Pol I to start synthesis of rRNA precursor; low resolution negative stain EM map of Pol I PIC is shown, on the left, pdb 6tps was fitted, extra densities could correspond to UAF and TBP, putative interaction sites for Net1-C are indicated.

UAF is the nucleating factor for Pol I PIC formation. It might associate shortly after replication with the promoter (Keener et al. 1997) and stably associates with the Pol I promoter during different cell stages and growth conditions (Claypool et al. 2004; Goetze et al. 2010). Histone proteins H3/4 could contribute to stable binding, other UAF subunits could support specific recognition of the rDNA promoter. Net1 might join the promoter complex already at this stage. Net1 interaction depends on UAF *in vivo* (Goetze et al. 2010), crosslinking-mass spectrometry of a reconstituted PIC identified putative interaction sites of Net1-C and UAF. Next, UAF would recruit TBP to the promoter interactions do not depend on DNA. TBP might engage with promoter DNA, or not, and stabilises CF at the promoter. My findings were in good agreement with a step-wise promoter assembly model, forming a 'committed' (UAF-TBP-CF-DNA) complex suggested by Steffan et. al. (Steffan et al. 1996). CF did not bind very specific to DNA and was competed with other DNA fragments. We did not find strong protein-protein crosslinking between UAF and CF. TBP could bridge between UAF and CF complex. Whereas interaction of UAF and TBP were robust, TBP interacted only weakly with CF. Protein-protein

interactions alone would hardly explain stabilisation of CF on promoter DNA in presence of UAF-TBP.UAF and TBP might introduce a certain DNA conformation that could be recognised by CF and stabilises CF association. At this step TBP-promoter engagement could play a role. TBP might utilise a different interface for promoter binding in Pol I complexes (Bric et al. 2004) and CF was suggested to recognise bound/bendable DNA (Engel et al. 2017). Once bound, the 'committed complex' was efficiently recruiting Pol I/Rrn3 and strongly supported transcription initiation. Effects like DNA-torsion introduced in the 'committed complex'-conformation could facilitate promoter melting. Our high resolution cryo-EM structure of an eiPIC suggested, that promoter melting and trapping of the template strand could occur spontaneously and Pol I association could disband UAF-TBP conformation. Further, we could expand the Pol I PIC model and included Net1. Net1-C could interact with UAF and Pol I components but stimulated steps after the formation of the committed complex. We found similarities to the acidic activation domain in mammalian UBF, which might be functionally conserved. Transient binding of the activation domain could stabilise initiation intermediates. Finally, Pol I starts synthesis of rDNA and leaves the promoter, Net1 and Rrn3 accompany the enzyme and dissociate shortly after the promoter (Huang and Moazed 2003; Beckouet et al. 2008; Herdman et al. 2017).

Outlook:

Our recombinant expressions system and the established *in vitro* system will allow mutational analysis of UAF components like histone tail truncations, or TBP mutagenesis. We did not address questions on the function of UAF in silencing of Pol II transcription at the rDNA promoter. UAF might occupy E-pro promoter elements and thereby silence transcription and/or act as an obstacle that avoids Pol II transcription into the 35S rRNA gene. TBP plays a central role in Pol I transcription, but the mechanism how it supports Pol I initiation is still not fully understood. We can assemble different complexes of the Pol I machinery. The bottleneck in cryo-EM methodology is the preparation of frozen hydrated samples, behavior of samples can't be predicted and requires empirical optimization. Iterative steps of biochemical stabilization, grid type, geometry and support materials are required to optimize sample-behavior and ice-quality for high-resolution data collection. Apo-UAF, UAF-TBP, UAF assembled on promoter DNA, DNA bound UAF-TBP-CF, and the complete PIC can be purified and resulted so far in low-resolution reconstructions of the complexes (partial results are shown in Figure 33). Thus we can reconstitute all complexes of the step-wise Pol I PIC assembly model proposed in the Nomura lab (Steffan et al. 1996). We will investigate these complexes in more detail with structural and biochemical assays to understand the assembly and function of the Pol I PIC.

4. Materials

4.1. Organisms

4.1.1. Yeast strains

Table 1: Yeast stains used during this study

Database	Name	Genotype	Origin
	GPY2	leu2-Δ1 ade2-101 trp1-Δ63 ura3-52 his3-Δ200 lys2-801 RPA43Δ::LEU2 pAS22 (TRP1)	Stefan Fath/Esther
y206	BY4741	MATa; his3-1; leu2-0; met15-0; ura3-0	Euroscarf
y531	Y531 A190 shuffle	trp1-1; his4-401; leu2-3,112; ura3-52; can r; rpa190::URA3; RPA135-ProtA::kanMX6	Jochen Gerber
y532	D101-I2-RPA135-ProtA	rpa43::LEU2, ade2-101, ura3-52, lys2-801, trpa-D63, his3-D200 leu2-D1, RPA135-ProtA::kanMX6	Jochen Gerber
y2089	D101-I2-Rrn3-ProtA	rpa43::LEU2, ade2-101, ura3-52, lys2-801, trpa-D63, his3-D200 leu2-D1, RRN3-ProtA::kanMX6	Jochen Gerber
y2183	BSY420 Rrn3-ProtA	ade2-1; can1-100; his3200; leu2-3, 112; trp1-1; ura3-1; RRN3-TEV-ProtA-His7(HIS)	Robert Steinbauer
y2423	A135-ProtA, AC40-SNAP-3xFlag	mata; his31; leu20; met150 leu20; ura30 leu20; RPA135-TEV-ProtA::kanMX6	Jochen Gerber
y2670	GalHA A49	his31, leu2-0, lys2-, ura3-0, RPA135-TEV-ProtA::kanMX6, HIS3MX::GAL::HA-RPA49	Jorge Perez-Fernandez
y2679	Gal HA-A12.2	his3-1, leu2-0, lys2-0, ura3-0, RPA135-TEV-ProtA::kanMX6, HIS3MX::GAL::HA-RPA12	Jorge Perez-Fernandez
y3546	BHX WT	trp1-1; his4-401; leu2-3,112; ura3-52; can r; rpa190::URA3; RPA135-ProtA::kanMX7	Michael Pilsl
y3547	BHX1 (A190 RS 1015/1016 > ET)	trp1-1; his4-401; leu2-3,112; ura3-52; can r; rpa190::URA3; RPA135-ProtA::kanMX8	Michael Pilsl
y3548	BHX2 (A190 RS 1015/1016 > DP)	trp1-1; his4-401; leu2-3,112; ura3-52; can r; rpa190::URA3; RPA135-ProtA::kanMX9	Michael Pilsl
y3549	BHX3 (A190 RS 1015/1016 > PS)	trp1-1; his4-401; leu2-3,112; ura3-52; can r; rpa190::URA3; RPA135-ProtA::kanMX10	Michael Pilsl
y3623	A135-(WT)-TAP	ura3-Δ0, his3-Δ1, leu2-Δ0, lys2-Δ0, -HIS3, A135-TAP	Gadal, Olivier

y3624	A135-(D157N)-TAP	ura3-Δ0, his3-Δ1, leu2-Δ0, lys2-Δ0, -HIS3, A135-TAP	Gadal, Olivier
y3625	A135-(F301S)-TAP	ura3-Δ0, his3-Δ1, leu2-Δ0, lys2-Δ0, -HIS3, A135-TAP	Gadal, Olivier
y3626	A135-(I913V)-TAP	ura3-Δ0, his3-Δ1, leu2-Δ0, lys2-Δ0, -HIS3, A135-TAP	Gadal, Olivier
y3627	A135-(WT)-TAP ΔA49	ura3-Δ0, his3-Δ1, leu2-Δ0, lys2-Δ0, rpa49Δ::HPH, -HIS3, A135-(WT)-TAP	Gadal, Olivier
y3628	A135-(D157N)-TAP ΔA49	ura3-Δ0, his3-Δ1, leu2-Δ0, lys2-Δ0, rpa49Δ::HPH, -HIS3, A135-(D157N)-TAP	Gadal, Olivier
y3629	A135-(F301S)-TAP ΔA49	ura3-Δ0, his3-Δ1, leu2-Δ0, lys2-Δ0, rpa49Δ::HPH, -HIS3, A135-(F301S)-TAP	Gadal, Olivier
y3630	A135-(I913V)-TAP ΔA49	ura3-Δ0, his3-Δ1, leu2-Δ0, lys2-Δ0, rpa49Δ::HPH, -HIS3, A135-(I913V)-TAP	Gadal, Olivier
y4094	A135-TAP, AC40-SNAP-3xFlag	ura3-Δ0, his3-Δ1, leu2-Δ0, lys2-Δ0, -HIS3, A135-TAP, -URA3, AC40-SNAP-3xFlag	Michael Pilsl
y4095	A135-ProtA, AC40-SNAP-3xFlag	mata; his31; leu20; met150 leu20; ura30 leu20; RPA135-TEV-ProtA::kanMX6	Michael Pilsl
y4096	A135-TAP, A43-SNAP-3xFlag	ura3-Δ0, his3-Δ1, leu2-Δ0, lys2-Δ0, -HIS3, A135-TAP, -URA3, A43-SNAP-3xFlag	Michael Pilsl
y4097	A135-ProtA, A43-SNAP-3xFlag	mata; his31; leu20; met150 leu20; ura30 leu20; RPA135-TEV-ProtA::kanMX6	Michael Pilsl

4.1.2. Bacteria

Table 2: E. coli strains used during this study

Cells	**Genotype**	**Origin**
BL21 (DE3) pLysS	F–, ompT, hsdSB (rB–, mB–), dcm, gal, l(DE3), pLysS, Cmr	Promega
BL21-CodonPlus(DE3)-RIL	F– ompT hsdS(rB– mB–) dcm+ Tetr gal λ(DE3) endA Hte [argU ileYleuW Camr]	Agilent
BL21(DE3)-R3-pRARE	Derived from BL21(DE3) and Rosetta2 (Merck). BL21(DE3) transformed with plasmid pRARE2 (isolated from Rosetta2 calls), which carries seven rare-codon tRNA genes.	SGC
XL1blue	recA1, endA1, gyrA96 thi-1, hsdR17, supE44, relA1, lac [F´proAB lacIqZΔM15 Tn10 (TetR)]	Stratagene
DH5alpha	F- _80*lac*Z_M15 _(_*lac*ZYA-*arg*F)U169 *rec*A1 *end*A1 *hsd*R17(rk-, mk+) *pho*A *sup*E44 *thi*-1 *gyr*A96 *rel*A1 _	Invitrogen
Pir+ 8c	Δ(argF-lac)169, ΔuidA3::pir+ , recA1, rpoS396(Am), endA9(del-ins)::FRT, rph-1, hsdR514, rob-1, creC510	Imre Berger

DH10Bac-eYFP	pMON7124 (bom+, tra-, mob-), bMON14272 – eYFP, F– mcrA (mrr-hsdRMS-mcrBC) 80lacZΔ M15 lacX74 recA1 endA1 araD139 (ara, leu)7697 galU galK – rpsL nupG	Imre Berger

4.1.3. Insect cells

Insect cell lines SF9 and SF21 used during this study were derived from ovaries of the Fall Army worm, *Spodoptera frugiperda*. Cell-line was provided by Imre Berger (Berger et al. 2004).

4.2. Nucleic acids

4.2.1. Oligonucleotides

Oligonucleotides and gene-synthesis products were purchased from Eurofins and IDT

Database	Name	Sequence
144	M13 rev pUC	AGCGGATAACAATTTCACACAGG
894	RRN3-Not1-f.	TTTTTTGCGGCCGCATGATGGCTTTTGAGAATAC
895	RRN3-Not1-r.	TTTTTTGCGGCCGCAGAAGTGGCGCGCCCTAG
896	RRN3-SP1	TTTCGATTGATGTCGAGTTAC
1616	RPA43-seq	gaaagataagagacaaacgtgg
2115	5'_for_tail_ primer	CGCTAGGCGCCGATATCACCTTACCCTATACTTACTCGCATTCCCTACAATTCTACTTCATACCAAACCAATTC
2207	Kompetitior – Oligo	CGAGTAAGTATAGGGTAAGGTGAT
2334	→H3-XhoI-forw	TTTTTTCTCGAGATGGCCAGAACAAAGCAAAC
2335	→H3-NheI-rev	TTTTTTGCTAGCCTATGATCTTTCACCTCTTA
2336	→H4-Bam-forw	TTTTTTGGATCCATGTCCGGTAGAGGTAAAGG
2337	→H4-XbaI-rev	TTTTTTTCTAGATTAACCACCGAAACCGTATA
2338	→Rrn10-BamI-forw	TTTTTTGGATCCATGGATAGAAATGTATATGA
2339	→Rrn10-XbaI-rev	TTTTTTTCTAGATCAGATATTACCTGGCGCAT
2340	→Rrn5-XmaI-for-new	TTTTTTCCCGGGATGGAGCACCAACAATTGCGGAAGT
2341	→Rrn5-HA-NheI-p24	TTTTTTGCTAGCGCGCGCCCTAGCACTGAGCAG
2342	Rrn9-XhoI-forw	TTTTTTCTCGAGATGAGTGATCTTGACGAAGA
2342	→Rrn9-XhoI-forw	TTTTTTCTCGAGATGAGTGATCTTGACGAAGA
2343	Rrn9-NheI-rev	TTTTTTGCTAGCTCATATGTTCCCATTAGGCA
2343	→Rrn9-NheI-rev	TTTTTTGCTAGCTCATATGTTCCCATTAGGCA
2344	Rrn9-NheI-Flag-rev	TTTTTTGCTAGCTCACATCGTCGTCATCCTTGTAATCACCACCACCTATGTTCCCATTAGGCAGTT
2344	→ Rrn9-NheI-Flag-rev	TTTTTTGCTAGCTCACATCGTCGTCATCCTTGTTTCCCATTAGGCAGTT
2345	Uaf30 BamHI fwd	TTTTTTGGATCCATGGCTGAATTAAACGATTA
2345	→ UAF30-Bam-forw	TTTTTTGGATCCATGGCTGAATTAAACGATTA
2346	Uaf30-7xHis-HindIII-rev	TTTTTTAAGCTTTTTAGAAGTGGCGCGCCCTA
2346	→ UAF30-7xHis-HindIII-rev-	TTTTTTAAGCTTTTTAGAAGTGGCGCGCCCTA
2742	A43-seq-1	tcagaaagataagagacaaacgtgg
2743	A43-seq-2	ccgaagggactatcgttatacact
2851	Gal EcoRI up	CAGTGAATTCTTATATTGAATTTC
2852	A43 XhoI do	GACACTCGAGCTAATCACTATCACTCGATTCACCAT
2857	Gal Eco Seq pRS314	CAAACGTGGATAAGAGTGGCAA
3095	pGEX3	ccgggagctgcatgtgtcagagg
4018	3´r_bio_601 1k	Biotin-CCTACAGCGTGAGCTATGAGAAAG
4018	3´r_bio_601 1k	Biotin-CCTACAGCGTGAGCTATGAGAAAG
4019	3´r_bio_601 2k	Biotin-GAAGCCATACCAAACGACGAGC

4019	3´r_bio_601 2k	Biotin-GAAGCCATACCAAACGACGAGC
4021	5‘ PIP bio rDNA	cgaggtcgaggggcacctgtcac
4022	5‘ for PIP rDNA	cgaggtcgaggggcacctgtcac
4163	Rrn3 NcoI rev	TTTTTTccatggAGAAGTGGCGCGCCCTAG
4164	Rrn3 NcoI neu gc fwd	TTTTTTccatgggcATGATGGCTTTTGAGAATAC
4165	Rrn3 NheI fwd	TTTTTTgctagcATGATGGCTTTTGAGAATAC
4166	Rrn10 Nde1 fwd	ttggcatatgGATAGAAATGTATATGAA
4167	Rrn10 XhoI rev	ttttctcgagGATATTACCTGGCGCATG
4168	Rrn5 NdeI fwd	ttttcatatgGAGCACCAACAATTGCGGA
4169	Rrn5 HindIII rev	ttgcaagcttTTTGGATAACCATTTTAGCA
4175	NcoI_PolI_Prom_1kb_up	ttttccatggggtccagacatgttcagt
4176	#pPIP rev 320 nt	ttactattgcggtaacattcat
4177	#pPIP rev 480 nt	atattgtgtggagcaaagaaat
4178	A34.5_NcoI_fwd	ttttccatgggaATGGGCTCCAAGCTTTCG
4179	A34 NotI rev	ttttgcggccgcATCTCTATGTTTCTTTTTCTTA
4180	A49_1-186-NotI_rev	ttttgcggccgctctatcgttggaagtaattt
4181	A49 1-110 NotI rev	ttttgcggccgctggacccccttagattctt
4182	A49 111 tWH Nhe1 fwd	ttttgctagcaaaataaaaagtaagagtgatactcg
4183	A49 NdeI fwd	ttttcatatgatgtccgtgaaaaggtctgtt
4184	A49 Not1 rev	tttgcggccgcacgtcttggacctcttcct
4185	A49 tWH NheI fwd	ttttgctagcccattagccaatatcgatgc
4186	A49 tWH HindIII rev	ttttaagcttctaacgtcttggacctcttc
4220	#tail fwd Kompetitor rev compl	ATCACCTTACCCTATACTTACTCG
4221	#tail fwd up	ttgtactgagagtgcaccatatg
4222	Amp fwd	ccacgatgcctgcagcaatg
4223	Amp rev	gcaataaaccagccagccgg
4224	TBP NheI fwd	TTTTgctagcATGGCCGATGAGGAACGTTT
4224	TBP NheI fwd	TTTTgctagcATGGCCGATGAGGAACGTTT
4225	TBP NotI rev	TTTTgcggccgcTCACATTTTTCTAAATTCACTTAG
4225	TBP NotI rev	TTTTgcggccgcTCACATTTTTCTAAATTCACTTAG
4226	Pho5 EcoRI neu	tttttgaattcccagcaagatgagccttacc
4227	Pho5 NcoI neu	ttttccatggtagacacgagcaccttgagg
4228	PIP_Reb1_fwd	ttacccggggcacctgtc
4229	PIP_Reb1_Cy5	ttacccggggcacctgtc
4230	PIP_rev_Bio	atcacctagcgactctctcc
4231	601 rev 263 nt	gcctgcaggtcgactctag
4232	Biotin-601 rev 263 nt	gcctgcaggtcgactctag
4233	601 rev 191 nt	atccccttggcggttaaaacg
4234	601 rev 448 nt	ctggcacgacaggtttccc
4235	601 rev no BS	taccgagctcgaattcgtttcc
4352	4339_NcoI	GAGccatggATGACTACTCTGCAGTCCAAGTCG
4353	4340_NsiI	ACGatgcatGTTGGAGTCAGAGTCTGAGG
4354	4351_NcoI	GAGccatggATGTACAAGGTGCACCTGGACCTC
4359	RNAPI-TS CE2	TTTCGCATGAAGTACCTCCCAACTACTTTTCCTCACACTTGTACTCCATGACTAAATTCCCC CTCCCATTACAAACTAAAATCTTACTTTT
4360	RNAPI-NTS CE2	AAAAGTAAGATTTTAGTTTGTAATGGGAGGGGGAATTTAGTCATGGAGTACAAGTGTGA GGAAAAGTAGTTGGGAGGTACTTCATGCGAAA

4361	v1b	TTGCCAGGAATTgaagtacctcccaactactttt
4362	v1_rev	ttcaacacaattaattaacctccacccatcttct
4363	v2.1g	TTGTGTTGAATTGCtttggtatgaagtacctccca
4364	v2.4g	TTGTGTTGAACCCCtttggtatgaagtacctccca
4365	v2_rev	ttaattaacctccacccatcttctccaaccctta
4366	CEop_fwd	aaaagtaagattttagtttgtaatggga
4367	pMax1_+530_NheI_fwd	caccgttgctagcctgctatgg
4368	pMax1_-990_SphI_rev	tggcatgcagaggtagtttcaagg
4369	-4_+8 rev	gtagttgggaggtacGAcCATGgTCGgcagttgaagacaag
4370	-4_+8 fwd	cttgtcttcaactgcCGAcCATGgTCgtacctcccaactac
4371	-4_+8 rev s	tgggaggtacGAcCATGgTCGgcagttgaag
4372	-4_+8 fwd s	cttcaactgcCGAcCATGgTCgtacctccca
4373	V1 rev	ggaggtacttcAATTCCTGgcagttgaagac
4374	V1 fwd	gtcttcaactgcCAGGAATTgaagtacctcc
4375	PIP -47 CEI only NTS	gtgaggaaaagtagttgGGAGGTACTTCATGCGAAA
4376	PIP -47 CEI only TS	TTTCGCATGAAGTACCTCCcaactacttttcctcac
4377	pMAX_NheI_bb_rev	catagcaggctagcaacggtg
4378	pMAX_ClaI_bb_fwd	cgacggtatcgataagcttgatatc
4379	pMAX_ClaI_rev	gatatcaagcttatcgataccgtcg
4380	PIP d-47 rev	tcatggagtacaagtgtgagga
4381	PIP d-28 rev	gtgaggaaaagtagttgggag
4382	PIP d+1 rev	ttttgtatcgataagcttgatatcatgcgaaagcagttgaagacaagtt
4383	PIP [-28 -17] rev	ggtttagtcatggagtacaagtCGACCATGGTCGagttgggaggtacttcAtgc
4384	PIP [-28 -17] fwd	gcaTgaagtacctcccaactCGACCATGGTCGacttgtactccatgactaaacc
4385	PIP [-28 -17] fwd2	ccaactCGACCATGGTCGacttgtactccatgactaaacc
4386	PIP [-28 -17] rev2	gtacaagtCGACCATGGTCGagttgggaggtacttcAtgc
4387	A43 SNAP Flag rev	TCAATAACGTATATCTTTATTTGTTTTGATTTTTTCTCATTTTTCCCGTCtacgactcactataggg
4388	A43 SNAP Flag fwd	acgaggaaaacaccagtgaaagcaatgatggtgaatcgagtgatagtgattccatggaaaagagaagC
4389	AC40 SNAP Flag rev	TTAAGTATTTAATATTTTTCTCAAACTGTGTTTTTTTTTATTAGTATGCAAAGTAGGAtacgactcactataggg
4390	AC40 SNAP Flag fwd	tccgtcaggattttaaagaataaggctgagtatttgaaaaactgtccaattacccaatccatggaaaagagaagC
4391	PIP -38	gagtacaagtgtgaggaaaagtag
4392	PIP -33	caagtgtgaggaaaagtagttgg
4393	PIP +1	Atgcgaaagcagttgaagacaag
4394	PIP d205 fwd	CTGGGTTAcccggTGAACAC
4395	Bubble 38 bp TS	AAGTCAAGTACTTACGCCTGGTCATTACTAGTACTGCC
4396	Bubble 38 bp NTS	GGCAGTACTAGTAAACTAGTATTGAAAGTACTTGACTT
4397	Cy5-RNA Bubble	UAUAUGCAUAAAGACCAGGC
4398	Cy5-RNA Cleavage	UGCAUAAAGACCAGGCuagc
4399	Clv 13 bp NTS	TAGTACTTGACTT
4400	CE LSM -4 +8 rev	CGAcCATGgTCgtacctcc
4401	CE rev neu	tttcgcaTgaagtacctcccaac
4402	dCE rev	atgcatGGTGGTGCTGACC
4403	UE fwd neu	agcttaaattgaagtttttctcgg
4404	Cy3 PIP_rev_119 nt	atcacctagcgactctctcc

4405	PIP_rev_119 nt	atcacctagcgactctctcc
4406	227 nt rev	ggcttaactatgcggcatcag
4407	147 nt rev	gcattctcgagacggtgtag
4408	PIP fragment fwd	gag tgc acc aat tgg gta cc
4409	PIP fragment rev	gga tcc aag cga gca aaa gc
4417	#pUC rev 485nt	agcgcagcgagtcagtgag
4418	Cy5-Footprint +17 fwd	tttccaaactcttttcgaacttgtc
4419	Footprint +17 fwd	tttccaaactcttttcgaacttgtc
4420	Footprint +17 rev	aaaagcaggTGCGGCCGC
4668	R7d46_56F	ttaacgacgatgaaacaagacgtctgaatcttaccaccaatgc
4669	R7d46_56R	ttcagacgtcttgtttcatcgtcgttaaattccacgtcacctt
4670	R7dl43-47F	aggtgacgtggaatttaacctcaacggcctcgg
4671	R7d43-47R	ccgaggccgttgaggttaaattccacgtcacct
4672	R7d46_50F	ttaacgacgatgaaCTCGGTGCAGGTGTTATCacaagacgtc
4673	R7d46_50R	AACACCTGCACCGAGttcatcgtcgttaaattccacgtcaccttccataacg
4674	R7d51_56F	ATGATCTCAACGGCacaagacgtctgaatcttaccaccaatg
4675	R7d51_56R	ttcagacgtcttgtGCCGTTGAGATCATCttcatcgtcg
4676	R7da4a209-220F	gatccagctgccacctttaatgggcaactgtacaacaaaatcg
4677	R7da4a209-220R	cccattaaaaggtggcagctggatcctccacgatttcggtagt
4678	R7d287_297F	gaacctgacactggtaagtaatcatgccgaactcagggtcctctc
4679	R7d287_297R	catgattacttaccagtgtcaggttccgaatgtctgtttcttcaaattcgataac
4680	R7d51_56l	ttcagacgtcttgtGCCGTTGAGATCATCttcatcgtcgttaaattc
4681	R746_56_3xGA_F	tttaacgacgatgaaGGTGCGGGCGCAGGTGCGacaagacgtctgaatcttaccaccaatg
4682	R746_56_3xGA_R	attcagacgtcttgtCGCACCTGCGCCCGCACCttcatcgtcgttaaattccacgtcaccttc
4683	R7_N49A_F	atgaaGATGATCTCgcgGGCCTCGGTGCAGGTGCAGGTGTTATC
4684	R7_N49A_R	CCTGCACCGAGGCCcgcGAGATCATCttcatcgtcgttaaattc
4685	PIP -155 R	agcttaaattgaagtttttctcggc
4686	PIP +28 F	tcgaacttgtcttcaactgctttc
4687	PIP +24 F	acttgtcttcaactgctttcgc
4688	PIP +8 F	tttcgcaTgaagtacctcccaac
4689	PIP -38+24 NTS	GAGTACAAGTGTGAGGAAAAGTAGTTGGGAGGTACTTCATGCGAAAGCAGTTGAAGAC AAG
4690	PIP -38+24 TS	CTTGTCTTCAACTGCTTTCGCATGAAGTACCTCCCAACTACTTTTCCTCACACTTGTACTC
4691	RNAPI-NTS-Bio_Atto647N C12	aaa agt aag att tta gtt tgt aat ggg agg ggg aat tta gtc atg gag tac aag tgt gag gaa aag tag ttg gga ggt act tcA TAC CAA AGG GGT TCA ACA CAA GGG T
4692	RNAPI-TS_Cy3 C13	ttt tca ttc taa aat caa aca tta ccc tcc ccc tta aat cag tac ctc atg ttc aca ctc ctt ttc atc aac cct cca tga agt ATG GTT TCC CCA AGT TGT GTT CCC A
4693	PIP NTS (-155 +8)	AGCTTAAATTGAAGTTTTTCTCGGCGAGAAATACGTAGTTAAGGCAGAGCGACAGAGAG GGCAAAAGAAAATAAAAGTAAGATTTTAGTTTGTAATGGGAGGGGGGGTTTAGTCATGG AGTACAAGTGTGAGGAAAAGTAGTTGGGAGGTACTTCATGCGAAA
4694	PIP TS (-155 +8)	TTTCGCATGAAGTACCTCCCAACTACTTTTCCTCACACTTGTACTCCATGACTAAACCCCCC CTCCCATTACAAACTAAAATCTTACTTTTATTTTCTTTTGCCCTCTCTGTCGCTCTGCCTTAA CTACGTATTTCTCGCCGAGAAAAACTTCAATTTAAGCT

4.2.2. Plasmids

Table 3: Plasmids used during this study

Data-base	Name	Marker	Description
1	pBluescript	Amp	Cloning
190	pNOY373	Amp	Pol I promoter
435	pMAX1	Amp	Pol I promoter
436	pMAX2	Amp	Pol I promoter
437	pMAX3	Amp	Pol I promoter
688	pET21a	Amp	expression vector
689	pET24a	Kan	expression vector
729	Ycplac111-GAL-Rrn3-TEV-ProtA-His7	Amp/Leu	Gal dependent overexpression of Rrn3-TEV-ProtA-His7
1127	pUCDM MultiBac vector Chl	Chl	MultiBac
1129	pSPL MultiBac vector Spec	Spec	MultiBac
1130	pFL MultiBac vector Amp/ Gent	Amp/Gen t	MultiBac
1211	pSPL-6xHis MultiBac vector Spec 6xHis-tag in MCS2	Spec	MultiBac
1212	pFL-Flag-TEV MultiBac vector Amp/Gent	Amp/Gen t	MultiBac
1247	pUC19 PIP g- 601	Amp	generation tail templates
1253	pUC19 tail G- 601	Amp	generation tail templates
1336	MultiBac UAF -H3/4	Amp/Gen t/Chl	MultiBac Expression UAF -H3/4 (Rrn5-3xHA/Rrn10-pUCDM- Rrn9-Flag/UAF30-7xHis -pFL)
1338	MultiBac UAF	Amp/Gen t/Spec/Ch l	MultiBac Expression UAF (Rrn5-3xHA/Rrn10-pUCDM-Rrn9-Flag/UAF30-7xHis -pFL- H3/H4-pSPL(UAF)0)
1573	pUC19 tail G- w/o BS	Amp	tail template
1573	pUC19 tail G- w/o BS	amp	tail template
1864	YCplac22-GAL-RPA43	Amp	conditional A43 expression
1868	YCplac22-GAL-FLAG-RPA43	Amp	conditional A43 expression
1884	pRS314 A43 WT Gal:A43	Amp	A43 Shuffle vector
1885	pRS314 A43 (S141/143A) Gal:A43	Amp	A43 Shuffle vector
1886	pRS314 A43 (S141/143D) Gal:A43	Amp	A43 Shuffle vector
1887	pRS314 A43 WT Gal:Flag-A43	Amp	A43 Shuffle vector
1888	pRS314 A43 (S141/143A) Gal:Flag-A43	Amp	A43 Shuffle vector
1889	pRS314 A43 (S141/143D) Gal:Flag-A43	Amp	A43 Shuffle vector

1932	MultiBac UAF+TBP	Amp/Gent/Spec/Chl	MultiBac Expression UAF+TBP
1959	pUC19 PIP G- w/o BS	Amp	Pol I promoter dependent transcription
1959	pUC19 PIP G- w/o BS	Amp	Pol I promoter dependent transcription
2250	pET28b A49/A34.5	Kan	expression of A49/A34.5 dimer
2313	pUC19 PIP g- elong 601	Amp	Extended g-less cassette für besseres Labeling in pulse chase Experimenten
2314	pUC19 PIP g- elong TER	Amp	Extended g-less cassette für besseres Labeling in pulse chase Experimenten
2315	pUC19 PIP g- elong w/o BS	Amp	Extended g-less cassette für besseres Labeling in pulse chase Experimenten
2315	pUC19 PIP g- elong w/o BS	Amp	Extended g-less cassettefor better Labeling in pulse chase Experiments
2316	pUC19 tail g- elong 601	Amp	Extended g-less cassette für besseres Labeling in pulse chase Experimenten
2317	pUC19 tail g- elong TER	Amp	Extended g-less cassette für besseres Labeling in pulse chase Experimenten
2318	pUC19 tail g- elong w/o BS	Amp	Extended g-less cassette für besseres Labeling in pulse chase Experimenten
2318	pUC19 tail g- elong w/o BS	Amp	Extended g-less cassettefor better Labeling in pulse chase Experiments
2400	pET28b His6-Rrn3	Kan	Expression His6-Rrn3
2400	pET28b His6-Rrn3	Kan	Expression His6-Rrn3
2401	pET Duet CF	Amp	Expression His6-Rrn6; His6-Rrn7; Rrn11
2402	pET24a Rrn3-TEV-ProtA-His7	Kan	expression Rrn3-TEV-ProtA-His7
2403	pET28b His6-A49 186-415 (tWH)	Kan	expression His6-A49-tWH (186- 415)
2404	pET28b His6-A49 111-415	Kan	expression His6-A49 111- 415
2405	pET28b A34.5-His6	Kan	expression A34.5-His6
2406	pET28b A34.5/A49 (1-186) -His6	Kan	expression A34.5/A49 (1-186) -His6
2407	pET28b A34.5/A49 (1-110) -His6	Kan	expression A34.5/A49 (1-110) -His6
2454	pET28b His6-TBP	Kan	Expression His6-TBP
2516	pEX A2 1 PIP ins 131 bp	Amp	Pol I Promoter cis element analysis: 131 bp insertion between UE -39 and CE -38
2517	pEX A2 2 PIP WT	Amp	Pol I Promoter WT
2518	pEX A2 3 PIP LSM [-4 +8]	Amp	Pol I Promoter cis element analysis: linker scanning mutant CE -4 +8 relative to TSS see Musters '89
2519	pEX A2 4 PIP Δ [-155 -28]	Amp	Pol I Promoter cis element analysis: Truncation UE (-155 -28)
2520	pEX A2 5 PIP Δ [-155 -76]	Amp	Pol I Promoter cis element analysis: Truncation UE (-155 -76)
2521	pEX A2 6 PIP LSM [-28 -17]	Amp	Pol I Promoter cis element analysis: linker scanning mutant CE -28 -17 relative to TSS see Musters '89
2522	pEX A2 7 PIP Δ [-204 -156]	Amp	Pol I Promoter cis element analysis: Pol I Promoter (-204 -156) deletion including Reb1 BS

2523	pEX A2 8 PIP LSM [-87 -76]	Amp	Pol I Promoter cis element analysis: linker scanning mutant CE -87 -76 relative to TSS see Musters '89
2524	pEX A2 9 PIP UE inv	Amp	Pol I Promoter cis element analysis: UE (-155 -39) inverted
2525	pEX A2 10 PIP Δ [-155 -91]	Amp	Pol I Promoter cis element analysis: Truncation UE (-155 -91)
2526	pEX A2 11 PIP Δ CE (-38 +7)	Amp	Pol I Promoter cis element analysis: deletion of CE (-38 +8)
2527	pEX A2 12 PIP Δ UE (-155 -39)	Amp	Pol I Promoter cis element analysis: deletion of UE (-155 -39)
2528	pEX A2 13 PIP LSM (-38 -28) +6	Amp	Pol I Promoter cis element analysis: linker scanning mutant CE -38 -28 relative to TSS plus 6 bp insertion
2529	pEX A2 14 PIP Ins 26 bp	Amp	Pol I Promoter cis element analysis: 26bp insertion between UE -39 and CE -38
2530	pPIP 1 ins 131 bp	Amp	Pol I Promoter cis element analysis: 131 bp insertion between UE -39 and CE -38
2531	pPIP 2 WT	Amp	Pol I Promoter WT
2532	pPIP 3 LSM [-4 +8]	Amp	Pol I Promoter cis element analysis: linker scanning mutant CE -4 +8 relative to TSS see Musters '89
2533	pPIP 4 Δ [-155 -28]	Amp	Pol I Promoter cis element analysis: Truncation UE (-155 -28)
2534	pPIP 5 Δ [-155 -76]	Amp	Pol I Promoter cis element analysis: Truncation UE (-155 -76)
2535	pPIP 6 LSM [-28 -17]	Amp	Pol I Promoter cis element analysis: linker scanning mutant CE -28 -17 relative to TSS see Musters '89
2536	pPIP 7 Δ [-204 -155]	Amp	Pol I Promoter cis element analysis: Pol I Promoter (-204 -156) deletion including Reb1 BS
2537	pPIP 8 LSM [-87 -76]	Amp	Pol I Promoter cis element analysis: linker scanning mutant CE -87 -76 relative to TSS see Musters '89
2538	pPIP 9 UE inv	Amp	Pol I Promoter cis element analysis: UE (-155 -39) inverted
2539	pPIP 10 Δ [-155 -91]	Amp	Pol I Promoter cis element analysis: Truncation UE (-155 -91)
2540	pPIP 11 Δ CE [-38 +7]	Amp	Pol I Promoter cis element analysis: deletion of CE (-38 +8)
2541	pPIP 12 Δ UE (-155 -39)	Amp	Pol I Promoter cis element analysis: deletion of UE (-155 -39)
2542	pPIP 13 LSM (-38 -28) +6	Amp	Pol I Promoter cis element analysis: linker scanning mutant CE -38 -28 relative to TSS plus 6 bp insertion
2543	pPIP 14 Ins 26 bp	Amp	Pol I Promoter cis element analysis: 26bp insertion between UE -39 and CE -38
2582	pEGFP-C1-hUBF1	Kan, Neo	May serve to express an EGFP-hUBF1 in mammalian cells.
2583	pFL_NET1	Amp	Expression of TAP-tagged Net1 in S. Frugiperda
2584	pFL_NET1ΔCTD	Amp	Expression of TAP-tagged net1(1-1051) in S. Frugiperda
2585	pFL_CTD	Amp	Expression of TAP-tagged Net1-CTD in S. Frugiperda
2595	pFL-TAP	Amp	Expression of TAP-tagged proteins in S. Frugiperda
2595	pFL-TAP	Amp	Expression of TAP-tagged proteins in S. Frugiperda
2617	pFL hUBF1-CTR-TAP	Amp	vector for recombinant expression of a hUBF1-CTR-TAP fusion protein in insect cells

2618	pFL HP hUBF1-CTR-TAP	Amp	vector for recombinant expression of a hUBF1-HP-CTR-TAP fusion protein in insect cells
2620	pEX A2 15 PIP UE inverted	Amp	Pol I Promoter cis element analysis: inversion of UE (-155 -39)
2621	pEX A2 16 PIP Δ [-68 -39]	Amp	Pol I Promoter cis element analysis: PIP Δ [-68 -39]
2622	pEX A2 17 PIP Δ [-155 -127]	Amp	Pol I Promoter cis element analysis: PIP Δ [-155 -127]
2623	pEX A2 18 PIP Δ [-97 -39]	Amp	Pol I Promoter cis element analysis: PIP Δ [-97 -39]
2624	pEX A2 19 PIP Δ [-126 -39]	Amp	Pol I Promoter cis element analysis: PIP Δ [-126 -39]
2625	pEX A2 20 PIP Δ [-126 -76]	Amp	Pol I Promoter cis element analysis: PIP Δ [-126 -76]
2626	pEX A2 21 PIP Δ [-155 -126 ; -68-39]	Amp	Pol I Promoter cis element analysis: PIP Δ [-155 -126 ; -68-39]
126(CE)	pET28b Rrn7 WT	Kan	expression Rrn7 WT
2827	pET28b Rrn7 Δ [7 - 94]	Kan	expression Rrn7 Δ [7 - 94]
2828	pET28b Rrn7 Δ [43 - 47]	Kan	expression Rrn7 Δ [43 - 47]
2829	pET28b Rrn7 Δ [46 - 56]	Kan	expression Rrn7 Δ [46 - 56]
2830	pET28b Rrn7 Δ [46 - 50]	Kan	expression Rrn7 Δ [46 - 50]
2831	pET28b Rrn7 Δ [51 - 56]	Kan	expression Rrn7 Δ [51 - 56]
2832	pET28b Rrn7 Δ [209 - 220]	Kan	expression Rrn7 Δ [209 - 220]
2833	pET28b Rrn7 Δ [287 - 297]	Kan	expression Rrn7 Δ [287 - 297]
2834	pET21a-Rrn6-Rrn11 (C-terminal 6xHIS tag on Rrn11)	Amp	expression CF (Rrn6, Rrn11)

4.3. Chemicals

Ultrapure water (< 18 Ω) was received from an Elga Purelab Ultra filtration device. Unless stated otherwise, all chemicals and solvents used in this work were purchased at the highest available purity from Sigma Aldrich, Merck, Roth or J.T.Baker.

4.3.1. Media

Table 4: Media used during this study

	media	**ingredients**	**concentration**
E. coli	LB	tryptone	1.2% (w/v)
		yeast extract	2.4% (w/v)
		NaCl	0.5% (w/v)
		agar (plates)	2% (w/v)
	TB	tryptone	1.2% (w/v)
		yeast extract	2.4% (w/v)
		glycerol	0.5% (v/v)
	10x TB salts	KH_2PO_4	170 mM

		K_2HPO_4 x $3H_2O$	720 mM
	50x TB induction additive (5052)	glucose	2.5% (w/v)
		α-Lactose	10% (w/v)
		glycerol	25% (v/v)
Antibiotics		Ampicilin	100 µg/ml
		Kanamycin	50 µg/ml
		Gentamycin	10 µg/ml
		Tetracyclin	10 µg/ml
		Spectinomycin	50 µg/ml
		Chloramphenicol	30 µg/µl
Blue-White Screening		IPTG	0.5 mM
		X-Gal (5-Bromo-4-chloro-3-indoxyl-β-D-galactopyranoside)	200 µg/ml
Yeast	YPD	yeast extract	1% (w/v)
		peptone	2% (w/v)
		glucose	2% (w/v)
		agar (plates)	2% (w/v)
	YPG	yeast extract	1% (w/v)
		peptone	2% (w/v)
		galactose	2% (w/v)
		agar (plates)	2% (w/v)
	YPR	yeast extract	1% (w/v)
		peptone	2% (w/v)
		raffinose	2% (w/v)
		agar (plates)	2% (w/v)
	SC medium (synthetic complete)	YNB	0.67% (w/v)
		glucose/galactose/raffinose	2% (w/v)
		CSM (Complete Supplement Mixture)	see product for inividual dropout media
		complemented with lacking	
		L-histidine	20 mg/L
		L-leucine	100 mg/L
		L-tryptophan	50 mg/L
		L-arginine	20 mg/L
		uracil	20 mg/L
		agar (plates)	2% (w/v)
		NaOH (plates)	1.25 mM
Insect cells	Sf-900 II SFM (Gibco/ThermoFisher)		
	FuGENE HD Transfection Reagent (Promega)		

4.3.2. Buffer

Table 5: Buffers used in this study

Assay	**Buffer**	**Ingredients**

Biotin-coupling	Reaction buffer 1x	5 mM Tris/HCl pH 7.5; 0.5 mM EDTA; 1 M NaCl
Biotin-coupling	1x TE	10 mM Tris/HCl pH 7.5; 1 mM EDTA
CF (BIIC) purification	lysis	50 mM HEPES/KOH pH 7,8; 100 mM KCl; 5 mM $MgAc_2$; 0.1% Tween-20; 1 mM DTT; 1x PI
CF (BIIC) purification	wash	20 mM HEPES/KOH pH 7,8; 200 mM KCl; 5 mM $MgAc_2$; 0.1% Tween-20; 1 mM DTT; 1x PI
CF (BIIC) purification	elution	20 mM HEPES/KOH pH 7,8; 200 mM KCl; 5 mM $MgAc_2$; 0.1% Tween-20; 1 mM DTT; 0.2 mg/ml FLAG-peptide
CF (E. coli) purification	lysis	50 mM HEPES/KOH; 10% glycerol; 10 mM $MgCl_2$; 0.35 M NaCl; 10 mM imidazole; 1 mM DTT; 1x PIs
CF (E. coli) purification	wash A	20 mM HEPES/KOH; 10% glycerol; 10 mM $MgCl_2$; 0.2 M NaCl; 25 mM imidazole; 1 mM DTT
CF (E. coli) purification	wash B	20 mM HEPES/KOH; 10% glycerol; 10 mM $MgCl_2$; 0.2 M NaCl; 50 mM imidazole; 1 mM DTT
CF (E. coli) purification	wash C	20 mM HEPES/KOH; 10% glycerol; 10 mM $MgCl_2$; 0.2 M NaCl; 50 mM imidazole; 1 mM DTT; 5 mM ATP; 2 mg/ml detaturated proteins
CF (E. coli) purification	wash D	20 mM HEPES/KOH; 10% glycerol; 10 mM $MgCl_2$; 0.2 M NaCl; 50 mM imidazole; 1 mM DTT
CF (E. coli) purification	elution	20 mM HEPES/KOH; 10% glycerol; 10 mM $MgCl_2$; 0.2 M NaCl; 350 mM imidazole; 1 mM DTT
CF (E. coli) purification	heparin A	20 mM HEPES/KOH; 10% glycerol; 1 mM $MgCl_2$; 3 mM DTT
CF (E. coli) purification	heparin B	20 mM HEPES/KOH; 10% glycerol; 1 mM $MgCl_2$; 2 M NaCl; 3 mM DTT
CF (E. coli) purification	SEC buffer	20 mM HEPES/KOH; 10% glycerol; 1 mM $MgCl_2$; 0.3 M NaCl; 10 µM $ZnCl_2$; 5 mM DTT
Coomassie	Coomassie Staining	methanol 40% (v/v); acetic acid 10% (v/v); Coomassie Brilliant Blue 0.25% (w/v)
Coomassie	Coomassie Destaining	methanol 40% (v/v); acetic acid 10% (v/v);
Dnase I Footprinting	reaction buffer (1x)	20 mM HEPES/KOH pH 7,8; 200 mM KCl; 10 mM $MgCl_2$; 3 mM DTT, 0,2 mg/ml BSA
Dnase I Footprinting	stop solution	450 mM NaAc pH 5,3; 20 mM EDTA; 20 mM EGTA, 40 ng/µl glycogen
Dnase I Footprinting	loading dye	95% formamide; 20 mM EDTA; 0,02% bromphenole blue
Dnase I Footprinting	sequencing gel	7% acrylamide; 8 M urea; 1x taurine buffer
EMSA	reaction buffer 1x	20 mM HEPES/KOH pH 7,8; 5 mM $MgCl_2$; 5 mM EGTA; 2.5 mM DTT; 0.02% NP40; 0.2 mg/ml BSA; 10 µM $ZnCl_2$
EMSA	native PAGE gel	0.5x TBE; 4-6% acrylamide
EMSA	running buffer	0.4x TBE
EMSA	loading dye	0.4x TBE; 60% glycerole; 0.02% organge G dye
In vitro transcription	Reaction buffer 1x	20 mM HEPES/KOH pH 7,8; 10 mM $MgCl_2$; 5 mM EGTA; 2.5 mM DTT; 0.2 mM ATP; 0.2 mM UTP; 0.2 mM GTP; 0.01 mM CTP
In vitro transcription	buffer H0	20 mM HEPES/KOH pH 7,8; 10% glycerol; 2 mM $MgCl_2$; 0.1 mM EDTA; 2.5 mM DTT

In vitro transcription	proteinase K buffer	10 mM Tris/HCl pH 7.5; 0.3 M NaCl; 0.55% SDS; 5 mM EDTA + proteinase K 0.5 mg/ml
In vitro transcription	loading dye	0.1x TBE; 80% formamid (de-ionised); 0.02% bromphenolblue; 0.02% xlencyanol
In vitro transcription	urea PAGE gel	1xTBE buffer; 6-20% acrylamide; 8 M urea
In vitro transcription	dilution buffer	20 mM HEPES/KOH pH 7,8; 10% glycerol; 2 mM $MgCl_2$; 0.2 KAc; 5 mM DTT; 0.2 mg/ml BSA
MonoQ/S	buffer A	20 mM HEPES/KOH pH 7,8; 10% glycerol; 2 mM $MgCl_2$; 3 mM DTT
MonoQ/S	buffer B (KAc)	20 mM HEPES/KOH pH 7,8; 10% glycerol; 2 mM $MgCl_2$; 2 M KAc; 3 mM DTT
MonoQ/S	buffer B (KCl)	20 mM HEPES/KOH pH 7,8; 10% glycerol; 2 mM $MgCl_2$; 1 M KCl; 3 mM DTT
MonoQ/S	buffer B (NaCl)	20 mM HEPES/KOH pH 7,8; 10% glycerol; 2 mM $MgCl_2$; 2 M NaCl; 3 mM DTT
Net1 purification	lysis	50 mM HEPES/KOH pH 7,8; 10% glycerol; 200 mM KCl; 5 mM $MgCl_2$; 1 mM DTT; complete protease inhibitor cocktail (Roche)
Net1 purification	wash 1	20 mM HEPES/KOH pH 7,8; 10% glycerol; 200 mM KCl; 2 mM $MgCl_2$; 0.05% NP40; 1 mM DTT; complete protease inhibitor cocktail (Roche)
Net1 purification	wash 2/elution	20 mM HEPES/KOH pH 7,8; 10% glycerol; 200 mM KCl; 2 mM $MgCl_2$; 0.05% NP40; 1 mM DTT
PA600-fraction	storage buffer	150 mM HEPES/KOH pH7,8; 40% glycerol; 60 mM $MgCl_2$; 1 mM DTT
PA600-fraction	Buffer T0	20 mM HEPES/KOH pH 7,8; 20% glycerol; 10 mM $MgCl_2$; 0,2 mM EDTA; 1 mM DTT, 1 x PIs
PA600-fraction	Buffer A90	20 mM HEPES/KOH pH 7,8; 20% glycerol; 10 mM $MgCl_2$; 90 mM KCl; 0,2 mM EDTA; 1 mM DTT, 1 x PIs
PA600-fraction	Buffer A350	20 mM HEPES/KOH pH 7,8; 20% glycerol; 10 mM $MgCl_2$; 350 mM KCl; 0,2 mM EDTA; 1 mM DTT, 1 x PIs
PA600-fraction	Buffer D0	20 mM HEPES/KOH pH 7,8; 20% glycerol; 2 mM $MgCl_2$; 0,2 mM EDTA; 1 mM DTT, 1 x PIs
PA600-fraction	P600	20 mM HEPES/KOH pH 7,8; 20% glycerol; 2 mM $MgCl_2$; 600 mM KAc; 1mM DTT or 5 mM β-mercapto-ethanol
Pol I purification	lysis	50 mM HEPES/KOH; 10% glycerol; 10 mM $MgCl_2$; 0.4 M $(NH_4)_2SO_4$; 1 mM DTT; 1x PIs
Pol I purification	wash buffer B1500	20 mM HEPES/KOH pH 7,8; 20% glycerol; 1,5 M KAc; 2 mM $MgCl_2$; 1 mM DTT
Pol I purification	wash buffer/TEV elution	20 mM HEPES/KOH pH 7,8; 20% glycerol; 0.2 M KAc; 2 mM $MgCl_2$; 0,05 % NP40; 10 µM $ZnCl_2$; 1 mM DTT
purification IgG magnetic beads	Binding (P600)	20 mM HEPES/KOH pH 7,8; 20% glycerol; 600 mM KAc; 2 mM MgCl2; 0,1 % NP40; 1 mM DTT; 1 x PIs
purification IgG magnetic beads	wash buffer B1500	20 mM HEPES/KOH pH 7,8; 20% glycerol; 1,5 M KAc; 2 mM $MgCl_2$; 0,1 % NP40; 1 mM DTT
purification IgG magnetic beads	wash buffer B200	20 mM HEPES/KOH pH 7,8; 20% glycerol; 0.2 M KAc; 2 mM $MgCl_2$; 0,05 % NP40; 1 mM DTT
purification Talon-resin	Binding (P600)	20 mM HEPES/KOH pH 7,8; 20% glycerol; 600 mM KAc; 2 mM MgCl2; 0,2 mM EDTA; 5 mM β-mercapto-ethanol; 1 x PIs
purification Talon-resin	wash buffer 1	20 mM HEPES/KOH pH 7,8; 20% glycerol; 1,5 M KAc; 2 mM MgCl2; 0,1% NP40; 5 mM β-mercapto-ethanol

purification Talon-resin	wash buffer 2	20 mM HEPES/KOH pH 7,8; 20% glycerol; 600 mM KAc; 2 mM MgCl2; 5 mM imidazole; 0,1% NP40; 5 mM β-mercapto-ethanol
purification Talon-resin	elution buffer	20 mM HEPES/KOH pH 7,8; 20% glycerol; 600 mM KAc; 2 mM MgCl2; 150 mM imidazole; 5 mM β-mercapto-ethanol
Rrn3 purification	lysis	50 mM HEPES/KOH; 10% glycerol; 0.2 M NaCl; 10 mM imidazole; 1 mM DTT; 1x PIs
Rrn3 purification	wash	20 mM HEPES/KOH; 10% glycerol; 0.2 M NaCl; 25 mM imidazole; 1 mM DTT
Rrn3 purification	elution	20 mM HEPES/KOH; 10% glycerol; 0.2 M NaCl; 150 mM imidazole; 1 mM DTT
Rrn3 purification	SEC buffer	20 mM HEPES at pH 7.8, 0.3 M NaCl, 5 mM DTT
SDS-PAGE	stacking gel	4-6% acrylamide; 1x upper tris; 0.7% APS; 0.1% TEMED
SDS-PAGE	separating gel	6-15% acrylamide; 1x lower tris; 0.7% APS; 0.1% TEMED
SDS-PAGE	upper tris 4x	0.5 M Tris/HCl pH 6,8; 0.4% SDS; 0.02% bromphenolblue
SDS-PAGE	lower tris 4x	1.5 M Tris/HCl pH 8,8; 0.4% SDS
SDS-PAGE	loading dye 4X	0.25 M Tris/HCl pH 6,8; 8.4% SDS; 40% glycerol; 1 mM EDTA; 0.01% bromphenolblue; 0.57 M β-mercapto-ethanol
SDS-PAGE	HU	0.2 M Tris/HCl pH 6,8; 5% SDS; 8 M urea; 1 mM EDTA; 0.01% bromphenolblue; 0.2 M β-mercapto-ethanol
Silver staining	fixation	methanol 50% (v/v); acetic acid 12% (v/v); formaldhyde 0.02% (v/v)
Silver staining	wash	50% ethanole (v/v)
Silver staining	preincubation	0.8 mM $Na_2S_2O_3$
Silver staining	staining	12 mM $AgNO_3$; formaldhyde 0.03% (v/v)
Silver staining	developping solution	0.56 M $NaCO_3$; 0.016 mM $Na_2S_2O_3$; formaldhyde 0.02% (v/v)
Silver staining	stop solution	acetic acid 1% (v/v)
TBE	1x TBE	455 mM Tris; 455 mM boric acid; 10 mM EDTA
TBP purification	lysis	50 mM HEPES/KOH; 10% glycerol; 10 mM $MgAc_2$; 0.2 M KCl; 10 mM imidazole; 5 mM β-mercaptoethanole; 1x PIs
TBP purification	wash 1	20 mM HEPES/KOH; 10% glycerol; 10 mM $MgAc_2$; 1 M KCl; 20 mM imidazole; 5 mM β-mercaptoethanole
TBP purification	wash 2	20 mM HEPES/KOH; 10% glycerol; 10 mM $MgAc_2$; 0.2 M KCl; 20 mM imidazole; 5 mM β-mercaptoethanole
TBP purification	elution	20 mM HEPES/KOH; 10% glycerol; 10 mM $MgAc_2$; 0.2 M KCl; 20 mM imidazole; 5 mM β-mercaptoethanole
TBP purification	SEC buffer	20 mM HEPES/KOH; 10% glycerol; 2 mM $MgCl_2$; 0.2 M KCl; 5 mM DTT
TE	1x TE	10 mM Tris/HCl pH 8; 1 mM EDTA
UAF purification	lysis	50 mM HEPES/KOH; 10% glycerol; 10 mM $MgCl_2$; 0.4 M $(NH_4)_2SO_4$; 10 mM imidazole; 1 mM DTT; 1x PIs
UAF purification	wash 1	20 mM HEPES/KOH; 10% glycerol; 5 mM $MgCl_2$; 1 M KCl; 10 mM imidazole; 1 mM DTT
UAF purification	wash 2	20 mM HEPES/KOH; 10% glycerol; 5 mM $MgCl_2$; 0.4 M KCl; 50 mM imidazole; 1 mM DTT

UAF purification	wash 3	20 mM HEPES/KOH; 10% glycerol; 2 mM $MgCl_2$; 0.4 M KCl; 1 mM DTT
UAF purification	elution	20 mM HEPES/KOH; 10% glycerol; 2 mM $MgCl_2$; 0.4 M KCl; 300 mM imidazole; 1 mM DTT
UAF purification	SEC buffer	20 mM HEPES/KOH; 10% glycerol; 2 mM $MgCl_2$; 0.4-1 M KCl; 5 mM DTT
Western Blot	transfer buffer	20% methanol (v/v); 25 mM Tris; 192 mM glycin; 0.05% SDS
Western Blot	1x PBS	137 mM NaCl; 2.7 mM KCl; 20 mM KH_2PO_4; 10 mM $Na_2HPO_4x2H_2O$
Western Blot	1x PBST	137 mM NaCl; 2.7 mM KCl; 20 mM KH_2PO_4; 10 mM $Na_2HPO_4x2H_2O$ + 0.02% Tween20
Western Blot	Ponceau S	0.1% Ponceau S; 1% acetic acid (v/v)
Western Blot	blocking	137 mM NaCl; 2.7 mM KCl; 20 mM KH_2PO_4; 10 mM $Na_2HPO_4x2H_2O$ + 0.02% Tween20 + 5% dry milk powder
Western Blot	blocking BSA	137 mM NaCl; 2.7 mM KCl; 20 mM KH_2PO_4; 10 mM $Na_2HPO_4x2H_2O$ + 0.02% Tween20 + 2% BSA

4.3.3. Antibodies

Table 6: Antibodies used in this study

Antibody	**Species**	**Dilution**	**Source**
Anti-Flag (M2)	rat	1:2500	Agilent
Anti-HA (3F10)	rat	1:5000	Roche
INDIA-His-HPR (peroxidase conjugated)		1:2500	Pierce
PAP	rabbit	1:5000	GenScript
anti-rabbit (peroxidase conjugated)	goat	1:5000	Dianova
anti-rat (peroxidase conjugated)	goat	1:5000	Dianova
Anit-A43	rabbit	1:10000	(Buhler et al. 1980)
Anti-A49	rabbit	1:50000	(Buhler et al. 1980)
Anti-Pol I	rabbit	1:10000	(Buhler et al. 1980)
Anti-A135	rabbit	1:30000	(Buhler et al. 1980)
Anti-TBP	rabbit	1:20000	

4.3.4. Kits

Table 7: Kits used during this study

Monarch PCR purification Kit	New England Biolabs (NEB)
peqGOLD Cycle Pure Kit	Peqlab
peqGOLD Plasmid Miniprep Kit II	Peqlab
Phusion High-Fidelity DNA Polymerase	New England Biolabs (NEB)
QIAEX II Gel Extraction Kit	Qiagen
QIAquick Gel Extraction Kit	Qiagen
QIAquick PCR purification Kit	Qiagen
Roche BM Chemiluminescence Western Blotting Substrate (POD)	Roche
Thermo Sequenase Cycle Sequencing Kit	USB

4.3.5. Commercial enzymes

Table 8: Commercial enzymes used during this study

Antarctic Phosphatase	New England Biolabs (NEB)
GoTaq polymerase	Promega
Herculase II Fusion DNA Polymerase	Agilent
Phusion High-Fidelity DNA Polymerase	New England Biolabs (NEB)
Proteinase K	Sigma Aldrich
Restriction Endonucleases	New England Biolabs (NEB)
RNaseA	Invitrogen
T4 DNA ligase	New England Biolabs (NEB)
T7 RNA-polymerase	New England Biolabs (NEB)
Thermo Sequenase DNA Polymerase	ThermoFischerScientific
Zymolyase 20T	Seikagaku Corp.

4.4. Equipment

Table 9: Equipment used during this study

1600TR Liquid Scintillation Analyzer	Packard
Äkta Pure	GE Healthcare
Äkta Purifier	GE Healthcare
Avanti J-26 XP Centrifuge	Beckman Coulter
Avanti J-26S XP Centrifuge	Beckman Coulter
Bc-Mag Separator-24	Bioclone
Bc-Mag Separator-50	Bioclone
Branson Sonifier S-250A	Branson
Centrikon T-1170 Ultracentrifuge	Contron
Clip Ring	Gatan
Clip Ring Tool	Gatan
Cressington 208 carbon coater	Cressington
equipped with 4k × 4k CMOS camera (TemCam-F416)	TVIPS
Ettan LC	Pharmacia
Gatan 626 Cryo Transfer Holder	Gatan
Gel Documentation System	Intas
Gel max UV transilluminator	Intas
Glow Discharge Device, Plasma Cleaner/Sterilizer PDC-3xG	Harrick
Gradient Master 107 IP	Biocomp
IKA-Vibrax VXR	IKA
Insect cell incubator	Binder
JEM 2100F	Jeol
LAS-3000 Chemiluminescence Imager	Fujifilm
MicroPulser Electroporation Apparatus	BioRad
Nanodrop ND-1000	Thermo Fisher Scientific
Optima L-80 XP Ultracentrifuge	Beckman Coulter
PCR Cycler Nexus mastercycler	Eppendorf
Pelco ‘EasiGlow’ plasma cleaner	TedPella
Precellys Evolution with Cryolys	Bertin Instruments
QIAcube	Qiagen

SMART FPLC system	Pharmacia
Speed Vac Concentrator	Savan
Trans-Blot SD Semi-dry transfer cell	BioRad
Typhoon FLA-9500	GE Healthcare
Vitrobot Mark IV	Thermo Fisher Scientific
XCell SureLock Mini-/Midi-Cell Electrophoresis	Thermo Fisher Scientific

5. Methods

5.1. DNA manipulation

5.1.1. Polymerase chain reaction (PCR)

A proofreading enzyme (Phusion polymerase, NEB) was used for cloning purposes. For analytical PCR reactions e.g. colony-PCRs GoTaq-Polymerase (Promega), or home-made Taq-polymerase were used. PCR reactions were performed in thin 0,2 ml tubes.

Table 10: Phusion PCR reaction

component	**50 µl reaction**		**final concentration**
5x Phusion HF buffer	10 µl		1x
dNTPs (10 mM each)	1 µl		200 µM
Primer 1 (10 µM)	2.5 µl		0.5 µM
Primer 2 (10 µM)	2.5 µl		0.5 µM
Template DNA (0.2-100 ng)	variable		0.2-100 ng
Phusion DNA Polymerase	0.5 µl		1 u/50 µl
H_2O	to 50 µl		
Phusion PCR	1x	98°C	2'
	30-35x	98°C	10''
		T_m-5°C	15''
		72°C	30'' + 30''/kb
	1x	72°C	5'

PCR products were purified using PCR purification kits and analyzed on agarose gels.

Table 11: GoTaq PCR

component	**25 µl reaction**		**final concentration**
5x green GoTaq buffer	5		1x
dNTPs (10 mM each)	0.5		200 µM
Primer 1 (10 µM)	0.5		0.2 µM
Primer 2 (10 µM)	0.5		0.2 µM
GoTaq Polymerase	0.15		0.75 u/25 µl
H_2O	to 25 µl		
GoTaq PCR	1x	95°C	3'
	35x	95°C	10''
		T_m-5°C	15''
		72°C	30''
	1x	72°C	5'

5.1.2. Restriction enzyme digestion

Sequence specific restriction endonucleases were purchased from (NEB). Enzymatic digest was performed according to manufacturer's instructions and in appropriate buffers. Analytical digests were typically performed in 20 µl reaction volume, 300 ng plasmid DNA, and 0,5 µl restriction enzyme. Preparative digestions were typically performed in 50 µl reaction volume, 1-2µg plasmid DNA, and 1 u restriction enzyme/ µg DNA. Restriction enzymes were heat inactivated when applicable.

5.1.3. De-phosphorylation

Antarctic phosphatase (NEB) was used to de-phosphorylate 5' ends of digested DNA. This prevents re-ligation of vector DNA. 10x Antarctic phosphatase buffer added to restriction enzyme digestions, 1 µl of enzyme was Antarctic phosphatase was added and incubated for 1-14 hours. Enzyme was heat inactivated 20 minutes at 65°C and DNA was purified.

5.1.4. Ligation

Ligation reaction contained 50-100 ng vector/backbone DNA and with 3-5-fold excess of insert DNA in 10 µl final reaction volume. 10x reaction buffer supplemented with ATP and 0,5 µl were added and incubated for 1-16 hours at 16°C. 1-3 µl were used for transformation of E. coli.

5.1.5. Ligation independent cloning

For mutagenesis, ligation independent methods as QuikChange (Agilent) or similar were used. Homologous recombination of overlapping DNA-fragments in E. coli allowed fast generation of point mutations. Therefore, plasmid DNA was amplified by a high-fidelity polymerase (Phusion) with partially overlapping primers containing mutations. Plasmid DNA was digested with DpnI enzyme (1 µl enzyme (20u)/50 µl PCR reaction) at 37°C for 2-16 hours. Reactions were purified on PCR purification columns and used for transformation of E. coli.

PCR Phusion	1x	98°C	1'
	20x	98°C	10''
		T_m-3°C	30''
		72°C	3'30'' (30 sec/kb)
	1x	72°C	15'

5.1.6. Plasmid purification

Plasmids were purified using kits from PeqLab, Qiagen or Invitrogen according manufacturer's instructions. Alkaline lysis of cells in buffers containing NaOH and SDS solubilized nucleic acids and proteins, RNaseA digested cellular RNA. Buffers containing high amounts of KAc precipitated proteins

and genomic DNA. Soluble DNA at acidic pH was bound to a silica-matrix and washed with different buffers. DNA was eluted by changing to neutral/slightly basic pH values and could be further purified by ethanol precipitation.

5.1.7. Purification of PCR products

PCR purification kits from PeqLab, Qiagen or NEB were used. DNA binds at acidic pH to silicate gel columns, short DNA fragments (<100 depending on manufacturer) as PCR-primers do not bind and are removed during washing-steps as other components of the PCR reactions. After wash-steps, DNA was eluted at neutral/slightly basic pH (10 mM TE buffer pH 8).

5.1.8. Purification of nucleic acids from agarose gels

DNA fragments separated on agarose gels were purified using the Qiaex II Gel extraction kit according manufacturer's instructions. SybrSafe stained DNA was visualized under blue light and gel-fragment was cut out. Gel was solubilized, bound to silicate particles, washed, precipitated and re-solubilized neutral/slightly basic pH (10 mM TE buffer pH 8).

5.1.9. Ethanol precipitation

DNA and RNA were purified and concentrated by ethanol precipitation. A volume of nucleic acid solution was supplemented with 1/10 volume 3 M KAc pH 5,3 and mixed. 2 volumes ethanol were added and incubated for one hour at -20°C. Nucleic acids were precipitated for 15 minutes in a table-top centrifuge (15.000 rmp, 4°C), washed with 170 µl 70% ethanol. Supernatant was discarded, pellet was air-dried and resuspended in water or TE buffer.

5.1.10. Agarose gel electrophoresis

Agarose gels (0,8% -2% depending on size of DNA fragment) in TBE buffer were used in this study. DNA was stained with SYBR-Safe stain (added in 1:20.000 dilution to agarose gel) and separated in an electric field of 3-5 V/cm. Size of DNA fragments was estimated from DNA marker bands, typically 2log DNA-ladder (NEB).

5.2. Protein analysis

5.2.1. Protein quantification

Protein concentration in cell lysates were determined using the BioRad Protein assay, based on the Bradford protein assay (Bradford 1976). 1 ml of the diluted BioRad dye solution was incubated with 1-10 µl of protein solution for 30-60 seconds before the absorbance was measured at 595 nm (OD595). Protein concentration is approximated from an BSA calibration curve with BSA, which resulted in the factor 23, which was multiplied with the OD_{595} value. The value is then divided by the sample volume to get the protein concentration in µg/µl.

Protein concentrations of purified proteins were determined with an BSA calibration curve on Coomassie stained SDS PAGE gels and/or UV absorbance at 280 nm. 0,1 – 2 µg BSA were loaded on

SDS PAGE gels, Coomassie stained bands were quantified using ImageJ software (Schneider et al. 2012).

Coomassie Brilliant Blue staining relies on hydrophobic interactions of the dye with aromatic amino-acids and ionic interactions with basic residues (Weist et al. 2008). For larger globular proteins (e.g. Pol I, CF, Rrn3) methods depending on Coomassie blue interactions like the Bradford assay (Bradford 1976) give a good approximation of protein quantities, however this must not be true for intrinsically disordered proteins. Disordered proteins have distinct amino acid composition, with few aromatic and hydrophobic residues and could be weaker bound by the Coomassie dye (Contreras-Martos et al. 2018).

5.2.1.1. Coomassie staining

Proteins separated on SDS-PAGE gels were stained in Coomassie staining solution for 2-16 hours. Gels were de-stained in Coomassie-de-staining solution on a shaker-plate. Commercial alternatives to classical Coomassie-staining were used according manufacturer's instructions. Simply blue safe stain (Invitrogen) was used, which is more sensitive, or Instant Blue protein stain (VWR), which is faster and more sensitive than the traditional method.

5.2.1.2. Silver staining

Low amounts of proteins were stained with the highly sensitive silver-staining procedure, that allows detection of few ng protein per band. First, proteins were fixated in the gel in fixation-solution for 1 h or overnight. The gel was washed in silver-stain-wash solution for 20 min, treated with preincubation solution for 1 min, directly followed by three 20 seconds wash steps with water. Next, the gel was incubated in staining-solution for 20 min and washed two times for 20 seconds with water. The stained protein bands became visible upon incubation with developing solution, development was stopped with 1 % acetic acid.

5.2.2. Protein extraction and precipitation

TCA precipitation or methanol/chloroform extraction can be used to concentrate samples for protein analysis.

5.2.2.1. Trichloroacetic Acid (TCA) Precipitation of Proteins

A defined sample volume is precipitated with a final concentration of 10% TCA and 2 µl 2 % (w/v) Deoxycholate (DOC). After 30 minutes incubation on ice, proteins were pelleted by centrifugation (13.000 rpm, 20 min, 4°C). The supernatant was discarded, the proteins were resolubilized with SDS loading buffer and neutralizes with gaseous NH_3.

5.2.2.2. Methanol/Chloroform precipitation of proteins

Proteins contain hydrophilic and hydrophobic parts, they enrich in the interphase between aqueous phase and organic solvents. Four volumes (600 µl) of methanol were mixed with aqueous protein solution (150 µl). One volume chloroform (150 µl) was added and mixed. After the addition of three volumes water (450 µl) the solution was thoroughly mixed and the phases start to separate and

proteins will enrich in the interphase. The solution was centrifuged (13.000 rpm, 5 min) and the supernatant was carefully removed, avoiding to perturbate the interface. In fractions containing very high salt concentrations, the aqueous phase might have a higher density than chloroform. To precipitate the proteins, three volumes of methanol (450 µl) were added and the sample pelleted by centrifugation (13.000 rpm, 5 min). Supernatant- was discarded, the pellet was dried and finally resuspended in SDS loading buffer.

5.2.3. Sodium dodecyl-sulphate polyacrylamide gel electrophoresis (SDS-PAGE)

During vertical discontinuous sodium dodecyl sulphate polyacrylamide gel electrophoresis, proteins were separated by their molecular weight (Laemmli 1970). Apparent molecular weight was approximated from a molecular weight standard (NEB).

The commercial NuPAGE system (Invitrogen) with MOPS or MES running buffer and 4-12% 0gradient-acrylamide gels have different separation properties and were used if certain bands should be unambiguously separated, or samples were prepared for mass-spectrometric analysis. Gel electrophoresis was performed according to the manufacturer's instructions.

5.2.4. Western Blot analysis

Proteins can be specifically detected via immune-staining of the sample. SDS-PAGE separated samples were transferred to an activated (30 seconds in methanol) polyvinyl difluoride (PVDF)-membrane in a semi-dry transfer cell (Bio-Rad). The activated membrane was equilibrated in transfer-buffer and placed onto three filter papers soaked in transfer buffer (Whatman). The SDS-PAGE gel was equilibrated in transfer buffer, placed on the membrane and another three soaked filter papers were stacked on top. Proteins were transferred voltage of 24 V for 60 minutes. Transfer of proteins was controlled by reversible Ponceau S staining. The membrane was incubated for three minutes with Ponceau S staining solution and de-stained with water. Unspecific interactions with the membrane were blocked with BSA, the membrane was therefore incubated for one hour in a 2% (w/v) solution of BSA, or 5% (w/v) milk powder, in PBS buffer. Antibodies were diluted in the corresponding blocking solution to their working concentration (table antibodies). Primary antibodies were incubated more than one-hour, secondary antibodies for 30 – 60 minutes. Following each antibody incubation step, the membrane was washed three times for 5 min in about 50 ml PBST on a shaker. Secondary antibodies were horseradish peroxidase (HRP) conjugated and can be used to detect specifically bound proteins. The membrane was incubated with 1 ml Chemiluminescence Blotting Substrate (Roche), containing H_2O_2 and luminol as substrate for the HRP. Light emitted during this reaction could be detected on a LAS-3000 imager (Fuji).

5.2.5. Phosphoprotein staining

SDS-polyacrylamide gels were stained with Pro Q Diamond Phosphoprotein stain (Invitrogen) according to the manufacturer's instructions and visualized on a 315 nm UV in a Typhoon FLA

9500. The same gel was then stained with SimplyBlue SafeStain (Invitrogen) for total protein staining.

5.3. Work with E. coli

5.3.1. Cultivation

E. coli cells were cultivated in LB medium supplemented with antibiotics (Table 4) for selection. Cell density was determined by measuring absorbance at 600 nm wavelength (OD_{600}).

5.3.2. Transformation E. coli

5.3.2.1. Electro-competent E. coli

For the preparation of electrocompetent bacteria the *E. coli* XL1-blue strain was cultured overnight in SOB medium to an OD600 ~ 3. Afterwards the culture was diluted 1:100 in prewarmed (37°C) SOB and grown while vigorous aeration was given through shaking (300rpm). When the culture reached an OD600 between 0.4 and 0.6 it was chilled on ice for 15min. Afterwards the cells were centrifuged and resuspended in 400ml ice-cold sterile water. After a second centrifugation step the cells were resuspended in 200ml ice-cold sterile water and centrifuged again. After resuspension in 10ml cold and sterile 10% (v/v) glycerol the cell suspension was transferred to a Falcon tube and centrifuged for a last time. The pellet was then resuspended in 1.5ml cold, sterile 10% (v/v) glycerol and aliquots of 50 to 100µl were stored at -80°C.

5.3.2.2. Electroporation

50 µl electro competent *E. coli* cells XL1 blue were thawed on ice. 1-3 µl ligation or ~10 ng circular plasmid were incubated in a pre-cooled electroporation cuvette (0,2 cm). Electroporation in Bio-Rad MicroPulser Electroporation apparatus was performed with program EC2 (2,5 kV pulse). 1 ml LB medium was added an incubated for 45-60 minutes at 37°C. 100 µl were plated on LB plates with selection antibiotics. Remaining cell suspension was pelleted, resuspended and plated on LB plates with selection antibiotics.

5.3.2.3. Chemical-competent E. coli

E. coli XL1-blue strain was cultured overnight in SOB medium to an OD600 ~ 3. Afterwards the culture was diluted 1:100 in prewarmed (37°C) SOB and grown while vigorous aeration was given through shaking (300rpm). When the culture reached an OD600 between 0.4 and 0.6 cells were harvested by centrifugation (10 minutes, 4000 g; 4°C), re-suspended in cold buffer Tfb-1, incubated on ice for 20 minutes and pelleted. Cells were re-suspended in 4 ml buffer Tfb-2, incubated for 20 minutes on ice. 50-100 µl aliquots were stored at -80°

5.3.3. Heat shock transformation

Chemical competent E. coli. were thawed on ice, mixed with 10-50 ng circular plasmid DNA and incubated for 15 minutes on ice. After 45 seconds heat-shock at 42°C, cells were incubated on ice for 10 more minutes. 1 ml LB medium was added and cells incubated for 45-60 minutes. 100 µl

were plated on LB plates with selection antibiotics. Remaining cell suspension was pelleted, resuspended and plated on LB plates with selection antibiotics.

5.4. Work with S. cerevisiae

5.4.1. Cultivation

S. cerevisiae strains were grown in appropriate medium at 30°C.

5.4.2. Transformation

Competent yeast cells and transformation was carried out as described by Schiebel (Knop et al. 1999). 50 ml yeast cells were harvested at OD_{600} ~ 0.5, washed with water and SORB-buffer and finally resuspended in 360 µl SORB-buffer. 40 µl carrier DNA (Salmon sperm DNA (10 mg/ml) denatured at 100C for 10 min and cooled on ice.) were added. Aliquots of competent cells were stored at -80°C.

For transformation circular plasmids (10-50 ng) or for homologous recombination linearized plasmids, or PCR products (up to 1-2 µg) were incubated with 50 µl competent cells. 300 µl PEG was added and incubated for 30 minutes. 40 µl DMSO (final concentration ~10%) was added and cells were incubated at 42°C for 15 minutes. Cells were sedimented and resuspended in SC-medium and plated on selective agar plates. In cases resistance marker *kanMX6* were used, the cells were resuspended in approximately 1 ml YPD, incubated on a shaker for 3-16 hours at 30°C, harvested and spread on a G418 plate.

5.4.3. Purification of genomic DNA

5 ml of an overnight culture were pelleted and resuspended in 0,5 ml DNA-extraction buffer. After 60' Zymolase (250 U/ml) at 37°C, spheroblasts were sedimented (10.000g, 1 minute) and resuspended in 500 µl TE buffer. 50 µl 10% SDS was added and sample was incubated for 30 minutes at 65°C. Proteins were precipitated by addition of 200 µl 5 M KAc for 60 minutes in ice and centrifuged at 10.000 g for 10 minutes. Supernatant was transferred to a fresh tube and nucleic acids were precipitated with an equal volume of isopropanol. After centrifugation, (10.000g, 1 minute) the pellet was air-dried and resuspended in 300 µl TE-buffer. RNA was digested with 20 µg RNaseA at 37°C for 30 minutes. Genomic DNA was precipitated by addition of 30 µl 3 M KAc pH 5,3 and 330 µl isopropanol. After centrifugation, (10.000g, 1 minute) the pellet was air-dried and resuspended in 100 µl TE-buffer.

5.4.4. Denaturing protein extraction from yeast

Equal cells numbers were estimated from OD_{600} measurements. Approximately 5 ml of a yeast culture at OD_{600} ~1 were suspended in 1 ml water and mixed with 150 µl pretreatment solution and incubated for 15 minutes on ice. 150 µl 55% trichloroacetic acid (TCA) was added and the sample was incubated for 10 minutes on ice. After centrifugation (20.000g, 10 minutes, 4°C) the pellet was resuspended in 200 µl HU buffer. pH was neutralized using gaseous NH_3, observing pH indication bromphenole blue in HU buffer. The precipitated proteins were solubilized and incubated for 10 minutes at 70°C. Cell debris and insoluble components were removed by centrifugation (~20.000g, 5 minutes).

5.5. The MultiBac expression system

For recombinant protein production, we used the MultiBac expression system developed by Imre Berger (Berger et al. 2004; Fitzgerald et al. 2006). This baculo-virus expression system was shown to be very suitable for expression and purification of multi-protein complexes. Further, an eukaryotic expression system is beneficial for overexpression of challenging of proteins that require eukaryotic chaperones and/or post-translational modifications (Barford et al. 2013; Abdulrahman et al. 2015). For virus generation, insect cell culture and baculo-virus infections we follow established protocols, described in great detail (Berger et al. 2004; Fitzgerald et al. 2006; Garzoni et al. 2012; Life Technologies 2013; Berger and Poterszman 2015; Abdulrahman et al. 2015).

5.5.1. Cultivation of insect cells

The SF21 and SF9 cell-lines originate from ovaries of a moth species, the Fall Army Worm (*Spodoptera frugiperda*). Cells grow adherent but also in suspension culures without serum. Cells were cultivated at 27°C and 100 rpm in SF-900 II medium (Gibco). Work with insect cells was carried out in a sterile hood. Cell density was determined every 24 hours with a Neubauer counting chamber and cells were diluted to 0,5 x 10^6 cells/ml. Cells showed a doubling time of 20 hours under these conditions within the first three weeks after thawing, and ~24 hours later on. Cell density was kept constantly between 0,5 x 10^6 to 2 x 10^6 cells/ml.

5.5.2. Bacmid generation

Expressions cassettes were integrated into the viral genome in DH10 MultiBac YFP cells using a transposase (Tn7). Therefore, expression-cassettes must contain Tn7 recognition sequences and are derivates of vectors pFL. The element is inserted into a mini attTn7 site in the virus precurser. Sucessful integration of the cassette will destroy expression of a lacZ marker gene, which allows blue-white screening. Positive clones can no more metabolise 5-Brom-4-chlor-3-indoxyl-β-D-galactopyranosid (X-Gal) and form white colonies.

50 ng of plasmid are transformed into chemical competent DH10 MultiBac YFP E.coli cells. Long regeneration times (6 -16 hours) were given, before plating onto adequate plates (LB agar plates containing: 10 µg/ml kanamycin; 100 µg/ml ampicilin; 10 µg/ml gentamycin; 30 µg/ml chloramphenicol; 50 µg/ml spectinomycin; 0,5 mM IPTG; 200 µg/ml X-Gal). Combination of antibiotics according to used plasmids. After overnight growth at 37°C, cell better developp blue/white color when placed to colder temperatures 4/16°C for several hours. White colonies were picked and streaked again on adequate plates together with a blue colony to verify proper staining and selection. Bacmid isolation was carried out with solutions of the PeqLab mini-prep kit. 4 ml of a positive colony was grown over night in LB medium containing antibiotics. Cells were pelleted and resuspended in 300 µl of solution I. 300 µl solution II was added, the tube was inverted and incubated for 5 minutes on RT, to digest RNA. 300 µl solution III was added and the lysate was centrifuged for 10’ at 13.000 rpm. Supernatant was carefully transferred to a new tube and centrifuged again 5’ at 13.000 rpm to avoid

contamination with the white precipitate, that can impair transfection. 700 µl of the supernatant were precipitated with 700 µl of isopropanol and centrifuged 10' at 13.000 rpm. The pellet was washed with 200 µl 70% cold ethanol and centrifuge 5 minutes at 13000rpm, 4°C. The supernatant was removed and the pellet was dried under the sterile hood and resuspended in 30 µl sterile water.

The bacmid solution was transfected with the FuGene transfection reagent (Promega). Per transfection 100 µl of SF900 II medium was mixed with 10 µl FuGene reagent. 20 µl of bacmid solution was mixed with 200 µl medium and supplemented with 100 µl of FuGene-medium mix. During 15-30 minutes incubation, lipid-vesicles from the transfection reagent containing bacmid DNA should form, which can be absorbed by the insect cells.

Per transfection, $1x10^6$ insect cells were seeded into a 6 well plate to adsorb for 15-30 minutes. The supernatant was removed and 3 ml fresh medium (SF900-II, Gibco) was added. As controls, medium only and cells only with water used for bacmid preparation were incubated. 160 µl of the transfection mix was added per well (two wells resulting in 6 ml virus per construct). Infection can be monitored by the occurrence of fluorescence from a YFP marker gene integrated into the virus genome. Cells are monitored after 24, and 48 hours. After 48-60 hours (approx. 5-10% cells YFP positive) the supernatant containing the V_0 virus was collected. For an initial expression test, 3 ml fresh medium was added and cells incubated for 72 hours. Infected cells can be harvested and expression monitored on SDS-gels and western blots.

5.5.3. Virus amplification

V0 virus is a low titer virus, not suitable for large scale infection of insect cells. Therefore, amplification of the initial virus is required. The multiplicity of infection (MOI = ratio of virus particles per cultured cell) during virus amplification should be around 0,1. After infection, insect cells should double at least once but amplification should not take longer than 5 (max. 7) days to prevent recombination events in infected cells which can cause loss of recombinant genes.

A 50 ml culture $0,5x10^6$ cells/ml was infected with 50-200 µl V_0 virus (depending on virus stock titer). Cell density was monitored every 24 hours. If density was $>1x10^6$cells/ml, cells were diluted to $0,5x10^6$ cells/ml. When density was $>1x10^6$cells/ml cells were incubated for another 24 hours. Infection could be also monitored using the YFP marker. This was continued until proliferation arrest of the cells was observed. V_1 virus was collected 48 hours after this proliferation arrest. Therefor cells were centrifuged at 800 rpm for 5 minutes, the supernatant was transferred to a sterile 50 ml falcon and contain the V_1 virus. The pellet was frozen in liquid nitrogen and used for a test-purification. V_2 virus was generated accordingly in large amounts from low MOI infections with V_1 virus. The high-titer V_1/V_2virus was used for large scale infections. 5-20 µl of V_1/V_2 virus were used to infect $1x10^6$ cells. Titer was determined in small scale infection reaction on 50 ml cultures. At optimal titers, cells number should not increase more than 10-20% and almost all cells should show clear signs of infection.

5.5.4. Large scale infection of insect cells

Virus infection in the suspension cultures follow gaussian distribution. Thus, at a MOI of 3 (3 viruses per cell), 99% of all cells should be infected with at least one virus-particle. Erlenmeyer flasks should be filled to a maximum of $1/5^{th}$ of the capacity to ensure sufficient air supply and exchange. In 5 L Erlenmeyer flasks up to 1 L insect cells could be cultivated. After seeding 250 ml cells ($0,5x10^6$cells/ml) the culture was expanded the next days until the final culture reached 1 L at a density of $1x10^6$cells/ml. The culture was infected with V_1 or V_2 virus (titer should have been determined in test infections; amounts of V_1/V_2 should be around 5-20 ml for 1 L culture) and harvested 48 after infection. Cells are flash frozen in liquid nitrogen and stored at -80°C.

5.6. Purification of Pol I/Rrn3

5.6.1. PA600 fraction

Early *in vitro* studies on Pol I were done with fractionated cell extracts. The Pol I initiation machinery precipitated under low salt conditions, could be specifically enriched and further fractionated. (Tschochner 1996; Milkereit and Tschochner 1998). Later, a Pol I purification protocol that relies on a low salt precipitation step was established (Gerber 2008; Gerber et al. 2008). I previously found that Pol I is enriched in the 'PA600'-fraction more than 350-fold relative to total protein amounts in whole cell lysates. The Pol I/Rrn3 complex was purified from a strain which overexpresses Rrn3 fused to a TEV cleavage site linked to a protein A-His7-tag under the control of a GAL1/10 promoter. A 20 L fermenter with YPR (raffinose) was inoculated with a preculture, cultivated in SCR-Leu medium, to OD600 ~ 0,05. When the culture reached an OD600 of ~2, overexpression was induced by addition of 2% w/v galactose final concentration. After three hours of overexpression, cells were harvested by centrifugation, washed with ice-cold water, resuspended in storage buffer (150 mM HEPES/KOH pH7,8, 40% glycerol, 60 mM $MgCl_2$) 1 ml buffer per gram cell-paste, frozen in liquid nitrogen and stored at -80°C. 200 -250 ml cell suspension was thawed on ice, $(NH_4)_2SO_4$ was added to a final concentration of 0,4 M of the salt, 1x protease inhibitors were added and lysed with a bead beater (Biospec) for 90 minutes (30 s bead-beating, 90s cooling in ice water, 0,5 mm glass beads). Glass beads were separated from the lysate and washed with lysis buffer. The lysate was centrifuges at 100,000 g for one hour. The middle layer containing the cleared lysate was collected. I tried to avoid the top lipid layer in the centrifuge tube and the turbid bottom fraction. The clear supernatant (WCE, whole cell lysate) was dialyzed against buffer T0 (20 mM HEPES/KOH pH 7,8; 20% glycerol;10 mM $MgCl_2$, 0,2 mM EDTA; 1 mM DTT, 1 x PIs) to reach the conductivity of buffer A90 (20 mM HEPES/KOH pH 7,8; 20% glycerol; 90 mM KCl;10 mM MgCl2, 0,2 mM EDTA, 1mM DTT; 1 x PIs). The dialyzed sample was loaded to a manually cast DEAE-Sepharose column (13x5,2 cm) equilibrated with buffer A90 and washed with 1 L buffer A90. Proteins were eluted with a step to buffer A350 (20 mM HEPES/KOH pH 7,8; 20% glycerol; 90 mM KCl;10 mM $MgCl_2$, 0,2 mM EDTA; 1mM DTT, 1 x PIs). Protein containing peak-fractions were dialyzed against buffer D0 (20 mM HEPES/KOH pH 7,8; 20% glycerol; 2 mM MgCl2; 0,2 mM EDTA; 1mM DTT; 1

x PIs). The dialyzed sample was centrifuged at 40,000 g for 30 minutes. The pellet containing Pol I and Pol I/Rrn3 was thoroughly resuspended in buffer P600 (20 mM HEPES/KOH pH 7,8; 20% glycerol; 600 mM KAc; 2 mM MgCl2; 0,2 mM EDTA; 1mM DTT or 5 mM β-mercapto-ethanol (DTT should be avoided for Talon purification); 1 x PIs). The resuspended protein solution (5-10 ml; 2,5-5 mg/ml) was centrifuged another 10 minutes at 40,000 g to remove insoluble protein aggregates.

The Pol I enriched PA600-fraction was used for subsequent purification steps, either an immune-precipitation using the TEV-cleavable protein A-tag, or with immobilized-metal-ion chromatography (IMAC).

5.6.2. Immuno-precipitation of Pol I/Rrn3

Equal protein amounts (10-20 mg) of a PA600-fraction were incubated with 200 µL of IgG -coupled magnetic beads, equilibrated three times with buffer P600 (20 mM HEPES/KOH pH 7,8; 20% glycerol; 600 mM KAc; 2 mM $MgCl_2$; 0,1 % NP40; 1 mM DTT; 1 x PIs), for 2 h on a rotating wheel. The beads are washed 4 times with 1 mL wash buffer B1500 (20 mM HEPES/KOH pH 7,8; 20% glycerol; 1,5 M KAc; 2 mM $MgCl_2$; 0,1 % NP40; 1 mM DTT; 1 x PIs) and then three times with 1 mL buffer B200 (20 mM HEPES/KOH pH 7,8; 20% glycerol; 200 mM KAc; 2 mM MgCl2; 0,05 % NP40; 1 mM DTT). The beads were resuspended in 200 µL buffer B200 supplemented with 11.7 µg TEV protease, and incubated for 2 h at 16°C under shaking with 800 rpm in a thermomixer, elution was repeated over night at 4°C. Supernatants were collected, the beads washed with 50 µl buffer B200 and the supernatant pooled with the eluted fractions. Further purification on ion-exchange columns is optional, preparations in my hands resulted in homogenous Pol I/Rrn3 complex. The eluates were frozen in liquid nitrogen and stored at -80°C.

5.6.3. IMAC purification of Pol I/Rrn3

100 µl of Talon-agarose per ml of 'PA600'-fraction were equilibrated in buffer P600 (20 mM HEPES/KOH pH 7,8; 20% glycerol; 600 mM KAc; 2 mM MgCl2; 0,2 mM EDTA; 5 mM β-mercapto-ethanol; 1 x PIs). 5 mM imidazole were added to PA600 fraction to avoid unspecific interactions with the affinity matrix and incubated for two hours with the equilibrated beads. Beads were washed with wash buffer 1 (20 mM HEPES/KOH pH 7,8; 20% glycerol; 1,5 M KAc; 2 mM $MgCl_2$; 0,1% NP40; 5 mM β-mercapto-ethanol; 1 x PIs), wash buffer 2 (20 mM HEPES/KOH pH 7,8; 20% glycerol; 600 mM KAc; 2 mM $MgCl_2$; 5 mM imidazole; 0,1% NP40; 5 mM β-mercapto-ethanol) and eluted with elution buffer (20 mM HEPES/KOH pH 7,8; 20% glycerol; 600 mM KAc; 2 mM MgCl2; 150 mM imidazole; 5 mM β-mercapto-ethanol). The elution fractions were diluted with MonoQ buffer A (20 mM HEPES/KOH pH 7,8; 20% glycerol; 2 mM MgCl2; 3 mM DTT) to 300 mM KAc and loaded to a MonoQ PC 1,6/5 column (Pharmacia) equilibrated in 15 % MonoQ buffer B (KAc) (20 mM HEPES/KOH pH 7,8; 20% glycerol; 2 M KAc; 2 mM MgCl2; 3 mM DTT). Proteins were fractionated in a gradient with 4 CV from 15% to 35% B, 17 CV to 75% B and 4 CV to 100% B. Pol I/Rrn3 eluted at ~1,05 M KAc (~50% B). Gradient fractions were

analyzed on Coomassie stained SDS-PAGE gels, Pol I/Rrn3 containing fractions were pooled and frozen in liquid nitrogen.

5.6.4. Purification of Pol I

Cell lysates were prepared as described in 5.6.1. Protein concentration was determined with the Bradford assay. 1 ml slurry IgG Sepharose per 1 g of total protein, or 2 ml coupled magnetic beads slurry (depends on bead capacity, should be titrated for each new batch of home-made IgG-magnetic beads) were equilibrated in lysis buffer (50 mM HEPES/KOH; 10% glycerol; 10 mM $MgCl_2$; 0.4 M $(NH_4)_2SO_4$; 1 mM DTT; 1x PIs). Beads were incubated for three hours with the lysate, washed with lysis buffer, wash buffer B1500 (20 mM HEPES/KOH pH 7,8; 20% glycerol; 1,5 M KAc; 2 mM $MgCl_2$; 0,1 % NP40; 1 mM DTT; 1 x PIs) and then wash buffer B200 (20 mM HEPES/KOH pH 7,8; 20% glycerol; 200 mM KCl; 2 mM $MgCl_2$; 0,05 % NP40; 10 µM $ZnCl_2$ 1 mM DTT). The beads were resuspended in buffer B200 supplemented with TEV protease, and incubated for 2 h at 16°C under shaking with 800 rpm in a thermomixer, elution was repeated over night at 4°C. Supernatants were collected, diluted with 1,5 volumes of MonoS buffer A and loaded on MonoS GL 5/5 column. Pol I was eluted with a gradient from 10% to 35% buffer MonoS B (KAc) with a plateau at 17,5%.

Pol I eluted in two peaks at ~450 mM KAc (23 mS/cm) and 520 mM KAc (25,5 mS/cm). Peak fractions were pooled, concentrated and frozen in liquid nitrogen. Peak fraction 2 was used.

5.7. Purification of Pol I transcription factors

5.7.1. His_6-TBP expression and purification

S. cerevisae TBP was cloned into vector pET28b via NheI/NotI restriction sites. Recombinant His_6-TBP protein was expressed in BL21(DE3) pRIL cells, by autoinduction in TB medium (1.2% tryptone; 2.4% yeast extract; 0.5% glycerol; 1/10 volume of a sterile solution containing 0.17M KH2PO4 and 0.72M K2HPO4 and 1/50 volume of a sterile solution containing 25% glycerol; 10% lactose and 1% glucose were added. A culture was grown at 37° C to an OD_{600} of 0.6, after cooling the culture on ice, incubation was continued at 16° C overnight. Cells were harvested (6,000g; 10min), resuspended in lysis buffer (50 mM HEPES/KOH; 10% glycerol; 10 mM $MgAc_2$; 200 mM KCl; 10 mM imidazole; 5mM β-mercaptoethanole; 1mM phenylmethylsulphonyl fluoride (PMSF); 2mM benzamidine), and lysed by sonication (Branson Sonifier 250 macrotip, cooling in ice water). The cell extract was cleared (40.000 g for 60 min at 4°C) and incubated with 1 ml equilibrated NiNTA Agarose (Qiagen) at 4 °C for 2 h on a rotating wheel. The resin war transferred to a polypropylene column (Bio-Rad), washed with wash buffer 1 (20 mM HEPES/KOH; 10% glycerol; 5mM $MgAc_2$; 1 M KCl; 20 mM imidazole; 5 mM b-mercaptoethanole), then wash buffer 2 (same as wash buffer 1 but 0.2M KCl) and finally eluted with elution buffer (20mM HEPES/KOH; 10% glycerol; 5mM $MgAc_2$; 0,2 M KCl; 200 mM imidazole; and 5mM b-mercaptoethanole). Subsequent purification on MonoS HR 5/5 cation exchange chromatography and/or gelfiltration on Superdex 75 Increase 10/300 SEC column removed remaining impurities.

5.7.2. Rrn3 expression and purification

Purification of Rrn3 followed an established protocol (Blattner et al. 2011). Rrn3 was expressed in BL21(DE3) pRARE cells, by autoinduction in TB medium (1.2% tryptone; 2.4% yeast extract; 0.5% glycerol); 1/10 volume of a sterile solution containing 0.17 M KH2PO4 and 0.72 M K2HPO4 and 1/50 volume of a sterile solution containing 25% glycerol; 10% lactose and 1% glucose were added. A culture was grown at 37 °C to an OD600 of 0.6, after cooling the culture on ice, incubation was continued at 18 °C overnight. Cells were harvested (6000 g; 10 min), resuspended in lysis buffer (50 mM HEPES at pH 7.8, 200 mM NaCl, 1 mM DTT, 10% glycerol; 1x PI). A 3 ml Ni-NTA column (Qiagen) was equilibrated with lysis buffer, the supernatant loaded, and the column was washed with lysis buffer containing 25 mM imidazole. Elution was carried out in lysis buffer containing 150 mM imidazole. Next, Rrn3 was further purified by anion exchange chromatography Mono Q GL 5/50. The column was equilibrated in MonoQ buffer A (50 mM HEPES at pH 7.8, 100 mM NaCl 5 mM DTT, 10% glycerol), and proteins were eluted with a linear gradient of 20 column volumes from 100 mM to 1M NaCl. After concentration (Amicon, 35 kDa cut-off), the sample was applied to a Superdex 200 increase 10/300 size exclusion column equilibrated with buffer Rrn3-SEC (20 mM HEPES at pH 7.8, 300 mM NaCl, 5 mM DTT) (Pilsl and Engel 2020).

5.7.3. CF expression and purification

In initial experiments CF was expressed and purified from baculo infected insect cells with a one-step Flag-immuno-precipitation on subunit Rrn7 (Merkl et al. 2014; Pilsl et al. 2016b). Later, protocols for recombinant CF purification from E.coli were published (Bedwell et al. 2012; Knutson et al. 2014; Engel et al. 2017). These strategies are cheaper and result in high yields of recombinant protein and I did not observe changes in activity when comparing CF purified from the different expression systems in *in vitro* transcription assays. Therefore I adapted the protocol established by Tobias Gubbey (Engel et al. 2017), which yields purest complex in my preparations.

5.7.3.1. Purification of recombinant CF from baculo-virus infected insect cells

CF subunits Rrn6, Rrn7 and Rrn11 were co-expressed in baculo-virus infected SF21 insect cells. For purification a Flag-epitope fused to the C-terminus of Rrn7 was used. $50x10^6$ cells were resuspended in 30 ml lysis buffer (50 mM HEPES/KOH pH 7,8; 100 mM KCl; 5 mM $MgAc_{2;}$ 0.1% Tween-20; 1 mM DTT; 1x PI) and lysed by sonication using a Branson Sonifier 250 (output 5, duty cycle 40%, 30 s pulse, 30 s cooling, six repeats). Lysate was cleared by centrifugation (40.000 x g for 45 min) and incubated with 200 µl anti-flag M2 Agarose (Sigma) for two hours. Beads were washed three times with lysis buffer and wash buffer (20 mM HEPES/KOH pH 7,8; 200 mM KCl; 5 mM $MgAc_{2;}$ 0.1% Tween-20; 1 mM DTT; 1x PI). CF was eluted with an excess of FLAG-peptide. 100 µl elution buffer (0,2 mg/ml FLAG peptide in wash buffer) were incubated for three hours with the beads and eluted proteins recovered from agarose beads by centrifugation (2.000 g).

5.7.3.2. Purification of recombinant CF from E. coli

CF subunits were co-expressed in E. coli BL21-CodonPlus (DE3)-RIL cells (Agilent) from two plasmids. A 2 L culture was grown in LB medium at 37 °C until OD600 reached 0.5–0.7. Cultures were cooled on ice for 20 min and expression was induced with 0.1 mM IPTG. Cells were grown at 18 °C overnight. Cells were harvested by centrifugation, washed with phosphate-buffered saline (PBS) at 4 °C, flash frozen in liquid nitrogen and stored at −80 °C. One pellet was suspended in buffer CF-A (20 mM imidazole, 350 mM NaCl, 10mM $MgCl_2$, 10% (v/v) glycerol, 50 mM HEPES pH 7.8, 1 mM DTT, 1x protease inhibitor). Cells were lysed by sonication using a Branson Sonifier, the lysate was cleared by centrifugation and the supernatant was filtered with a 0.22 µm filter (Millipore) to remove cell debris. Cell lysate was then applied to a Ni-NTA column (5 ml, GE Healthcare) and bound CF washed with 5 CV of buffer CF-B (25 mM imidazole, 200 mM NaCl, 10 mM MgCl2, 10% (v/v) glycerol, 20mM HEPES pH 7.8, 1 mM DTT) at 4 °C. The column was transferred to room temperature, washed with 2.5 CV of buffer CF-C (50 mM imidazole, 200 mM NaCl, 10mM MgCl2, 10% (v/v) glycerol, 20 mM HEPES pH 7.8, 1 mM DTT, 5 mM ATP, 2 mg/ml denatured protein), incubated for 10 min, and washed again with 2.5 CV buffer CF-C. The column was transferred to 4 °C and washed with 5 CV buffer CF-D (50 mM imidazole, 200mM NaCl, 10 mM MgCl2, 10% (v/v) glycerol, 20 mM HEPES pH 7.8, 1 mM DTT). Elution was performed with 5 CV of buffer CF-E (350 mM imidazole, 200 mM NaCl, 10 mM $MgCl_2$, 10% (v/v) glycerol, 20 mM HEPES pH 7.8, 1 mM DTT). Protein was then loaded on a 1 ml heparin column (GE Healthcare) in buffer CF-F (200 mM NaCl, 1 mM $MgCl_2$, 10% (v/v) glycerol, 20mM HEPES pH 7.8, 1 mM DTT) and eluted with a gradient ranging from 0.2 to 2.0 M NaCl, including a plateau at 550mM NaCl of 4 CVs. CF-containing fractions were concentrated using a 100 kDa cut-off centrifugal filter (Millipore). Size exclusion chromatography was carried out with a Superose 6 increase 10/300 column (GE Healthcare) in buffer CF-SEC (300 mM NaCl, 1 mM $MgCl_2$, 10% (v/v) glycerol, 20 mM HEPES pH 7.8, 10 µM $ZnCl_2$, 5 mM DTT). CF-containing fractions were concentrated using a 100 kDa cut-off centrifugal filter and flash frozen in liquid nitrogen for storage at −80 °C (Pilsl and Engel 2020).

5.7.4. UAF and UAF/TBP expression and purification

UAF was purified from baculovirus infected insect cells, co-expressing Rrn5, Rrn9, Rrn10, Uaf30 and the yeast histone proteins H3 and H4. Subunit Rrn5 was fused to the 3xHA-tag (derived from human influenza hemagglutinin), Rrn9 was marked with the Flag-epitope and Uaf30 with a 7x His-tag. Another virus was co-expressing yeast Spt15/TBP together with the six UAF subunits.

Insect cells culture, virus generation and infection of cultures were guided by established protocols and described in methods 5.5.

$2x10^9$ cells derived from 2 L baculovirus infected insect cells were resuspended in 100 ml UAF lysis buffer (50 mM HEPES pH 7.8, 400 mM $(NH_4)_2SO_4$, 10 mM $MgCl_2$, 10% (v/v) glycerol, 10 mM imidazole, 1 mM DTT, protease inhibitors). Cells were lysed by sonication using a Branson Sonifier 10x30 seconds, 1-minute cooling in ice-water between pulses, the lysate was cleared by centrifugation and the

supernatant was filtered with a 0.22 µm filter (Millipore) to remove cell debris. The lysate was added to 3 ml NiNTA agarose (Qiagen) equilibrated in lysis buffer and incubated for two hours. The beads were transferred to a polypropylene column, washed subsequently with wash-buffer 1 (20 mM HEPES pH 7.8, 1 M KCl, 5 mM $MgCl_2$, 10% (v/v) glycerol, 10 mM imidazole, 1 mM DTT), wash-buffer 2 (20 mM HEPES pH 7.8, 400 mM KCl, 5 mM $MgCl_2$, 10% (v/v) glycerol, 50 mM imidazole, 1 mM DTT), wash-buffer 3 (20 mM HEPES pH 7.8, 400 mM KCl, 2 mM $MgCl_2$, 10% (v/v) glycerol, 1 mM DTT) and eluted in 2 ml fractions with UAF elution buffer (20 mM HEPES pH 7.8, 400 mM KCl, 2 mM $MgCl_2$, 10% (v/v) glycerol, 300 mM imidazole 1 mM DTT). UAF-protein containing fractions were pooled diluted with 1/6 volume buffer A MonoS (20 mM HEPES pH 7.8, 2 mM $MgCl_2$, 10% (v/v) glycerol, 3 mM DTT) and loaded to a MonoS HR 5/5 column equilibrated in 40% buffer MonoS B (KCl) (20 mM HEPES pH 7.8, 1 M KCl, 2 mM $MgCl_2$, 10% (v/v) glycerol, 3 mM DTT). UAF eluted in a step gradient with wash-steps of five column volumes at 40% and 48% B respectively at 72% buffer B (720 mM KCl). The elution fractions contained almost homogenous UAF-complexes. Subsequent gelfiltration (Superdex 200 Increase or Superose 6 Increase) removed remaining impurities (optional) buffer UAF SEC (20 mM HEPES pH 7.8, 600 mM KCl, 2 mM $MgCl_2$, 10% (v/v) glycerol, 5 mM DTT). Fractions were concentrated using a 100 kDa cut-off centrifugal filter and flash frozen in liquid nitrogen for storage at −80 °C.

5.7.5. Expression and purification of full length Net1 and truncations in BIICs

Expression of and initial purification of Net1 and its truncation was initially established by Andreas Maier, Jochen Gerber and Joachim Griesenbeck. Full length Net1 and truncations were expressed as C-terminal TAP fusion proteins in BIICs. Insect cells culture, virus generation and infection of cultures were guided by established protocols as described below (methods 5.5). $1x10^8$ cells derived from 100 mL baculovirus infected insect cells were resuspended in 40 ml Net1 lysis buffer (50 mM HEPES pH 7.8, 200 mM KCl, 10 mM MgCl2, 10% (v/v) glycerol, 1 mM DTT, complete protease inhibitor cocktail (Roche)). Cells were lysed by sonication using a Branson Sonifier, 8x30 seconds, 1-minute cooling in ice-water between pulses, the lysate was cleared by centrifugation and the supernatant was filtered with a 0.22 µm filter. The lysate was added to 0,5 ml IgG Sepharose (GE healthcare) equilibrated in lysis buffer and incubated for two hours. The beads were transferred to a polypropylene column, washed with Net1 ~ 20 bed volumes of wash buffer (20M HEPES pH 7.8, 200 mM KCl, 2 mM MgCl2, 10% (v/v) glycerol, 0,05% NP40, 1 mM DTT) with and without protease inhibitor cocktail. Finally, proteins were eluted with proteolytic cleavage by TEV-protease. Two elution steps, 2 hours at 16 °C and over-night digestion (~ 14 hours) at 4°C were pooled.

5.8. Cryo electron microscopy and the resolution revolution

In the field of RNA polymerase (Pol) I research, a number of cryo-EM studies contributed to understanding the highly specialized mechanisms underlying the transcription of ribosomal RNA genes. During the past years, development of more powerful microscopes, new direct electron

detectors and advances in computational image processing caused a ‘resolution revolution’ (Kühlbrandt 2014) in the field of cryo-electron microscopy (cryo-EM). This culminated in the award of the Nobel Prize in Chemistry to three scientists driving these developments: Joachim Frank, Richard Henderson, and Jacques Dubochet in 2017.

With its increasing popularity, the technique is now more easily accessible and widely used in many areas of structural biology research. Hence, cryo-EM studies on Pol I complexes became possible and advanced our understanding of the molecular mechanisms employed by this highly specialized enzyme (Pilsl et al. 2016a; Engel et al. 2016; Tafur et al. 2016; Han et al. 2017; Sadian et al. 2019; Pilsl and Engel 2020).

The workflow of biochemical purification and sample preparation of Pol I complexes and the optimization of cryo-grid preparation containing frozen, hydrated single particle specimens with the goal of acquiring high resolution images for structure determination, is described below.

We summarized strategies for the purification and stabilization of Pol I complexes and present an efficient workflow for cryo-grid preparation and optimization in a chapter in ‘methods in molecular biology’ (in press). This chapter emphasized technical aspects and describes strategies for cryo-grid preparation in more detail. Still the most limiting factor of high-resolution structure determination by electron cryo-microscopy is sample and grid-preparation (Stark and Chari 2016).

5.8.1. Assembly and purification of Pol I PIC complexes

The assembly of the complete PIC or subcomplexes relied on the detailed *in vitro* characterization of these complexes as describes above (

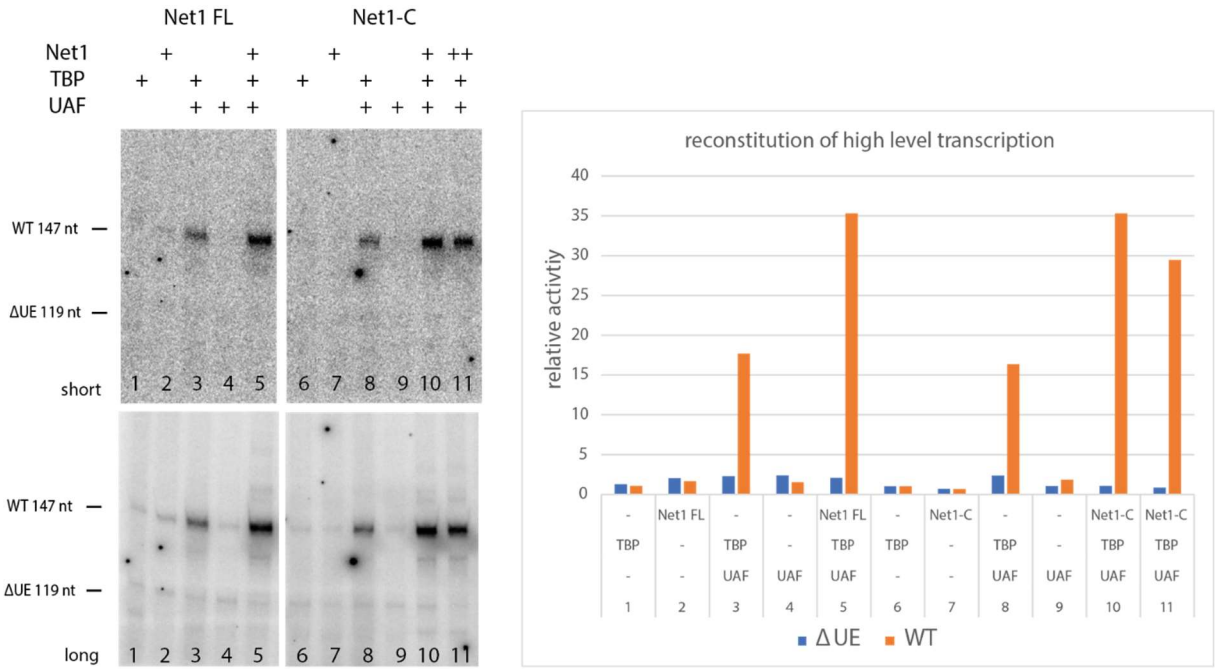

Figure 14). Conditions optimized for maximal DNA, binding and/or transcriptional output where applied as well as the determined order of addition was used. A micro-volume FPLC system (Ettan LC,

Pharmacia) was used, that allowed the application of small sample quantities. For analytical SEC runs, 20 µg protein in 50 µl was applied, which was scaled up to 200 µg of crosslinked complex.

5.8.2. Protein crosslinking

Crosslinking of protein-protein or protein-nucleic acid complexes can improve their stability during the grid preparation process. Dissociation of (sub)-complexes can be prevented, as denaturation at the air-water interface can be inhibited. This crosslinking can be coupled to a purification step (as in GraFix), or preformed directly before grid-plunging. These preparation techniques can also be combined, e. g. carrying out a SEC run after batch-crosslinking. Such a strategy combines the advantages of sample stabilization and purification while directly including the transition to a suitable buffer system but requires larger quantities of sample.

Glutaraldehyde is a crosslinker with higher reactivity, its carbonyl groups target amine groups. Glutaraldehyde was used for batch crosslinking at 4°C, 0,1% concentration for 1 minute, or in GraFix gradients at a maximal concentration of 0,025%.

DSS (disuccinimidyl suberate) is a membrane-permeable crosslinker that contains an amine-reactive N-hydroxy succinimide (NHS) ester at each end of an 8-carbon spacer arm. NHS esters react with primary amines at pH 7-9 to form stable amide bonds. DSS must first dissolved in an organic solvent such as DMF or DMSO, then added to the aqueous crosslinking reaction (Thermo Scientific Pierce 2020).

BS3 (Sulfo-DSS) is bis(sulfosuccinimidyl)suberate, is the water-soluble analogue of DSS with essentially the same crosslinking activity to primary amines.

Concentration of the crosslinking reagents was determined in titration experiments. At optimal concentrations, the single protein chains on SDS Coomassie gel shift to a defined higher molecular mass band. Over-crosslinking can lead to aggregation caused by massive inter-particle crosslinks. Crosslinking with DSS or BS3 was done at a concentration of 1 mM at 30°C for 30 minutes, reaction was quenched for another 15 minutes with ammonium bicarbonate at a final concentration of 100 mM. The crosslinked complex was concentrated at applied to a gelfiltration column to eliminate unbound factors or subcomplexes.

EDC (1-Ethyl-3-[3-dimethylaminopropyl]carbodiimide hydrochloride) is a water-soluble zero-length crosslinker that activates carboxyl groups for spontaneous reaction with primary amines. *N*-hydroxysulfosuccinimide (NHS) was included to increase efficiency of the reaction. EDC and NHS were added at a final concentration of 100 mM each to the protein-nucleic acid complex for 30 minutes at 25 °C, before the reaction was quenched with ammonium bicarbonate at a final concentration of 100 mM.

5.8.3. negative staining

Negative staining allows fast assessment of particle homogeneity and concentration. A saturated uranyl formate solution was prepared freshly by dissolving little amounts (~ 20 mg) of uranyl formate salt in 400 µl bidest water by vortexing for two minutes and pelleting undissolved salt by centrifugation for 10 minutes at 15.000 g. 5 µl of sample were applied to a freshly glow-discharged carbon coated EM grids and allowed to adsorb for 30 seconds. Next, the sample was washed in a 900 µl droplet of water and stained two times with 5 µl uranyl formate solution for 20 seconds and one time for 30 seconds. The liquid was blotted in between with pieces of filter-paper. Negative stain images were used to evaluate sample homogeneity, complex stability, concentration or factor occupancy.

5.8.4. Preparation of grid for Cryo-Electron microscopy

Liquid ethane is the mostly used cryogen for cryo-grid freezing. The temperature of the cryogen is critical for the vitrification process. At temperatures higher than 133 K (-140°C), vitreous water will be transformed into cubic or hexagonal ice, the grid is no longer usable. Ethane should be used close to its melting point (90,4 K, -182.8°C) but is still liquid at higher temperatures (boiling point ethane: 184,6 K, -88.4°C) not suitable for sample vitrification (Dubochet et al. 1988). Ethane was condensed in the cryogen container under a fume hood. To ensure the right temperature, it was waited until solid ethane precipitated at the edges of the cryogen container.

Holey carbon grids were glow discharged, carbon side up in a Pelco EasiGlow system two times 100 seconds; 15 mA; 0,4 mbar; for grids coated with ultrathin carbon film: 30 seconds; 15 mA; 0,4 mbar Grids were prepared on a Vitrobot Mark IV (Thermo Fisher) operated at 4°C and 100% humidity to minimize evaporation effects. 3 µl sample was applied to a freshly glow-discharged grid. Holey carbon grids were prepared using following conditions: Blotting settings: wait 0 sec, blot 5 sec, drain 0 sec, Blot force 12. If grids with an extra ultrathin carbon support-film were used, the sample was incubated for 30-60 seconds on the grid before blotting-plunging procedure (blotting settings: wait 30-60 sec, blot 5 sec, drain 0 sec, Blot force 12).

5.8.5. Electron microscopy of Pol I/Rrn3, Pol I monomers and dimers

Grid preparation and optimization, EM data collection and processing on Pol I/Rrn3, Pol I monomers and dimers were performed in the group of Patrick Schultz under guidance of Corinne Crucifix at the IGBMC Strasbourg and previously presented (Pilsl et al. 2016a).

Purified Pol I or Pol I/Rrn3 was cross-linked with 0.1% of glutaraldehyde for two minutes, diluted to a final concentration of 7 ng/µl in EM-buffer (20mM HEPES/KOH pH 7,8; 150 mM KAc; 2 mM $MgCl_2$; 3 mM DTT). The specimen was adsorbed for 60 minutes on a small piece of carbon partially floated off a mica sheet at the surface of a Teflon well containing 37 µl (total amount Pol I: 260 ng) of sample. Next, the carbon film was transferred onto a holey carbon EM copper grid (R2/2; Quantifoil) and frozen in liquid ethane using an automated plunger (Vitrobot Mark IV, FEI) with controlled blotting time (4 s.), blotting force (5), humidity (95%) and temperature (20 °C). The particles were imaged on a Cs-

corrected Titan Krios transmission electron microscope (FEI) operated at 300 kV. Images were recorded under low-dose condition using the automated data collection software EPU (FEI) on a 4.096x4.096 direct detector camera (Falcon II, FEI) at a magnification of 59.000x resulting in a pixel size of 1,08 Å. Movies containing 17 frames with an electron dose of 3,2 $e^-/Å^2$/frame were collected and frames 2-8 (total dose of 22 $e^-/Å^2$) were aligned using the optical flow protocol (Abrishami et al. 2015) and averaged for further analysis. Molecular images of the Pol I-Rrn3 complex were extracted from 4,121 frames, while the WT Pol I molecule were selected from 2,934 frames. A high dose image (54 $e^-/Å^2$), generated by summing all frames, was used as reference for frame alignment and for particle selection. The contrast transfer function of the microscope was determined for each micrograph using CTFFIND3 (Mindell and Grigorieff 2003) within the RELION software package (Scheres 2012), and the image phases were flipped accordingly. Semiautomated particle picking was done using the boxer application in the EMAN2 software package (Ludtke et al. 1999). Molecular images were subjected to reference-free classification in RELION to produce representative 2D class averages that were used as cross-correlation references for automated particle picking in all movies with the gEMpicker software (Hoang et al. 2013b). The full data set was then partitioned in 2D classified to eliminate images containing contamination or bad particles. Structure refinement was done in RELION using a starting model obtained from a previously determined 3D model of Pol I derived from 2D crystals (Schultz et al. 1993). Three-dimensional reconstruction, structure refinement, 3D clustering and post-processing were carried out in RELION. The Pol I dimer structure was first refined without imposing any symmetry constrains. The two-fold symmetry axis was clearly identified on fitting the atomic structures of the monomers and was oriented in the z-direction before performing a 3D refinement with symmetry imposed. The initial rigid body fitting of the atomic structure of Pol I into the cryo-EM map was performed using gEMfitter (Hoang et al. 2013a). Normal mode-based flexible fitting of the atomic structure of Pol I into the cryo-EM structures was performed using iMODFIT and ISOLDE plugin in ChimeraX (Lopéz-Blanco and Chacón 2013; Goddard et al. 2018). Local resolution estimation was performed using ResMap (Kucukelbir et al. 2014). The data set was split randomly into two halves to obtain two reconstructions that were used to estimate the local resolution. The maps were colored based on the local resolution estimation using the 'Surface color' tool implemented in Chimera.

5.8.6. Electron microscopy of an early intermediate Pol I pre-initiation complex

High resolution cryo-EM data collection of an early PIC intermediate was done at the IGBMC Strasbourg with support by Corinne Crucifix, Gabor Papai and Patrick Schultz.

4 µl sample was applied to a freshly glow discharged (60 seconds, Argon-Oxygen 90:10) grid (R 2/1 + 2 nm carbon, Quantifoil), incubated for 30 s, blotted 4 s with blot force '8', at 100% humidity and 4 °C in a Vitrobot Mark IV (FEI) and plunged into liquid ethane.

Images were collected on a Cs-corrected Titan Krios microscope (FEI), operated at 300 kV using the multi-shot feature of the SerialEM software (Mastronarde 2005) for automated data collection. Movie frames were acquired on a 4k × 4k Gatan K2 summit direct electron detector (Gatan) in super-resolution mode at a nominal magnification of 105.000x, which yielded a pixel size of 0,545 Å. Forty movie frames were recorded at a dose of 1,4 electrons per $Å^2$ per frame corresponding to a total dose of 56 $e^-/Å^2$. Movie frames were aligned, dose-weighted, binned by a factor of 2 and averaged using MotionCor2 (Zheng et al. 2017). Contrast Transfer Function (CTF) parameters were estimated with the Gctf program (Zhang 2016). The RELION 3-beta suite (Zivanov et al. 2018) was used for the whole-image processing workflow unless stated otherwise. The dataset was divided into four subsets with ~1000 images each. In a first step the reference-free auto-picking procedure based on a Laplacian-of-Gaussian (LoG) filter was used to identify ~100.000 starting coordinates (per subset), which were used to extract particles with threefold binning in a 140-pixel box and the particles were grouped by reference-free 2D classification. Classes with contamination and damaged particles were discarded and the remaining particles were aligned on a reference generated from the PDB entry 5G5L low-pass filtered to 40 Å. Three-dimensional (3D) classes containing only Pol I and Rrn3, or damaged particles were discarded. The remaining 227.718 particles from the four subsets were merged, re-extracted without binning and refined against an initial model generated in RELION. CTF Refinement and Bayesian polishing was performed and the polished particles were refined and 2D and 3D classification without alignment were performed to remove misaligned particles and the remaining 168.532 particles were subjected to a second round of CTF refinement. A 3D classification without sampling and a CF-only mask revealed one class with partial CF occupancy and another with damaged particles that were both discarded. Refinement of the remaining 122.099 particles resulted in an early intermediate PIC reconstruction. For details, compare Supplemental Figure 10. During post-processing in RELION, a B-factor of −75 $Å^2$ was determined and applied for map sharpening, resulting in an overall resolution of 3,5 Å. Focused refinements the with a Pol-I-Rrn3 mask (3.5 Å after post-processing) or a CF-DNA mask (3,9 Å after post-processing) were additionally carried out to assist subdomain conformation determination and aid CF chain tracing, respectively. Directional FSC were calculated as described (Tan et al. 2017).

At a resolution of 3,5 Å, we derive an atomic model of an early intermediate PIC. We first placed Pol I domains as described for PDB 5G5L originating from the crystal structure (PDB 4C2M), an Rrn3 monomer (PDB 3TJ1), a CF monomer (PDB 5O7X) and an ITC DNA (PDB 5W66) in the unsharpened eiPIC map generated with RELION 3(beta version) (Zivanov et al. 2018). Using COOT (Emsley et al. 2010), we adjusted protein backbone traces consulting focused maps of CF or the Pol-I-Rrn3 complex and finally build side chain residues where appropriate. DNA-sequences were mutated to poly-A (-T, -G, -C). For the structure-based modelling of the TFIIB-related domains in the N-terminal region of Rrn7,

the strong density for aromatic residue Phe70 was used as a marker. The final model was refined using the real-space refinement tool of the Phenix suite (Adams et al. 2010) and evaluated using MolProbity (Chen et al. 2010). Figures were prepared with UCSF Chimera (Pettersen et al. 2004), ChimeraX (Goddard et al. 2018) or PyMOL (pymol.org).

5.9. Crosslinking mass-spectrometry of Pol I initiation complexes

Beside the stabilizing effects on protein-complexes during EM-grid preparation, coupled with mass spectrometry the defined length of the spacer arm can be used to derive architectural information of the complex. Only lysine residues or the N-terminal amino-groups of protein chains that are within 30 Å distance to each other can be crosslinked by BS3 or DSS. This distance restraints can be used to position subunits or domains, to identify interactions sites or flexibilities and to guide structural modelling. The same SEC elution-fractions could be used for EM-grid preparation as well as for mass-spectrometry experiments. Mass-spectrometric analysis of cross-linked initiation complexes were done by Alexandra Stützer and Momchil Ninov in the lab of Henning Urlaub (Max Planck Institute for Biophysical Chemistry, Göttingen).

5.10. Functional and biochemical assays

5.10.1. *In vitro* DNase I Footprinting

End-labelled DNA fragments were generated by PCR amplification with fluorescently labelled oligonucleotides. One primer binds at position -212 and allows to map the (distal) UE. To monitor digestion of the other strand, a reverse primer annealing at position +23 was used, which showed better resolution in the CE and proximal UE on UREA-PAGE gels. For DNase I footprinting assays, complexes were assembled on DNA scaffolds essentially as described above (EMSA), but with four-fold concentration of all components. One fourth of the reaction was loaded to a native acrylamide gel, to monitor complex formation. The remaining 75% of the reaction (containing 120 fmol Cy5 labelled DNA) were digested with 0,4 u RQ-DNase I (Promega) for three minutes at room-temperature in reaction buffer (20 mM HEPES/KOH pH 7,8; 200 mM KCl; 10 mM $MgCl_2$; 3 mM DTT, 0,2 mg/ml BSA). Reaction was stopped with 100 µl stop solution (450 mM NaAc pH 5,3; 20 mM EDTA; 20 mM EGTA, 40 ng/µl glycogen). Digested DNA was precipitated with 300 µl ethanol, washed with 70% ethanol and the dried pellet was resuspended in 15 µl loading dye (95% formamide; 20 mM EDTA; 0,02% bromphenole blue). Samples were denaturated for three minutes at 90°C and loaded on a sequencing gel (7% acrylamide; 8 M urea; 1x taurine buffer). The same plasmid and oligo used for labelling and amplification of the DNA template were used in sequencing reactions. Sequencing reactions were performed with the Thermo Sequenase Cycle Sequencing kit (USB) following instructions of the kit. Sequencing reactions were stopped by addition of loading dye (95% formamide; 20 mM EDTA; 0,02% bromphenole blue), denaturated for two minutes and loaded on the sequencing gel. The sequencing reactions allow a precise mapping of the DNase I digested DNA fragments.

5.10.2. Electrophoretic mobility shift assay (EMSA)

Electrophoretic mobility shift assays (EMSA) were used to analyze interactions of promoter DNA with transcription factors. These assays measured, the mobility of nucleic acids in native (acrylamide) gels in an electric field. When components interact with DNA or RNA, migration in gels becomes slower.

DNA fragment were PCR amplified using fluorescently labelled oligo-nucleotides. Binding of transcription factors to two amplicons labelled with different fluorescence dyes was directly compared. Reactions contained a reference template that was used to normalize reactions and compare affinity and a second template containing mutated sequences labelled with different fluorescent dye.

45 *f*mol of each DNA fragment were supplemented with 5x reaction buffer. Then protein factors were added. When UAF and Net1-C binding was analyzed, 1-5 pmol Net1-C were added first to the DNA templates, then UAF and TBP were added. Volume and salt-concentration were adjusted with water and 1 M KCl. Reactions contained final salt concentration of 200 mM KCl in 15 µl reaction volume. Reactions incubated for 30 minutes at room temperature. 3 µl loading dye was added and sample was loaded to a pre-run (45 minutes, 100 V) native acrylamide gel in 0,4x TBE buffer at 120 V for 90-120 minutes. Imaging of individual fluorescence signals was done on a Typhoon FLA 9500.

5.10.3. In vitro transcription assay

Many studies on Pol I mechanisms and regulation were performed using complex in vitro systems reconstituted from more or less purified fractions. Promoter specific and unspecific tailed template transcriptions were performed during this study. Protocols were originally established with fractionated yeast extracts (Tschochner 1996; Milkereit and Tschochner 1998). Whereas, highly purified components could be used in later studies, the transcription assay was only slightly modified (Pilsl et al. 2016b). Linearized plasmid DNA or mainly PCR-amplified DNA was used as template for transcription. PCR templates avoided potential RNase contaminations from plasmid preparations and did not depend on restriction enzyme cleavage sites.

5.10.4. Promoter dependent assay

5.10.4.1. Minimal assay

Pol I was preincubated with 14-fold molar excess of recombinant Rrn3 for at least 3 hours or over-night. *Ex vivo* purified Pol I/Rrn3 could be directly used. For a minimal initiation assay, 0,1-0,125 pmol Pol I in complex with Rrn3 was incubated with 0,125 pmol promoter DNA template and 1 pmol CF for 30 minutes. Volume and salt-concentration were adjusted with buffer H0 and 2,5 M KAc. Reactions contained final salt concentration of 150 mM KAc in 25 µl reaction volume. Reactions were started by addition of 5 µl 5x transcription buffer supplemented with 0,3 µCi α^{32}P-CTP or α^{32}P-GTP. After 30 minutes, reaction was stopped by addition of 200 µl proteinase K buffer (supplemented with 0,5 mg/ml proteinase K and glycogen 20 ng/µl). Proteins were digested for 15 minutes at 56°C. 700 µl ethanol was added and sample was incubated at -20°C for 1-14 hours. RNA was pelleted (13.000 rpm, 15

minutes, 4°C), washed with 165 µl ice cold ethanol (13.000 rpm, 10 minutes, 4°C). Supernatants were discarded, RNA pellet was dried at 90°C for 10-20 seconds and resolved in loading dye. Samples were denaturated at 90°C for 2 minutes and loaded on a pre-run urea-PAGE gel. RNAs were separated at 25 W for 30-40 minutes. Gel was washed in water for 5 minutes, and dried for 1-2 hours at 80°C in a vacuum dryer. Radiolabeled transcripts were visualized on phosphoscreens in a Typhoon FLA 9500 phospho-imager.

5.10.4.2. Complete Pol I initiation assay

For in vitro transcription initiation containing the full set of initiation factors, I first assembled UAF to promoter DNA templates. 0,075 -0,125 pmol DNA templates supplemented with 1 µl 5x reaction buffer without NTPs. 1-5 pmol Net1-C were added first to the DNA templates, then UAF, TBP and finally CF were added. Volume and salt-concentration were adjusted with water and 1 M KCl. Reactions contained final salt concentration of 200 mM KCl in 5 µl reaction volume. Reactions were incubated for 30 minutes to 2 hours over night.

0,125 pmol Pol I preincubated over night with 1,75 pmol Rrn3 were added, salt concentration and volume were adjusted with buffer H0 and 2,5 M KAc and reactions were incubated another 30 minutes on room temperature. Final reactions contained 50 mM KAc and 50 mM KCl in a total volume of 25 µl. Transcription reactions were started by addition of NTP containing transcription buffer. After 30 minutes, reactions were stopped by addition of proteinase K buffer and samples were treated as described in methods 5.10.4.1.

Optimal reactions with constant amounts of 0,125 pmol Pol I contained: 75-125 fmol of both DNA templates, 1,75 pmol Rrn3 (preincubated with Pol I); 1-5 pmol Net1-C; 0,35-0,5 pmol UAF; 0,5-1 pmol TBP, and 0,5 pmol CF.

5.10.5. Radioactive labelled RNA marker

Century RNA Plus marker (Ambion) was transcribed by T7-RNA-polymerase (NEB) according manufacturer's instructions in appropriate 10x reaction buffer supplemented with 1 µl α^{32}P-CTP. Reactions were stopped by addition of loading dye and stored at -20°C. 1-4 µl were loaded onto urea-page gels to estimate transcript size.

5.10.6. Tailed template assay

5.10.6.1. Tail-template preparation

RNA polymerase can start transcription from 3' overhangs (Dedrick and Chamberlin 1985). 3'OH overhangs were generated by digestion of double stranded DNA with nicking endo-nuclease Nb.BsmI (NEB). Double stranded DNA, including enzyme cleavage site, was PCR amplified and digested with Nb.BsmI (4 u/pmol DNA) in NEB 3.1 at 65°C for 90 minutes. Enzyme was inactivated for 10 minutes at 80°C. Competitor oligo-nucleotide was added in 10x molar excess to input DNA and reaction was incubated another 10 minutes at 80°C. Reaction was slowly cooled down (1°C/minute) to room-

temperature. Sample was purified and concentrated by ethanol precipitation and resuspended in water.

5.10.6.1. Tailed template transcription

0,125 pmol tailed templates were incubated with 0,125 pmol RNA-polymerase for 30 minutes on room-temperature. Volume and salt-concentration were adjusted with buffer H0 and 2,5 M KAc. Reactions contained final salt concentration of 120 mM KAc in 25 µl reaction volume. Reactions were started by addition of 5 µl 5x transcription buffer supplemented with α^{32}P-CTP or α^{32}P-GTP. After 30 minutes, reaction was stopped by addition of 200 µl proteinase K buffer (supplemented with 0,5 mg/ml proteinase K and glycogen 20 ng/µl). Proteins were digested for 15 minutes at 56°C. Samples were processed as described in methods

6. References

Abascal-Palacios, Guillermo; Ramsay, Ewan Phillip; Beuron, Fabienne; Morris, Edward; Vannini, Alessandro (2018): Structural basis of RNA polymerase III transcription initiation. In *Nature* 553 (7688), pp. 301–306. DOI: 10.1038/nature25441.

Abdulrahman, Wassim; Radu, Laura; Garzoni, Frederic; Kolesnikova, Olga; Gupta, Kapil; Osz-Papai, Judit et al. (2015): The production of multiprotein complexes in insect cells using the baculovirus expression system. In *Methods in molecular biology (Clifton, N.J.)* 1261, pp. 91–114. DOI: 10.1007/978-1-4939-2230-7_5.

Abrishami, Vahid; Vargas, Javier; Li, Xueming; Cheng, Yifan; Marabini, Roberto; Sorzano, Carlos Óscar Sánchez; Carazo, José María (2015): Alignment of direct detection device micrographs using a robust Optical Flow approach. In *Journal of structural biology* 189 (3), pp. 163–176. DOI: 10.1016/j.jsb.2015.02.001.

Adams, Paul D.; Afonine, Pavel V.; Bunkóczi, Gábor; Chen, Vincent B.; Davis, Ian W.; Echols, Nathaniel et al. (2010): PHENIX: a comprehensive Python-based system for macromolecular structure solution. In *Acta Crystallogr. D Biol. Crystallogr.* 66 (Pt 2), pp. 213–221. DOI: 10.1107/S0907444909052925.

Albert, B.; Leger-Silvestre, I.; Normand, C.; Ostermaier, M. K.; Perez-Fernandez, J.; Panov, K. I. et al. (2011): RNA polymerase I-specific subunits promote polymerase clustering to enhance the rRNA gene transcription cycle. In *The Journal of Cell Biology* 192 (2), pp. 277–293. DOI: 10.1083/jcb.201006040.

Albert, Benjamin; Colleran, Christine; Léger-Silvestre, Isabelle; Berger, Axel B.; Dez, Christophe; Normand, Christophe et al. (2013): Structure-function analysis of Hmo1 unveils an ancestral organization of HMG-Box factors involved in ribosomal DNA transcription from yeast to human. In *Nucleic Acids Res.* 41 (22), pp. 10135–10149. DOI: 10.1093/nar/gkt770.

Anderson, Susan J.; Sikes, Martha L.; Zhang, Yinfeng; French, Sarah L.; Salgia, Shilpa; Beyer, Ann L. et al. (2011): The transcription elongation factor Spt5 influences transcription by RNA polymerase I positively and negatively. In *J Biol Chem* 286 (21), pp. 18816–18824. DOI: 10.1074/jbc.M110.202101.

Andrews, Andrew J.; Luger, Karolin (2011): Nucleosome structure(s) and stability: variations on a theme. In *Annual review of biophysics* 40, pp. 99–117. DOI: 10.1146/annurev-biophys-042910-155329.

Appling, Francis D.; Scull, Catherine E.; Lucius, Aaron L.; Schneider, David A. (2018): The A12.2 Subunit Is an Intrinsic Destabilizer of the RNA Polymerase I Elongation Complex. In *Biophysical Journal* 114 (11), pp. 2507–2515. DOI: 10.1016/j.bpj.2018.04.015.

Aprikian, P.; Moorefield, B.; Reeder, R. H. (2000): TATA binding protein can stimulate core-directed transcription by yeast RNA polymerase I. In *Mol. Cell. Biol.* 20 (14), pp. 5269–5275.

Aprikian, P.; Moorefield, B.; Reeder, R. H. (2001): New model for the yeast RNA polymerase I transcription cycle. In *Mol. Cell. Biol.* 21 (15), pp. 4847–4855. DOI: 10.1128/MCB.21.15.4847-4855.2001.

Arakawa, T.; Tsumoto, K.; Kita, Y.; Chang, B.; Ejima, D. (2007): Biotechnology applications of amino acids in protein purification and formulations. In *Amino acids* 33 (4), pp. 587–605. DOI: 10.1007/s00726-007-0506-3.

Arents, G.; Burlingame, R. W.; Wang, B. C.; Love, W. E.; Moudrianakis, E. N. (1991): The nucleosomal core histone octamer at 3.1 A resolution. A tripartite protein assembly and a left-handed superhelix. In *Proc Natl Acad Sci U S A* 88 (22), pp. 10148–10152.

Arents, G.; Moudrianakis, E. N. (1993): Topography of the histone octamer surface. Repeating structural motifs utilized in the docking of nucleosomal DNA. In *Proc Natl Acad Sci U S A* 90 (22), pp. 10489–10493.

Arents, G.; Moudrianakis, E. N. (1995): The histone fold. A ubiquitous architectural motif utilized in DNA compaction and protein dimerization. In *Proc Natl Acad Sci U S A* 92 (24), pp. 11170–11174.

Armache, Karim-Jean; Mitterweger, Simone; Meinhart, Anton; Cramer, Patrick (2005): Structures of complete RNA polymerase II and its subcomplex, Rpb4/7. In *J. Biol. Chem.* 280 (8), pp. 7131–7134. DOI: 10.1074/jbc.M413038200.

Azzam, Ramzi; Chen, Susan L.; Shou, Wenying; Mah, Angie S.; Alexandru, Gabriela; Nasmyth, Kim et al. (2004): Phosphorylation by cyclin B-Cdk underlies release of mitotic exit activator Cdc14 from the nucleolus. In *Science* 305 (5683), pp. 516–519. DOI: 10.1126/science.1099402.

Bairwa, Narendra K.; Zzaman, Shamsu; Mohanty, Bidyut K.; Bastia, Deepak (2010): Replication fork arrest and rDNA silencing are two independent and separable functions of the replication terminator protein Fob1 of Saccharomyces cerevisiae. In *J. Biol. Chem.* 285 (17), pp. 12612–12619. DOI: 10.1074/jbc.M109.082388.

Barford, David; Takagi, Yuichiro; Schultz, Patrick; Berger, Imre (2013): Baculovirus expression: tackling the complexity challenge. In *Curr. Opin. Struct. Biol.* 23 (3), pp. 357–364. DOI: 10.1016/j.sbi.2013.03.009.

Beckouet, Frédéric; Labarre-Mariotte, Sylvie; Albert, Benjamin; Imazawa, Yukiko; Werner, Michel; Gadal, Olivier et al. (2008): Two RNA polymerase I subunits control the binding and release of Rrn3 during transcription. In *Mol. Cell. Biol.* 28 (5), pp. 1596–1605. DOI: 10.1128/MCB.01464-07.

Bedwell, Gregory J.; Appling, Francis D.; Anderson, Susan J.; Schneider, David A. (2012): Efficient transcription by RNA polymerase I using recombinant core factor. In *Gene* 492 (1), pp. 94–99. DOI: 10.1016/j.gene.2011.10.049.

Berger, Imre; Fitzgerald, Daniel J.; Richmond, Timothy J. (2004): Baculovirus expression system for heterologous multiprotein complexes. In *Nat Biotechnol* 22 (12), pp. 1583–1587. DOI: 10.1038/nbt1036.

Berger, Imre; Poterszman, Arnaud (2015): Baculovirus expression: old dog, new tricks. In *Bioengineered* 6 (6), pp. 316–322. DOI: 10.1080/21655979.2015.1104433.

Bernecky, Carrie; Herzog, Franz; Baumeister, Wolfgang; Plitzko, Jürgen M.; Cramer, Patrick (2016): Structure of transcribing mammalian RNA polymerase II. In *Nature* 529 (7587), pp. 551–554. DOI: 10.1038/nature16482.

Bier, Mirko; Fath, Stephan; Tschochner, Herbert (2004): The composition of the RNA polymerase I transcription machinery switches from initiation to elongation mode. In *FEBS Lett.* 564 (1-2), pp. 41–46. DOI: 10.1016/S0014-5793(04)00311-4.

Bischler, Nicolas; Brino, Laurent; Carles, Christophe; Riva, Michel; Tschochner, Herbert; Mallouh, Veronique; Schultz, Patrick (2002): Localization of the yeast RNA polymerase I-specific subunits. In *EMBO J* 21 (15), pp. 4136–4144.

Blattner, C. (2011): Molecular Basis of Rrn3-regulated RNA Polymerase I Initiation. Edited by Ludwig–Maximilians–Universität München. Ludwig–Maximilians–Universität München.

Blattner, C.; Jennebach, S.; Herzog, F.; Mayer, A.; Cheung, A. C. M.; Witte, G. et al. (2011): Molecular basis of Rrn3-regulated RNA polymerase I initiation and cell growth. In *Genes & Development* 25 (19), pp. 2093–2105. DOI: 10.1101/gad.17363311.

Bordi, L.; Cioci, F.; Camilloni, G. (2001): In vivo binding and hierarchy of assembly of the yeast RNA polymerase I transcription factors. In *Mol Biol Cell* 12 (3), pp. 753–760.

Boyaci, Hande; Chen, James; Jansen, Rolf; Darst, Seth A.; Campbell, Elizabeth A. (2019): Structures of an RNA polymerase promoter melting intermediate elucidate DNA unwinding. In *Nature* 565 (7739), pp. 382–385. DOI: 10.1038/s41586-018-0840-5.

Bradford, Marion M. (1976): A rapid and sensitive method for the quantitation of microgram quantities of protein utilizing the principle of protein-dye binding. In *Anal Biochem* 72 (1-2), pp. 248–254. DOI: 10.1016/0003-2697(76)90527-3.

Bric, Anka; Radebaugh, Catherine A.; Paule, Marvin R. (2004): Photocross-linking of the RNA polymerase I preinitiation and immediate postinitiation complexes. Implications for promoter recruitment. In *The Journal of biological chemistry* 279 (30), pp. 31259–31267. DOI: 10.1074/jbc.M311828200.

Brueckner, Florian; Cramer, Patrick (2008): Structural basis of transcription inhibition by alpha-amanitin and implications for RNA polymerase II translocation. In *Nat Struct Mol Biol* 15 (8), pp. 811–818. DOI: 10.1038/nsmb.1458.

Buhler, J. M.; Huet, J.; Davies, K. E.; Sentenac, A.; Fromageot, P. (1980): Immunological studies of yeast nuclear RNA polymerases at the subunit level. In *J Biol Chem* 255 (20), pp. 9949–9954.

Bushnell, D. A.; Cramer, P.; Kornberg, R. D. (2002): Structural basis of transcription: α-Amanitin–RNA polymerase II cocrystal at 2.8 Å resolution. In *Proceedings of the National Academy of Sciences of the United States of America* 99 (3), pp. 1218–1222. DOI: 10.1073/pnas.251664698.

Cavanaugh, Alice H.; Hirschler-Laszkiewicz, Iwona; Hu, Qiyue; Dundr, Miroslav; Smink, Tom; Misteli, Tom; Rothblum, Lawrence I. (2002): Rrn3 phosphorylation is a regulatory checkpoint for ribosome biogenesis. In *The Journal of biological chemistry* 277 (30), pp. 27423–27432. DOI: 10.1074/jbc.M201232200.

Chen, Bo-Shiun; Hampsey, Michael (2004): Functional interaction between TFIIB and the Rpb2 subunit of RNA polymerase II: implications for the mechanism of transcription initiation. In *Mol Cell Biol* 24 (9), pp. 3983–3991. DOI: 10.1128/mcb.24.9.3983-3991.2004.

Chen, Shoudeng; Rufiange, Anne; Huang, Hongda; Rajashankar, Kanagalaghatta R.; Nourani, Amine; Patel, Dinshaw J. (2015): Structure-function studies of histone H3/H4 tetramer maintenance during transcription by chaperone Spt2. In *Genes Dev.* 29 (12), pp. 1326–1340. DOI: 10.1101/gad.261115.115.

Chen, Vincent B.; Arendall, W. Bryan; Headd, Jeffrey J.; Keedy, Daniel A.; Immormino, Robert M.; Kapral, Gary J. et al. (2010): MolProbity: all-atom structure validation for macromolecular crystallography. In *Acta Crystallogr. D Biol. Crystallogr.* 66 (Pt 1), pp. 12–21. DOI: 10.1107/S0907444909042073.

Cheung, Alan C. M.; Cramer, Patrick (2011): Structural basis of RNA polymerase II backtracking, arrest and reactivation. In *Nature* 471 (7337), pp. 249–253. DOI: 10.1038/nature09785.

Cheung, Alan C. M.; Cramer, Patrick (2012): A movie of RNA polymerase II transcription. In *Cell* 149 (7), pp. 1431–1437. DOI: 10.1016/j.cell.2012.06.006.

Choe, S. Y.; Schultz, M. C.; Reeder, R. H. (1992): In vitro definition of the yeast RNA polymerase I promoter. In *Nucleic Acids Res* 20 (2), pp. 279–285.

Claypool, Jonathan A.; French, Sarah L.; Johzuka, Katsuki; Eliason, Kristilyn; Vu, Loan; Dodd, Jonathan A. et al. (2004): Tor pathway regulates Rrn3p-dependent recruitment of yeast RNA polymerase I to the promoter but does not participate in alteration of the number of active genes. In *Mol. Biol. Cell* 15 (2), pp. 946–956. DOI: 10.1091/mbc.E03-08-0594.

Clemente-Blanco, Andres; Mayan-Santos, Maria; Schneider, David A.; Machin, Felix; Jarmuz, Adam; Tschochner, Herbert; Aragon, Luis (2009): Cdc14 inhibits transcription by RNA polymerase I during anaphase. In *Nature* 458 (7235), pp. 219–222. DOI: 10.1038/nature07652.

Conconi, Antonio; Widmer, Rosa M.; Koller, Theo; Sogo, JoséM. (1989): Two different chromatin structures coexist in ribosomal RNA genes throughout the cell cycle. In *Cell* 57 (5), pp. 753–761. DOI: 10.1016/0092-8674(89)90790-3.

Contreras-Martos, Sara; Nguyen, Hung H.; Nguyen, Phuong N.; Hristozova, Nevena; Macossay-Castillo, Mauricio; Kovacs, Denes et al. (2018): Quantification of Intrinsically Disordered Proteins: A Problem Not Fully Appreciated. In *Frontiers in Molecular Biosciences* 5, p. 83. DOI: 10.3389/fmolb.2018.00083.

Cormack, B. P.; Struhl, K. (1992): The TATA-binding protein is required for transcription by all three nuclear RNA polymerases in yeast cells. In *Cell* 69 (4), pp. 685–696.

Cramer, P.; Armache, K-J; Baumli, S.; Benkert, S.; Brueckner, F.; Buchen, C. et al. (2008): Structure of eukaryotic RNA polymerases. In *Annu Rev Biophys* 37, pp. 337–352. DOI: 10.1146/annurev.biophys.37.032807.130008.

Cramer, P.; Bushnell, D. A.; Kornberg, R. D. (2001): Structural basis of transcription: RNA polymerase II at 2.8 angstrom resolution. In *Science* 292 (5523), pp. 1863–1876. DOI: 10.1126/science.1059493.

Cramer, Patrick (2002): Multisubunit RNA polymerases. In *Curr Opin Struct Biol* 12 (1), pp. 89–97.

Cramer, Patrick (2019): Organization and regulation of gene transcription. In *Nature* 573 (7772), pp. 45–54. DOI: 10.1038/s41586-019-1517-4.

Dammann, R.; Lucchini, R.; Koller, T.; Sogo, J. M. (1993): Chromatin structures and transcription of rDNA in yeast Saccharomyces cerevisiae. In *Nucleic Acids Res* 21 (10), pp. 2331–2338.

Darrière, Tommy; Pilsl, Michael; Sarthou, Marie-Kerguelen; Chauvier, Adrien; Genty, Titouan; Audibert, Sylvain et al. (2019): Genetic analyses led to the discovery of a super-active mutant of the RNA polymerase I. In *PLoS genetics* 15 (5), e1008157. DOI: 10.1371/journal.pgen.1008157.

Dedrick, R. L.; Chamberlin, M. J. (1985): Studies on transcription of 3'-extended templates by mammalian RNA polymerase II. Parameters that affect the initiation and elongation reactions. In *Biochemistry* 24 (9), pp. 2245–2253. DOI: 10.1021/bi00330a019.

Dienemann, Christian; Schwalb, Björn; Schilbach, Sandra; Cramer, Patrick (2019): Promoter Distortion and Opening in the RNA Polymerase II Cleft. In *Mol Cell* 73 (1), 97-106.e4. DOI: 10.1016/j.molcel.2018.10.014.

Douet, Julien; Tutois, Sylvie; Tourmente, Sylvette; Ecker, Joseph R. (2009): A Pol V–Mediated Silencing, Independent of RNA–Directed DNA Methylation, Applies to 5S rDNA. In *PLoS Genet* 5 (10), pp. e1000690. DOI: 10.1371/journal.pgen.1000690.

Dubochet, J.; Adrian, M.; Chang, J. J.; Homo, J. C.; Lepault, J.; McDowall, A. W.; Schultz, P. (1988): Cryo-electron microscopy of vitrified specimens. In *Quarterly reviews of biophysics* 21 (2), pp. 129–228. DOI: 10.1017/s0033583500004297.

Emsley, P.; Lohkamp, B.; Scott, W. G.; Cowtan, K. (2010): Features and development of Coot. In *Acta Crystallogr. D Biol. Crystallogr.* 66 (Pt 4), pp. 486–501. DOI: 10.1107/S0907444910007493.

Engel, Christoph; Gubbey, Tobias; Neyer, Simon; Sainsbury, Sarah; Oberthuer, Christiane; Baejen, Carlo et al. (2017): Structural Basis of RNA Polymerase I Transcription Initiation. In *Cell* 169 (1), 120-131.e22. DOI: 10.1016/j.cell.2017.03.003.

Engel, Christoph; Neyer, Simon; Cramer, Patrick (2018): Distinct Mechanisms of Transcription Initiation by RNA Polymerases I and II. In *Annual review of biophysics* 47, pp. 425–446. DOI: 10.1146/annurev-biophys-070317-033058.

Engel, Christoph; Plitzko, Jurgen; Cramer, Patrick (2016): RNA polymerase I-Rrn3 complex at 4.8 A resolution. In *Nature communications* 7, p. 12129. DOI: 10.1038/ncomms12129.

Engel, Christoph; Sainsbury, Sarah; Cheung, Alan C.; Kostrewa, Dirk; Cramer, Patrick (2013): RNA polymerase I structure and transcription regulation. In *Nature* 502 (7473), pp. 650–655. DOI: 10.1038/nature12712.

Engel, Krysta L.; French, Sarah L.; Viktorovskaya, Olga V.; Beyer, Ann L.; Schneider, David A.: Spt6 is Essential for rRNA Synthesis by RNA Polymerase I. In *Mol. Cell. Biol.*, p. 1499. DOI: 10.1128/MCB.01499-14.

Erijman, Ariel; Kozlowski, Lukasz; Sohrabi-Jahromi, Salma; Fishburn, James; Warfield, Linda; Schreiber, Jacob et al. (2020): A High-Throughput Screen for Transcription Activation Domains Reveals Their Sequence Features and Permits Prediction by Deep Learning. In *Mol Cell* 78 (5), 890-902.e6. DOI: 10.1016/j.molcel.2020.04.020.

Esbin, Meagan N.; Tjian, Robert (2020): Distinct Handoff Mechanism for TBP-TATA DNA Engagement Revealed by SAGA Structures. In *Biochemistry* 59 (17), pp. 1647–1649. DOI: 10.1021/acs.biochem.0c00190.

Fath, S.; Milkereit, P.; Peyroche, G.; Riva, M.; Carles, C.; Tschochner, H. (2001): Differential roles of phosphorylation in the formation of transcriptional active RNA polymerase I. In *Proc. Natl. Acad. Sci. U.S.A.* 98 (25), pp. 14334–14339. DOI: 10.1073/pnas.231181398.

Fath, Stephan; Kobor, Michael S.; Philippi, Anja; Greenblatt, Jack; Tschochner, Herbert (2004): Dephosphorylation of RNA polymerase I by Fcp1p is required for efficient rRNA synthesis. In *J Biol Chem* 279 (24), pp. 25251–25259. DOI: 10.1074/jbc.M401867200.

Feklistov, Andrey; Bae, Brian; Hauver, Jesse; Lass-Napiorkowska, Agnieszka; Kalesse, Markus; Glaus, Florian et al. (2017): RNA polymerase motions during promoter melting. In *Science* 356 (6340), pp. 863–866. DOI: 10.1126/science.aam7858.

Fernández-Tornero, Carlos (2018): RNA polymerase I activation and hibernation. Unique mechanisms for unique genes. In *Transcription*, pp. 1–7. DOI: 10.1080/21541264.2017.1416267.

Fernández-Tornero, Carlos; Böttcher, Bettina; Riva, Michel; Carles, Christophe; Steuerwald, Ulrich; Ruigrok, Rob W. H. et al. (2007): Insights into transcription initiation and termination from the electron microscopy structure of yeast RNA polymerase III. In *Molecular Cell* 25 (6), pp. 813–823. DOI: 10.1016/j.molcel.2007.02.016.

Fernández-Tornero, Carlos; Moreno-Morcillo, María; Rashid, Umar J.; Taylor, Nicholas M. I.; Ruiz, Federico M.; Gruene, Tim et al. (2013): Crystal structure of the 14-subunit RNA polymerase I. In *Nature* 502 (7473), pp. 644–649. DOI: 10.1038/nature12636.

Fitzgerald, D. J.; Berger, P.; Schaffitzel, C.; Yamada, K.; Richmond, T. J.; Berger, I. (2006): Protein complex expression by using multigene baculoviral vectors. In *Nature methods* 3 (12), pp. 1021–1032. DOI: 10.1038/nmeth983.

Fitzgerald, Daniel J.; Schaffitzel, Christiane; Berger, Philipp; Wellinger, Ralf; Bieniossek, Christoph; Richmond, Timothy J.; Berger, Imre (2007): Multiprotein expression strategy for structural biology of eukaryotic complexes. In *Structure (London, England : 1993)* 15 (3), pp. 275–279. DOI: 10.1016/j.str.2007.01.016.

French, Sarah L.; Osheim, Yvonne N.; Cioci, Francesco; Nomura, Masayasu; Beyer, Ann L. (2003): In exponentially growing Saccharomyces cerevisiae cells, rRNA synthesis is determined by the summed RNA polymerase I loading rate rather than by the number of active genes. In *Mol. Cell. Biol.* 23 (5), pp. 1558–1568.

Gadal, O.; Mariotte-Labarre, S.; Chedin, S.; Quemeneur, E.; Carles, C.; Sentenac, A.; Thuriaux, P. (1997): A34.5, a nonessential component of yeast RNA polymerase I, cooperates with subunit A14 and DNA topoisomerase I to produce a functional rRNA synthesis machine. In *Mol Cell Biol* 17 (4), pp. 1787–1795. DOI: 10.1128/mcb.17.4.1787.

Gadal, Olivier; Labarre, Sylvie; Boschiero, Claire; Thuriaux, Pierre (2002): Hmo1, an HMG-box protein, belongs to the yeast ribosomal DNA transcription system. In *EMBO J.* 21 (20), pp. 5498–5507.

Ganley, Austen R. D.; Hayashi, Kouji; Horiuchi, Takashi; Kobayashi, Takehiko (2005): Identifying gene-independent noncoding functional elements in the yeast ribosomal DNA by phylogenetic footprinting. In *Proceedings of the National Academy of Sciences of the United States of America* 102 (33), pp. 11787–11792. DOI: 10.1073/pnas.0504905102.

Garzoni, Frederic; Bieniossek, Christoph; Berger, Imre (2012): The MultiBac BEVS for producing proteins and their complexes (Prot54). In *EMBL Grenoble Outstation*. Available online at https://www.epigenesys.eu/index.php/en/protcols/complex-purificationproteomics/328-the-multibac-bevs-for-producing-proteins-and-their-complexes.

Geiger, Sebastian R.; Kuhn, Claus.-D.; Leidig, Christoph; Renkawitz, Jörg; Cramer, Patrick (2008): Crystallization of RNA polymerase I subcomplex A14/A43 by iterative prediction, probing and removal of flexible regions. In *Acta Crystallogr F Struct Biol Cryst Commun* 64 (5), pp. 413–418. DOI: 10.1107/S174430910800972X.

Geiger, Sebastian R.; Lorenzen, Kristina; Schreieck, Amelie; Hanecker, Patrizia; Kostrewa, Dirk; Heck, Albert J.R; Cramer, Patrick (2010): RNA Polymerase I Contains a TFIIF-Related DNA-Binding Subcomplex. In *Molecular Cell* 39 (4), pp. 583–594. DOI: 10.1016/j.molcel.2010.07.028.

Gerber, Jochen (2008): Site-specific phosphorylation of yeast RNA polymerase I. Dissertation Jochen Gerber 2008. Available online at https://epub.uni-regensburg.de/10735/1/Diss_Gerber_08.pdf.

Gerber, Jochen; Reiter, Alarich; Steinbauer, Robert; Jakob, Steffen; Kuhn, Claus-Dieter; Cramer, Patrick et al. (2008): Site specific phosphorylation of yeast RNA polymerase I. In *Nucleic Acids Res.* 36 (3), pp. 793–802. DOI: 10.1093/nar/gkm1093.

Gietl, Andreas; Holzmeister, Phil; Blombach, Fabian; Schulz, Sarah; von Voithenberg, Lena Voith; Lamb, Don C. et al. (2014): Eukaryotic and archaeal TBP and TFB/TF(II)B follow different promoter DNA bending pathways. In *Nucleic Acids Research* 42 (10), pp. 6219–6231. DOI: 10.1093/nar/gku273.

Gnatt, A. L.; Cramer, P.; Fu, J.; Bushnell, D. A.; Kornberg, R. D. (2001): Structural basis of transcription: an RNA polymerase II elongation complex at 3.3 A resolution. In *Science* 292 (5523), pp. 1876–1882. DOI: 10.1126/science.1059495.

Goddard, Thomas D.; Huang, Conrad C.; Meng, Elaine C.; Pettersen, Eric F.; Couch, Gregory S.; Morris, John H.; Ferrin, Thomas E. (2018): UCSF ChimeraX: Meeting modern challenges in visualization and analysis. In *Protein Science : A Publication of the Protein Society* 27 (1), pp. 14–25. DOI: 10.1002/pro.3235.

Goetze, H.; Wittner, M.; Hamperl, S.; Hondele, M.; Merz, K.; Stoeckl, U.; Griesenbeck, J. (2010): Alternative Chromatin Structures of the 35S rRNA Genes in Saccharomyces cerevisiae Provide a Molecular Basis for the Selective Recruitment of RNA Polymerases I and II. In *Molecular and Cellular Biology* 30 (8), pp. 2028–2045. DOI: 10.1128/MCB.01512-09.

Gong, X.; Radebaugh, C. A.; Geiss, G. K.; Simon, M. N.; Paule, M. R. (1995): Site-directed photo-cross-linking of rRNA transcription initiation complexes. In *Mol Cell Biol* 15 (9), pp. 4956–4963. DOI: 10.1128/mcb.15.9.4956.

Gouge, Jerome; Guthertz, Nicolas; Kramm, Kevin; Dergai, Oleksandr; Abascal-Palacios, Guillermo; Satia, Karishma et al. (2017a): Molecular mechanisms of Bdp1 in TFIIIB assembly and RNA polymerase III transcription initiation. In *Nat Comms* 8 (1), p. 130. DOI: 10.1038/s41467-017-00126-1.

Gouge, Jerome; Guthertz, Nicolas; Kramm, Kevin; Dergai, Oleksandr; Abascal-Palacios, Guillermo; Satia, Karishma et al. (2017b): Molecular mechanisms of Bdp1 in TFIIIB assembly and RNA polymerase III transcription initiation. In *Nat Comms* 8 (1), p. 130. DOI: 10.1038/s41467-017-00126-1.

Gouge, Jerome; Satia, Karishma; Guthertz, Nicolas; Widya, Marcella; Thompson, Andrew James; Cousin, Pascal et al. (2015): Redox Signaling by the RNA Polymerase III TFIIB-Related Factor Brf2. In *Cell* 163 (6), pp. 1375–1387. DOI: 10.1016/j.cell.2015.11.005.

Graham, Martin; Combe, Colin; Kolbowski, Lars; Rappsilber, Juri (2019): xiView: A common platform for the downstream analysis of Crosslinking Mass Spectrometry data.

Haag, Jeremy R.; Pikaard, Craig S. (2011): Multisubunit RNA polymerases IV and V: purveyors of non-coding RNA for plant gene silencing. In *Nature reviews. Molecular cell biology* 12 (8), pp. 483–492. DOI: 10.1038/nrm3152.

Hamperl, Stephan; Brown, Christopher R.; Garea, Ana Villar; Perez-Fernandez, Jorge; Bruckmann, Astrid; Huber, Katharina et al. (2014): Compositional and structural analysis of selected chromosomal domains from Saccharomyces cerevisiae. In *Nucleic Acids Res.* 42 (1), e2. DOI: 10.1093/nar/gkt891.

Han, Yan; Yan, Chunli; Nguyen, Thi Hoang Duong; Jackobel, Ashleigh J.; Ivanov, Ivaylo; Knutson, Bruce A.; He, Yuan (2017): Structural mechanism of ATP-independent transcription initiation by RNA polymerase I. In *eLife* 6. DOI: 10.7554/elife.27414.

Hannig, Katharina (2016): Net1 - ein modular aufgebautes und multifunktionales Protein im Nukleolus der Hefe Saccharomyces cerevisiae. Universtität Regensburg. Available online at https://epub.uni-regensburg.de/32428/.

Hannig, Katharina; Babl, Virginia; Hergert, Kristin; Maier, Andreas; Pilsl, Michael; Schächner, Christopher et al. (2019): The C-terminal region of Net1 is an activator of RNA polymerase I transcription with conserved features from yeast to human. In *PLoS Genet* 15 (2). DOI: 10.1371/journal.pgen.1008006.

He, Yuan; Yan, Chunli; Fang, Jie; Inouye, Carla; Tjian, Robert; Ivanov, Ivaylo; Nogales, Eva (2016): Near-atomic resolution visualization of human transcription promoter opening. In *Nature* 533 (7603), pp. 359–365. DOI: 10.1038/nature17970.

Heiss, Florian B.; Daiß, Julia L.; Becker, Philipp; Engel, Christoph (2021): Conserved strategies of RNA polymerase I hibernation and activation. In *Nat Comms* 12 (1), p. 758. DOI: 10.1038/s41467-021-21031-8.

Herdman, Chelsea; Mars, Jean-Clement; Stefanovsky, Victor Y.; Tremblay, Michel G.; Sabourin-Felix, Marianne; Lindsay, Helen et al. (2017): A unique enhancer boundary complex on the mouse ribosomal RNA genes persists after loss of Rrn3 or UBF and the inactivation of RNA polymerase I transcription. In *PLoS Genet* 13 (7), e1006899. DOI: 10.1371/journal.pgen.1006899.

Herr, A. J.; Jensen, M. B.; Dalmay, T.; Baulcombe, D. C. (2005): RNA polymerase IV directs silencing of endogenous DNA. In *Science* 308 (5718), pp. 118–120. DOI: 10.1126/science.1106910.

Hirai, Hiroyuki; Tani, Tetsuya; Kikyo, Nobuaki (2010): Structure and functions of powerful transactivators. VP16, MyoD and FoxA. In *The International journal of developmental biology* 54 (11-12), pp. 1589–1596. DOI: 10.1387/ijdb.103194hh.

Hirschler-Laszkiewicz, Iwona; Cavanaugh, Alice H.; Mirza, Ayoub; Lun, Mingyue; Hu, Qiyue; Smink, Tom; Rothblum, Lawrence I. (2003): Rrn3 becomes inactivated in the process of ribosomal DNA transcription. In *J Biol Chem* 278 (21), pp. 18953–18959. DOI: 10.1074/jbc.M301093200.

Hoang, Thai V.; Cavin, Xavier; Ritchie, David W. (2013a): gEMfitter: a highly parallel FFT-based 3D density fitting tool with GPU texture memory acceleration. In *Journal of structural biology* 184 (2), pp. 348–354. DOI: 10.1016/j.jsb.2013.09.010.

Hoang, Thai V.; Cavin, Xavier; Schultz, Patrick; Ritchie, David W. (2013b): gEMpicker: a highly parallel GPU-accelerated particle picking tool for cryo-electron microscopy. In *BMC structural biology* 13, p. 25. DOI: 10.1186/1472-6807-13-25.

Hoffmann, Niklas A.; Jakobi, Arjen J.; Moreno-Morcillo, María; Glatt, Sebastian; Kosinski, Jan; Hagen, Wim J. H. et al. (2015): Molecular structures of unbound and transcribing RNA polymerase III. In *Nature* 528 (7581), pp. 231–236. DOI: 10.1038/nature16143.

Hontz, R. D.; French, S. L.; Oakes, M. L.; Tongaonkar, P.; Nomura, M.; Beyer, A. L.; Smith, J. S. (2008): Transcription of Multiple Yeast Ribosomal DNA Genes Requires Targeting of UAF to the Promoter by Uaf30. In *Molecular and Cellular Biology* 28 (21), pp. 6709–6719. DOI: 10.1128/MCB.00703-08.

Huang, Julie; Moazed, Danesh (2003): Association of the RENT complex with nontranscribed and coding regions of rDNA and a regional requirement for the replication fork block protein Fob1 in rDNA silencing. In *Genes & Development* 17 (17), pp. 2162–2176. DOI: 10.1101/gad.1108403.

Iida, Tetsushi; Kobayashi, Takehiko (2019a): How do cells count multi-copy genes?: "Musical Chair" model for preserving the number of rDNA copies. In *Current genetics*. DOI: 10.1007/s00294-019-00956-0.

Iida, Tetsushi; Kobayashi, Takehiko (2019b): RNA Polymerase I Activators Count and Adjust Ribosomal RNA Gene Copy Number. In *Mol Cell* 73 (4), 645-654.e13. DOI: 10.1016/j.molcel.2018.11.029.

Ishibashi, Toyotaka; Dangkulwanich, Manchuta; Coello, Yves; Lionberger, Troy A.; Lubkowska, Lucyna; Ponticelli, Alfred S. et al. (2014): Transcription factors IIS and IIF enhance transcription efficiency by differentially modifying RNA polymerase pausing dynamics. In *Proc Natl Acad Sci U S A* 111 (9), pp. 3419–3424. DOI: 10.1073/pnas.1401611111.

Jackobel, Ashleigh J.; Zeberl, Brian J.; Glover, Danea M.; Fakhouri, Aula M.; Knutson, Bruce A. (2019): DNA binding preferences of S. cerevisiae RNA polymerase I Core Factor reveal a preference for the GC-minor groove and a conserved binding mechanism. In *Biochimica et biophysica acta. Gene regulatory mechanisms* 1862 (9), p. 194408. DOI: 10.1016/j.bbagrm.2019.194408.

Jennebach, S.; Herzog, F.; Aebersold, R.; Cramer, P. (2012): Crosslinking-MS analysis reveals RNA polymerase I domain architecture and basis of rRNA cleavage. In *Nucleic Acids Research* 40 (12), pp. 5591–5601. DOI: 10.1093/nar/gks220.

Jochem, Laura; Ramsay, Ewan P.; Vannini, Alessandro (2017): RNA polymerase I, bending the rules? In *The EMBO journal*. DOI: 10.15252/embj.201797924.

Kadesch, T R; Chamberlin, M J (1982): Studies of in vitro transcription by calf thymus RNA polymerase II using a novel duplex DNA template. In *J. Biol. Chem.* 257 (9), pp. 5286–5295.

Keaveney, Marie; Struhl, Kevin (1998): Activator-Mediated Recruitment of the RNA Polymerase II Machinery Is the Predominant Mechanism for Transcriptional Activation in Yeast. In *Mol Cell* 1 (6), pp. 917–924. DOI: 10.1016/S1097-2765(00)80091-X.

Keener, J.; Dodd, J. A.; Lalo, D.; Nomura, M. (1997): Histones H3 and H4 are components of upstream activation factor required for the high-level transcription of yeast rDNA by RNA polymerase I. In *Proc. Natl. Acad. Sci. U.S.A.* 94 (25), pp. 13458–13462.

Keener, J.; Josaitis, C. A.; Dodd, J. A.; Nomura, M. (1998): Reconstitution of yeast RNA polymerase I transcription in vitro from purified components. TATA-binding protein is not required for basal transcription. In *J. Biol. Chem.* 273 (50), pp. 33795–33802.

Kettenberger, Hubert; Armache, Karim-Jean; Cramer, Patrick (2003): Architecture of the RNA Polymerase II-TFIIS Complex and Implications for mRNA Cleavage. In *Cell* 114 (3), pp. 347–357. DOI: 10.1016/S0092-8674(03)00598-1.

Kettenberger, Hubert; Armache, Karim-Jean; Cramer, Patrick (2004): Complete RNA polymerase II elongation complex structure and its interactions with NTP and TFIIS. In *Mol Cell* 16 (6), pp. 955–965. DOI: 10.1016/j.molcel.2004.11.040.

Keys, D. A.; Lee, B. S.; Dodd, J. A.; Nguyen, T. T.; Vu, L.; Fantino, E. et al. (1996): Multiprotein transcription factor UAF interacts with the upstream element of the yeast RNA polymerase I promoter and forms a stable preinitiation complex. In *Genes Dev* 10 (7), pp. 887–903.

Keys, D. A.; Vu, L.; Steffan, J. S.; Dodd, J. A.; Yamamoto, R. T.; Nogi, Y.; Nomura, M. (1994): RRN6 and RRN7 encode subunits of a multiprotein complex essential for the initiation of rDNA transcription by RNA polymerase I in Saccharomyces cerevisiae. In *Genes Dev* 8 (19), pp. 2349–2362.

Khatter, Heena; Vorländer, Matthias K.; Müller, Christoph W. (2017): RNA polymerase I and III. Similar yet unique. In *Current opinion in structural biology* 47, pp. 88–94. DOI: 10.1016/j.sbi.2017.05.008.

Kim, J. L.; Nikolov, D. B.; Burley, S. K. (1993a): Co-crystal structure of TBP recognizing the minor groove of a TATA element. In *Nature* 365 (6446), pp. 520–527. DOI: 10.1038/365520a0.

Kim, Nam Ah; Hada, Sharvron; Thapa, Ritu; Jeong, Seong Hoon (2016): Arginine as a protein stabilizer and destabilizer in liquid formulations. In *International journal of pharmaceutics* 513 (1-2), pp. 26–37. DOI: 10.1016/j.ijpharm.2016.09.003.

Kim, T. K.; Roeder, R. G. (1994): Involvement of the basic repeat domain of TATA-binding protein (TBP) in transcription by RNA polymerases I, II, and III. In *The Journal of biological chemistry* 269 (7), pp. 4891–4894.

Kim, Y.; Geiger, J. H.; Hahn, S.; Sigler, P. B. (1993b): Crystal structure of a yeast TBP/TATA-box complex. In *Nature* 365 (6446), pp. 512–520. DOI: 10.1038/365512a0.

Klinge, Sebastian; Woolford, John L. (2019): Ribosome assembly coming into focus. In *Nature reviews. Molecular cell biology* 20 (2), pp. 116–131. DOI: 10.1038/s41580-018-0078-y.

Klinger, C.; Huet, J.; Song, D.; Petersen, G.; Riva, M.; Bautz, E. K. et al. (1996): Localization of yeast RNA polymerase I core subunits by immunoelectron microscopy. In *EMBO J* 15 (17), pp. 4643–4653. DOI: 10.1002/j.1460-2075.1996.tb00841.x.

Knop, M.; Siegers, K.; Pereira, G.; Zachariae, W.; Winsor, B.; Nasmyth, K.; Schiebel, E. (1999): Epitope tagging of yeast genes using a PCR-based strategy: more tags and improved practical routines. In *Yeast* 15 (10B), pp. 963–972. DOI: 10.1002/(SICI)1097-0061(199907)15:10B<963::AID-YEA399>3.0.CO;2-W.

Knutson, B. A.; Hahn, S. (2011): Yeast Rrn7 and Human TAF1B Are TFIIB-Related RNA Polymerase I General Transcription Factors. In *Science* 333 (6049), pp. 1637–1640. DOI: 10.1126/science.1207699.

Knutson, Bruce A.; Hahn, Steven (2013): TFIIB-related factors in RNA polymerase I transcription. In *Biochim. Biophys. Acta* 1829 (3-4), pp. 265–273. DOI: 10.1016/j.bbagrm.2012.08.003.

Knutson, Bruce A.; Luo, Jie; Ranish, Jeffrey; Hahn, Steven (2014): Architecture of the Saccharomyces cerevisiae RNA polymerase I Core Factor complex. In *Nat. Struct. Mol. Biol.* DOI: 10.1038/nsmb.2873.

Knutson, Bruce A.; Smith, Marissa L.; Belkevich, Alana E.; Fakhouri, Aula M. (2020): Molecular Topology of RNA Polymerase I Upstream Activation Factor. In *Mol. Cell. Biol.* DOI: 10.1128/MCB.00056-20.

Kobayashi, T.; Nomura, M.; Horiuchi, T. (2001): Identification of DNA cis elements essential for expansion of ribosomal DNA repeats in Saccharomyces cerevisiae. In *Mol Cell Biol* 21 (1), pp. 136–147. DOI: 10.1128/MCB.21.1.136-147.2001.

Kobayashi, Takehiko (2011): Regulation of ribosomal RNA gene copy number and its role in modulating genome integrity and evolutionary adaptability in yeast. In *Cellular and molecular life sciences : CMLS* 68 (8), pp. 1395–1403. DOI: 10.1007/s00018-010-0613-2.

Kobayashi, Takehiko; Ganley, Austen R. D. (2005): Recombination regulation by transcription-induced cohesin dissociation in rDNA repeats. In *Science* 309 (5740), pp. 1581–1584. DOI: 10.1126/science.1116102.

Kornberg, R. D. (1974): Chromatin structure: a repeating unit of histones and DNA. In *Science* 184 (4139), pp. 868–871. DOI: 10.1126/science.184.4139.868.

Kornberg, R. D.; Stryer, L. (1988): Statistical distributions of nucleosomes: nonrandom locations by a stochastic mechanism. In *Nucl Acids Res* 16 (14A), pp. 6677–6690. DOI: 10.1093/nar/16.14.6677.

Kornberg, Roger D.; Lorch, Yahli (2020): Primary Role of the Nucleosome. In *Mol Cell* 79 (3), pp. 371–375. DOI: 10.1016/j.molcel.2020.07.020.

Kostrewa, Dirk; Kuhn, Claus D.; Engel, Christoph; Cramer, Patrick (2015): An alternative RNA polymerase I structure reveals a dimer hinge. 4ym7. In *Acta crystallographica. Section D, Biological crystallography* 71 (Pt 9), pp. 1850–1855. DOI: 10.1107/S1399004715012651.

Kownin, Preecha; Bateman, Erik; Paule, Marvin R. (1987): Eukaryotic RNA polymerase I promoter binding is directed by protein contacts with transcription initiation factor and is DNA sequence-independent. In *Cell* 50 (5), pp. 693–699. DOI: 10.1016/0092-8674(87)90327-8.

Kramm, Kevin; Engel, Christoph; Grohmann, Dina (2019): Transcription initiation factor TBP: old friend new questions. In *Biochemical Society transactions* 47 (1), pp. 411–423. DOI: 10.1042/BST20180623.

Kucukelbir, Alp; Sigworth, Fred J.; Tagare, Hemant D. (2014): Quantifying the local resolution of cryo-EM density maps. In *Nature methods* 11 (1), pp. 63–65. DOI: 10.1038/nmeth.2727.

Kühlbrandt, Werner (2014): Biochemistry. The resolution revolution. In *Science (New York, N.Y.)* 343 (6178), pp. 1443–1444. DOI: 10.1126/science.1251652.

Kuhn, Claus-D; Geiger, Sebastian R.; Baumli, Sonja; Gartmann, Marco; Gerber, Jochen; Jennebach, Stefan et al. (2007): Functional Architecture of RNA Polymerase I. In *Cell* 131 (7), pp. 1260–1272. DOI: 10.1016/j.cell.2007.10.051.

Kujirai, Tomoya; Ehara, Haruhiko; Fujino, Yuka; Shirouzu, Mikako; Sekine, Shun-Ichi; Kurumizaka, Hitoshi (2018): Structural basis of the nucleosome transition during RNA polymerase II passage. In *Science* 362 (6414), pp. 595–598. DOI: 10.1126/science.aau9904.

Kulkens, T.; Riggs, D. L.; Heck, J. D.; Planta, R. J.; Nomura, M. (1991): The yeast RNA polymerase I promoter: ribosomal DNA sequences involved in transcription initiation and complex formation in vitro. In *Nucleic Acids Res* 19 (19), pp. 5363–5370.

Kulkens, T.; van der Sande, C. A.; Dekker, A. F.; van Heerikhuizen, H.; Planta, R. J. (1992): A system to study transcription by yeast RNA polymerase I within the chromosomal context: functional analysis of the ribosomal DNA enhancer and the RBP1/REB1 binding sites. In *EMBO J* 11 (12), pp. 4665–4674. DOI: 10.1002/j.1460-2075.1992.tb05568.x.

Laemmli, U. K. (1970): Cleavage of structural proteins during the assembly of the head of bacteriophage T4. In *Nature* 227 (5259), pp. 680–685.

Laferté, Arnaud; Favry, Emmanuel; Sentenac, André; Riva, Michel; Carles, Christophe; Chédin, Stéphane (2006): The transcriptional activity of RNA polymerase I is a key determinant for the level of all ribosome components. In *Genes Dev.* 20 (15), pp. 2030–2040. DOI: 10.1101/gad.386106.

Lalo, D.; Carles, C.; Sentenac, A.; Thuriaux, P. (1993): Interactions between three common subunits of yeast RNA polymerases I and III. In *Proc. Natl. Acad. Sci. U.S.A.* 90 (12), pp. 5524–5528.

Lalo, D.; Steffan, J. S.; Dodd, J. A.; Nomura, M. (1996): RRN11 encodes the third subunit of the complex containing Rrn6p and Rrn7p that is essential for the initiation of rDNA transcription by yeast RNA polymerase I. In *J. Biol. Chem.* 271 (35), pp. 21062–21067.

Lang, W. H.; Reeder, R. H. (1993): The REB1 site is an essential component of a terminator for RNA polymerase I in Saccharomyces cerevisiae. In *Mol. Cell. Biol.* 13 (1), pp. 649–658. DOI: 10.1128/MCB.13.1.649.

Léger-Silvestre, I.; Trumtel, S.; Noaillac-Depeyre, J.; Gas, N. (1999): Functional compartmentalization of the nucleus in the budding yeast Saccharomyces cerevisiae. In *Chromosoma* 108 (2), pp. 103–113. DOI: 10.1007/s004120050357.

Life Technologies (2013): Bac-to-Bac Baculovirus Expression System 10359 Rev A.0.

Lin, C. W.; Moorefield, B.; Payne, J.; Aprikian, P.; Mitomo, K.; Reeder, R. H. (1996): A novel 66-kilodalton protein complexes with Rrn6, Rrn7, and TATA-binding protein to promote polymerase I transcription initiation in Saccharomyces cerevisiae. In *Mol. Cell. Biol.* 16 (11), pp. 6436–6443.

Lindell, T. J.; Weinberg, F.; Morris, P. W.; Roeder, R. G.; Rutter, W. J. (1970): Specific inhibition of nuclear RNA polymerase II by alpha-amanitin. In *Science* 170 (3956), pp. 447–449. DOI: 10.1126/science.170.3956.447.

Lisica, Ana; Engel, Christoph; Jahnel, Marcus; Roldán, Édgar; Galburt, Eric A.; Cramer, Patrick; Grill, Stephan W. (2016): Mechanisms of backtrack recovery by RNA polymerases I and II. In *Proceedings of the National Academy of Sciences of the United States of America*. DOI: 10.1073/pnas.1517011113.

Liu, Wallace H.; Roemer, Sarah C.; Port, Alex M.; Churchill, Mair E. A. (2012): CAF-1-induced oligomerization of histones H3/H4 and mutually exclusive interactions with Asf1 guide H3/H4 transitions among histone chaperones and DNA. In *Nucleic Acids Res.* 40 (22), pp. 11229–11239. DOI: 10.1093/nar/gks906.

Liu, Xiangyang; Farnung, Lucas; Wigge, Christoph; Cramer, Patrick (2018): Cryo-EM structure of a mammalian RNA polymerase II elongation complex inhibited by α-amanitin. In *J. Biol. Chem.* 293 (19), pp. 7189–7194. DOI: 10.1074/jbc.RA118.002545.

Lopéz-Blanco, José Ramón; Chacón, Pablo (2013): iMODFIT: efficient and robust flexible fitting based on vibrational analysis in internal coordinates. In *Journal of structural biology* 184 (2), pp. 261–270. DOI: 10.1016/j.jsb.2013.08.010.

Ludtke, S. J.; Baldwin, P. R.; Chiu, W. (1999): EMAN: semiautomated software for high-resolution single-particle reconstructions. In *Journal of structural biology* 128 (1), pp. 82–97. DOI: 10.1006/jsbi.1999.4174.

Luger, K.; Mäder, A. W.; Richmond, R. K.; Sargent, D. F.; Richmond, T. J. (1997): Crystal structure of the nucleosome core particle at 2.8 A resolution. In *Nature* 389 (6648), pp. 251–260. DOI: 10.1038/38444.

Mason, S. W.; Wallisch, M.; Grummt, I. (1997): RNA polymerase I transcription termination: similar mechanisms are employed by yeast and mammals. In *J. Mol. Biol.* 268 (2), pp. 229–234. DOI: 10.1006/jmbi.1997.0976.

Mastronarde, David N. (2005): Automated electron microscope tomography using robust prediction of specimen movements. In *Journal of structural biology* 152 (1), pp. 36–51. DOI: 10.1016/j.jsb.2005.07.007.

Mattiroli, Francesca; Gu, Yajie; Yadav, Tejas; Balsbaugh, Jeremy L.; Harris, Michael R.; Findlay, Eileen S. et al. (2017): DNA-mediated association of two histone-bound complexes of yeast Chromatin Assembly Factor-1 (CAF-1) drives tetrasome assembly in the wake of DNA replication. In *eLife* 6. DOI: 10.7554/eLife.22799.

Mayer, Christine; Bierhoff, Holger; Grummt, Ingrid (2005): The nucleolus as a stress sensor: JNK2 inactivates the transcription factor TIF-IA and down-regulates rRNA synthesis. In *Genes & Development* 19 (8), pp. 933–941. DOI: 10.1101/gad.333205.

Mayer, Christine; Zhao, Jian; Yuan, Xuejun; Grummt, Ingrid (2004): mTOR-dependent activation of the transcription factor TIF-IA links rRNA synthesis to nutrient availability. In *Genes & Development* 18 (4), pp. 423–434. DOI: 10.1101/gad.285504.

McClintock, Barbara (1934): The relation of a particular chromosomal element to the development of the nucleoli in Zea mays. In *Z.Zellforsch* 21 (2), pp. 294–326. DOI: 10.1007/BF00374060.

McStay, B.; Frazier, M. W.; Reeder, R. H. (1991): xUBF contains a novel dimerization domain essential for RNA polymerase I transcription. In *Genes & Development* 5 (11), pp. 1957–1968. DOI: 10.1101/gad.5.11.1957.

McStay, B.; Sullivan, G. J.; Cairns, C. (1997): The Xenopus RNA polymerase I transcription factor, UBF, has a role in transcriptional enhancement distinct from that at the promoter. In *EMBO J* 16 (2), pp. 396–405. DOI: 10.1093/emboj/16.2.396.

McStay, Brian (2016): Nucleolar organizer regions: genomic 'dark matter' requiring illumination. In *Genes Dev* 30 (14), pp. 1598–1610. DOI: 10.1101/gad.283838.116.

Merkl, Philipp; Perez-Fernandez, Jorge; Pilsl, Michael; Reiter, Alarich; Williams, Lydia; Gerber, Jochen et al. (2014): Binding of the termination factor Nsi1 to its cognate DNA site is sufficient to terminate RNA polymerase I transcription in vitro and to induce termination in vivo. In *Mol Cell Biol* 34 (20), pp. 3817–3827. DOI: 10.1128/MCB.00395-14.

Merkl, Philipp E.; Pilsl, Michael; Fremter, Tobias; Schwank, Katrin; Engel, Christoph; Längst, Gernot et al. (2020): RNA polymerase I (Pol I) passage through nucleosomes depends on Pol I subunits binding its lobe structure. In *J. Biol. Chem.* DOI: 10.1074/jbc.RA119.011827.

Merz, K.; Hondele, M.; Goetze, H.; Gmelch, K.; Stoeckl, U.; Griesenbeck, J. (2008): Actively transcribed rRNA genes in S. cerevisiae are organized in a specialized chromatin associated with the high-mobility group protein Hmo1 and are largely devoid of histone molecules. In *Genes & Development* 22 (9), pp. 1190–1204. DOI: 10.1101/gad.466908.

Milkereit, P.; Schultz, P.; Tschochner, H. (1997): Resolution of RNA polymerase I into dimers and monomers and their function in transcription. In *Biol. Chem.* 378 (12), pp. 1433–1443.

Milkereit, P.; Tschochner, H. (1998): A specialized form of RNA polymerase I, essential for initiation and growth-dependent regulation of rRNA synthesis, is disrupted during transcription. In *EMBO J.* 17 (13), pp. 3692–3703. DOI: 10.1093/emboj/17.13.3692.

Miller, O. L.; Beatty, B. R. (1969): Visualization of nucleolar genes. In *Science* 164 (3882), pp. 955–957. DOI: 10.1126/science.164.3882.955.

Mindell, Joseph A.; Grigorieff, Nikolaus (2003): Accurate determination of local defocus and specimen tilt in electron microscopy. In *Journal of structural biology* 142 (3), pp. 334–347. DOI: 10.1016/s1047-8477(03)00069-8.

Moorefield, B.; Greene, E. A.; Reeder, R. H. (2000): RNA polymerase I transcription factor Rrn3 is functionally conserved between yeast and human. In *Proc Natl Acad Sci U S A* 97 (9), pp. 4724–4729. DOI: 10.1073/pnas.080063997.

Moss, T.; Langlois, F.; Gagnon-Kugler, T.; Stefanovsky, V. (2007): A housekeeper with power of attorney: the rRNA genes in ribosome biogenesis. In *Cell. Mol. Life Sci.* 64 (1), pp. 29–49. DOI: 10.1007/s00018-006-6278-1.

Moss, Tom (2004): At the crossroads of growth control; making ribosomal RNA. In *Curr. Opin. Genet. Dev.* 14 (2), pp. 210–217. DOI: 10.1016/j.gde.2004.02.005.

Moss, Tom; Stefanovsky, Victor Y. (2002): At the center of eukaryotic life. In *Cell* 109 (5), pp. 545–548.

Musters, W.; Knol, J.; Maas, P.; Dekker, A. F.; van Heerikhuizen, H.; Planta, R. J. (1989): Linker scanning of the yeast RNA polymerase I promoter. In *Nucleic Acids Res* 17 (23), pp. 9661–9678.

Naidu, S.; Friedrich, J. K.; Russell, J.; Zomerdijk,J. C. B. M. (2011): TAF1B Is a TFIIB-Like Component of the Basal Transcription Machinery for RNA Polymerase I. In *Science* 333 (6049), pp. 1640–1642. DOI: 10.1126/science.1207656.

Németh, Attila; Perez-Fernandez, Jorge; Merkl, Philipp; Hamperl, Stephan; Gerber, Jochen; Griesenbeck, Joachim; Tschochner, Herbert (2013): RNA polymerase I termination: Where is the end? In *Biochim. Biophys. Acta* 1829 (3-4), pp. 306–317. DOI: 10.1016/j.bbagrm.2012.10.007.

Neyer, Simon; Kunz, Michael; Geiss, Christian; Hantsche, Merle; Hodirnau, Victor-Valentin; Seybert, Anja et al. (2016): Structure of RNA polymerase I transcribing ribosomal DNA genes. In *Nature*. DOI: 10.1038/nature20561.

Nielsen, S.; Yuzenkova, Y.; Zenkin, N. (2013): Mechanism of Eukaryotic RNA Polymerase III Transcription Termination. In *Science* 340 (6140), pp. 1577–1580. DOI: 10.1126/science.1237934.

Nogi, Y.; Vu, L.; Nomura, M. (1991a): An approach for isolation of mutants defective in 35S ribosomal RNA synthesis in Saccharomyces cerevisiae. In *Proceedings of the National Academy of Sciences of the United States of America* 88 (16), pp. 7026–7030.

Nogi, Y.; Yano, R.; Nomura, M. (1991b): Synthesis of large rRNAs by RNA polymerase II in mutants of Saccharomyces cerevisiae defective in RNA polymerase I. In *Proc. Natl. Acad. Sci. U.S.A.* 88 (9), pp. 3962–3966.

Oakes, M.; Siddiqi, I.; Vu, L.; Aris, J.; Nomura, M. (1999): Transcription factor UAF, expansion and contraction of ribosomal DNA (rDNA) repeats, and RNA polymerase switch in transcription of yeast rDNA. In *Mol. Cell. Biol.* 19 (12), pp. 8559–8569.

Pacheco, Derek; Warfield, Linda; Brajcich, Michelle; Robbins, Hannah; Luo, Jie; Ranish, Jeff; Hahn, Steven (2018): Transcription Activation Domains of the Yeast Factors Met4 and Ino2: Tandem Activation Domains with Properties Similar to the Yeast Gcn4 Activator. In *Mol. Cell. Biol.* 38 (10). DOI: 10.1128/MCB.00038-18.

Papai, Gabor; Frechard, Alexandre; Kolesnikova, Olga; Crucifix, Corinne; Schultz, Patrick; Ben-Shem, Adam (2020): Structure of SAGA and mechanism of TBP deposition on gene promoters. In *Nature* 577 (7792), pp. 711–716. DOI: 10.1038/s41586-020-1944-2.

Patel, Avinash B.; Louder, Robert K.; Greber, Basil J.; Grünberg, Sebastian; Luo, Jie; Fang, Jie et al. (2018): Structure of human TFIID and mechanism of TBP loading onto promoter DNA. In *Science* 362 (6421). DOI: 10.1126/science.aau8872.

Peters, Jason M.; Vangeloff, Abbey D.; Landick, Robert (2011): Bacterial transcription terminators: the RNA 3'-end chronicles. In *Journal of molecular biology* 412 (5), pp. 793–813. DOI: 10.1016/j.jmb.2011.03.036.

Petes, T. D. (1979): Yeast ribosomal DNA genes are located on chromosome XII. In *Proc Natl Acad Sci U S A* 76 (1), pp. 410–414.

Pettersen, Eric F.; Goddard, Thomas D.; Huang, Conrad C.; Couch, Gregory S.; Greenblatt, Daniel M.; Meng, Elaine C.; Ferrin, Thomas E. (2004): UCSF Chimera--a visualization system for exploratory research and analysis. In *Journal of computational chemistry* 25 (13), pp. 1605–1612. DOI: 10.1002/jcc.20084.

Peyroche, G.; Milkereit, P.; Bischler, N.; Tschochner, H.; Schultz, P.; Sentenac, A. et al. (2000): The recruitment of RNA polymerase I on rDNA is mediated by the interaction of the A43 subunit with Rrn3. In *EMBO J* 19 (20), pp. 5473–5482. DOI: 10.1093/emboj/19.20.5473.

Philippi, A.; Steinbauer, R.; Reiter, A.; Fath, S.; Leger-Silvestre, I.; Milkereit, P. et al. (2010): TOR-dependent reduction in the expression level of Rrn3p lowers the activity of the yeast RNA Pol I machinery, but does not account for the strong inhibition of rRNA production. In *Nucleic Acids Research* 38 (16), pp. 5315–5326. DOI: 10.1093/nar/gkq264.

Pikaard, C. S. (2006): Cell biology of the Arabidopsis nuclear siRNA pathway for RNA-directed chromatin modification. In *Cold Spring Harb. Symp. Quant. Biol.* 71, pp. 473–480. DOI: 10.1101/sqb.2006.71.046.

Pilsl, Michael (2013): Analyse von heterolog exprimierten RNA-Polymerase I abhängigen Transkriptionsfaktoren. Master Thesis.

Pilsl, Michael; Crucifix, Corinne; Papai, Gabor; Krupp, Ferdinand; Steinbauer, Robert; Griesenbeck, Joachim et al. (2016a): Structure of the initiation-competent RNA polymerase I and its implication for transcription. In *Nature communications* 7, p. 12126. DOI: 10.1038/ncomms12126.

Pilsl, Michael; Engel, Christoph (2020): Structural basis of RNA polymerase I pre-initiation complex formation and promoter melting. In *Nat Comms* 11 (1), p. 1206. DOI: 10.1038/s41467-020-15052-y.

Pilsl, Michael; Merkl, Philipp E.; Milkereit, Philipp; Griesenbeck, Joachim; Tschochner, Herbert (2016b): Analysis of S. cerevisiae RNA Polymerase I Transcription In Vitro. In *Methods in molecular biology (Clifton, N.J.)* 1455, pp. 99–108. DOI: 10.1007/978-1-4939-3792-9_8.

Plaschka, C.; Hantsche, M.; Dienemann, C.; Burzinski, C.; Plitzko, J.; Cramer, P. (2016): Transcription initiation complex structures elucidate DNA opening. In *Nature* 533 (7603), pp. 353–358. DOI: 10.1038/nature17990.

Plaschka, C.; Larivière, L.; Wenzeck, L.; Seizl, M.; Hemann, M.; Tegunov, D. et al. (2015): Architecture of the RNA polymerase II-Mediator core initiation complex. In *Nature* 518 (7539), pp. 376–380. DOI: 10.1038/nature14229.

Powers, T.; Walter, P. (1999): Regulation of ribosome biogenesis by the rapamycin-sensitive TOR-signaling pathway in Saccharomyces cerevisiae. In *Mol. Biol. Cell* 10 (4), pp. 987–1000.

Prescott, Elizabeth M.; Osheim, Yvonne N.; Jones, Hannah S.; Alen, Claudia M.; Roan, Judith G.; Reeder, Ronald H. et al. (2004): Transcriptional termination by RNA polymerase I requires the small subunit Rpa12p. In *Proc. Natl. Acad. Sci. U.S.A.* 101 (16), pp. 6068–6073. DOI: 10.1073/pnas.0401393101.

Radebaugh, C. A.; Matthews, J. L.; Geiss, G. K.; Liu, F.; Wong, J. M.; Bateman, E. et al. (1994): TATA box-binding protein (TBP) is a constituent of the polymerase I-specific transcription initiation factor TIF-IB (SL1) bound to the rRNA promoter and shows differential sensitivity to TBP-directed reagents in polymerase I, II, and III transcription factors. In *Mol Cell Biol* 14 (1), pp. 597–605. DOI: 10.1128/MCB.14.1.597.

Ramsay, Ewan Phillip; Abascal-Palacios, Guillermo; Daiß, Julia L.; King, Helen; Gouge, Jerome; Pilsl, Michael et al. (2020): Structure of human RNA polymerase III. In *Nat Comms* 11 (1), p. 6409. DOI: 10.1038/s41467-020-20262-5.

Raska, Ivan; Shaw, Peter J.; Cmarko, Dušan (2006): New Insights into Nucleolar Architecture and Activity. In Kwang W. Jeon (Ed.): International review of cytology. A survey of cell biology., vol. 255. Amsterdam: Elsevier (International Review of Cytology, v. 255), pp. 177–235.

Ravarani, Charles N. J.; Flock, Tilman; Chavali, Sreenivas; Anandapadamanaban, Madhanagopal; Babu, M. Madan; Balaji, Santhanam (2020): Molecular determinants underlying functional innovations of TBP and their impact on transcription initiation. In *Nature communications* 11 (1), p. 2384. DOI: 10.1038/s41467-020-16182-z.

Reeder, Ronald H.; Roeder, Robert G. (1972): Ribosomal RNA synthesis in isolated nuclei. In *J. Mol. Biol.* 67 (3), pp. 433–441. DOI: 10.1016/0022-2836(72)90461-5.

Reines, D.; Ghanouni, P.; Li, Q. Q.; Mote, J. (1992): The RNA polymerase II elongation complex. Factor-dependent transcription elongation involves nascent RNA cleavage. In *J Biol Chem* 267 (22), pp. 15516–15522.

Reiter, Alarich (2011): PhD thesis Alarich Reiter. *In vivo* analysis of RNA-PolI elongation and termination in *Saccharomyces cerevisiae*.

Reiter, Alarich; Hamperl, Stephan; Seitz, Hannah; Merkl, Philipp; Perez-Fernandez, Jorge; Williams, Lydia et al. (2012): The Reb1-homologue Ydr026c/Nsi1 is required for efficient RNA polymerase I termination in yeast. In *EMBO J* 31 (16), pp. 3480–3493. DOI: 10.1038/emboj.2012.185.

Rhee, Ho Sung; Pugh, B. Franklin (2012): Genome-wide structure and organization of eukaryotic pre-initiation complexes. In *Nature* 483 (7389), pp. 295–301. DOI: 10.1038/nature10799.

Riggs, D. L.; Nomura, M. (1990): Specific transcription of Saccharomyces cerevisiae 35 S rDNA by RNA polymerase I in vitro. In *J. Biol. Chem.* 265 (13), pp. 7596–7603. Available online at http://www.jbc.org/content/265/13/7596.full.pdf.

Roeder, R. G.; Rutter, W. J. (1969): Multiple forms of DNA-dependent RNA polymerase in eukaryotic organisms. In *Nature* 224 (5216), pp. 234–237.

Roeder, R. G.; Rutter, W. J. (1970): Specific nucleolar and nucleoplasmic RNA polymerases. In *Proc Natl Acad Sci U S A* 65 (3), pp. 675–682.

Rossi, Matthew J.; Kuntala, Prashant K.; Lai, William K. M.; Yamada, Naomi; Badjatia, Nitika; Mittal, Chitvan et al. (2021): A high-resolution protein architecture of the budding yeast genome. In *Nature*, pp. 1–6. DOI: 10.1038/s41586-021-03314-8.

Rothblum, Katrina; Hu, Qiyue; Penrod, Yvonne; Rothblum, Lawrence I. (2014): Selective inhibition of rDNA transcription by a small-molecule peptide that targets the interface between RNA polymerase I and Rrn3. In *Molecular cancer research : MCR* 12 (11), pp. 1586–1596. DOI: 10.1158/1541-7786.MCR-14-0229.

Rudra, Dipayan; Warner, Jonathan R. (2004): What better measure than ribosome synthesis? In *Genes Dev.* 18 (20), pp. 2431–2436. DOI: 10.1101/gad.1256704.

Russell, Jackie; Zomerdijk, Joost C B M (2006): The RNA polymerase I transcription machinery. In *Biochem Soc Symp* (73), pp. 203–216.

Sadian, Yashar; Baudin, Florence; Tafur, Lucas; Murciano, Brice; Wetzel, Rene; Weis, Felix; Müller, Christoph W. (2019): Molecular insight into RNA polymerase I promoter recognition and promoter melting. In *Nat Comms* 10 (1), p. 5543. DOI: 10.1038/s41467-019-13510-w.

Sadian, Yashar; Tafur, Lucas; Kosinski, Jan; Jakobi, Arjen J.; Wetzel, Rene; Buczak, Katarzyna et al. (2017): Structural insights into transcription initiation by yeast RNA polymerase I. In *The EMBO journal*. DOI: 10.15252/embj.201796958.

Sainsbury, Sarah; Niesser, Jürgen; Cramer, Patrick (2013): Structure and function of the initially transcribing RNA polymerase II-TFIIB complex. In *Nature* 493 (7432), pp. 437–440. DOI: 10.1038/nature11715.

Sanz-Murillo, Marta; Xu, Jun; Belogurov, Georgiy A.; Calvo, Olga; Gil-Carton, David; Moreno-Morcillo, María et al. (2018): Structural basis of RNA polymerase I stalling at UV light-induced DNA damage. In *PNAS* 115 (36), pp. 8972–8977. DOI: 10.1073/pnas.1802626115.

Sauer, Paul Victor; Timm, Jennifer; Liu, Danni; Sitbon, David; Boeri-Erba, Elisabetta; Velours, Christophe et al. (2017): Insights into the molecular architecture and histone H3-H4 deposition mechanism of yeast Chromatin assembly factor 1. In *eLife* 6. DOI: 10.7554/eLife.23474.

Scheres, Sjors H. W. (2012): RELION: implementation of a Bayesian approach to cryo-EM structure determination. In *Journal of structural biology* 180 (3), pp. 519–530. DOI: 10.1016/j.jsb.2012.09.006.

Schmidt, Carla; Urlaub, Henning (2017): Combining cryo-electron microscopy (cryo-EM) and cross-linking mass spectrometry (CX-MS) for structural elucidation of large protein assemblies. In *Curr. Opin. Struct. Biol.* 46, pp. 157–168. DOI: 10.1016/j.sbi.2017.10.005.

Schneider, Caroline A.; Rasband, Wayne S.; Eliceiri, Kevin W. (2012): NIH Image to ImageJ: 25 years of image analysis. In *Nat Methods* 9 (7), pp. 671–675. DOI: 10.1038/nmeth.2089.

Schneider, David A.; Michel, Antje; Sikes, Martha L.; Vu, Loan; Dodd, Jonathan A.; Salgia, Shilpa et al. (2007): Transcription elongation by RNA polymerase I is linked to efficient rRNA processing and ribosome assembly. In *Molecular Cell* 26 (2), pp. 217–229. DOI: 10.1016/j.molcel.2007.04.007.

Schneider, David Alan (2012): RNA polymerase I activity is regulated at multiple steps in the transcription cycle: Recent insights into factors that influence transcription elongation. In *Gene* 493 (2), pp. 176–184. DOI: 10.1016/j.gene.2011.08.006.

Schultz, M. C.; Reeder, R. H.; Hahn, S. (1992): Variants of the TATA-binding protein can distinguish subsets of RNA polymerase I, II, and III promoters. In *Cell* 69 (4), pp. 697–702.

Schultz, P.; Célia, H.; Riva, M.; Sentenac, A.; Oudet, P. (1993): Three-dimensional model of yeast RNA polymerase I determined by electron microscopy of two-dimensional crystals. In *EMBO J* 12 (7), pp. 2601–2607.

Scull, Catherine E.; Ingram, Zachariah M.; Lucius, Aaron L.; Schneider, David A. (2019): A Novel Assay for RNA Polymerase I Transcription Elongation Sheds Light on the Evolutionary Divergence of Eukaryotic RNA Polymerases. In *Biochemistry*. DOI: 10.1021/acs.biochem.8b01256.

Shou, W.; Sakamoto, K. M.; Keener, J.; Morimoto, K. W.; Traverso, E. E.; Azzam, R. et al. (2001): Net1 stimulates RNA polymerase I transcription and regulates nucleolar structure independently of controlling mitotic exit. In *Mol. Cell* 8 (1), pp. 45–55.

Shou, W.; Seol, J. H.; Shevchenko, A.; Baskerville, C.; Moazed, D.; Chen, Z. W. et al. (1999): Exit from mitosis is triggered by Tem1-dependent release of the protein phosphatase Cdc14 from nucleolar RENT complex. In *Cell* 97 (2), pp. 233–244.

Siddiqi, I.; Keener, J.; Vu, L.; Nomura, M. (2001a): Role of TATA Binding Protein (TBP) in Yeast Ribosomal DNA Transcription by RNA Polymerase I: Defects in the Dual Functions of Transcription Factor UAF Cannot Be Suppressed by TBP. In *Molecular and Cellular Biology* 21 (7), pp. 2292–2297. DOI: 10.1128/MCB.21.7.2292-2297.2001.

Siddiqi, I. N.; Dodd, J. A.; Vu, L.; Eliason, K.; Oakes, M. L.; Keener, J. et al. (2001b): Transcription of chromosomal rRNA genes by both RNA polymerase I and II in yeast uaf30 mutants lacking the 30 kDa subunit of transcription factor UAF. In *EMBO J.* 20 (16), pp. 4512–4521. DOI: 10.1093/emboj/20.16.4512.

Sigurdsson, Stefan; Dirac-Svejstrup, A. Barbara; Svejstrup, Jesper Q. (2010): Evidence that Transcript Cleavage Is Essential for RNA Polymerase II Transcription and Cell Viability. In *Molecular Cell* 38 (2), pp. 202–210. DOI: 10.1016/j.molcel.2010.02.026.

Silva, Daniel-Adriano; Weiss, Dahlia R.; Pardo Avila, Fatima; Da, Lin-Tai; Levitt, Michael; Wang, Dong; Huang, Xuhui (2014): Millisecond dynamics of RNA polymerase II translocation at atomic resolution.

In *Proceedings of the National Academy of Sciences of the United States of America* 111 (21), pp. 7665–7670. DOI: 10.1073/pnas.1315751111.

Smith, Marissa L.; Cui, Weidong; Jackobel, Ashleigh J.; Walker-Kopp, Nancy; Knutson, Bruce A. (2018): Reconstitution of RNA Polymerase I Upstream Activating Factor and the Roles of Histones H3 and H4 in Complex Assembly. In *Journal of molecular biology*. DOI: 10.1016/j.jmb.2018.01.003.

Soutourina, J.; Wydau, S.; Ambroise, Y.; Boschiero, C.; Werner, M. (2011): Direct Interaction of RNA Polymerase II and Mediator Required for Transcription in Vivo. In *Science* 331 (6023), pp. 1451–1454. DOI: 10.1126/science.1200188.

Srivastava, A. K.; Schlessinger, D. (1991): Structure and organization of ribosomal DNA. In *Biochimie* 73 (6), pp. 631–638. DOI: 10.1016/0300-9084(91)90042-y.

Stark, Holger; Chari, Ashwin (2016): Sample preparation of biological macromolecular assemblies for the determination of high-resolution structures by cryo-electron microscopy. In *Microscopy (Oxf)* 65 (1), pp. 23–34. DOI: 10.1093/jmicro/dfv367.

Steffan, J. S.; Keys, D. A.; Dodd, J. A.; Nomura, M. (1996): The role of TBP in rDNA transcription by RNA polymerase I in Saccharomyces cerevisiae: TBP is required for upstream activation factor-dependent recruitment of core factor. In *Genes & Development* 10 (20), pp. 2551–2563. DOI: 10.1101/gad.10.20.2551.

Steffan, J. S.; Keys, D. A.; Vu, L.; Nomura, M. (1998): Interaction of TATA-binding protein with upstream activation factor is required for activated transcription of ribosomal DNA by RNA polymerase I in Saccharomyces cerevisiae in vivo. In *Mol. Cell. Biol.* 18 (7), pp. 3752–3761.

Steinbauer, Robert (2010): PhD thesis Robert Steinbauer 2010. Growth-dependent regulation of ribosome biogenesis and the role of Rrn3p in RNA polymerase I transcription. Edited by Universtität Regensburg. Universtität Regensburg.

Stepanchick, A.; Zhi, H.; Cavanaugh, A. H.; Rothblum, K.; Schneider, D. A.; Rothblum, L. I. (2013): DNA Binding by the Ribosomal DNA Transcription Factor Rrn3 Is Essential for Ribosomal DNA Transcription. In *Journal of Biological Chemistry* 288 (13), pp. 9135–9144. DOI: 10.1074/jbc.M112.444265.

Straight, A. F.; Shou, W.; Dowd, G. J.; Turck, C. W.; Deshaies, R. J.; Johnson, A. D.; Moazed, D. (1999): Net1, a Sir2-associated nucleolar protein required for rDNA silencing and nucleolar integrity. In *Cell* 97 (2), pp. 245–256.

Tafur, Lucas; Sadian, Yashar; Hanske, Jonas; Wetzel, Rene; Weis, Felix; Müller, Christoph W. (2019): The cryo-EM structure of a 12-subunit variant of RNA polymerase I reveals dissociation of the A49-A34.5 heterodimer and rearrangement of subunit A12.2. In *eLife* 8. DOI: 10.7554/eLife.43204.

Tafur, Lucas; Sadian, Yashar; Hoffmann, Niklas A.; Jakobi, Arjen J.; Wetzel, Rene; Hagen, Wim J.H. et al. (2016): Molecular Structures of Transcribing RNA Polymerase I. In *Molecular Cell*. DOI: 10.1016/j.molcel.2016.11.013.

Tan, Yong Zi; Baldwin, Philip R.; Davis, Joseph H.; Williamson, James R.; Potter, Clinton S.; Carragher, Bridget; Lyumkis, Dmitry (2017): Addressing preferred specimen orientation in single-particle cryo-EM through tilting. In *Nature methods* 14 (8), pp. 793–796. DOI: 10.1038/nmeth.4347.

Thermo Scientific Pierce (2020). Available online at https://www.thermofisher.com/order/catalog/product/21655#/21655, updated on 3/3/2020, checked on 3/3/2020.

Thuillier, V.; Stettler, S.; Sentenac, A.; Thuriaux, P.; Werner, M. (1995): A mutation in the C31 subunit of Saccharomyces cerevisiae RNA polymerase III affects transcription initiation. In *EMBO J* 14 (2), pp. 351–359.

Tollervey, David (2004): Molecular biology: termination by torpedo. In *Nature* 432 (7016), pp. 456–457. DOI: 10.1038/432456a.

Torreira, Eva; Louro, Jaime Alegrio; Pazos, Irene; Gonzalez-Polo, Noelia; Gil-Carton, David; Duran, Ana Garcia et al. (2017): The dynamic assembly of distinct RNA polymerase I complexes modulates rDNA transcription. In *eLife* 6. DOI: 10.7554/eLife.20832.

Tschochner, H. (1996): A novel RNA polymerase I-dependent RNase activity that shortens nascent transcripts from the 3' end. In *Proc. Natl. Acad. Sci. U.S.A.* 93 (23), pp. 12914–12919.

Tuan, J. C.; Zhai, W.; Comai, L. (1999): Recruitment of TATA-binding protein-TAFI complex SL1 to the human ribosomal DNA promoter is mediated by the carboxy-terminal activation domain of upstream binding factor (UBF) and is regulated by UBF phosphorylation. In *Mol Cell Biol* 19 (4), pp. 2872–2879. DOI: 10.1128/mcb.19.4.2872.

Ucuncuoglu, Suleyman; Engel, Krysta L.; Purohit, Prashant K.; Dunlap, David D.; Schneider, David A.; Finzi, Laura (2016): Direct Characterization of Transcription Elongation by RNA Polymerase I. In *PLoS ONE* 11 (7), e0159527. DOI: 10.1371/journal.pone.0159527.

van Mullem, Vincent; Landrieux, Emilie; Vandenhaute, Jean; Thuriaux, Pierre (2002): Rpa12p, a conserved RNA polymerase I subunit with two functional domains. In *Molecular microbiology* 43 (5), pp. 1105–1113.

Vannini, Alessandro; Cramer, Patrick (2012): Conservation between the RNA polymerase I, II, and III transcription initiation machineries. In *Mol. Cell* 45 (4), pp. 439–446. DOI: 10.1016/j.molcel.2012.01.023.

Viktorovskaya, Olga V.; Appling, Francis D.; Schneider, David A. (2011): Yeast transcription elongation factor Spt5 associates with RNA polymerase I and RNA polymerase II directly. In *J Biol Chem* 286 (21), pp. 18825–18833. DOI: 10.1074/jbc.M110.202119.

Viktorovskaya, Olga V.; Schneider, David A. (2015): Functional divergence of eukaryotic RNA polymerases: unique properties of RNA polymerase I suit its cellular role. In *Gene* 556 (1), pp. 19–26. DOI: 10.1016/j.gene.2014.10.035.

Visintin, R.; Hwang, E. S.; Amon, A. (1999): Cfi1 prevents premature exit from mitosis by anchoring Cdc14 phosphatase in the nucleolus. In *Nature* 398 (6730), pp. 818–823. DOI: 10.1038/19775.

Vogelauer, M.; Cioci, F.; Camilloni, G. (1998): DNA protein-interactions at the Saccharomyces cerevisiae 35 S rRNA promoter and in its surrounding region. In *J. Mol. Biol.* 275 (2), pp. 197–209. DOI: 10.1006/jmbi.1997.1451.

Voit, R.; Schnapp, A.; Kuhn, A.; Rosenbauer, H.; Hirschmann, P.; Stunnenberg, H. G.; Grummt, I. (1992): The nucleolar transcription factor mUBF is phosphorylated by casein kinase II in the C-terminal hyperacidic tail which is essential for transactivation. In *EMBO J* 11 (6), pp. 2211–2218.

Vorländer, Matthias K.; Khatter, Heena; Wetzel, Rene; Hagen, Wim J. H.; Müller, Christoph W. (2018): Molecular mechanism of promoter opening by RNA polymerase III. In *Nature* 553 (7688), pp. 295–300. DOI: 10.1038/nature25440.

Vu, L.; Siddiqi, I.; Lee, B. S.; Josaitis, C. A.; Nomura, M. (1999): RNA polymerase switch in transcription of yeast rDNA. Role of transcription factor UAF (upstream activation factor) in silencing rDNA transcription by RNA polymerase II. In *Proc Natl Acad Sci U S A* 96 (8), pp. 4390–4395.

Wang, D.; Bushnell, D. A.; Huang, X.; Westover, K. D.; Levitt, M.; Kornberg, R. D. (2009): Structural basis of transcription: backtracked RNA polymerase II at 3.4 angstrom resolution. In *Science (New York, N.Y.)* 324 (5931), pp. 1203–1206. DOI: 10.1126/science.1168729.

Warner, J. R. (1999): The economics of ribosome biosynthesis in yeast. In *Trends Biochem Sci* 24 (11), pp. 437–440.

Weijers, Mireille; Broersen, Kerensa; Barneveld, Peter A.; Cohen Stuart, Martien A.; Hamer, Rob J.; Jongh, Harmen H. J. de; Visschers, Ronald W. (2008): Net charge affects morphology and visual properties of ovalbumin aggregates. In *Biomacromolecules* 9 (11), pp. 3165–3172. DOI: 10.1021/bm800751e.

Weist, Stephanie; Eravci, Murat; Broedel, Oliver; Fuxius, Sandra; Eravci, Selda; Baumgartner, Andreas (2008): Results and reliability of protein quantification for two-dimensional gel electrophoresis strongly depend on the type of protein sample and the method employed. In *Proteomics* 8 (16), pp. 3389–3396. DOI: 10.1002/pmic.200800236.

Wieland, T. (1968): Poisonous principles of mushrooms of the genus Amanita. Four-carbon amines acting on the central nervous system and cell-destroying cyclic peptides are produced. In *Science* 159 (3818), pp. 946–952. DOI: 10.1126/science.159.3818.946.

Wittner, Manuel; Hamperl, Stephan; Stöckl, Ulrike; Seufert, Wolfgang; Tschochner, Herbert; Milkereit, Philipp; Griesenbeck, Joachim (2011): Establishment and Maintenance of Alternative Chromatin States at a Multicopy Gene Locus. In *Cell* 145 (4), pp. 543–554. DOI: 10.1016/j.cell.2011.03.051.

Woolford, John L.; Baserga, Susan J. (2013): Ribosome biogenesis in the yeast Saccharomyces cerevisiae. In *Genetics* 195 (3), pp. 643–681. DOI: 10.1534/genetics.113.153197.

Yamamoto, R. T.; Nogi, Y.; Dodd, J. A.; Nomura, M. (1996): RRN3 gene of Saccharomyces cerevisiae encodes an essential RNA polymerase I transcription factor which interacts with the polymerase independently of DNA template. In *EMBO J.* 15 (15), pp. 3964–3973.

Zhang, Kai (2016): Gctf: Real-time CTF determination and correction. In *Journal of structural biology* 193 (1), pp. 1–12. DOI: 10.1016/j.jsb.2015.11.003.

Zhang, Yinfeng; Sikes, Martha L.; Beyer, Ann L.; Schneider, David A. (2009): The Paf1 complex is required for efficient transcription elongation by RNA polymerase I. In *Proc. Natl. Acad. Sci. U.S.A.* 106 (7), pp. 2153–2158. DOI: 10.1073/pnas.0812939106.

Zhang, Yinfeng; Smith, Archer D.; Renfrow, Matthew B.; Schneider, David A. (2010): The RNA polymerase-associated factor 1 complex (Paf1C) directly increases the elongation rate of RNA polymerase I and is required for efficient regulation of rRNA synthesis. In *The Journal of biological chemistry* 285 (19), pp. 14152–14159. DOI: 10.1074/jbc.M110.115220.

Zhang, Zhengjian; English, Brian P.; Grimm, Jonathan B.; Kazane, Stephanie A.; Hu, Wenxin; Tsai, Albert et al. (2016): Rapid dynamics of general transcription factor TFIIB binding during preinitiation complex assembly revealed by single-molecule analysis. In *Genes & Development* 30 (18), pp. 2106–2118. DOI: 10.1101/gad.285395.116.

Zheng, Shawn Q.; Palovcak, Eugene; Armache, Jean-Paul; Verba, Kliment A.; Cheng, Yifan; Agard, David A. (2017): MotionCor2: anisotropic correction of beam-induced motion for improved cryo-electron microscopy. In *Nature methods* 14 (4), pp. 331–332. DOI: 10.1038/nmeth.4193.

Zivanov, Jasenko; Nakane, Takanori; Forsberg, Björn O.; Kimanius, Dari; Hagen, Wim Jh; Lindahl, Erik; Scheres, Sjors Hw (2018): New tools for automated high-resolution cryo-EM structure determination in RELION-3. In *eLife* 7. DOI: 10.7554/eLife.42166.

Zlatanova, Jordanka; Bishop, Thomas C.; Victor, Jean-Marc; Jackson, Vaughn; van Holde, Ken (2009): The nucleosome family: dynamic and growing. In *Structure (London, England : 1993)* 17 (2), pp. 160–171. DOI: 10.1016/j.str.2008.12.016.

7. Supplemental Figures

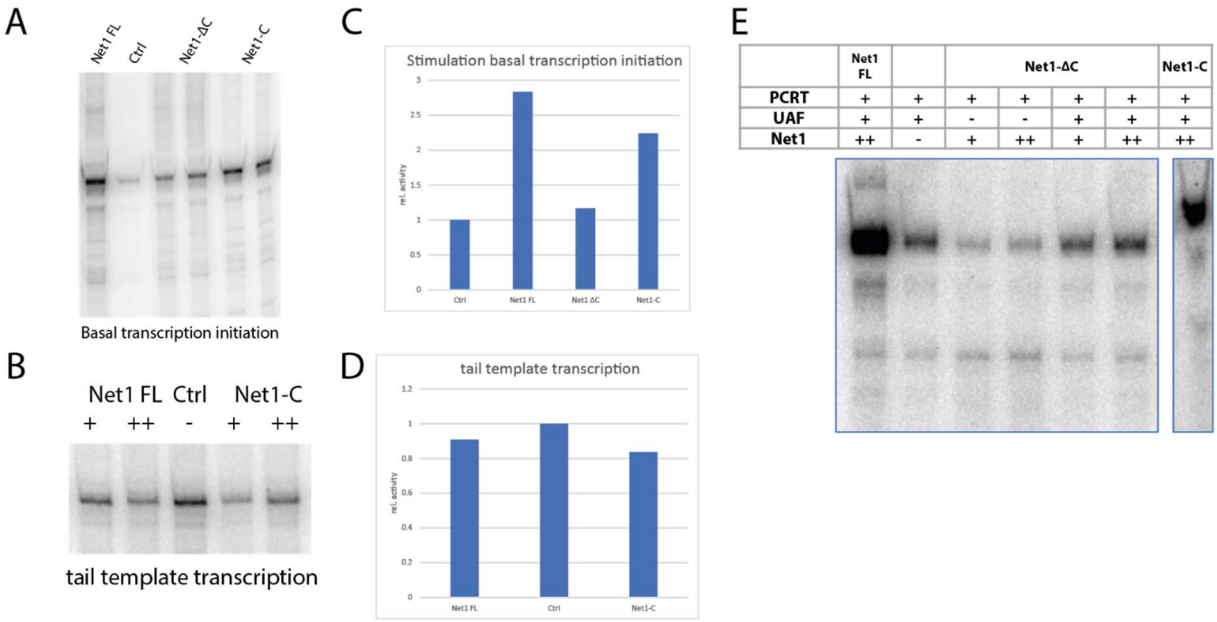

Supplemental Figure 1: Stimulatory activity of Net1 can be assigned to its C-terminus
Net 1 FL, Net1-ΔC and Net1-C were tested in different in vitro transcription assays. A) Basal initiation assay containing constant amounts Pol I, Rrn3 and CF plus Net1-protein as indicated and a buffer control reaction; B) Tail template transcription assay, Net 1 FL, Net1-ΔC and Net1-C were added to Pol I containing reactions as indicated C) Quantification of basal transcription initiation assay in A; D) Quantification of tail template assay in B; D) Complete transcription initiation assay Net 1 FL, Net1-ΔC and Net1-C were added to transcription reactions as indicated

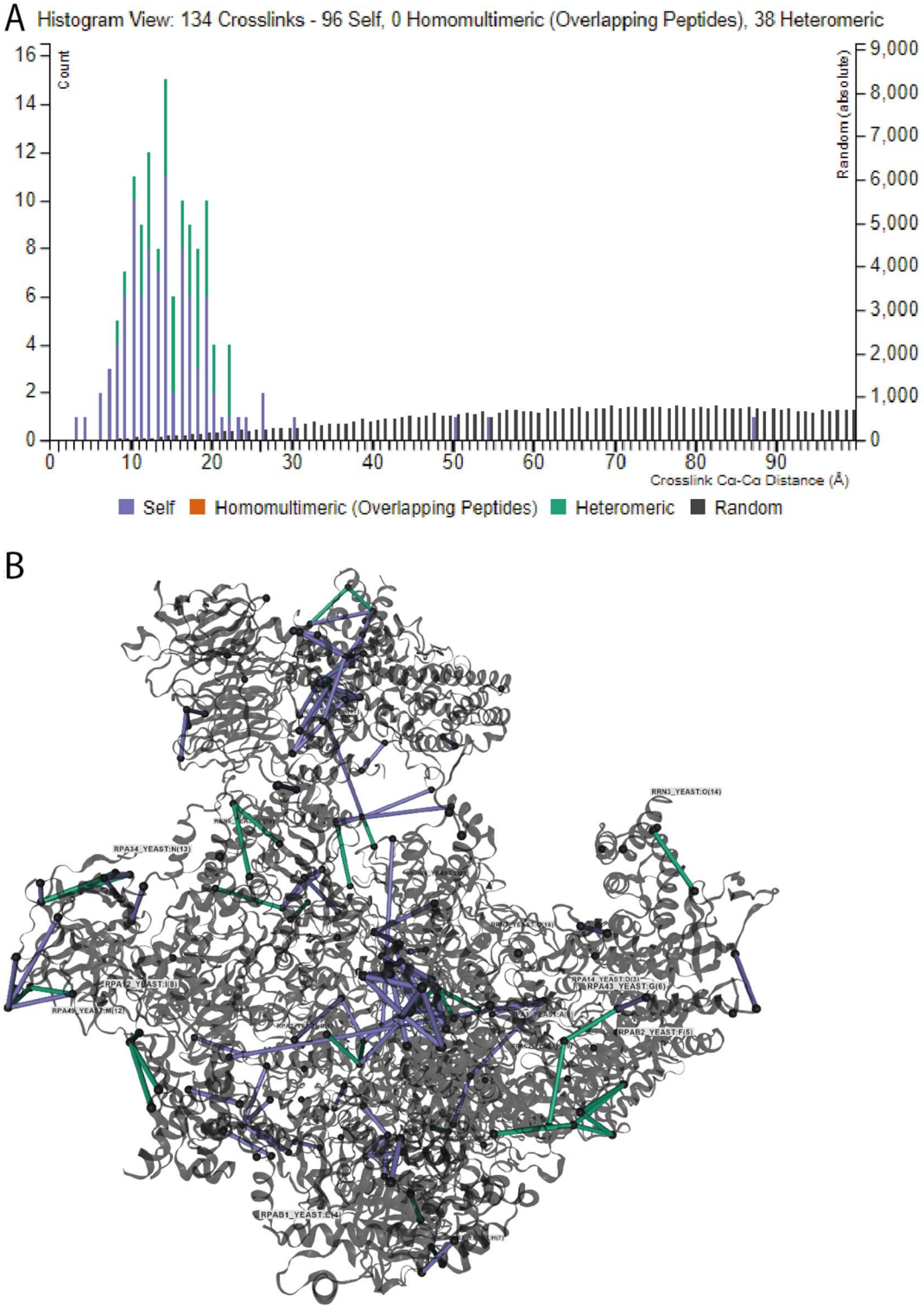

Supplemental Figure 2: Quality assessment X-link MS data
Mapping of BS3 crosslinks of complete PIC sample eiPIC structure (pdb: 6TPS) shows high quality of mass-spectrometry analysis. 131 out of 136 (96%) crosslinked residue pairs full-fill distance restrains of 30 Å Cα-Cα distance. A) Histogram of Cα-Cα distance; intra-subunit crosslinks are displayed in blue (self), inter-protein crosslinks in green (heteromeric). B) Crosslinks visualized on molecular PIC structure (6TPS), intra-subunit crosslinks are displayed in blue, inter-protein crosslinks in green. Protein interaction network at the Pol I PIC visualized with xiview webserver (xiVIEW | Home).

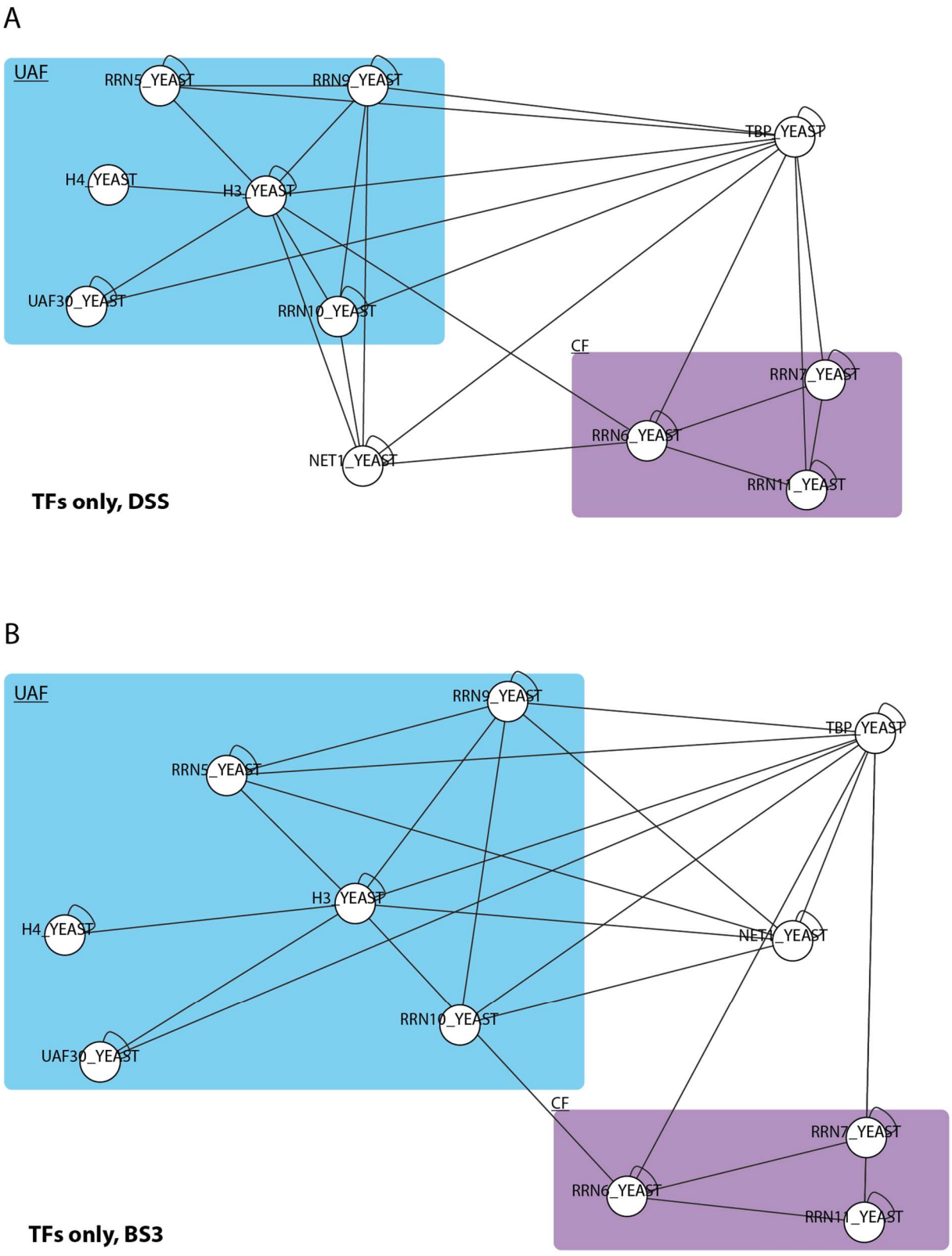

Supplemental Figure 3: X-link MS data of UAF-TBP-CF-Net1-C complex
Protein-protein interaction network at reconstituted promoter bound complex. A) crosslinked with DSS B) crosslinked with BS3. Protein interaction network at the visualized with xiview webserver (xiVIEW | Home) https://xiview.org/.

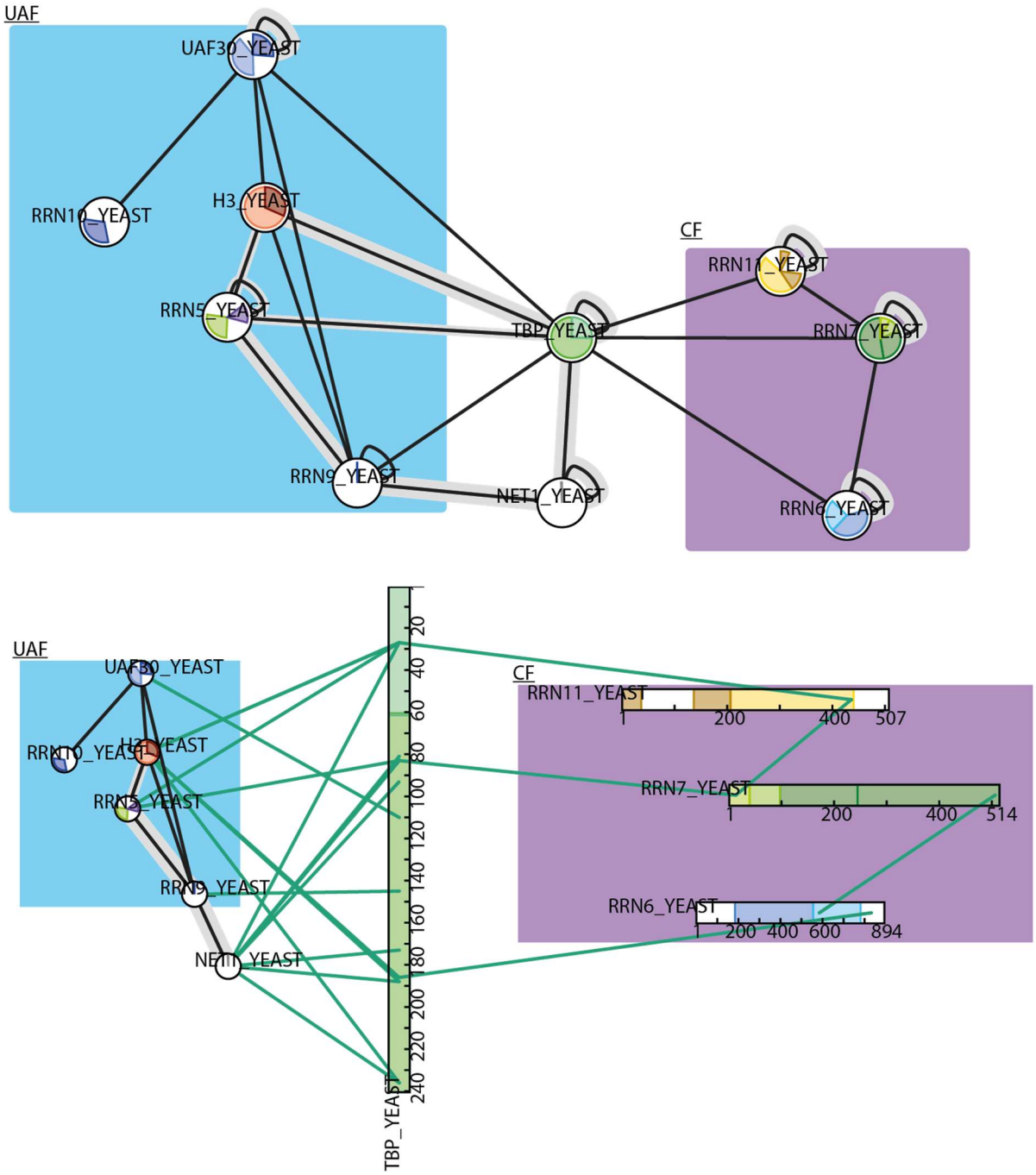

Supplemental Figure 4: X-link MS data of EDC crosslinked UAF-TBP-CF-Net1-C complex
Protein interaction network at the Pol I PIC visualized with xiview webserver (xiVIEW | Home). UAF subunits highlighted with blue background, CF in violet. Flexible TBP-N-terminal part is shown in light green, core TBP in dark green. Bottom: TBP was enlarged to visualizes interacting residues.

A

	1	2	3	4	5	6	7	8	9	10	11	12	13	14	15
	G	A	T	C											
DnaseI						+	+	+	+	+	+	+	+	+	-
UAF							+	+	+	+	+	+			
Net1-C							+	+	+	+	+	+			
CF								+	+	+	+	+			
TBP									+	+	+	+			
Pol I+Rrn3										0,5	2	4	0,5	4	

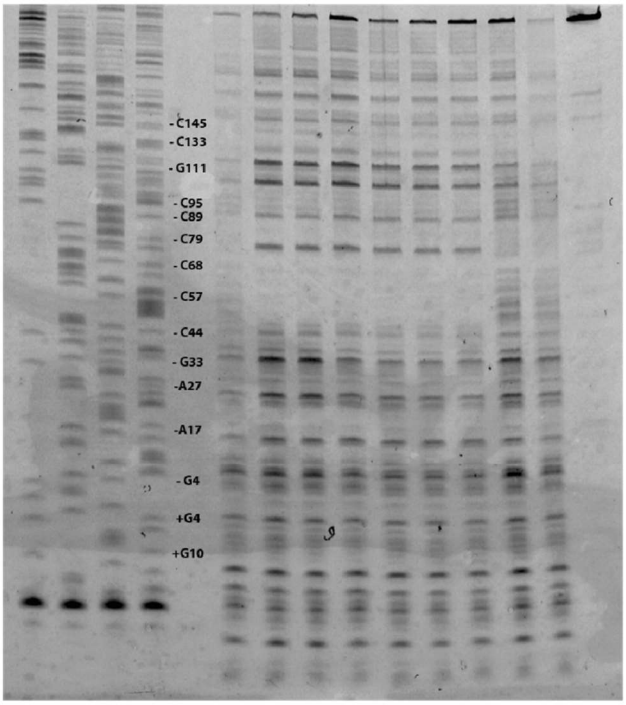

B

	6	7	8	9	10	11	12	13	14	15
UAF		+	+	+	+	+	+			
Net1-C		+	+	+	+	+	+			
CF			+	+	+	+	+			
TBP				+	+	+	+			
Pol I+Rrn3					0,5	2	4	0,5	4	

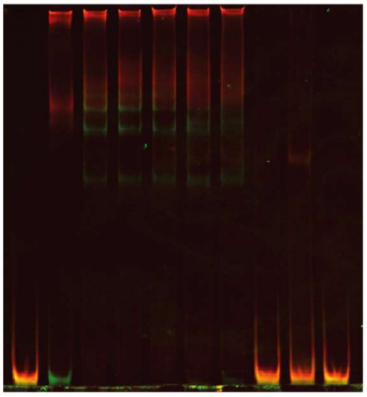

C

	1	2	3	4	5	6	7	8	9	10	11	12	13	14	15
ddNTP	G	A	T	C											
DnaseI						+	+	+	+	+	+	+	+	+	-
UAF							+	+	+	+	+	+			
Net1-C							+	+	+	+	+	+			
CF								+	+	+	+	+			
TBP									+	+	+	+			
Pol I+Rrn3										0,5	2	4	0,5	4	

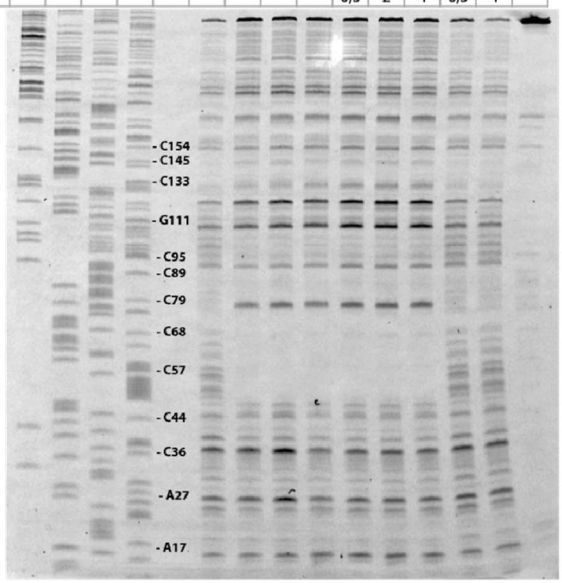

Supplemental Figure 5: DNase I Footprinting Pol I PIC

A) 7% UREA-PAGE sequencing gel of DNase I footprinting reaction; sequencing reactions with di-deoxy-nucleotides (ddNTPs) allowed mapping of DNA fragments, the di-deoxy-nucleotides used in the respective sequencing reaction are indicated on top of each lane. Selected bases are indicated relative to the TSS; reactions contain factors as indicated and were digested with constant amounts of DNase

I. Reactions in lane contained Cy5-labelled WT DNA and equal amounts of Cy3-labelled ΔUE DNA, only Cy5 signal is shown. B) EMSA experiments confirmed DNA occupancy. An aliquot of the assembly reaction was loaded onto a native PAGE gel prior to DNA digestion; reactions contained Cy5-labelled WT DNA and equal amounts of Cy3-labelled ΔUE DNA Merged Cy3 and Cy5 channels are depicted C) 7% UREA-PAGE sequencing gel of DNase I footprinting reaction; experiment in A) was repeated with prolonged gel-run for better separation around position -80 -120. Selected bases are indicated relative to the TSS of the template strand.

	1	2	3	4	5	6	7	8	9	10	11	12	15	16	17	18
ddNTP	G	A	T	C	-							-	G	A	T	C
DnaseI						-	+	+	+	+	+					
Net1-C							+		+	+						
UAF								+	+	+						
TBP										+						

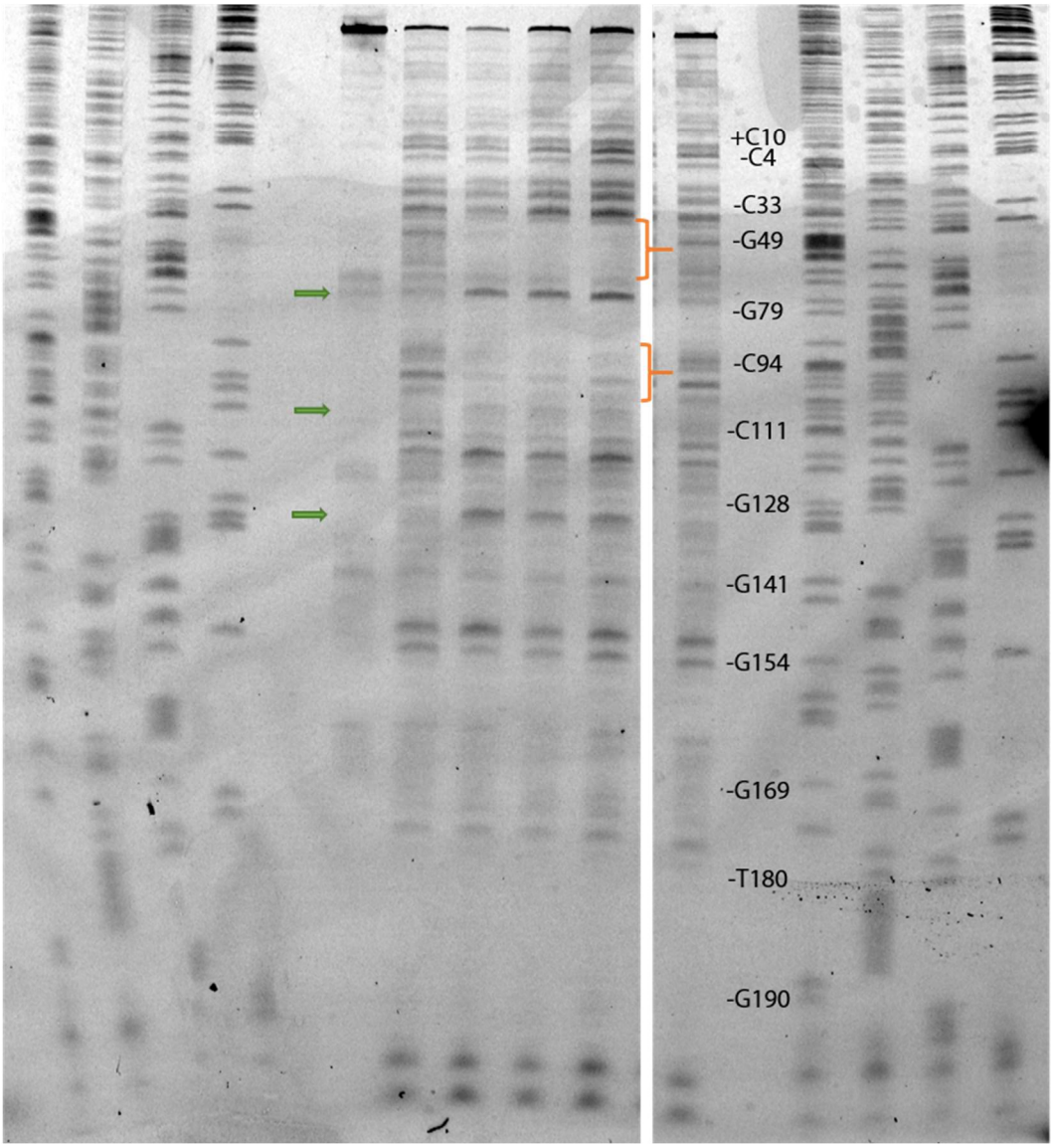

Supplemental Figure 6: DNase I Footprinting Non-Template Strand
A) 7% UREA-PAGE sequencing gel of DNase I footprinting reaction, Non-template strand was fluorescently labelled with Cy5. Selected bases are indicated relative to the TSS. Green arrows highlighted hypersensitive sites, brackets highlight protected areas by UAF.

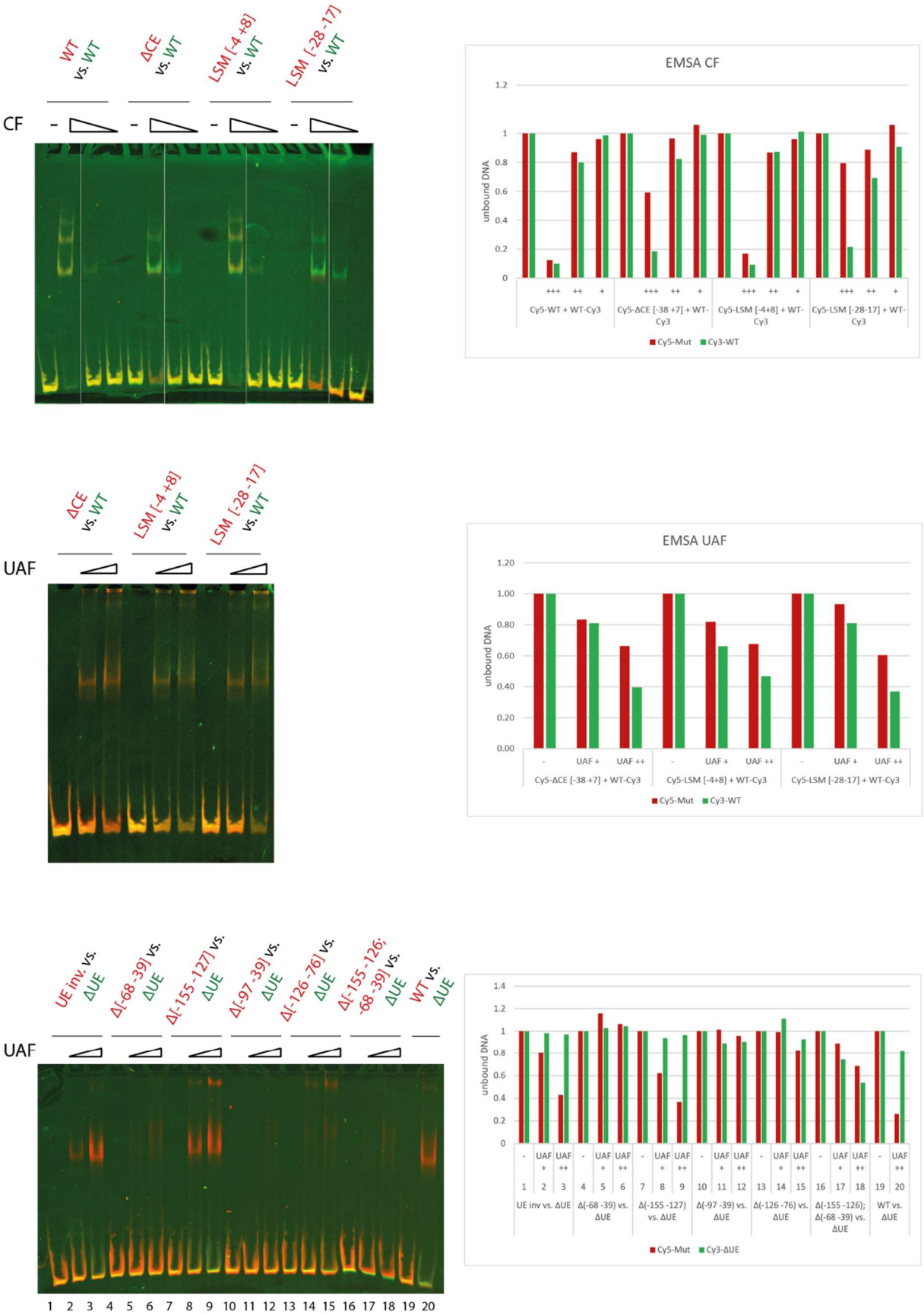

Supplemental Figure 7: Gel shift assays of Pol I promoter variants

EMSA of different Pol I promoter variants, left: native PAGE gels, competition between indicated mutant (Cy5 labelled, red) and ΔUE reference template (Cy3, green), merged channels are depicted; right: quantification of unbound DNA in each channel are depicted

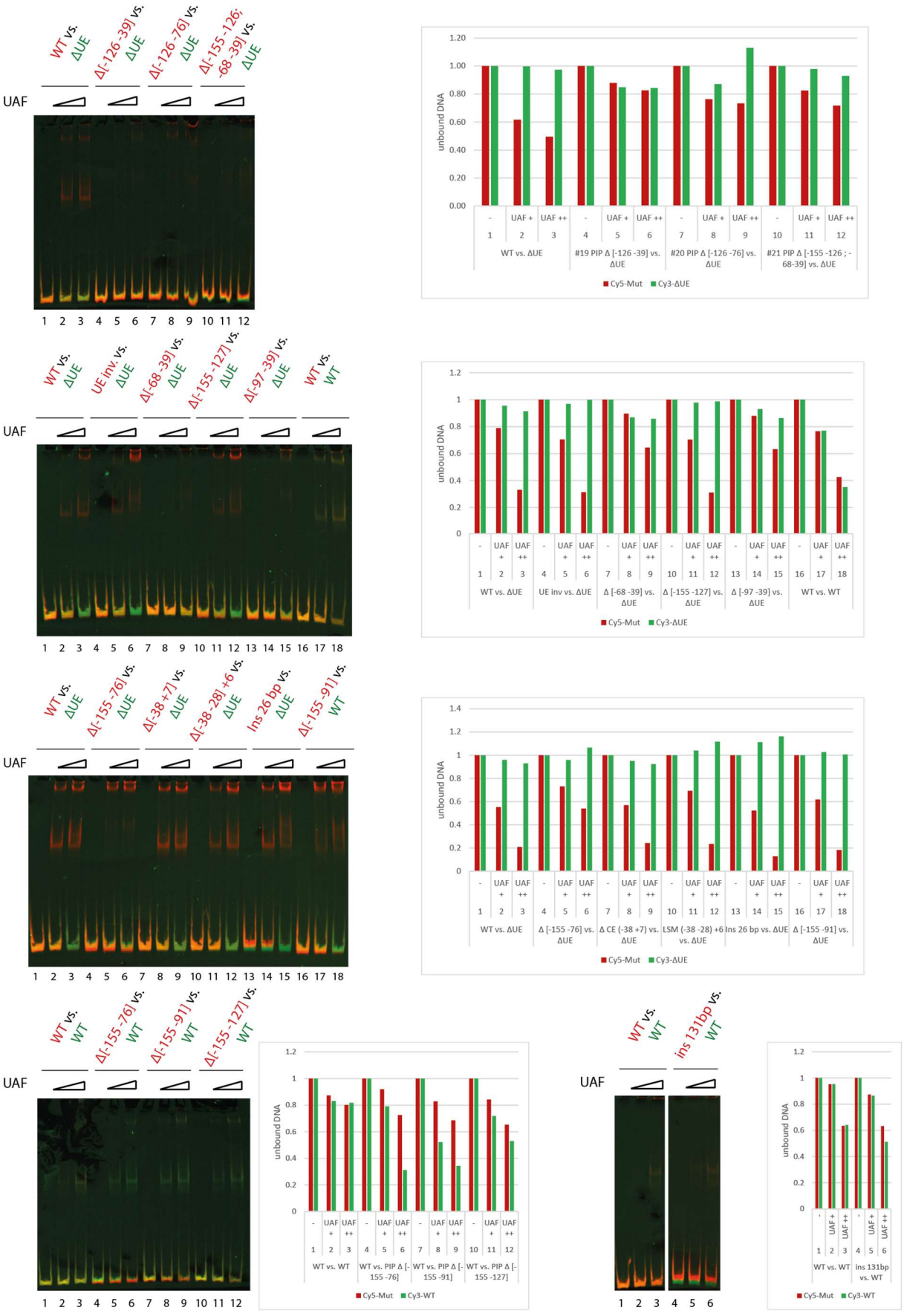

Supplemental Figure 8: Gel shift assays of Pol I promoter variants

EMSA of different Pol I promoter variants, left: native PAGE gels, competition between indicated mutant (Cy5 labelled, red) and ΔUE reference template (Cy3, green), merged channels are depicted; right: quantification of unbound DNA in each channel are depicted

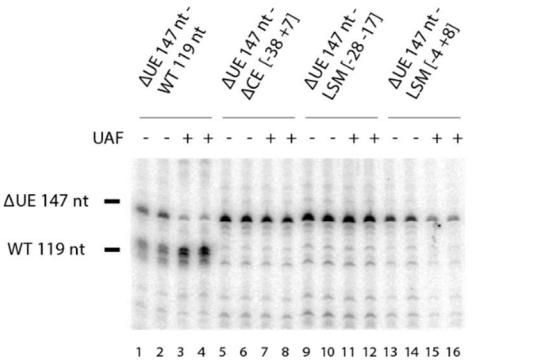
ΔUE 147 nt - WT 119 nt
ΔUE 147 nt - ΔCE [-38 +7]
ΔUE 147 nt - LSM [-28 -17]
ΔUE 147 nt - LSM [-4 +8]
UAF
ΔUE 147 nt
WT 119 nt
1 2 3 4 5 6 7 8 9 10 11 12 13 14 15 16

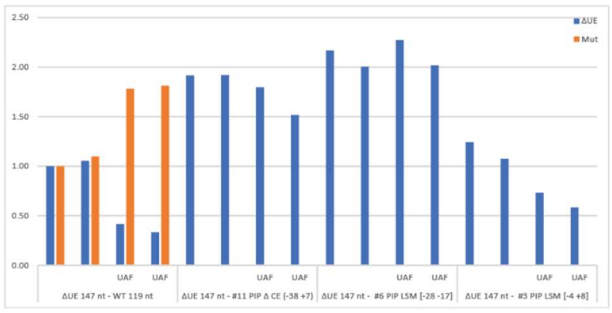
ΔUE
Mut
ΔUE 147 nt - WT 119 nt
ΔUE 147 nt - #11 PIP Δ CE [-38 +7]
ΔUE 147 nt - #6 PIP LSM [-28 -17]
ΔUE 147 nt - #3 PIP LSM [-4 +8]

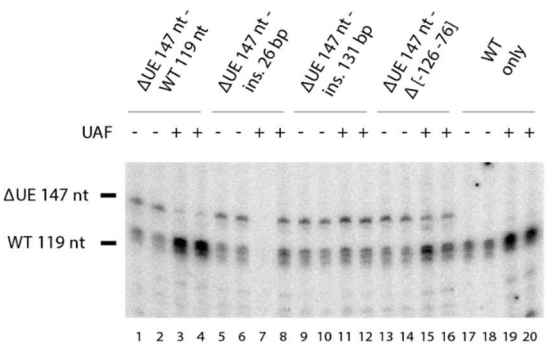
ΔUE 147 nt - WT 119 nt
ΔUE 147 nt - ins. 26 bp
ΔUE 147 nt - ins. 131 bp
ΔUE 147 nt - Δ [-126 -76]
WT only
UAF
ΔUE 147 nt
WT 119 nt
1 2 3 4 5 6 7 8 9 10 11 12 13 14 15 16 17 18 19 20

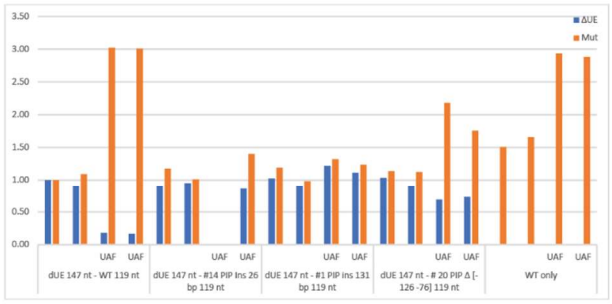
ΔUE
Mut
dUE 147 nt - WT 119 nt
dUE 147 nt - #14 PIP Ins 26 bp 119 nt
dUE 147 nt - #1 PIP ins 131 bp 119 nt
dUE 147 nt - # 20 PIP Δ [-126 -76] 119 nt
WT only

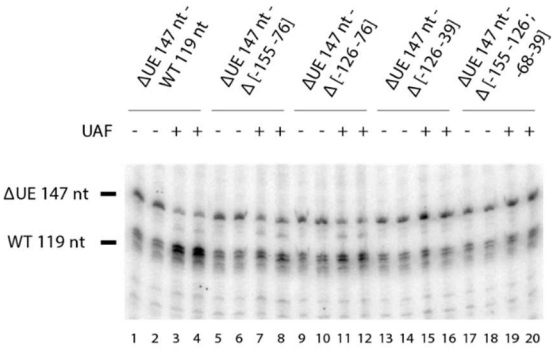
ΔUE 147 nt - WT 119 nt
ΔUE 147 nt - Δ [-155 -76]
ΔUE 147 nt - Δ [-126 -76]
ΔUE 147 nt - Δ [-126 -39]
ΔUE 147 nt - Δ [-155 -126 ; -68-39]
UAF
ΔUE 147 nt
WT 119 nt
1 2 3 4 5 6 7 8 9 10 11 12 13 14 15 16 17 18 19 20

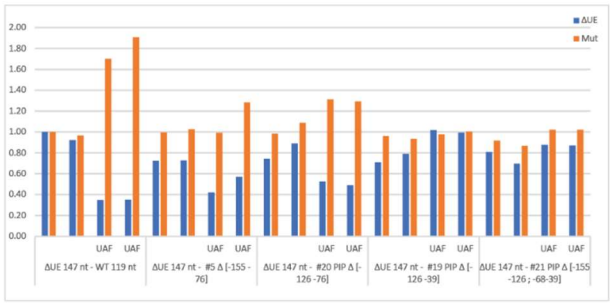
ΔUE
Mut
ΔUE 147 nt - WT 119 nt
ΔUE 147 nt - #5 Δ [-155 -76]
ΔUE 147 nt - #20 PIP Δ [-126 -76]
ΔUE 147 nt - #19 PIP Δ [-126 -39]
ΔUE 147 nt - #21 PIP Δ [-155 -126 ; -68-39]

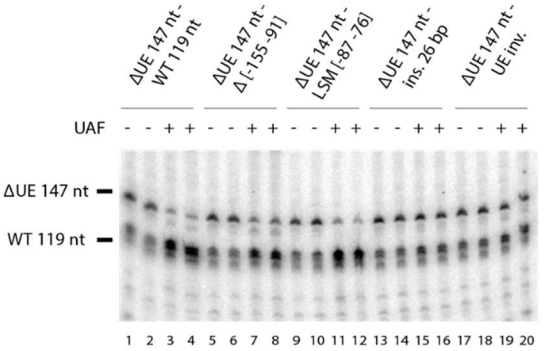
ΔUE 147 nt - WT 119 nt
ΔUE 147 nt - Δ [-155 -91]
ΔUE 147 nt - LSM [-87 -76]
ΔUE 147 nt - ins. 26 bp
ΔUE 147 nt - UE inv.
UAF
ΔUE 147 nt
WT 119 nt
1 2 3 4 5 6 7 8 9 10 11 12 13 14 15 16 17 18 19 20

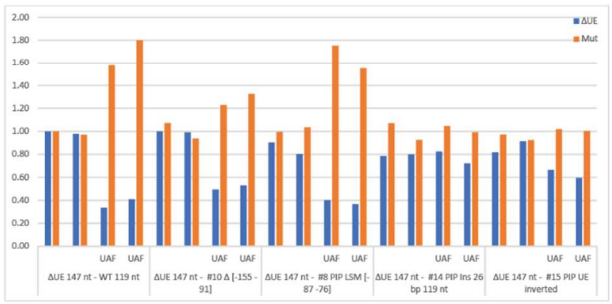
ΔUE
Mut
ΔUE 147 nt - WT 119 nt
ΔUE 147 nt - #10 Δ [-155 -91]
ΔUE 147 nt - #8 PIP LSM [-87 -76]
ΔUE 147 nt - #14 PIP Ins 26 bp 119 nt
ΔUE 147 nt - #15 PIP UE inverted

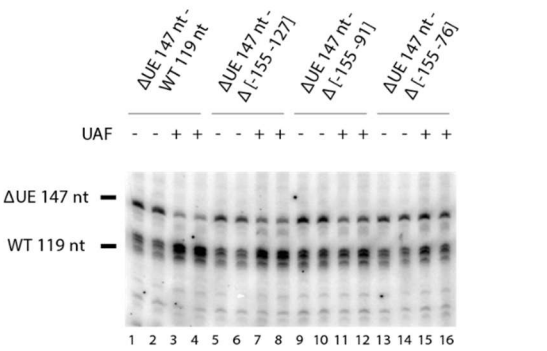
ΔUE 147 nt - WT 119 nt
ΔUE 147 nt - Δ [-155 -127]
ΔUE 147 nt - Δ [-155 -91]
ΔUE 147 nt - Δ [-155 -76]
UAF
ΔUE 147 nt
WT 119 nt
1 2 3 4 5 6 7 8 9 10 11 12 13 14 15 16

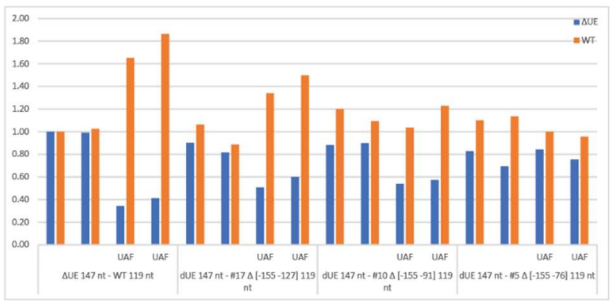
ΔUE
WT
ΔUE 147 nt - WT 119 nt
dUE 147 nt - #17 Δ [-155 -127] 119 nt
dUE 147 nt - #10 Δ [-155 -91] 119 nt
dUE 147 nt - #5 Δ [-155 -76] 119 nt

Supplemental Figure 9: in vitro transcription reactions of Pol I promoter variants
In vitro transcription of different Pol I promoter variants, left: autoradiograms of reactions. Reactions contained DNA templates as indicated and same amounts of Pol I, Rrn3, CF, TBP and Net1 and UAF or respective buffer. Right quantification of transcription from each template.

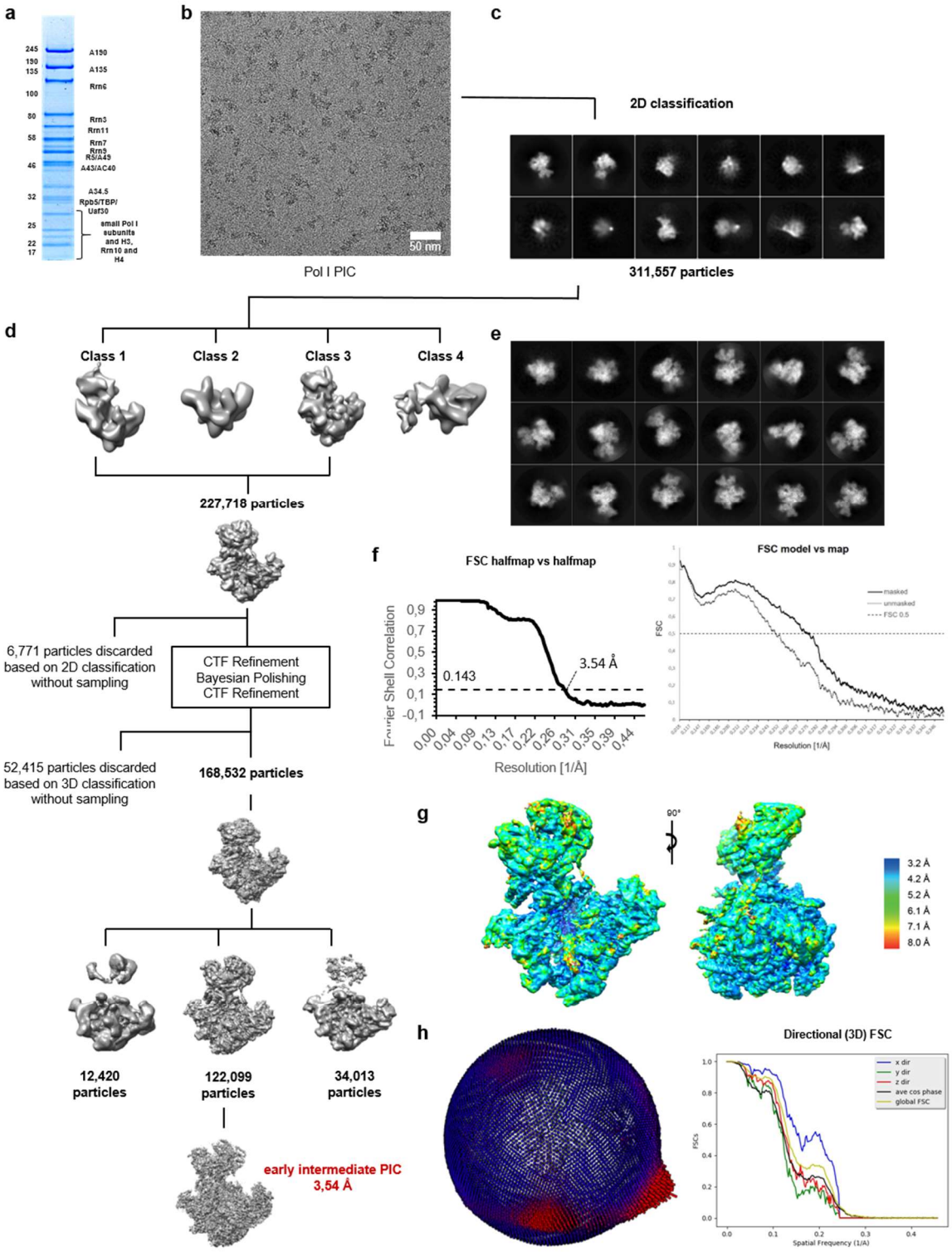

Supplemental Figure 10: Formation and cryo-EM processing of eiPIC
A Coomassie-stained SDS-PAGE of non-crosslinked PIC samples shows the presence of all polypeptide chains in approximately stoichiometric amounts. **B** Representative raw cryo-electron micrograph. **C** Representative reference-free 2D class averages of initially extracted particles. **D** 3D classification of

the Pol I PIC data set (Methods). The particles were subjected to a hierarchical process, which encompassed several rounds of classification. The number of particles contributing to each class is indicated. First round of 2D and 3D classification was performed with four subsets and threefold binning. **E** Representative 2D class averages of particles in final reconstruction. **F** Fourier shell correlation of eiPIC half-datasets with the estimated resolution at the gold-standard FSC (FSC = 0.143) and model vs. map FSC. **G** Local Resolution estimation. **H** Orientational distribution of the particles contributing to the eiPIC reconstruction, left panel: height of the surface bars indicates the relative number of particles in a given orientation, right panel: directional FSC (compare Methods).

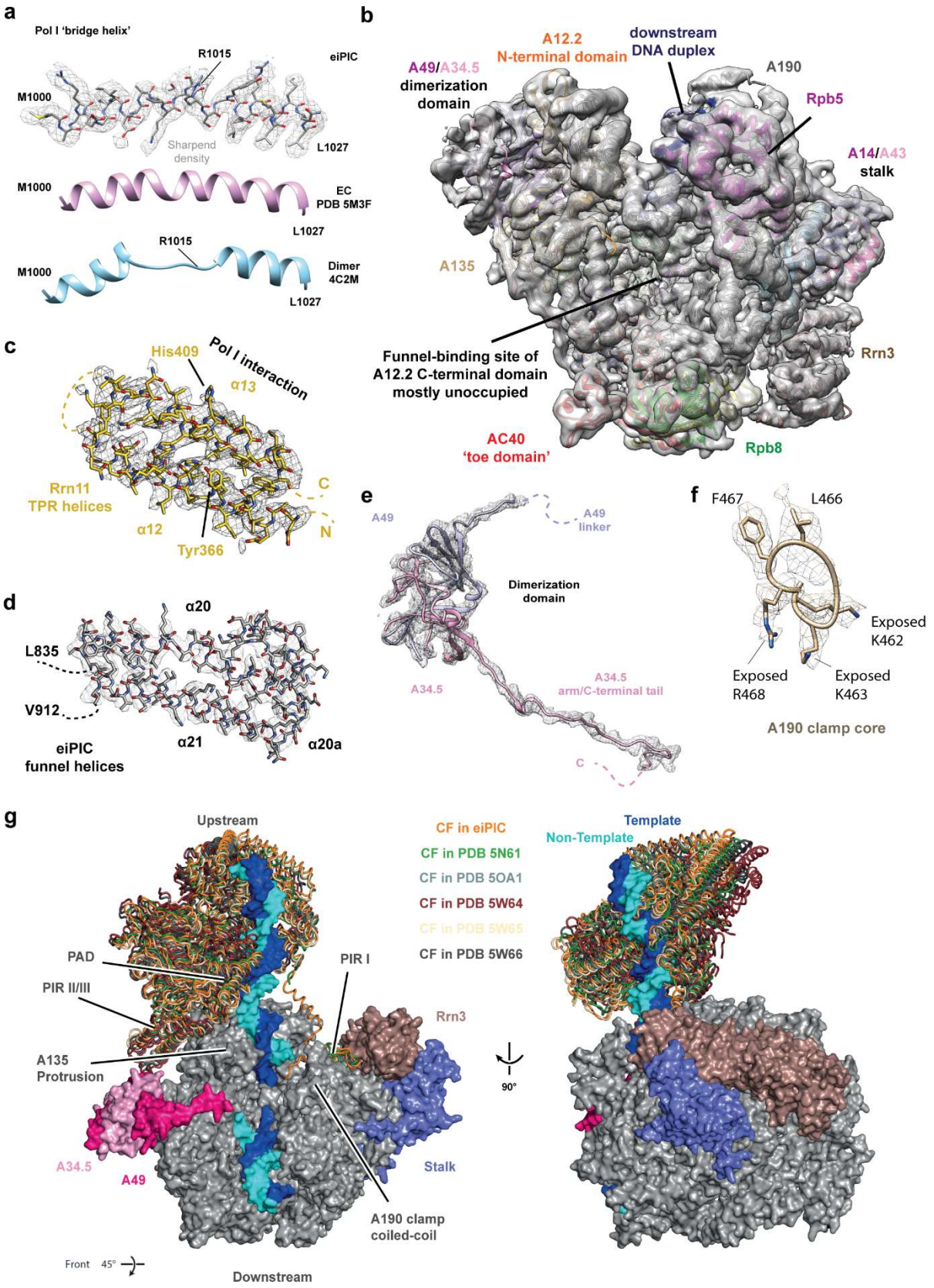

Supplemental Figure 11: Cryo-EM density and factor occupation of eiPIC reconstruction
A Central bridge helix is refolded in eiPIC reconstruction. Sharpened eiPIC density (Focused on Pol I – Rrn3) is depicted as grey mesh and superimposed with atomic model. Models of completely folded bridge helix in a Pol I EC (pink, PDB 5M3F) and the unfolded helix in Pol I dimers (light blue, PDB 4C2M)

shown for comparison. **B** eiPIC cryo-EM density (grey, transparent envelope) superimposed with the eiPIC structural model indicates low to no evidence of A12.2 C-terminal domains presence. **C** Rrn11-TPR density is depicted as grey mesh and superimposed with atomic model. **D** Atomic model of the funnel helices within Pol I subunit A190 overlaid with sharpened eiPIC density (grey mesh). **E** eiPIC density (grey mesh) shows a well-defined A49/A34.5 sub-complex (ribbon). **F** Exposed positive charges in A190 clamp core, atomic model overlaid with sharpened eiPIC density (grey mesh). **G** Location of CF in Pol I initiation complexes. 10-subunit core of Pol I is shown in gray with the A14/A43 stalk sub-complex in slate, Rrn3 in dark red and the A49/A34.5 dimerization domain in pink (space filling). PDB models were superposed via the subunit A135. The CF location is similar in all structures as shown by ribbon models of the subunits Rrn6, Rrn7, and Rrn11 in orange eiPIC, green (5N61), tin (5OA1), brown (5W64), wheat (5W65), and dark grey (5W66).

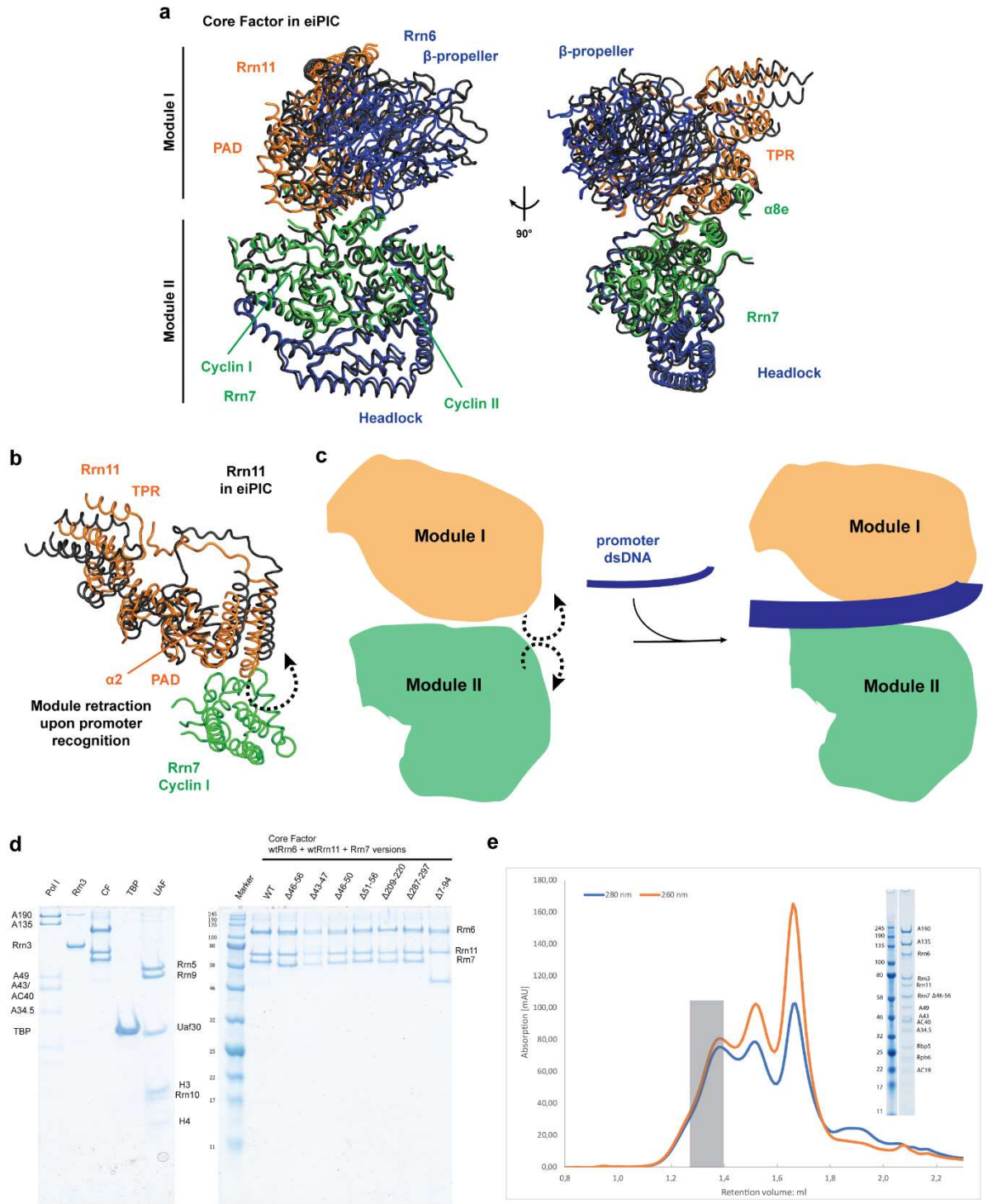

Supplemental Figure 12: Core Factor modules retract upon promoter recruitment.
A Structure of free CF (PDB 5O7X; subunits Rrn6, Rrn7 and Rrn11 in blue, green and orange, respectively) overlaid with promoter-bound CF (black) via their Rrn7 cyclin domains. **B** CF modules retract from each other to expose phosphate-backbone-interacting regions (Colors as in a). **C** Schematic representation of CF module retraction upon DNA binding, module I depicted in orange, module II in green and DNA in blue. Arrows with dotted line indicate movement of modules. **D** Coomassie-stained SDS-PAGE shows the used complexes, single proteins and CF-mutants for comparison. **E** SEC of CF mutant version with deleted Rrn7 B-reader loop. The mutant still assembles with Pol I and Rrn3 on promoter DNA. Right panel: Coomassie-stained SDS-PAGE of marked elution fraction.

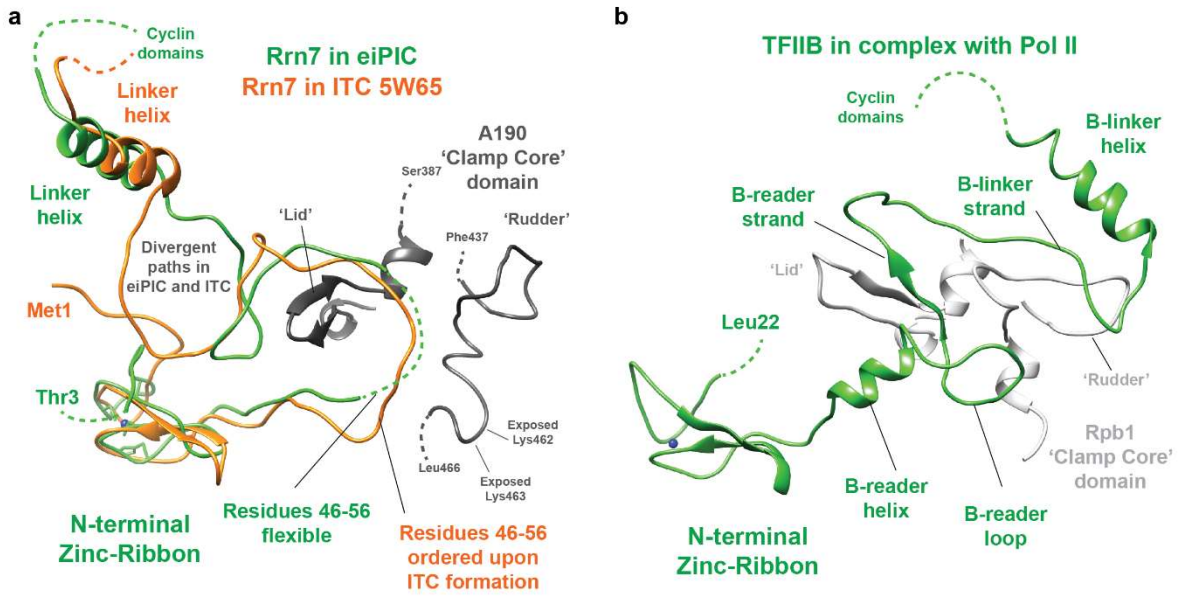

Supplemental Figure 13: Rrn7 path in the Pol I cleft
A Structure of Rrn7 in the eiPIC (green) compared to the ITC (PDB 5W65, orange). While the residues 46 to 56 are disordered in the eiPIC, they are mostly structured in the ITC. Divergent chain traces upon Pol I exit may indicate different stages of Rrn7 action, they may also result from different interpretation of densities (compare Fig. 3). **B** For comparison, the path of TFIIB in an ITC crystal structure is indicated (PDB 4BBS, green).

8. Figures

9. Tables

10. Summary

In fast growing cells, up to 60% of total transcription is devoted to ribosomal RNA synthesis. In eukaryotes a specialized enzyme, RNA polymerase I (Pol I), synthesizes a polycistronic precursor rRNA which is the 35S ribosomal RNA (rRNA) in the yeast S. cerevisiae. Whereas Pol II and Pol III use similar mechanisms to initiate transcription, the processes underlying Pol I promoter recognition, initiation complex formation and DNA melting substantially diverge. The transcription initiation factor CF (core factor) together with Pol I and the Pol I-bound initiation factor Rrn3 initiates *in vitro* transcription at a basal level. Binding of Upstream-Activating-Factor (UAF) and TATA-Binding-Protein (TBP) to the upstream promoter element (UE) enhance Pol I transcription initiation *in vitro* and are essential for Pol I-dependent rRNA synthesis *in vivo*. I reconstituted Pol I transcription initiation from highly purified factors to understand molecular mechanisms underlying this process. I combined biochemical characterisation of Pol I and its transcription factors with electron cryo microscopy (cryo EM). We obtained a cryo EM density of a highly active Pol I/Rrn3 complex at 7,5 Å and compared it with monomeric and dimeric Pol I. Rrn3 binds at the Pol I stalk and contacts subunits AC40 and A190. Rrn3 binding occludes A43-connector association and thereby prevents dimerization. Rrn3-bound and monomeric Pol I differ from the dimeric enzyme in cleft opening, and localization of the A12.2 C-terminus in the active center. Rrn3 stabilizes monomeric Pol I and drives pre-initiation complex formation (PIC). I used a fully reconstituted transcription system to better define contributions of individual PIC components to highly efficient Pol I initiation. My results suggested that UAF recruits TBP to the promoter, UAF and TBP stabilize CF and form a stable 'committed' complex. Net1-C might be associated with this complex, and acts as an activation domain which could be functionally conserved in mammalian UBF. Further, re-investigation of Pol I promoter elements allowed a more precise description of cis-acting elements and their interaction with Pol I transcription factors. Finally, we obtained a high-resolution cryo-EM reconstruction of a Pol I early initiation intermediate at 3,5 Å resolution. Our analysis showed, how efficient promoter-backbone interactions were achieved by re-arrangement of flexible regions in CF subunits Rrn7 and Rrn11. Destabilization of the melted DNA region correlated with a contraction of the polymerase cleft upon transcription activation, thereby combining promoter recruitment with DNA melting.

11. Acknowledgements

Ich möchte mich herzlich bei Allen bedanken, die mich im Laufe dieser Arbeit begleitet und unterstützt haben.

Bei Herbert Tschochner für die Möglichkeit und das Vertrauen diese Arbeit anzufertigen, die Vergabe des interessanten Themas und die gute Betreuung.

Danke an alle ehemaligen und aktuellen Mitglieder des Lehrstuhls Biochemie III und der AG Engel.

Ein großer Dank geht an Joachim Griesenbeck und Philipp Milkereit sowie allen Teilnehmern der Transkription/Chromatin Sub-Gruppe für die konstruktiven Diskussionen.

Danken möchte ich auch Kinga und Caroline für die Organisation der Graduiertenschule, der Graduate Research Academy *RNA Biology* für die Organisation von Methodenkursen, der Finanzierung von Hilfs-Studenten und der Finanzierung des Kurses (EMBO-course integrative structural modelling).

Bei Patrick Schultz und Corinne Crucifix möchte ich mich für die Einführung in die Elektronen-Mikroskopie und die gute Kooperation bedanken.

Ein großes Dankeschön geht an Christoph Engel für seine Unterstützung und dass ich mit ihm das Projekt fortführen darf. Danke für die vielen Diskussionen und die Einführung sowie Vertiefung in struktur-biologische Arbeitstechniken.

Ein besonderes Dankeschön geht an meine Labor-Mitbewohnerin Gisela, für die tatkräftige und moralische Unterstützung während der ganzen Zeit.

Danken möchte ich auch Norbert und Gerhard für die Unterstützung mit der Rechen-Infrastruktur und Mona für allerlei Hilfe im Labor.

Der größte Dank gebührt meiner Familie, insbesondere meiner Frau Kathrin die meine Launen während der Anfertigung dieser Arbeit ertragen musste und meinen Kindern Frieda, Carla und Anton die auch zu oft zurückstecken mussten. Ohne euch hätte ich diese Arbeit nicht erstellen können, vielen Dank für eure Unterstützung. Ein extra Dank an Frieda für die guten Anregungen zur Farbgestaltung.